



2015-06-01

Synthesis, RNA Binding and Antibacterial Studies of 2-DOS Mimetics AND Development of Polymer Supported Nanoparticle Catalysts for Nitroarene and Azide Reduction

Venkata Reddy Udumula
Brigham Young University

Follow this and additional works at: <https://scholarsarchive.byu.edu/etd>

 Part of the [Chemistry Commons](#)

BYU ScholarsArchive Citation

Udumula, Venkata Reddy, "Synthesis, RNA Binding and Antibacterial Studies of 2-DOS Mimetics AND Development of Polymer Supported Nanoparticle Catalysts for Nitroarene and Azide Reduction" (2015). *All Theses and Dissertations*. 6031.
<https://scholarsarchive.byu.edu/etd/6031>

This Dissertation is brought to you for free and open access by BYU ScholarsArchive. It has been accepted for inclusion in All Theses and Dissertations by an authorized administrator of BYU ScholarsArchive. For more information, please contact scholarsarchive@byu.edu, ellen_amatangelo@byu.edu.

Synthesis, RNA Binding and Antibacterial Studies of 2-DOS Mimetics

AND

Development of Polymer Supported Nanoparticle Catalysts

for Nitroarene and Azide Reduction

Venkata Reddy Udumula

A dissertation submitted to the faculty of
Brigham Young University
in partial fulfillment of the requirements for the degree of

Doctor of Philosophy

David J. Michaelis, Chair
Paul B. Savage
Merritt B. Andrus
Matt A. Peterson
Roger G. Harrison

Department of Chemistry & Biochemistry

Brigham Young University

June 2015

Copyright © 2015 Venkata Reddy Udumula

All Rights Reserved

ABSTRACT

Synthesis, RNA Binding and Antibacterial Studies of 2-DOS Mimetics AND Development of Polymer Supported Nanoparticle Catalysts for Nitroarene and Azide Reduction

Venkata Reddy Udumula
Department of Chemistry & Biochemistry, BYU
Doctor of Philosophy

Project I 2-Deoxystreptamine (2-DOS), the most conserved central scaffold of aminoglycosides, is known to specifically recognize the 5'-GU-'3 sequence step through highly conserved hydrogen bonds and electrostatic interactions within and without the context of aminoglycosides. We proposed that a novel monomeric unnatural amino acid building block using 2-DOS as a template would allow us to develop RNA binding molecules with higher affinity and selectivity than those currently available. Conjugating two or more of the monomeric building blocks by an amide bond would introduce extra hydrogen bonding donors and acceptors that are absent in natural aminoglycosides and increase specificity of binding to a target RNA through a network of hydrogen bonds. In addition, the amide conjugation between the monomeric building blocks places two GU-base recognizing amines at 5 Å distance, which is equal to the distance of neighboring base stacks in dsRNAs. We hypothesized that targeting dsRNAs containing multiple consecutive 5'-GU-'3 sequence steps would become possible by connecting two or more of the monomeric building blocks by amide bonds. According to the proposed hypothesis, we designed three dimeric 2-DOS compounds connected by an amide bond. These three targets include the dimeric 2-DOS substrate connected by an amide bond, the dimeric 2-DOS containing the sugar moiety from Neamine, and a dimeric 2-DOS connected by a urea linker. These compounds were then tested for sequence specific binding against 8 different RNA strands, and for antibacterial activity against *E. coli*, *actinobacter baumannii* and *klebsiella*.

Key Words: aminoglycosides, RNA binding studies, 2-DOS, antibiotics

Project II A dual optimization approach was used for to enhance the catalytic activity and chemoselectivity for nitro reduction. In this approach the composition of the nanoparticles and electronics effects of the polymer were studied towards nitro reduction. Bimetallic Ruthenium–Cobalt nanoparticles showed exceptional catalytic activity and chemoselectivity compared to monometallic Ruthenium nanoparticles. The electronic effects of the polymer also had a significant effect on the catalytic activity of the bimetallic nanoparticles. The electron-deficient poly(4-trifluoromethylstyrene) supported bimetallic nanoparticles undergo nitro reduction in 20 minutes at room temperature, whereas electron-rich poly(4-methylstyrene) and poly(4-methoxystyrene) supported bimetallic nanoparticles to longer reaction times to go to completion. Electronics of the polymers also effects the change in mechanism of nitroreduction. Polystyrene bimetallic Ruthenium–Cobalt nanoparticles showed excellent yields and chemoselectivity towards nitro functional group in the presence of easily reducible functional groups like alkenes, alkynes, allyl ethers, propargyl ethers.

Monometallic ruthenium nanoparticles also showed excellent reactivity and chemoselectivity towards azide reduction in the presence of easily reducible functional groups. Interestingly monometallic ruthenium nanoparticles showed regioselective reduction of primary azides in the presence of secondary and benzylic azides, also aromatic azides can be selectively reduced in the presence of secondary azides. These polystyrene supported nanoparticles are heterogeneous and are easily separated from the reaction mixture and reused multiple times without significant of catalytic activity.

Key words: bimetallic nanoparticle, nitroarene reduction, polymer support, metal-support interaction

ACKNOWLEDGEMENTS

I am very grateful to Dr. David J. Michaelis for accepting me into his research group after Dr. Ham left the university and for the support I received throughout the project. Dr. Michaelis' passion and dedication for chemistry is inspiring. I am fortunate to be part of his research group. This thesis would not have been possible without the guidance and suggestions from Dr. Michaelis.

I thank Dr. Young Wan Ham for accepting me into his research group and for the suggestions and help I received throughout the time I was in his lab. I thank all my committee members--Dr. Paul B. Savage, Dr. Merritt B. Andrus, Dr. Matt A. Peterson and Dr. Roger G. Harrison--for teaching me the classes and for their guidance and suggestions.

I would like to thank Brigham Young University and the Department of Chemistry & Biochemistry for giving me the opportunity to pursue my PhD studies in this beautiful university. I also would like to thank Janet Fonoimoana, our assistant graduate coordinator, for her help in reminding the students about registering for classes and answering the questions regarding the PhD program.

I also would like to thank our lab members Hadi S. Nazari, Whitney K. Walker, Diana L. Anderson, Jefferson H. Tyler, and Mike Talley for their support through my time in the lab.

I want to thank my father, Malla Reddy, and my mother, Vara Lakshmi, for their support and love throughout my studies and for giving me everything without asking anything in return. I cannot express enough gratitude to my mother and father. I want to dedicate this thesis for them.

Table of Contents

Chapter-1	1
Aminoglycoside Antibiotics and Selective RNA Binding Molecules	1
1.1 Introduction.....	1
1.1.1 RNA as Drug target	1
1.1.2 RNA structure.....	3
1.2 Aminoglycosides.....	4
1.3 Toxicity and Resistance in Aminoglycoside Antibiotics.....	7
1.4 Molecular Mechanism of Action of Aminoglycosides.....	9
1.5 2-Deoxystreptamine Mimetics.....	12
1.6 Conclusion	19
1.7 References.....	20
Chapter-2	24
Rational Design of Novel 2-DOS Mimics for sequence specific RNA Recognition	24
2.1 Introduction.....	24
2.2 Rational for Proposed RNA Specific Analogs of 2-DOS.....	25
2.3 Synthesis of Novel 2-DOS Analog with Peptidyl and Urea Connectivity as Monomeric Building Block.....	28
2.3.1 Synthesis of Bis-Azide 4 as a Common Synthetic Intermediate	29
2.3.2 Synthesis of the Amine containing monomeric 2-DOS analog building block 8	30
2.3.3 Synthesis of the Acid containing monomeric 2-DOS analog building block 9.....	31
2.3.4 Synthesis of 2-DOS Mimic 1.....	32
2.3.5 Synthesis of 2-DOS Mimic 2.....	33
2.3.6 Synthesis of 2-DOS Mimic 3.....	33
2.4 Conclusion	34

2.5 References.....	34
2.6 Experimental Procedures	35
2.6.1 Characterization of compounds synthesized	35
Chapter-3	46
RNA Binding Studies and Antibacterial Activity of 2-deoxystreptamine Antibiotic Mimics	46
3.1 RNA Binding Studies and Anti-bacterial Activity	46
3.2 Evaluating RNA Binding.....	46
3.2.1 RNA Binding Studies of Compound 1	47
3.2.2 RNA Binding Studies of Compound 2	51
3.2.3 RNA Binding Studies of Compound 3	52
3.3 Antibacterial Activity.....	53
3.3.1 Antibacterial Activity of Novel 2-DOS Mimics 1–3.....	53
3.3.2 Comparison of RNA binding Affinity and Antibacterial Activity.....	54
3.4 Conclusion	57
3.5. References.....	58
3.6 Experimental Procedures	59
3.6.1 Fluorescence Binding Assay Condition, Procedures, and Titration Curves.....	59
3.6.2 Fluorescence Binding Assay	60
Chapter-4	61
Polymer-Supported Nanoparticle Catalysts for Organic Synthesis	61
4.1 Introduction.....	61
4.2 Preparation Strategies for Nanoparticle Catalysts	63
4.3 The Impact of Nanoparticle Structure on Catalytic Activity	64
4.3.1 Nanoparticle Size and Catalytic Activity	64
4.3.2 Nanoparticle Shape and Catalytic Activity	65

4.3.3 Supporting Ligands and Catalytic Activity	67
4.4 Preparation and Catalytic Performance of Nanoparticle Catalysts for Organic Synthesis	69
4.4.1 Preparation and Catalytic Activity of Unsupported Metal Nanoparticles	69
4.4.2 Preparation and Catalytic Applications of Supported Nanoparticles	76
4.5 Conclusion and Outlook	87
4.6 References	90
Chapter-5	100
A Dual Nanoparticle Approach to Bimetallic Nanoparticle Catalysis: Impact of $M_1:M_2$ Ratio and Supporting Polymer on Reactivity in Nitroarene Reductions	100
5.1 Introduction	100
5.2 Results and Discussion	104
5.2.1 Catalyst Optimization Studies	104
5.2.2 Recyclability studies	107
5.2.3 Leaching Studies	108
5.2.4 Effect of Polymer Structure on Catalyst Activity	109
5.2.5 Mechanism of Nitroarene Reduction	111
5.2.6 Analysis of Nanoparticles	112
5.3. Conclusion	114
5.4 References	115
5.5 Experimental Section	118
5.6 Nanoparticle Characterization	134
Characterization of Ru-Co/polystyrene nanoparticles	134
5.7 References	137
5.8 XPS and ToF-SIMS Studies:	138
5.9 Instrumentation	142

5.10 References for XPS and ToF-SIMS studies.....	143
Chapter-6	145
Chemo and Regioselective Alkyl and Aryl Azide Reductions with Recoverable Heterogeneous Nanoparticle Catalysts	145
6.1 Introduction.....	145
6.2. Results and Discussions.....	149
6.2.1 Catalyst Preparation.....	149
6.2.3 Substrate Scope of azide reduction.....	151
6.2.4 Recyclability studies.....	154
6.2.5 Leaching Studies.....	155
6.2.6 Regioselectivity in Azide Reductions.....	156
6.3 Conclusion	160
6.4 References.....	161
6.5 Experimental Section.....	162
Appendix A.....	171
Spectral images for Chapters 2, 5 and 6	171

List of Figures

Chapter-1

Figure 1.1 Possible secondary structures of RNA.....	4
Figure 1.2 Chemical structures of the three aminoglycoside subclasses	5
Figure 1.3 Structures of aminoglycosides based on connectivity around central scaffold 2-DOS-6	
Figure 1.4 Ring structure of aminoglycosides.....	9
Figure 1.5 Crystal structure of the 30S particle.....	11

Figure 1.6 Sequence specific recognition of A-site RNA by rings I and II -----	13
Figure 1.7 Loss of binding affinity of paromomycin when G 1494 is mutated to A-----	14
Figure 1.8 Sequence specific recognition of 5'-GU-'3 base steps by a 2-DOS monomer -----	15
Figure 1.9 RNA binding molecules with one or no aminosugar subunit-----	16
Figure 1.10 Amide conjugated 2-deoxystreptamine analogs-----	17
Figure 1.11 2-DOS analogs conjugated with heterocyclic compounds-----	17
Figure 1.12 Binding 2-DOS dimers to RNA stem loops-----	18
Figure 1.13 Conformationally restricted aminoglycosides-----	19

Chapter-2

Figure 2.1 Simplified binding mode of 2-DOS to its target RNAs based on crystal structures of various aminoglycosides -----	27
Figure 2.2 Aminoglycoside connected amide bond showing ring I, ring II and ring III-----	28
Figure 2.3 Distances between the two neighboring amino groups in the neighboring 2-DOS analogs in the dimer-----	30
Figure 2.4 Conversion of 4 into (a) amine 8 and (b) carboxylic acid 9 -----	31
Figure 2.5 Compound 1 : Dimeric 2-DOS connected by amide bond and aminosugar; 2 : Dimeric 2-DOS connected by amide bond without sugar 3) Dimeric 2-DOS connected by urea bond----	31
Figure 2.6 Preparation of 4 from 1,4-cyclohexadiene-----	32

Chapter-3

Figure 3.1 Structures of Compounds 1, 2 and 3-----	49
Figure 3.2 Design of sequence specific RNA binding molecules-----	51
Figure 3.3 Sequences of RNA targets-----	52
Figure 3.4 Conserved H-bonding and electrostatic interactions between aminoglycosides and RNA-----	53
Figure 3.5 titration curve between RNA 1 and Neomycin and Sample titration curve between RNA 2 and Compound 1-----	54
Figure 3.6 Titration curve between RNA 1 and Neomycin and Sample titration curve between RNA 6 and Compound 2-----	55
Figure 3.7 Figure 3.7 (a) titration curve between RNA 1 and Neomycin. (b) Sample titration curve between RNA 6 and Compound 3-----	56
Figure 3.8 Members of pyranmycin and neomycin family used to compare antibacterial activity and binding affinity-----	58

Chapter-4

Figure 4.1 Hydrogenation of pyrrole over platinum NPs of different sizes-----	69
Figure 4.2 Shape sensitivity in palladium nanoparticle-catalyzed Suzuki-Miyaura cross coupling reaction-----	70
Figure 4.3 Tetrahedral Pt NPs catalyzed Suzuki- Miyaura coupling reaction-----	70

Figure 4.4 Schematic representation of stabilization of nanoparticles using different protecting groups-----	71
Figure 4.5 PVP stabilized gold NPs catalyzed oxidation of benzyl alcohol -----	74
Figure 4.6 Ionic polymer stabilized Au NPs for 4-nitrophenol reduction-----	75
Figure 4.7 PVA, THPC, Citrate stabilized Au NPs for aerobic oxidation of glycerol-----	76
Figure 4.8 PVP-Pd NPs catalyzed Suzuki cross coupling-----	77
Figure 4.9 Chiral Phosphine stabilized Pd NPs for enantioselective Suzuki-Miyaura coupling reactions-----	77
Figure 4.10 Tetraalkylammonium carboxylate-stabilized Pd NPs for Heck reactions-----	78
Figure 4.11 PVP stabilized Ru NPs for deuteration of amines-----	79
Figure 4.12 Aryl and alkyl groups containing phosphine stabilized Ru NPs for Hydrogenation-----	79
Figure 4.13 Silica supported Platinum NPs for Hydroarylation-----	82
Figure 4.14 Silica supported silver NPs for Diels-Alder reactions-----	82
Figure 4.15 TiO ₂ supported gold NPs catalyzed aerobic oxidation of alcohols-----	83
Figure 4.16 Aerobic oxidation of 1-phenylethanol using polymer incarcerated gold NPs-----	85
Figure 4.17 PI Gold NPs prepared by cross linking the epoxide and alcohol functional groups of the polymer-----	85

Figure 4.18 schematic representation of copolymer used to prepare Pd NPs for Suzuki-Miyaura coupling-----	86
Figure 4.19 Corriu-Kumada-Tamao reaction-----	87
Figure 4.20 Nickel NPs stabilized in the cross-linked imidazolium-containing polymer with N-heterocyclic carbene-----	87
Figure 4.21 PATP-Stabilized Gold Nanoparticle Catalysts for Suzuki-Miyaura Coupling -----	88
Figure 4.22 Polyaniline supported Pd NPs for Suzuki coupling-----	89
Figure 4.23 Polymer incarcerated (PI) Au/Co NPs for amide synthesis from alcohols and amines-----	90
Figure 4.24 Selectivity to different products using bimetallic nanoparticles-----	91
Figure 4.25 Modifying the nanoparticle composition and tuning the metal-support interaction for nitro reduction-----	92
Figure 4.26 Selective reduction of azides in the presence of nitro group and partial reduction of nitro group to form diarylhydrazine product-----	93

Chapter-5

Figure 5.1 Possible electron donations from polymers to platinum nanoparticles-----	105
Figure 5.2 polymer supported nanoparticle catalysts-----	106
Figure 5.3 Synthesis of bimetallic nanoparticle catalysts-----	108
Figure 5.4 Substrate Scope of Nitroarene Reduction-----	110

Figure 5.5 Test for homogeneous nanoparticles-----	112
Figure 5.6 Electronic effects of polymer supports-----	113
Figure 5.7 Electronic effects of Lewis basic functional groups on catalysis-----	114
Figure 5.8 Nanoparticle Characterization-----	116
Figure S5.1 Nanoparticle Leaching study-----	129
Figure S5.2 STEM image Ru-Co polystyrene catalyst-----	138
Figure S5.3 STEM image of Ru-Co poly (4-Methylstyrene) catalyst-----	138
Figure S5.4 STEM image Ru-Co poly (4-methoxystyrene) catalyst-----	139
Figure S5.5 Ru-Co poly (4-CF ₃ styrene) catalyst-----	139
Figure S5.6 XPS survey spectrum of Co-Ru nanoparticles in a polystyrene matrix-----	141
Figure S5.7 XPS narrow scans of Co-Ru nanoparticles in a polystyrene matrix-----	141
Figure S5.8 Positive ion time-of-flight (TOF)-secondary ion mass spectrometry of Co-Ru nanoparticles in a polystyrene matrix-----	145

Chapter-6

Figure 6.1 Common methods used for azide reductions to amines -----	150
Figure 6.2 Reduction of azides to amines using iron oxide nanoparticles-----	152
Figure 6.3 Reduction of azides to amines using copper nanoparticles-----	152
Figure 6.4 Reduction of aromatic azides to amines using CdS/CdSe nanoparticles-----	153

Figure 6.5 Reduction of 1-azido-4-nitrobenzene using Ru NPs supported on polystyrene-----	154
Figure 6.6 Aliphatic substrates used in azide reduction. Yield/Selectivity-----	159
Figure 6.7 Regioselective reduction of bis-azides using trimethyl phosphine-----	161
Figure 6.8 Effect of polymer support on regioselectivity-----	162
Figure 6.9 Regioselective reduction of bis-azides-----	165

List of Schemes

Chapter-2

Scheme 1 Synthesis of monomeric 2-DOS analog building block 8-----	33
Scheme 2 Syntheses of monomeric analog acid building block 9-----	34
Scheme 3 Synthesis of compound 1-----	35
Scheme 4 Syntheses of Compound 2-----	35
Scheme 5 Syntheses of 2-DOS mimic 3-----	36

Chapter-5

Scheme 5.1 Catalyst Recyclability Studies-----	111
Scheme 5.2 Intermediate formation in nitroarene reduction-----	115

Chapter-6

Scheme 6.1 Catalyst Recyclability Studies-----	160
--	-----

List of Tables

Chapter-3

Table 3.1 K_d values (μM) for compound 1 against mutant RNA-----	54
Table 3.2 K_d values (μM) for Compound 2 against RNA mutants-----	55
Table 3.3 K_d values (μM) for Compound 3-----	56
Table 3.4 Binding affinity ($K_d = \mu\text{M}$) a and minimum inhibitory concentrations (MIC's)-----	60

Chapter-5

Table 5.1 Catalyst Optimization Studies-----	109
Table S5.1 Loading of catalysts determined by ICP-----	126
Table S5.2. Positions of the Co $2p_{3/2}$, Co $2p_{1/2}$, Ru $3p_{3/2}$, and Ru $3p_{1/2}$ peaks in metallic Co and Ru (from the literature), and from Co/Ru nanoparticles in a polystyrene matrix-----	144
Table S5.3 Natural abundances of Ru isotopes and experimental peak areas of Ru^+ signals from Co/Ru nanoparticles in a polystyrene matrix-----	145

Chapter-6

Table 6.1 Optimization of the catalyst-----	155
Table 6.2 Effect of metal loading and nanoparticle composition on catalytic activity-----	156
Table 6.3 Aromatic compounds used in azide reduction. Yields/Selectivity-----	157
Table 6.4 Optimization of regioselectivity by changing the temperature-----	162

List of abbreviations

RNA	ribonucleic acid
mRNA	messenger RNA
tRNA	transfer RNA
rRNA	ribosomal RNA
RNAi	RNA interference
TAR	trans activation response
HIV-1 RRE	human immunodeficiency virus-1 rev response element
2-DOS	2-deoxystreptamine
Å	angstrom
HATU	1-[Bis (dimethylamino) methylene]-1H-1,2,3-triazolo[4,5-b]pyridinium 3-oxid hexafluorophosphate
HOAt	1-Hydroxy-7-azabenzotriazole
DIPEA	<i>N,N</i> -Diisopropylethylamine
DIAD	diisopropyl azodicarboxylate
TFA	trifluoroacetic acid
MOM Cl	chloromethyl methyl ether

LiOH	lithium hydroxide
MeOH	methanol
HCl	hydrochloric acid
DCM	dichloromethane
$[\alpha]_D^{24}$	specific rotation
AIBN	2,2'-azobisisobutyronitrile
aq.	Aqueous
Boc	tert-butoxycarbonyl
Bn	benzyl
DMF	N,N'-dimethylformamide
THF	tetrahydrofuran
Tf ₂ O	trifluoromethanesulfonic anhydride
DMS	dimethyl sulfide
MS	molecular sieves
NPs	nanoparticles
TiO ₂	titanium dioxide
Al ₂ O ₃	aluminum oxide

SiO ₂	silicon dioxide
CeO ₂	cerium oxide
ZrO ₂	zirconium dioxide
CO	carbon monoxide
nm	nanometers
Nb ₂ O ₅	niobium pentoxide
MW	molecular weight
Hz	hertz
<i>J</i>	coupling constant
g	gram(s)
mg	milligram(s)
mL	milliliter(s)
μL	microliter(s)
h	hour(s)
mmol	millimole(s)
mol	mole(s)
MS	mass spectrometry

Chapter-1

Aminoglycoside Antibiotics and Selective RNA Binding Molecules

1.1 Introduction

1.1.1 RNA as Drug Target

Ribonucleic acid or RNA, along with DNA and proteins, is one of the important biological macromolecules used by all forms of life. The genetic information in a cell flows from DNA to RNA, and then from RNA to proteins. “DNA makes RNA makes protein”. Proteins are the workhorses of the cell and play important roles as enzymes and structural components. DNA carries all of the genetic information required for the cell to grow, to take in nutrients, and to propagate. When a cell requires a protein, the portion of DNA that codes for that protein gets activated and produces multiple copies of mRNA. These copies of mRNA, with the help of ribosomes, are then used to build proteins. Until recently, RNA was believed to be important only in protein synthesis as mRNA, tRNA and rRNA. However, scientists begun to realize that the functions of RNA are much broader. Ribozymes are catalytic RNAs that help to speed chemical reactions. In several clinically important viruses, RNA has also been shown to carry genetic information rather than DNA.

Until recently pharmaceutical companies focus on targeting proteins for drug discovery, but with the discovery of several other functions of RNA, researchers started designing of RNA binding small molecules as a part of drug discovery efforts. Targeting RNA has several advantages compared to protein targeted drugs due to several reasons First, RNA provides unprecedented access to targets that have not been susceptible to conventional drug discovery efforts. Traditional drug discovery has focused targeting on only a few hundred endogenous

proteins such as receptors, enzymes and ion channels, which accounts for about 17 % of the human genome.¹ Second, targeting mRNAs is a much more economical approach compared to targeting proteins because the cellular pathways may be controlled one step ahead of protein translation with relatively fewer numbers of targets and structural diversities. In addition, Human mRNA molecules are frequently tissue or disease specific, and mRNAs encoding oncogenic proteins often contain unique sequences that are not found in normal cells.⁴ Thus, RNA has received increasing attention as a proven drug target over the past few years. Ribosomal RNAs (rRNAs) are targets of numerous antibiotics.² Naturally occurring antibiotics also bind to viral mRNA such as HIV-I RRE (Rev Response Element) and TAR³ (Trans Activation Response), and reduce HIV-1 replication rates.

Antisense and RNAi (RNA interference) technology are also commonly used strategies to target RNA for preventing and controlling disease⁵. In this approach, nucleic acid strand or antisense strand is synthesized complementary to mRNA produced by that gene that causes a disease. The synthesized antisense strand is delivered into cytoplasm which binds to the mRNA and forms double helix, thus preventing them from synthesizing the proteins responsible for that disease. However these strategies have several disadvantages like the toxicity, instability and also lack of efficient delivery mechanism of the RNAi and antisense molecules. Due to these disadvantages these strategies are limited in practical therapeutic application⁶ so, due to several disadvantages of these strategies it is necessary to design and develop small molecules that bind selectively to RNA and prevent the proteinsynthesis responsible for that disease.

1.1.2 RNA Structure

The binding of several ligands to RNA is due to the ability of the RNA to have several different tertiary conformations⁷. The structure of the RNA has been elucidated by variety of spectroscopic and chemical probing experiments⁸ which made little easier to find the binding sites of the RNA. RNA has structural characters that are similar to both DNA and proteins. DNA exists as a double helix, while RNA exists largely as a single stranded nucleotide chains. However RNA can fold on itself by base pairing, forming small self-complementary stands, which results in tertiary structures. The folded RNA is stabilized by a variety of interactions, the most important of which are hydrogen bonding and base stacking. RNA can assume several different secondary and tertiary conformations similar to proteins⁹ via hydrogen bonding and base stacking between base pairs. Naturally occurring RNAs largely exists in A-form conformations or exists as spherical double helix connected by single stranded regions (Figure 1.1). RNA A- helix has major and minor groove similar to DNA, the major groove largely contributes to the binding of the proteins and small molecules. The mismatched bases of major groove of A-helix RNA widen the major groove allowing the binding of small molecules.

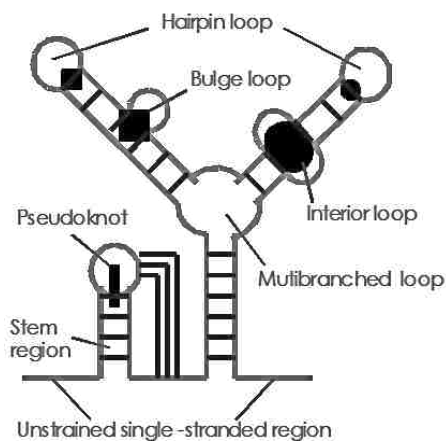


Figure 1.1 Possible secondary structures of RNA

The secondary and tertiary interactions of the RNA form complex three-dimensional structures containing bulges, hairpins, loops and pseudoknots (Figure 1.1). Rational design of RNA binding small molecules is a challenge due to the complex three-dimensional structure of RNA. There are few reports on how small molecules bind to RNA with high affinity and specificity¹⁰ However there are no specific rules or model for the structure-based rational design of small molecules to target specific RNA sequences and structures.

1.2 Aminoglycosides

The aminoglycosides are a class of antibiotics whose mode of action involves specific binding to RNA. The important structural features of the aminoglycoside antibiotics is a 1, 3-diaminocyclohexanetriol core structure termed known as 2-deoxystreptamine or 2-DOS (Figure 1.2). 2-Deoxystreptamine is important for the biological activity of the aminoglycosides, which form a large class of clinically important antibiotics with a broad antibacterial spectrum, particularly against Gram-negative bacteria.^{10b} Naturally occurring aminoglycosides can be readily isolated from actinomycetes of either genus *Streptomyces* or *Micromonospora*.¹¹ Most of the aminoglycosides contain amino sugars, which are either mono 6-amino or 2,6-diamino substituted.

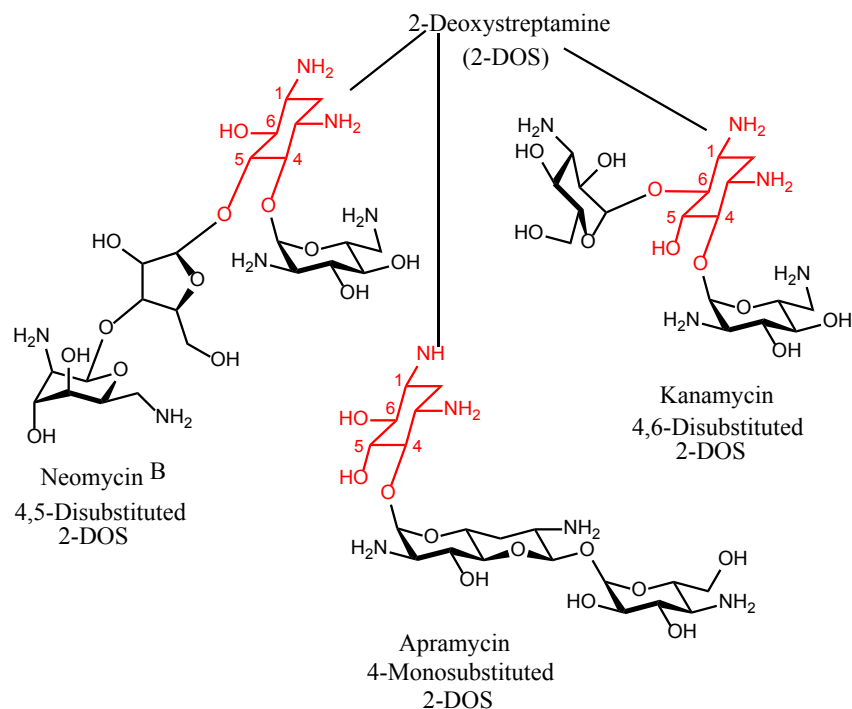


Figure 1.2 Chemical structures of the three aminoglycoside subclasses and their substitution sites. The central scaffold 2-DOS is shown in the red color and is present in all types of aminoglycoside antibiotics.

The streptamine core structure of the aminoglycosides contains a highly conserved 1,3-diamino functional groups. Apart from this conserved structure, streptamine also contains hydroxyl groups at various positions. Streptamine itself contains hydroxyl groups at each of the 4 carbons not containing amine functionality. If streptamine contains only 3-hydroxyl groups, which is most common among the aminoglycoside antibiotics, then the core structure is called 2-deoxystreptamine. The hydroxyl groups of the streptamine core act as anchoring points for the attachment of various aminosugars. Based on the substitution pattern of the streptamine ring, the aminoglycosides can be categorized as 4-monosubstituted 4,5-disubstituted or 4, 6-disubstituted (Figure 1.3). The presence of various amino group in the aminoglycosides, which are protonated and charged under physiological conditions, explains their strong affinity towards negatively charged nucleotides.

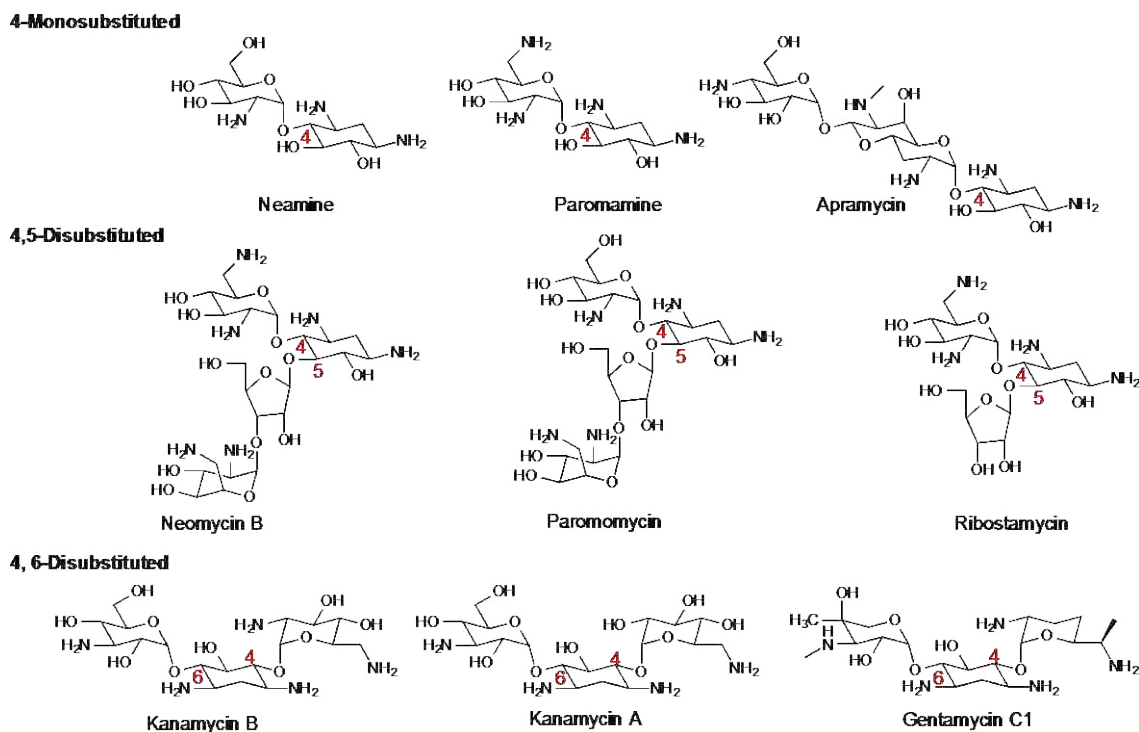


Figure 1.3 Structures of aminoglycosides based on connectivity around central scaffold 2-DOS

Aminoglycoside antibiotics bind to the aminoacyl site or A-site decoding region of the bacterial 16S ribosomal RNA within the 30S subunit and prevent the translocation of peptidyl t-RNA from A-site to P-site thereby inhibiting the synthesis of proteins necessary for bacteria to grow, leading to cell death ¹². Aminoglycosides are shown to have high promiscuous binding towards A-site RNA which means they bind to different to several different structural elements of RNA such as Bulges, internal loops, hairpin loops and stem junctions without any specificity ³. Many nucleic acid intercalating molecules such as 2, 6-diaminopurine-linked acridine, ethidium-arginine, acrine-4-carboxamide derivatives, and tetracationic diphenylfuran derivatives are also shown to have high promiscuous binding towards RNA ¹³. Aminoglycosides are also shown to have strong binding affinity towards RRE (Rev Response Element) of HIV-1 thereby preventing the growth of the virus. Neomycin is shown to bind to HIV TAR and HIV RRE

prevents the growth of HIV virus³. The strong binding affinity of the aminoglycosides to A-site RNA is due to the noncovalent interaction or hydrogen bonding between the amino groups of aminoglycosides and the hydroxyl groups of the RNA bases and also due to the electrostatic interactions between the negatively charged phosphate backbone of RNA and positively charged ammonium groups of the aminoglycosides.

All these studies showed that aminoglycosides serve as potential antibiotics. Aminoglycosides are also shown to have binding towards viral RNA and inhibits viral replication which opens the door for further drug development of antiviral drugs.

1.3 Toxicity and Resistance in Aminoglycoside Antibiotics

Aminoglycosides are highly potent, broad spectrum antibiotics. Despite their broad application, the high levels of ototoxicity (hearing loss) and nephrotoxicity (kidney damage) caused by treatment with these aminoglycosides often limits their use.¹⁴ Nephrotoxicity is usually reversible, while ototoxicity is permanent and not reversible. Nephrotoxicity is caused by the accumulation of aminoglycosides in the renal cortex. Ototoxicity results from a combination of different mechanisms, one mechanism resulting from the structural similarity between bacterial rRNA and mitochondrial rRNA. Aminoglycosides also bind to mitochondrial 12S rRNA and cause misreading in mitochondrial protein synthesis. Thus, tissues rich in mitochondria are predominantly effected.¹⁶ Aminoglycosides also decrease mitochondrial ATP synthesis, which in turn decreases ion pump activity. Reduced ion pump activity in strial intermediate cells could ultimately lead to a progressive decrease of the endocochlear potential¹⁷. The main cause of the toxicity of the aminoglycosides is due to the basicity of the amine groups. It has been shown that a decrease in the number of amine groups in aminoglycosides results in lower toxicity. In addition, a decrease in the number of hydroxyl group's results in higher

toxicity.¹⁸ For example, it was shown that neomycin is more toxic than paromycin because of the presence of the greater number of amine groups in neomycin. Also removing hydroxyl groups, which are electron-withdrawing groups significantly increases the toxicity of aminoglycosides. Displacement of 5-OH in 2-DOS with a fluorine group results in a decrease in toxicity in amikacin. This decrease is due to a lowering of the basicity of the amine groups by the electron withdrawing fluorine group.¹⁹ N-acetylated aminoglycosides also possess considerably lower toxicity than their free amine compounds, further substantiating this hypothesis.²⁰

The increasing resistance of bacteria to the major classes of antibiotics alarms the development of novel antibiotics. Bacteria develops resistance to aminoglycoside antibiotics via three different mechanisms. 1) Mutation of the ribosomal target, 2) Reduced permeability for the antibiotics, 3) enzymatic modification of drugs leading to inactivation²². Among these three resistance pathways, enzymatic modification is the most significant source of resistance development.²³ Based on their mode of action of the enzymes that modify aminoglycosides, they are classified in to different types. They include N-acetyltransferases (AACs), O-adenyl transferases (ANTs) and O-phosphotransferases (APHs). These enzymes modify aminoglycosides through N-acetylation of amino groups, or by adenylation and phosphorylation of hydroxyl groups.

Information on the structure-activity profile of aminoglycoside antibiotics has also been reported. Recent studies on tobramycin, kanamycin A and B, amikacin and gentamicin showed that differences in ring III did not alter the interaction of aminoglycosides with target rRNA, but variations in ring I and II significantly affected the binding of aminoglycosides to RNA (Figure 1.4).²⁴ It is the I and II rings that make the highly conserved interactions with the target RNA. Acetylation of amines, adenylation and phosphorylation of hydroxyl groups results in loss of

ability to form hydrogen bonding and electrostatic interactions between aminoglycosides and target RNAs, ultimately causing the aminoglycosides to lose binding affinity completely for RNA targets.²⁵ Therefore, while it is necessary to discover new aminoglycosides that are less prone to enzymatic modification and that have low toxicity, modification of the 2-deoxystreptamine core of the aminoglycosides (rings I and II) may be a good starting point for these pursuits.

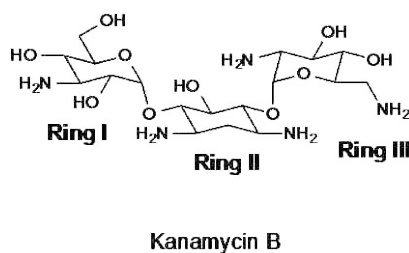


Figure 1.4 Ring structure of aminoglycosides.

1.4 Molecular Mechanism of Action of Aminoglycosides

Aminoglycosides are traditionally gram-negative antibacterial therapeutic agents and act by inhibiting protein synthesis. This is mainly due to their promiscuous structural properties, which allow them to bind to different types of RNA targets such as prokaryotic ribosomal A-site, HIV TAR, HIV RRE, Group 1 intron, RNase P, and tmRNA. Aminoglycosides are known to induce miscoding during protein synthesis. The binding site of aminoglycosides was found to be located at the aminoacyl-tRNA decoding site (A-site) on the 16S ribosomal RNA of the bacterial 30S ribosomal sub unit.²⁶ This binding prevents the translocation of peptidyl-tRNA from the A-site to the P-site. This inhibits synthesis of vital bacterial proteins or leads to the synthesis of nonfunctional misfolded proteins, eventually killing the bacteria. Puglisi et al. prepared a small model oligonucleotide that mimics A-site RNA to study the important nucleotides of A-site RNA that effect the binding of aminoglycosides²⁷⁻²⁸. This finding initiated the characterization of

aminoglycoside molecules that bind to A-site RNA at molecular level. This section will summarize the molecular mechanism of aminoglycoside antibiotic recognition by the ribosomal RNA from the available crystal structures of the various aminoglycoside/A-site complexes

Ramakrishnan et al. reported the high-resolution structure of the 30S ribosomal subunit from *Thermus thermophilus* in both free form²⁹ and 30S subunit complexed with paromomycin³⁰. These crystal structures help in understanding the mechanism of action of antibiotics. Paromomycin has one specific binding site called the A-site in the 30S particle. The A-site of the bacterial ribosome has certain features that help in binding of the aminoglycosides. The strong binding affinity of aminoglycosides is attributed to the hydrogen bonding and electrostatic interactions that they form in the narrow drug pocket of the A-site. It is believed that the wobble base pair U1495-U1406; bases A1408, A1492 and A1493; as well as the base pair C1409-G1491 are responsible for hydrogen bonding ability in the A-site³¹ (Figure 1.5).

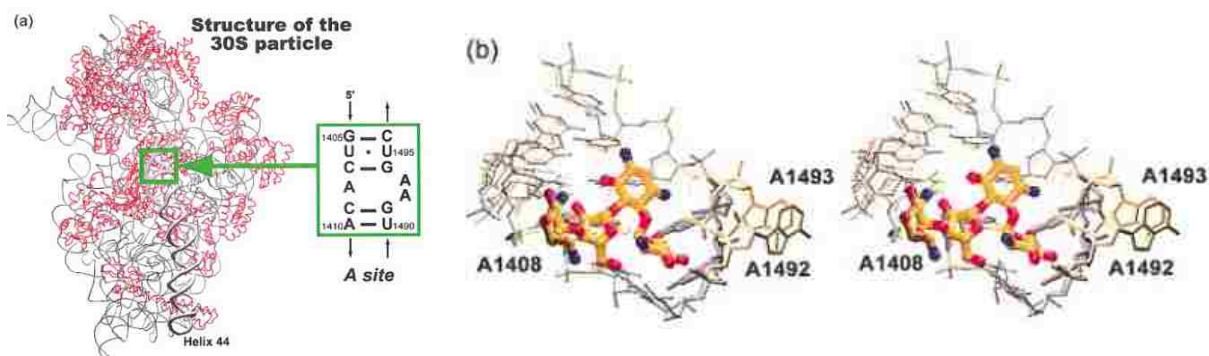


Figure 1.5³¹ Crystal structure of the 30S particle. (a) View of the 50S-facing side, with the 16SrRNA and the proteins shown in grey and red, respectively.⁸ The A site (green box) is located at the foot of helix 44 (bold). The conserved A-site sequence and its corresponding numbering in *E. coli* are specified. (b) Superimposition (based on the sugar-phosphate backbone atoms) of the A site free (grey)⁸ and bound to paromomycin (gold)³¹ inside the 30S particle

The currently accepted mechanism for the primary mode of action of most of 4, 5- and 4, 6-disubstituted 2-DOS aminoglycosides suggests that these aminoglycosides bind to the

ribosomal A-site and lock the A-site conformation in active (open) state in the absence of cognate the tRNA-mRNA complex.³² This increases the affinity of A-site to non-cognate tRNA-mRNA complexes which unable the ribosome to distinguish between non-cognate and cognate complexes. This results in the synthesis of mistranslated proteins and eventually the death of the bacterial cell.³¹

The A-site RNA is made up of three Watson-Crick G=C pairs, one U=U wobble base pair, and an internal loop made of three adenines (A1408, A1492 and A1493) in which A1492 and A1493 fold back within the helix (Figure 1.5). When aminoglycoside paromomycin binds to the ribosomal A-site RNA, the puckered sugar I (figure 1.4) is inserted into the A-site helix by stacking against the G1491 residue by forming two hydrogen bonds to the Watson-Crick sites of the universally conserved A1408. This causes A1492 and A1493 to fully bulge out from the helix³¹.

The first step of translation is the formation of a helix between the codon of the mRNA and the anticodon of the cognate aminoacyl-tRNA, which helps in selection of the aminoacyl-tRNA, this happens at the A-site near A1492 and A1493⁴¹. When the complex is formed between the tRNA-mRNA, the two adenines (A1492 and A1493) flip out from the A-site helix. This molecular switch decides the continuation of translation⁴². The stability of the conformations of A-site is increased only when cognate tRNA-mRNA complex is formed, but when aminoglycosides like paromomycin binds to mRNA the stability of the non-cognate aminoacyl-tRNA binding to A-site is also increased and this disturbs the translation as the ribosome is unable to discriminate between cognate and noncognate tRNA-mRNA complexes. This results in the synthesis of mistranslated proteins and eventually the death of bacteria.³¹

1.5 2-Deoxystreptamine Mimetics

This section describes some of the most recent research on 2-deoxystreptamine (2-DOS) aminoglycoside mimetics, as well as provides the background that led to the design of our research. Aminoglycosides provide very important insights through their binding to RNA at a molecular level through X-ray crystal structures of aminoglycosides complexed with the 30S ribosomal particle or the A-site 16S rRNA²⁹. Aminoglycosides have been shown to bind to RNAs, such as A-site rRNA, ribozymes, and HIV-1, RRE and TAR³. These RNAs contain 5'-GU-3' or 5'-GG-3' base steps in common next to bulge nucleotides. A similar binding pattern was observed without exception for 2-DOS, the central scaffold of aminoglycosides, regardless of its substitution positions. For instance, the crystal structure of six aminoglycoside antibiotics (neamine, gentamycin, C1A, kanamycin A, ribostamycin, lividomycin A and neomycin B) and oligonucleotides containing the decoding A-site of bacterial ribosome revealed that the rings I and II (2-DOS) are essential for sequence-specific recognition (Figure 1.6). Up to eight direct hydrogen bonds are conserved in rings I and II (2-DOS) of the six aminoglycosides. The puckered sugar ring I is inserted into the A-site helix by stacking against G1491 and forms of pseudo base pair with two hydrogen bonds to the Watson-Crick sites of the universally conserved A1408³³ (figure 1.6).

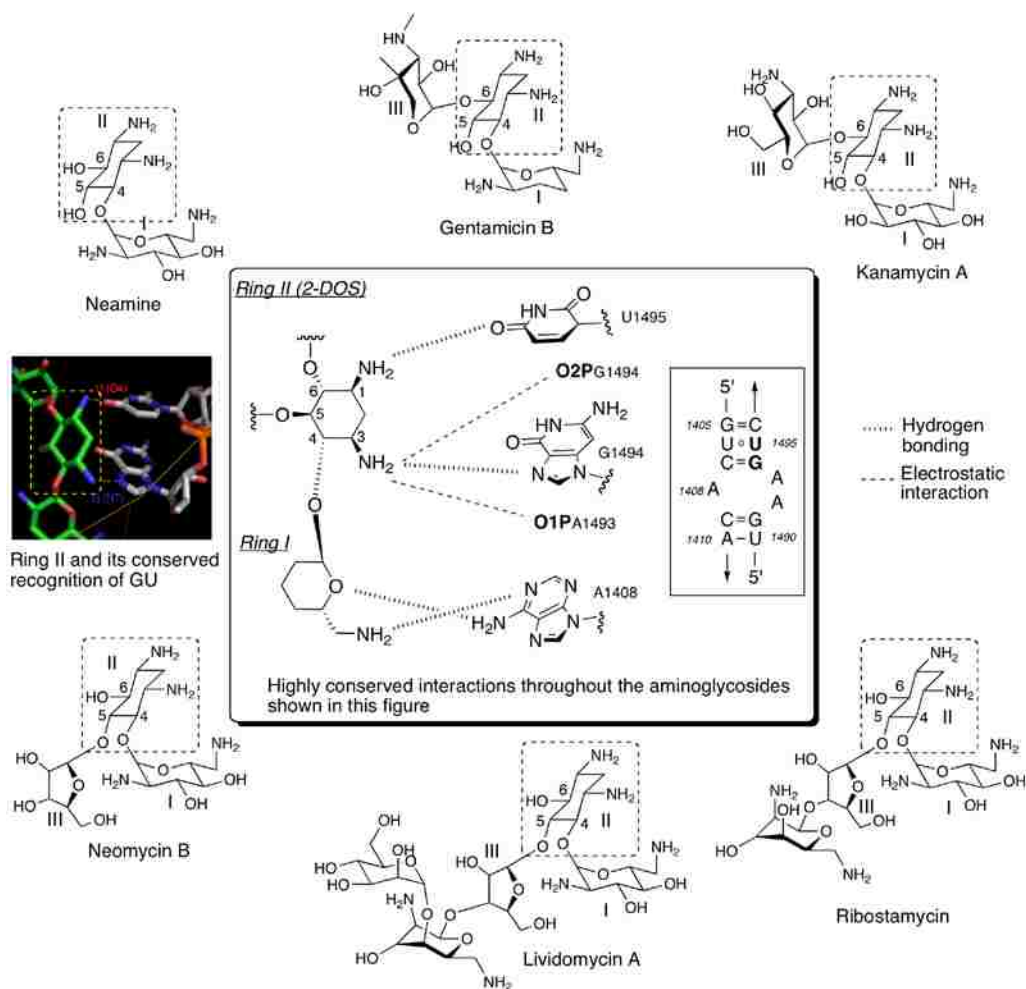


Figure 1.6 Sequence specific recognition of A-site RNA by rings I and II (2-DOS) in six different aminoglycosides. Hydrogen bonding (.....) and electrostatic interactions (-----) that are conservative throughout the aminoglycosides are indicated with dashed lines. Ring I shows highly conserved binding pattern with A1408. The 2-DOS (ring II) unanimously recognizes the 5'-GU-'3 base step (bold) in A-site regardless of aminosugar substitution among different aminoglycosides. The contact made by 2-DOS to the RNA is independent of their structural context of aminosugar subunits and more dependent on helical sequence.³³

This central interaction helps to maintain A1492 and A1493 in a bilged-out conformation. The ring II (2-DOS) unanimously recognizes the same 5'-GU-'3 step in A-site in spite of the different aminosugar substitution at various locations of 2-DOS (Figure 1.6). 2-DOS specifically recognizes 5'-GU-'3 base step in A-site through hydrogen bonding with N7 of G1494 and O4 of U1495 and electrostatic interactions with negatively charged phosphate

backbone (Figure 1.6)³³. Recently it was reported that the replacement of G1494A in the target A-site RNA with other base pairs results in weaker binding of paromomycin to the A-site RNA (Figure 1.7).³⁴ This shows that the 2-DOS ring of paromomycin strictly recognizes the 5'-G(N7)-U(O4)-'3 sequence step.

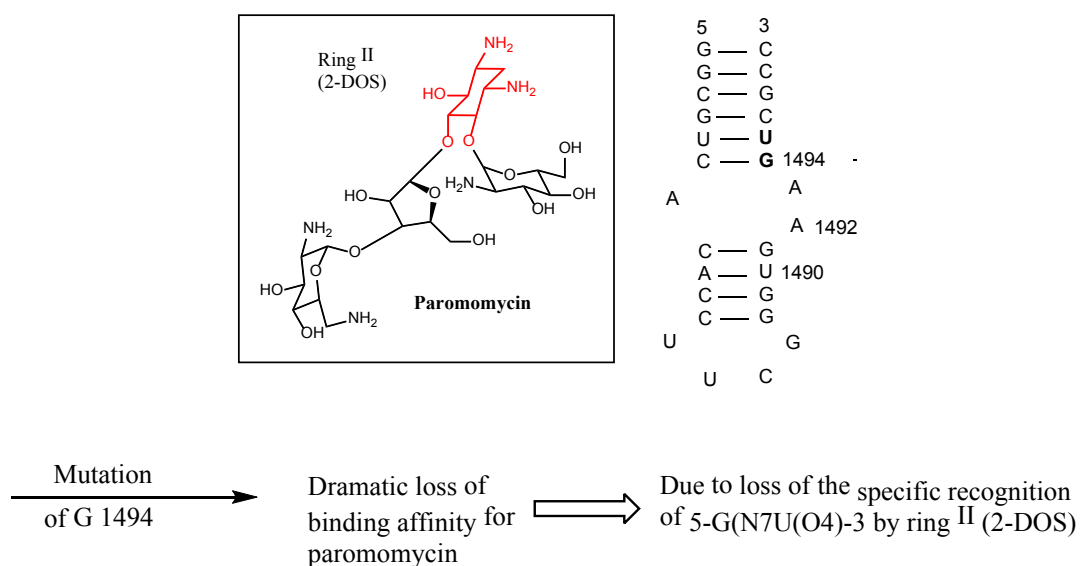


Figure 1.7 Loss of binding affinity of paromomycin when G 1494 is mutated to A. This indicates that the 2-DOS ring of paromomycin strictly recognizes the 5-G(N7)-U(O4)-3 sequence step (highlighted in bold) but not 5'-A(N7)-U(O4)-'3.

Puglisi et al. isolated 2-DOS, without the aminosugar subunit and treated with the wild type A-site of 16S rRNA (Figure 1.8).³⁵ The binding activity between the 2-DOS and A-site RNA was monitored by high resolution NMR techniques. It was reported that 2-DOS specifically recognizes the two 5'-GU-'3 base steps (G1494-U1495 and G1405-U1406) with a binding affinity of 1mM.

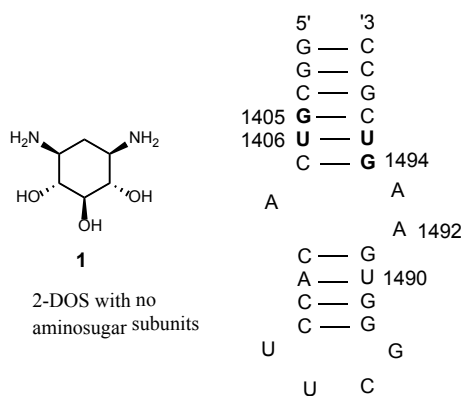


Figure 1.8 Sequence specific recognition of 5-GU-3 base steps by a 2-DOS monomer that does not have any aminosugar substitution

2-Deoxystreptamine with no aminosugar subunit attached is increasingly recognized as a platform for the design of novel RNA-binding molecules because it has demonstrated RNA-binding capability within and without the context of aminoglycosides. Wang et al. recently reported two examples of novel aminoglycoside antibiotics by removing one or both aminosugars from the original aminoglycoside structures. This modification leaves the core 2-DOS as the sole or main component of the compounds (Figure 1.9).³⁶ Both compounds demonstrated strong affinity to the target RNA A-site and inhibited bacterial translation. It is important to note that the deoxystreptamine compound with no aminosugar subunits still binds to the RNA target with K_d value of 88 μM . This suggests the likely success of generating libraries of mimics that maintain the conformation/function of aminoglycosides yet lack the aminosugars.

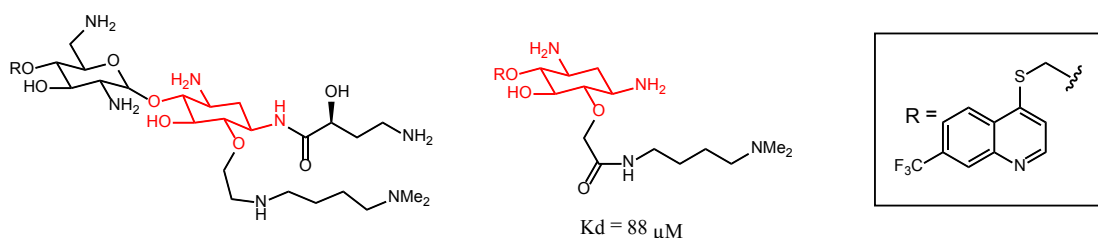
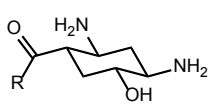


Figure 1.9 RNA binding molecules with one or no aminosugar subunit

Herman et al.³⁷ synthesized a small library of monomeric 2-DOS analogs conjugated with a small number of heterocycles via an amide bond (Figure 1.10). Although some compounds have shown slightly improved binding affinity to the target RNA A-site, most did not demonstrate enhanced binding activity. It is somewhat contrary to the above observation that one unit of the 2-DOS amide showed a dramatic increase in binding affinity with the addition of an alkyl tertiary amine, even though the amide functionality was present in a different. The heterocycles employed in this experiment may not be able to make electrostatic or hydrogen bonding interaction, possibly because of the inappropriate positions of amino groups in the rigid structures. The more flexible alkylamino arm in the Wang example participated in the electrostatic interactions with a phosphate backbone and increased the binding affinity. This signifies the importance of the subunits connected to the 2-DOS in the interactions with the target RNA, which becomes apparent in the following example.



The figure shows the chemical structure of 2-deoxystreptamine, a bicyclic molecule with a decalin core. It features a hydroxyl group at the 2-position, an amino group at the 3-position, and an amide group at the 4-position. The amide group is attached to an R group.

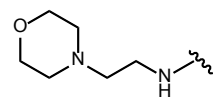
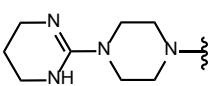
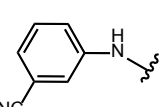
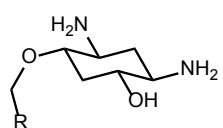
R =	IC ₅₀ (μM)
H	>1000
	>1000
	>1000
	450

Figure 1.10 Amide conjugated 2-deoxystreptamine analogs

Ding et al.³⁸ also prepared heterocyclic 2-DOS derivatives as neamine mimics (Figure 1.11). Most of the compounds demonstrated a modest increase in binding affinity with a

conjugation of a variety of heterocycles, while the binding affinity of the compound containing an electron-withdrawing (CF_3) did not show any increase. This implies that the subunit conjugated to the deoxystrptamine analog plays an important role in RNA-binding; therefore careful selection of the subunit may be essential element in improving binding affinity in the design of 2-DOS- based RNA-binding molecules.



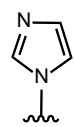
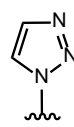
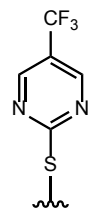
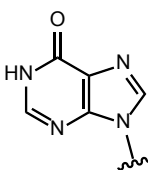
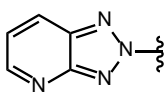
R					
K_d (μM)	275	355	1079	100	554

Figure 1.11 2-DOS analogs conjugated with heterocyclic compounds

Recently, two molecules of 2-DOS were utilized in the design of RNA-binding molecules by Hergenrother et al.³⁹ This example provides convincing evidence of the strong binding affinity between 2-DOS and RNA (Figure 1.12). The presence of the bivalent structure of 2-DOS shows low micromolar binding to RNA hairpin loops. These dimers demonstrated strong binding affinity to RNA hairpin loops of a variety of sizes containing two 5-GU-3 steps for recognition. Standard RNA-binding molecules such as aminoglycosides do not generally recognize those hairpin loops. Considering that the library was constructed by connecting two 2-DOS compounds with simple alkyl or aryl linkers of various lengths, the enhanced binding affinity is believed to result from the existence of one extra 2-DOS molecule. This is because the simple alkyl chain will not affect the binding affinity because of the lack of an adequate binding motif.

This example clearly demonstrates that novel RNA-binding molecules may be designed based solely on the 2-DOS structure.

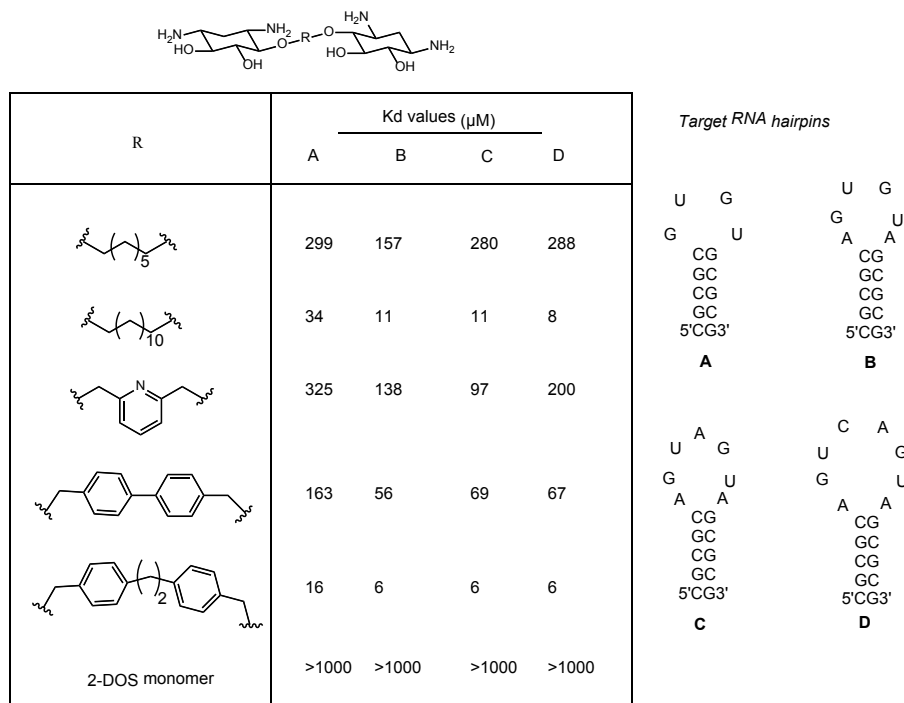


Figure 1.12 Binding 2-DOS dimers to RNA stem loops

According to the studies discussed so far, RNA-binding molecules containing two or more 2-DOS analogs may be able to bind to target RNAs with strong binding affinity, while those molecules containing one deoxystreptamine analog bind with only moderate affinity. However, the studies mentioned did not address sequence specificity, despite the promising observation of 2-DOS in sequence-specific recognition of RNAs. Therefore, building dimeric and trimeric compounds using the monomeric building block may result in small RNA-binding ligands with both strong binding affinity and sequence-specific recognition capability.

Tor et al.⁴⁰ synthesized conformationally restricted neomycin and paromomycin by covalently connecting aminosugar ring I with aminosugar ring III to reduce the number of

available conformations caused by the flexible glycosidic linkages (Figure 1.13). These two conformationally restricted aminoglycosides were tested for specific binding against two different RNA (TAR-RNA and A-site RNA) to see if the conformationally restricted aminoglycosides will show any discrimination between different types of RNA. However, these conformationally restricted aminoglycosides did not show any discrimination between TAR-RNA and A-site RNA, which suggests that the structure of target RNA and its flexibility also play an important role for specific binding.

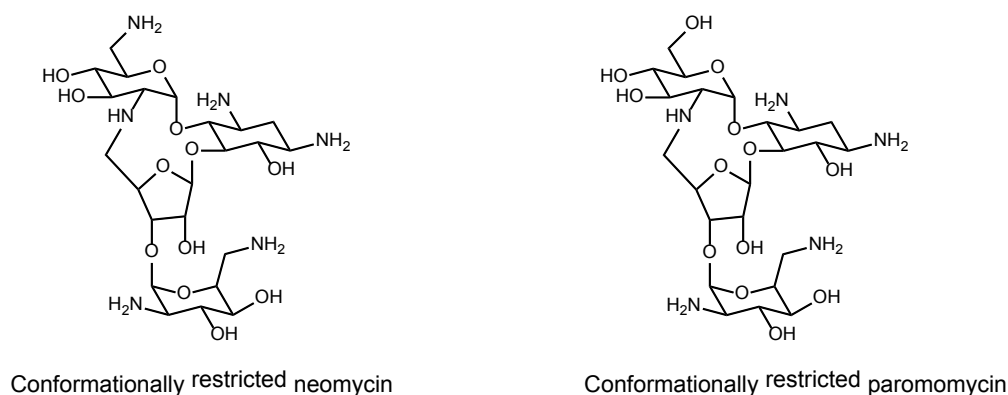


Figure 1.13 *Conformationally restricted aminoglycosides*

1.6 Conclusion

According to the studies discussed so far, RNA-binding molecules containing two or more 2-DOS analogs may be able to bind to target RNAs with strong binding affinity, while those molecules containing one deoxystreptamine analog bind with only moderate affinity. However, the studies mentioned did not address sequence specificity despite the promising observation of 2-DOS in sequence-specific recognition of RNAs. Therefore, building dimeric and trimeric 2-DOS compounds using the monomeric building block 1 (figure 1.8) may result in small RNA-binding ligands with both strong binding affinity and sequence-specific recognition capability.

1.7 References

1. Zaman, G. J. R.; Michiels, P. J. A.; van Boeckel, C. A. A. *Drug Discovery Today*, **2003**, *8*, 297.
2. Brink, M. F.; Brink, G.; Verbeet, M. P.; Debeor, H. A. *Nucleic Acids Research*, **1994**, *22*, 325. (b) Wang, Y.; Hamasaki, K.; Rando, R. R. *Biochemistry*, **1997**, *36*, 768. (c) Kaul, M.; Barbieri, C.M.; Pilch, D .S. *J. Am. Chem. Soc.* **2006**, *128*, 1261.
3. Renner, S.; Ludwig, V.; Boden, O.; Scheffer, U.; Gobel, M.; Schneider, G. *ChemBioChem*, **2005**, *6*, 1119. (b) Mei, H. Y.; Cui, M.; Czarnik, A. W.; Lemrow, S. M.; Truong, H. N.; Loo, J. A.; Sanneslowery, K. A.; Heldsinger, A.; Sharmeen, L.; Wang, S.; Huber, P. W. *J. Am. Chem. Soc.* **1997**, *213*, 71. (c) Tassew, N.; Thompson, M. *Biophysical Chem.* **2003**, *106*, 241. (d) Blount, K. F.; Tor, Y. *Nucleic Acids Research*, **2003**, *31*, 5490.
4. Tok, J. B. H.; Cho, J. H.; Rando, R. R. *Biochemistry*, **1999**, *38*, 199.
5. Popescu, F. D. *J. Cell. Mol. Med.* **2005**, *9*, 840. (b) Rayburn, E. R.; Zhang, R. *Drug Discov. Today*. **2008**, *13* 513. (c) Aagaard, L.; Rossi, J. J. *Advanced Drug Delivery Reviews*, **2007**, *59*, 75. (d) Capodici, J.; Kariko, K.; Weissman, D. *J. Immunol.* **2002**, *169*, 5196.
6. Benimetskaya, L.; Stein, C. A. *Clin. Prostate Cancer*. **2002**, *1*, 20.
7. Zhang, Q.; Al-Hashimi, H. M. *RNA*. **2009**, *15*, 1941.
8. Puglisi, J.; Williamson, J. *Current Opinion in Structural Biology*, **2010**, *20*, 295. (b) Merino, E.J.; Wilkinson, K.A.; Coughlan, J.L.; Weeks, K.M. *J. Am. Chem. Soc.* **2005**, *127*, 4223.
9. Thomas, J. R.; ergenrother, P. J. *Chemical Reviews*, **2008**, *108*, 1173.

10. Thomas, J. R.; Liu, X. J.; Hergenrother, P. J. *Biochemistry*, **2006**, *45*, 10928. (b) Busscher, G. F.; Rutjes, F.; van Delft, F. L. *Chemical Reviews*, **2005**, *105*, 775.
11. Zembower, T. R.; Noskin, G. A.; Postelnick, M. J.; Nguyen, C.; Peterson, L. R. *Int. J. Antimicrob. Agents*, **1998**, *10*, 95.
12. Wong, C.H.; Hendrix, M.; Priestley, E. S.; Greenberg, W. A. *Chem Biol*. **1998**, *5*, 397.
13. Carlson, C. B.; Stephens, O. M.; Beal, P.A. *Biopolymers*, **2003**, *70*, 86.
14. Schacht, J.; Talaska, A. E.; Rybak, L. P. *Anat Rec (Hoboken)*. **2012**, *295*, 1837. (b) Croes, S.; Koop, A.H.; van Gils, S.A.; Neef, C. *Eur. J Pharm. Sci*. **2012**, *23*, 90.
15. Mingeot-Leclercq, M-P.; Tulkens, P. M. *Antimicrob Agents Chemother*. **1999**, *43*, 1003.
16. Selimoglu, E. *Curr Pharm Des*. **2007**, *13*, 119.
17. Xing, G.; Chen, Z.; Cao, X. *Cell Research*, **2007**, *17*, 227.
18. Chen, L.; Hainrichson, M.; Bourdetsky, D.; Mor, A.; Yaron, S.; Baasov, T. *Bioorg Med Chem*. **2008**, *16*, 8940.
19. Shitara, T.; Kobayashi, Y.; Tsuchiya, T.; Umezawa, S. *Carbohydr Res*. **1992**, *232*, 273. (b)
20. Takahashi, Y.; Ueda, C.; Tsuchiya, T.; Kobayashi, Y. *Carbohydr Res*. **1993**, *249*, 57.
21. Owada, K. *Chemotherapia*. **1962**, *5*, 277.
22. Latorre, M.; Peñalver, P.; Revuelta, J.; Asensio, J. L.; Garcia-Junceda, E.; Bastida, A. *Chem Commun*. **2007**, *19*, 2829.
23. Smith, C. A.; Baker, E. N. *Curr Drug Targets Infect Disord*. **2002**, *2*, 143.

24. Fourmy, D.; Recht, M. I.; Blanchard, S. C.; Puglisi, J. D. *Science*. **1996**, *274*, 1367.
25. Hobbie, S. N.; Pfister, P.; Brull, C.; Westhof, E.; Bottger, E. C. *Antimicrob Agents Chemother*. **2005**, *49*, 5112.
26. Moazed, D.; Noller, H. F. *Nature*, **1987**, *327*, 389. (b) Fourmy, D.; Recht, M. I.; Blanchard, S.I.; Puglisi, J. D. *Science*. **1996**, *274*, 1367.
27. Recht, M. I.; Fourmy, D.; Blanchard, S. C.; Dahlquist, K. D.; Puglisi, J. D. *J Mol Biol*. **1996**, *262*, 421.
28. Purohit, P.; Stern, S. *Nature*, **1994**, *370*, 659.
29. Wimberly, B. T.; Brodersen, D. E.; Clemons, W. M., Jr.; Morgan-Warren, R. J.; Carter, A. P.; Vornrhein, C.; Hartsch, T.; Ramakrishnan, V. *Nature*, **2000**, *407*, 327.
30. Carter, A. P.; Clemons, W. M.; Brodersen, D. E.; Morgan-Warren, R. J.; Wimberly, B. T.; Ramakrishnan, V. *Nature*, **2000**, *407*, 340.
31. Vicens, Q.; Westhof, E. *Biopolymers*, **2003**, *70*, 42.
32. Kondo, J.; Francois, B.; Urzhumtsev, A.; Westhof, E. *Angew. Chem. Int. ed*. **2006**, *45*, 3310.
33. Francois, B.; Russell, R. J. M.; Murray, J. B.; Aboul-ela, F.; Masquida, B.; Vicens, Q.; Westhof, E. *Nucleic Acids Research*, **2005**, *33*, 5677.
34. Recht, M. I.; Fourmy, D.; Blanchard, S. C.; Dahlquist, K. D.; Puglisi, J. D. *J Mol Biol*. **1996** *262*, 421. (b) Peytou, V.; Condom, R.; Patino, N.; Guedj, R.; Aubertin, A. M.; Gelus, N.; Bailly, C.; Terreux, R.; Cabrol-Brass, D. *J. Med. Chem*. **1999**, *42*, 4042. (c) Bailly, C.; Colson, P.; Houssier, C.; Hmy, F. *Nucleic Acids Research*, **1996**, *24*, 1460.

35. Yoshizawa, S.; Fourmy, D.; Eason, R. G.; Puglisi, J. D. *Biochemistry*, **2002**, *41*, 6263.
36. Wang, X. J.; Migawa, M. T.; Sannes-Lowery, K. A.; Swayze, W. E. *Bioorg. Med. Chem. Lett.* **2005**, *15*, 4919.
37. Vourloumis, D.; Takahashi, M.; Winters, G. C.; Simonsen, K. B.; Ayida, B. K.; Herman, T. *Bioorg Med Chem Lett.* **2002**, *12*, 3367.
38. Ding, Y.; Hofstadler, S. A.; Swayze, E. E.; Griffey, R. H. *Org Lett.* **2001**, *3*, 1621.
39. Liu, X.; Thomas, J. R.; Hergenrother, P. J. *J Am Chem Soc.* **2004**, *126*, 9196.
40. Blount, K. F.; Zhao, F.; Hermann, T.; Yitzhak, T. *J. Am. Chem. Soc.* **2005**, *127*, 9818.
41. Moore, P. B.; Steitz, T. A. *Nature*, **2002**, *418*, 229.
42. Pape, T.; Wintermeyer, W.; Rodnina, M. V. *Nat Struct Biol*, **2000**, *7*, 104.

Chapter-2

Rational Design of Novel 2-DOS Mimics for Sequence Specific RNA Recognition

2.1 Introduction

To date, few examples of RNA-binding molecules have been reported with their structural basis on 2-DOS without an aminosugar subunit attached (ring 1 figure 2.2)³⁷⁻³⁹. This is likely because both the mechanism of action of aminoglycosides and the sequence specific mode of the 2-DOS binding was reported only recently. Therefore, the potential of designing RNA-binding molecules based on this structural information is just beginning to unfold. Despite the promising observation of sequence specific recognition of RNA bases by 2-DOS,¹ none of the existing studies addressed sequence specificity or selectivity in the design of 2-DOS based compounds. This may be attributed to the lack of novel linker strategies other than glycosidic linkages between two or more 2-DOS subunits.

Upon close inspection of the crystal structures of aminoglycoside RNA complexes mentioned in Chapter 1, it is evident that two amino functional groups at 1- and 3-positions in 2-DOS participate in recognizing RNA bases through hydrogen bonding and electrostatic interactions.² In addition, glycosidic linkages at the 4- and 6- positions serve as linkers to extend the aminoglycoside structures to the aminosugar subunits (Figure 2.1). In our research, we propose that modification of the hydroxyl group (or connectivity unit) of 2-DOS would provide a novel approach to generating more selective RNA binding motifs. In this chapter we will describe our efforts to synthesize novel carboxylic acid and urea derivatives of 2-DOS that enable additional linkers for generating selective RNA recognizing molecules based on the 2-DOS framework. The hydroxyl functional group at position 5 was omitted in the design of 2-

DOS mimics to increase the simplicity of chemistry used to synthesize our mimics. We expect that this deletion of the should not cause loss of activity because subunits substituted on the 5-position of 2-DOS project out of the target RNA helix and do not participate in elongation of the unit along the helix axis.

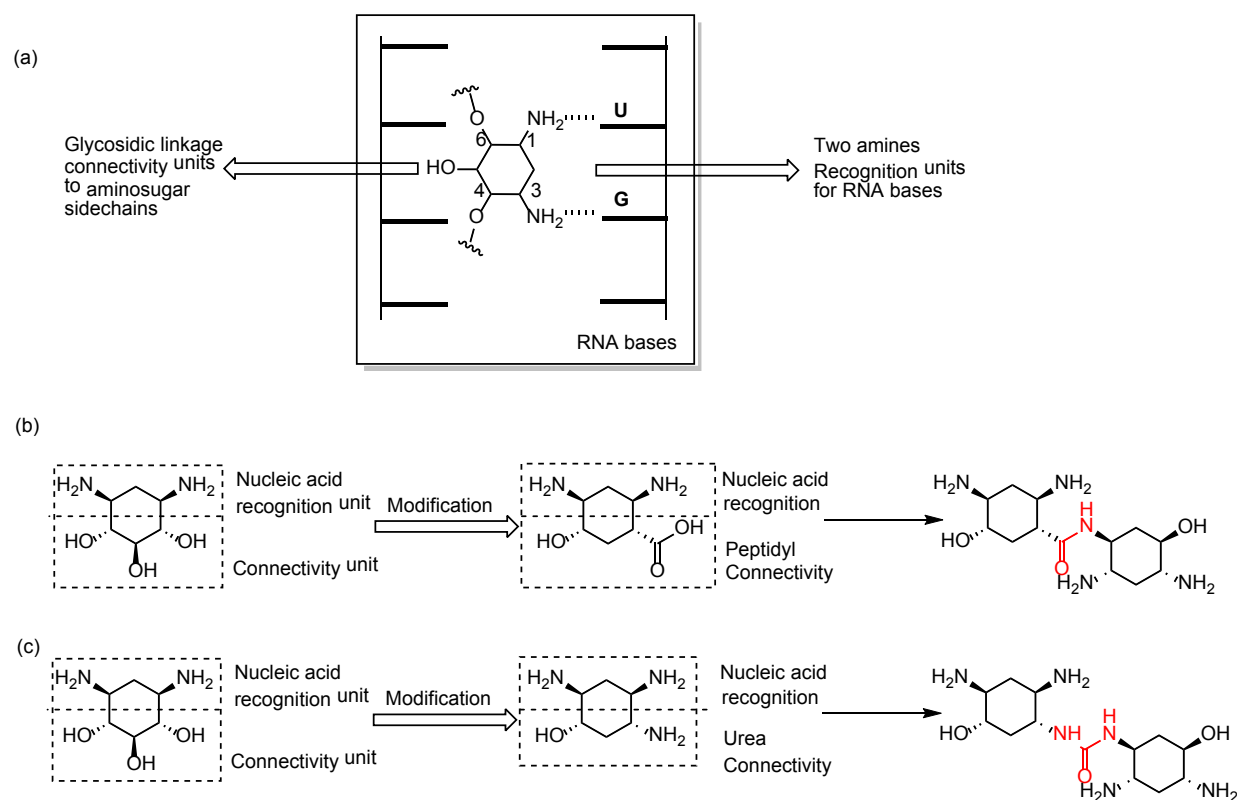


Figure 2.1 Simplified binding mode of 2-DOS to its target RNAs based on crystal structures of various aminoglycosides mentioned in Figure 2.1. (b) Structure based rational design of novel 2-DOS analog with peptidyl connectivity. (c) Structure based rational design of novel 2-DOS analog with urea connectivity.

2.2 Rational for Proposed RNA Specific Analogs of 2-DOS

It is hypothesized that targeting RNA double helices containing certain GU-rich sequence steps would be possible by connecting two or more of the monomeric 2-DOS building blocks through amide bonds within or without the structural context of ring-I (Figure 2.2). This strategy may provide several advantages in designing RNA-binding small molecules with high sequence

specificity and strong binding affinity. First, the 2-DOS analog is used as the exclusive building block in the design of sequence-specific RNA-binding molecules. The free amino groups of the aminosugar subunits in aminoglycosides are the source of the nonspecific binding characteristics of aminoglycosides³ and are no longer present in our designed ligands. Instead, an additional specific recognition unit (2-DOS) is introduced in place of the aminosugars, resulting in molecules with fewer amino functional groups. This may limit the possibility of nonspecific electrostatic interactions and promote specificity in binding.

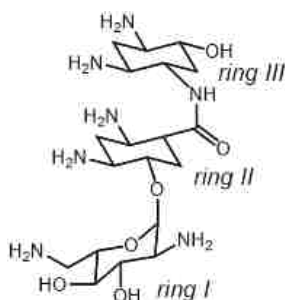


Figure 2.2 *Aminoglycoside connected amide bond showing ring I, ring II and ring III.*

Second, the ambiguous binding characteristic of aminoglycosides originates not only from the electrostatically driven mode but also from the conformational adaptability of aminoglycosides⁴. The glycosidic connection assumes a variety of conformations and permits aminoglycosides to structurally adjust to diverse RNA targets. The glycosidic linkage in the proposed targets is replaced by an amide connectivity, which introduces extra hydrogen bonding donors and acceptors. The amide connectivity will restrict the flexibility of the RNA-binding ligands through a network of extensive hydrogen bonds. This connectivity may also help discriminate nucleotide bases upon binding to target RNAs. Hydrogen bonding has been shown to play a key role in specific ligand recognition as observed with various aptamers for amino acids, oligosaccharides, peptides, and proteins.⁵ Amide bonds were proven to be a very useful

tool in differentiating DNA bases in the context of the Dervan's polypyrrole and imidazole DNA-binding agents in the minor groove and may play a similar role in the context of RNA-binding molecules.^{6, 7}

Third, this strategy makes it possible to target certain RNA sequences that contain four or more consecutive nucleotides such as 5-GUGU-3 for the first time. In order to recognize consecutive RNA base steps, proper distance between the neighboring amino functional groups in the ligands is essential. Introduction of an amide bond between the two neighboring 2-DOS building blocks not only brings extra hydrogen bonding acceptors and donors but also provides the desired distance between the amino functional groups in the adjoining monomeric building blocks (Figure 2.3a). According to a model of the dimeric compound, the neighboring amino groups adjacent to the monomeric building blocks are spaced by 5.1 Å, which would be slightly different depending on the degree of rotation between the two adjoining building blocks. In fact, the nitrogen atoms of amino groups at 1- and 3- positions in 2-DOS are spaced by 4.93 Å, which allows hydrogen bonding with the G1494 (N7)-U1495 (O4) step of the free A-site RNA.⁸ The average distance between the RNA steps in the A-site is known to be 5.2 ± 0.3 Å⁹ and is indeed very close to the distance between the amines observed in the model of the dimer ligand (Figure 2.3b). Therefore, introducing the amide bond between the two building blocks may bring the neighboring two amines to match the distance of the RNA bases, which is essential for sequence recognition and discrimination of different RNA bases.

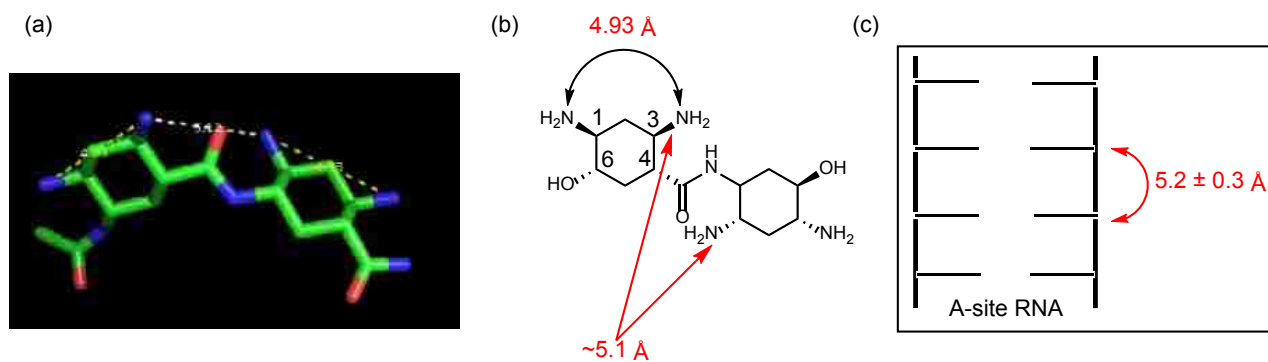


Figure 2.3 (a) Distances between the two neighboring amino groups in the neighboring 2-DOS analogs in the dimer. (b) Distances between the amino groups located at 1- and 3- positions of the 2-DOS. (c) Average distance between the base stacks in A-site RNA.

Fourth, the proposed RNA binding molecules may slow down the emergence of resistance. Aminosugar residues are the structural features most recognized by aminoglycoside modifying enzymes.¹⁰ Therefore, the absence of those amino sugars in the designed molecules may improve *in vivo* bioavailability of the ligands and can provide a novel strategy to combat emergence of the prevalent viral and bacterial resistance in the clinic.

2.3 Synthesis of Novel 2-DOS Analog with Peptidyl and Urea Connectivity as Monomeric Building Block

In this chapter, we will describe our synthesis of three 2-DOS mimics for application to selective RNA recognition. Our synthesis of three designed RNA binding molecules relies on use of a known diazide **4**¹¹ to access the desired building blocks containing amine (**8**, Figure 2.4a) and carboxylic acid (**9**, Figure 2.4b) functional groups. These monomeric building blocks will be assembled either via amide bond formation (carboxylic acid) or through urea formation (amine) to access our desired 2-DOS mimics **1–3** (Figure 2.5). These synthetic studies will provide access to dimeric 2-DOS mimics where two neamine core units are assembled through a rigid amide bond (**2**), or a more flexible urea bond (**3**). In addition, we will explore the specificity of the dimeric neamine core containing an aminosugar moiety (**1**)

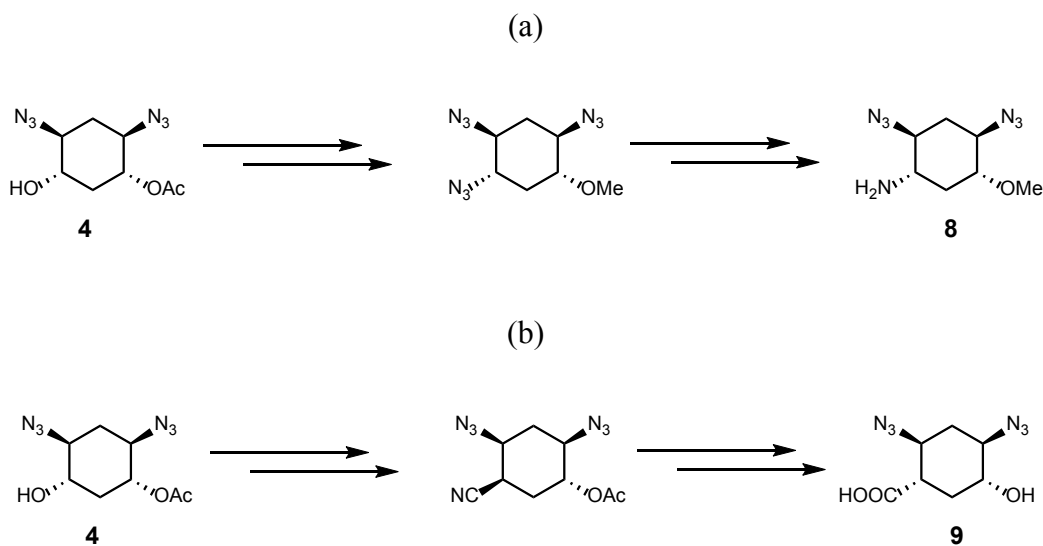


Figure 2.4 Conversion of **4** into (a) amine **8** and (b) carboxylic acid **9** to enable amide and urea bond formation.

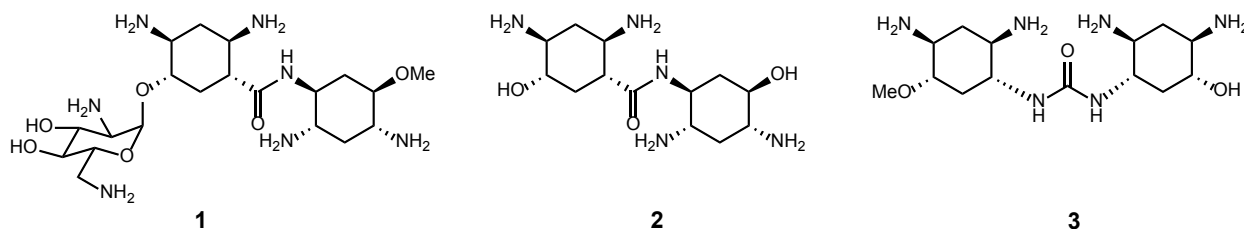


Figure 2.5 Compound **1**: Dimeric 2-DOS connected by amide bond and aminosugar; **2**: Dimeric 2-DOS connected by amide bond without sugar; **3**: Dimeric 2-DOS connected by urea bond.

2.3.1 Synthesis of Bis-Azide **4** as a Common Synthetic Intermediate

Our proposed synthesis of 2-DOS mimics relies on ready and scalable access to a bis-azide intermediate that can be derivatized to provide the desired functional building blocks. Jacques and coworkers previously reported a synthesis that uses cyclohexadiene to make bis-azide **4**.¹¹ Cyclohexadiene is first converted to a cis-bis-epoxide, which is then ring-opened to provide the racemic bis-azide intermediate shown below (Figure 2.6). Desymmetrization of the diol with the *candida rugose* lipase in presence of vinyl acetate provided enantiopure bis-azide **4**, which was employed as a common intermediate for the synthesis of our 2-DOS mimics.

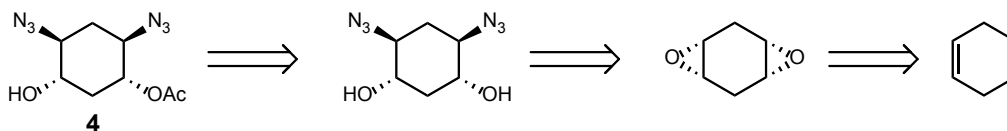
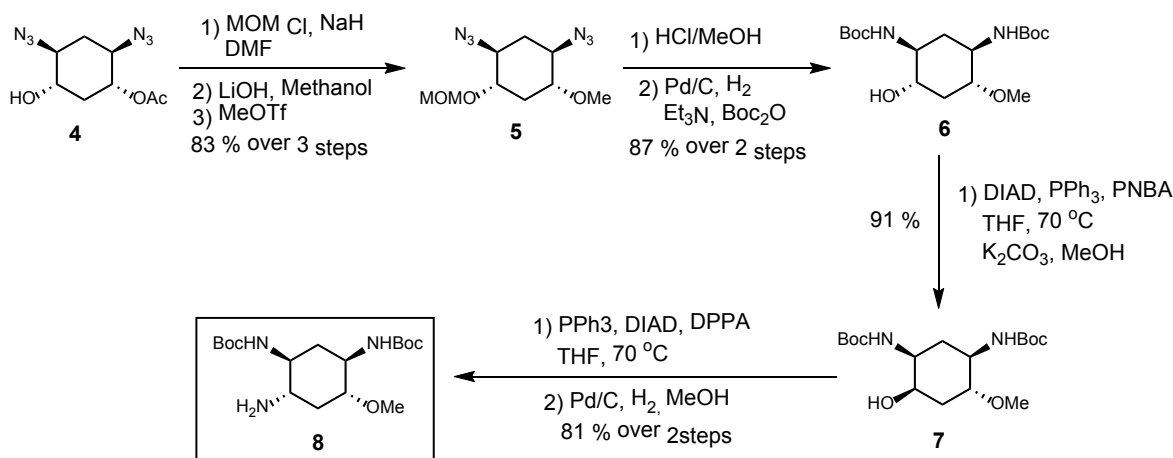


Figure 2.6 Preparation of 4 from 1, 4-cyclohexadiene.

2.3.2 Synthesis of the Amine containing monomeric 2-DOS analog building block 8

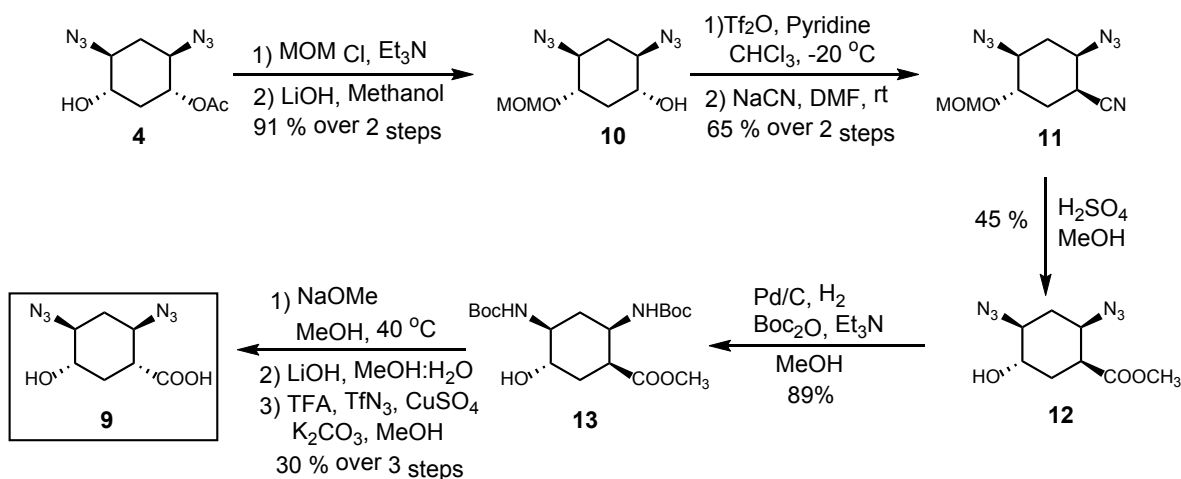
Compound **8** was prepared starting from asymmetric bis azide **4** following the procedures shown in Scheme 1. Compound **4** was first protected as the methoxy methyl ether, then acetyl deprotection and methylation of the resulting alcohol gave compound **5**. MOM deprotection, followed by hydrogenation of bisazide and Boc protection of both amines gave compound **6**. The hydroxyl group in compound **6** was epimerized to compound **7** using Mitsunobu reaction¹². Compound **6** was first converted to benzoate ester via a Mitsunobu protocol followed by hydrolysis of the ester gave compound **7**. The hydroxyl group in the compound **7** was converted to azide by the second Mitsunobu reaction with an azide nucleophile provided the azide with the desired stereochemistry, reduction of azide using palladium on carbon in presence of hydrogen gave our desired building block amine **8**.



Scheme 1 Synthesis of monomeric 2-DOS analog building block **8**.

2.3.3 Synthesis of the Acid Containing Monomeric 2-DOS Analog Building Block 9

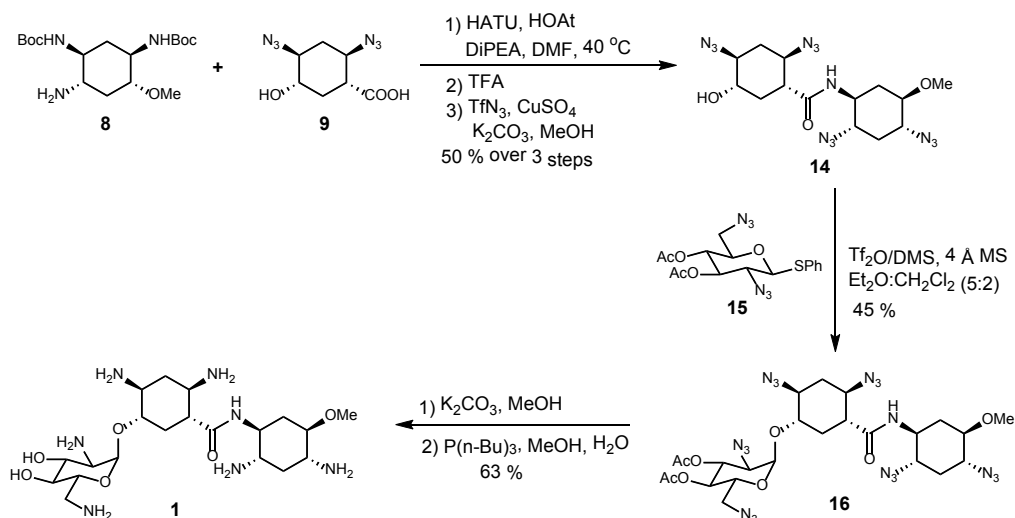
Acid-containing compound **9** was prepared starting from the same asymmetric bisazide **4** following the procedures shown in Scheme 2. The hydroxyl group in the compound **4** was again protected as the MOM-ether and the acetyl group was removed in the presence of LiOH to give alcohol **10**. Alcohol **10** was then treated with triflic anhydride and pyridine at $-20\text{ }^{\circ}\text{C}$ in the presence of NaCN to give nitrile **11**. The nitrile was next converted to ester **12** via hydrolysis using H_2SO_4 in methanol. Reduction of the two azides in **12** with H_2 gas and Pd/C was directly followed by *N*-Boc protection of diamine to afford ester **13**. Compound **13** was epimerized using sodium methoxide in presence of methanol at $40\text{ }^{\circ}\text{C}$ to provide the desired trans stereochemistry at the carboxylic acid center. ¹² Hydrolysis of ester to acid was then accomplished using lithium hydroxide. The NHBoc groups were next converted back to azides by deprotection of the Boc group (TFA in CH_2Cl_2), followed by treatment with trifluoromethanesulfonyl azide¹³ to give compound **9** (Scheme 2).



Scheme 2 Syntheses of monomeric analog acid building block **9**.

2.3.4 Synthesis of 2-DOS Mimic 1

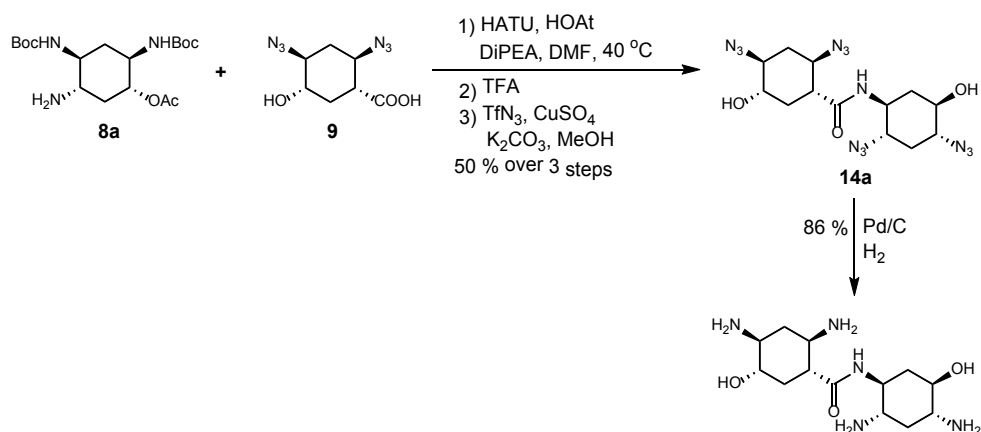
Synthesis of our desired dimeric 2-DOS mimic **1** required coupling of our monomeric 2-DOS analogs **8** and **9**, followed by addition of the desired amino sugar and finally alcohol deprotection followed by reduction of azides gave compound **1** (Scheme 3). The amino compound **8** was coupled to acid compound **9** using HOAT and HATU as coupling agents at 40 °C, followed by Boc deprotection and conversion of the resulting amines to azides using trifluoromethanesulfonyl azide gave intermediate **14**. The glycosylation reaction was performed between compound **14** and protected sugar **15** using the procedure developed by Fugedi¹⁴ gave compound **16**. Protected sugar was prepared by a literature procedure¹⁵ from a commercially available 2-acetamido-2-deoxy-D-glucopyranose. Compound **15** was finally deprotected, first with potassium carbonate and methanol to remove the acetates and then with tributyl phosphine to reduce all six azides, providing compound **1** in 63 % yield over 2 steps.



Scheme 3 Synthesis of compound **1**

2.3.5 Synthesis of 2-DOS Mimic 2

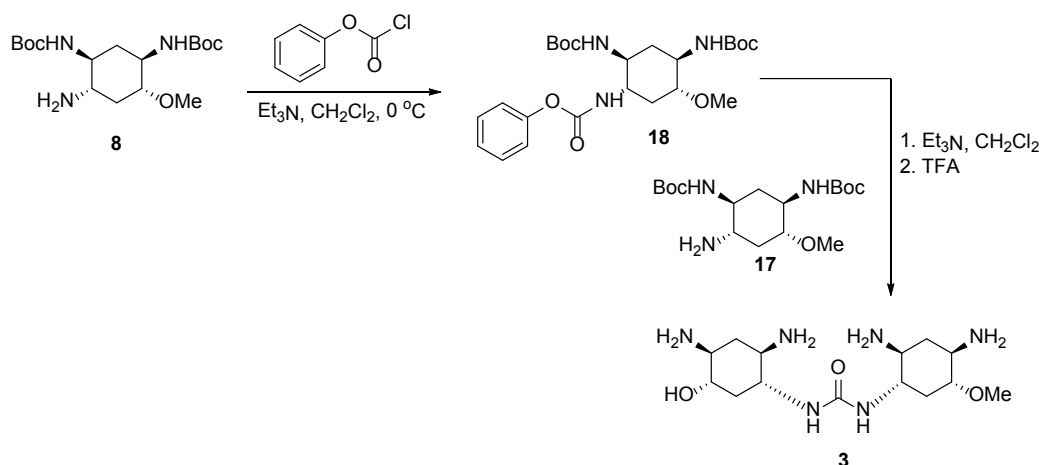
The synthesis of dimeric 2-DOS mimic required a simple coupling reaction followed by global reduction of the 4 azides. The coupling of compounds **8a** and **9** using HATU and HOAt provided the dimer 45 % yield. Deprotection of Boc groups and conversion of amines to azides in the presence of triflyl azide then gave tetra azide **14a**. The tetra azide was then reduced to tetra amine in the presence of palladium on carbon and hydrogen to give compound **2** (Scheme 4)



Scheme 4 Syntheses of Compound **2**

2.3.6 Synthesis of 2-DOS Mimic 3

The synthesis of 2-DOS mimic **3** was accomplished via stepwise dimerization of amine **17** and amine **8** with a phosgene equivalent (Scheme 4). Compound **17** was treated with phenyl chloroformate in presence of triethyl amine at 0 °C gave carbamate **18**. Intermediate **18** was then condensed with amine **8** in presence of triethyl amine to give compound **19**. Final deprotection of the Boc groups with TFA provided the desired compound **3** with an overall yield of 65% from **17** (Scheme 5).



Scheme 5 Syntheses of 2-DOS mimic **3**

2.4 Conclusion

The synthesis of dimeric 2-DOS mimics **1-3** was readily accomplished due to the ease of access of monomeric core structures **8**, **9** and **17**. These synthetic studies lay the ground work for the synthesis of an entire library of 2-DOS mimics where the RNA binding activity can be modified by changing the number of streptomycin core units, the linker between units and the glycosylation state of each scaffold structure. The next chapter will discuss RNA binding assays and anti-bacterial studies with compounds **1-3** to ascertain their potential to act as specific RNA binding molecules for use as antibiotics.

2.5 References

1. Yoshizawa, S.; Fourmy, D.; Eason, R. G.; Puglisi, J. D. *Biochemistry*, **2002**, *41*, 6263.
2. Francois, B.; Russel, R. J. M.; Murray, J. B.; Aboula-ela, F.; Masquida, B.; Vicens, Q.; Westhof, E. *Nucleic Acids Res.* **2005**, *33*, 5677.
3. Zhao, F.; Zhao, Q.; Blount, K. F.; Han, Q.; Tor, Y.; Herman, T. *Angew. Chem.Int. Ed*, **2005**, *44*, 5329.

4. Blount, K. F.; Zhao, F.; Herman, T.; Tor, Y.; *J. Am. Chem. Soc.* **2005**, *127*, 9818.
5. Hermann, T.; Patel, D. J.; *Science*, **2000**, *287*, 820.
6. Devran, P. B.; Edelson, B. S.; *Current Opinion in Structural Biology* **2003**, *13*, 284.
7. Devran, P. B.; Burli, R. W. *Current Opinion in Structural Biology* **1999**, *3*, 688.
8. Fourmy, D.; Recht, M. I.; Puglisi, J. D. *J. Mol. Bio.* **1998**, *277*, 347.
9. Yoshizawa, S.; Fourmy, D.; Eason, R. G.; Puglisi, J. D. *Biochemistry*, **2002**, *41*, 6263.
10. Vicens, Q.; Westhof, E.; *Chemistry & Biology*, **2002**, *9*, 747.
11. Chenevert, R.; Jacques, F. *Tetrahedron Lett.* **2006**, *17*, 1017.
12. Roberts, S.; Chittapragada, M.; Pendem, K.; Leavitt, B. J.; Mahler, J. W.; Ham, Y.- W. *Tetrahedron Lett.* **2010**, *51*, 1779.
13. Nyffeler, P. T.; Liang, C-H.; Koeller, K. M.; Wong, C-H. *J. Am. Chem. Soc.*, **2002**, *124*, 10773.
14. Fugedi, P.; Tatai, J. *Org. Lett.* **2007**, *9*, 4647.
15. Pang, L-J.; Wang, D.; Zhou, J.; Zhang, L-H.; Ye, X-S. *Org. Biomol. Chem.* **2009**, *7*, 4252.

2.6 Experimental Procedures

2.6.1 Characterization of compounds synthesized

Di-tert-butyl ((1R,3S,4S,6R)-4-hydroxy-6-methoxycyclohexane-1,3-diyl)dicarbamate (6). To a solution of compound 5 (1.1 g, 4.29 mmol) was dissolved in methanol (50 mL) and added aqueous HCl (10 mL), the reaction mixture was heated to reflux for 1 h after completion of the

reaction, it was cooled to room temperature, neutralized with sodium bicarbonate and extracted with methylene chloride (3×100 mL), the combined extracts were dried over anhydrous MgSO₄, the solvent was concentrated to give the desired product as colorless liquid (0.8 g, 88%), which was dissolved in methanol (40 mL) were added 10% Pd/C, triethylamine (1.3 mL, 9.43 mmol), and di-*t*-butyl dicarbonate (2.47 g, 11.3 mmol). The reaction mixture was stirred for 12 h at room temperature under hydrogen atmosphere. After completion of reaction, the catalyst was removed by filtration using microfiber filter paper. Evaporation of solvent, followed by column purification (1:1 hexanes: ethyl acetate) afford compound 6 as a white solid (1 g, 74%). ¹H NMR (500MHz, CDCl₃) δ 4.75 (brs, 2H), 3.81 (brs, 1H), 3.42-3.35 (m, 3H), 3.36 (s, 3H), 3.14-3.04 (m, 1H), 2.5-2.36 (m, 2H), 2.1-2.0 (m, 1H), 1.44 (s, 18H), 1.4-1.2 (m, 1H). ¹³C NMR (125MHz, CDCl₃) δ 155.9, 80.3, 79.5, 78.6, 56.3, 54.6, 53, 36, d 28. HRMS (ESI) m/z [M+H]⁺ caclcd 361.2339, found 361.2331. [α]_D²⁴ = -37.14° (42 mg/6 mL DCM). mp 206- 208 °C.

di-tert-butyl ((1R,3S,4R,6R)-4-hydroxy-6-methoxycyclohexane-1,3-diyl)dicarbamate (7). To a solution of 6 (2.5 g, 6.93 mmol), PPh₃ (5.45 g, 20.8 mmol), and 4-nitrobenzoic acid (3.47 g, 20.8 mmol) in dry THF (150 mL) was added DIAD (4 mL, 20.8 mmol) in one portion with stirring at rt under Nitrogen. The resulting solution was refluxed for 2 h after which the solvent was removed in vacuum. The crude mixture was dissolved in dry methanol (100 mL) to which K₂CO₃ (10-15 equiv.) was added. After stirring for 30 min at room temperature, the solvent was evaporated and reaction mixture was diluted with methylene chloride (200mL), the organic layer was washed with water (2×100 mL) and dried over anhydrous MgSO₄, Evaporation of solvent, followed by column purification on silica gel (1:1 hexanes: ethyl acetate) yielded compound 7 as a colorless oily liquid (2.2 g, 88%). ¹H NMR (500 MHz, CDCl₃) δ 5.17 (brs, 1H), 4.9 (brs, 1H), 4.14-4.0 (m, 1H), 3.71-3.58 (m, 1H), 3.54-3.36 (m, 2H), 3.35 (s, 3H), 3.32-3.18 (m, 1H), 2.34-

2.26 (m, 1H), 2.1-2.0 (m, 1H), 1.76-1.61 (m, 1H), 1.44 (s, 9H), 1.43 (s, 9H). ¹³C NMR (125MHz, CDCl₃) δ 155.8, 155.4, d 79.4, 76.8, 68.1, 56.5, 53, 51, 34.7, 31.8, 28.4, 28.3. HRMS (ESI) m/z [M+H]⁺ caclcd 361.2339, found 361.2338. [α]_D²⁴ = -31.4° (65mg/6 mL DCM). mp 86–88 °C

di-tert-butyl ((1R,3S,4S,6R)-4-amino-6-methoxycyclohexane-1,3-diyl)dicarbamate (8). To a solution of 7 (900 mg, 2.5 mmol), PPh₃ (1.96 g, 7.5 mmol), and DPPA (1.6 mL, 7.5 mmol) in dry THF (150 mL) was added DIAD (1.47 mL, 7.5 mmol) in one portion with stirring at rt, under nitrogen. The resulting solution was refluxed for 3 hours. The solvent was removed in vacuum and the crude reaction mixture was purified by flash chromatography (3:1 hexanes: ethyl acetate) to give product as colorless oil, which was dissolved in MeOH (30 mL) and added Pd/C (100 mg). The mixture was stirred for 12h at room temperature under hydrogen atmosphere and the catalyst was removed by filtration using microfiber filter paper. Evaporation of the solvent followed by column purification on silica gel (1:1 MeOH: ethyl acetate) yielded compound 8 as white crystalline solid (400 mg, 44%). ¹H NMR (500MHz, CDCl₃) δ 3.44-3.38 (m, 1H), 3.37 (s, 3H), 3.21 (t, 1H J = 10Hz), 3.08 (dt, 1H, J = 5Hz, 10 Hz), 2.5 (dt, 1H, J = 5Hz, 10Hz), 2.40-2.26 (m, 1H), 2.05 (d, 1H, J = 15Hz), 1.34-1.06 (m, 2H). ¹³C NMR (125MHz, CDCl₃) δ 156.8, 156.6, 79.7, 78.7, 55.9, 54.6, 52, 48, 36, 27.4, 27.3. HRMS (ESI) m/z [M+H]⁺ caclcd 360.2499, found 360.2580. [α]_D²⁴ = -9.28° (110 mg/6mL methanol). mp 168-170 °C

(1R,2R,4S,5S)-2,4-diazido-5-(methoxymethoxy)cyclohexanol (10). To a solution of 4 (6 g, 25 mmol) in dry dimethylformamide and dry triethylamine (8.7 mL, 62.5 mmol) was added methoxymethylchloride (3.8 ml, 50 mmol) was added under argon gas and the reaction mixture was refluxed for 1hour. The reaction mixture was cooled down, solvent was concentrated under high vacuum and the product was dissolved in dichloromethane (2×100 mL). Organic layer was washed with water and brine and dried over anhydrous MgSO₄ and the solvent was removed

under vacuum to give compound as yellow oil. (6.1 g, 85% yield). The crude product was (6.1 g, 21.45. mmol) was dissolved in methanol and the reaction mixture was cooled to 0 °C and LiOH was added (1g, 44.0 mmol) and stirred for 1 hour, solvent was removed and crude product was dissolved in dichloromethane. Organic layer was washed with water and dried over anhydrous MgSO₄ and the solvent was removed under vacuum to give compound 10 as yellow oil (4.95 g, 95% yield). ¹H NMR (500 MHz, CDCl₃) δ 4.78 (m, 2H), 3.50-3.40 (m, 3H), 3.40 (s, 3H), 3.30 (m, 1H) 2.60 (br s, 1H), 2.40 (dt, 1H, *J* = 13.18, 3.91 Hz), 2.20 (dt, 1H, *J* = 13.18, 3.91 Hz), 1.50 (q, 1H, *J* = 11.48 Hz), 1.35 (q, 1H, *J* = 11.48 Hz); ¹³C NMR (125 MHz, CDCl₃) δ 96, 76, 71, 64, 62, 56, 36, 32; HRMS (ESI) found 243.12 [M + H]⁺, calcd 242.11; [α]_D 24 = -31.09° (c 1.22, CHCl₃).

(1S,2R,4S,5S)-2, 4-diazo-5-(methoxymethoxy)cyclohexanecarbonitrile (11). To a solution of 10 (6 g, 24.7 mmol) in dry dichloromethane was cooled to -20 °C, then pyridine (10 mL, 123.5 mmol) was added, followed by drop wise addition of trifluoromethanesulfonic anhydride (16.6 mL, 99 mmol) under argon gas, after complete consumption of starting material, the reaction mixture was washed with ice water and the organic layer was dried over anhydrous MgSO₄ and the solvent was removed under vacuum with no heat to give the product as orange liquid (8.5 g 92 %) The crude product was (8.5 g, 22.7 mmol) was dissolved in Minimal amounts of dimethylformamide (20 mL), followed by the addition of excess sodium cyanide (10-15 equiv) at 0 °C. The reaction was allowed to stir for 2h at room temperature, the solvent was removed under high vacuum. The resulting reaction mixture was then dissolved in dichloromethane and washed with water and brine until all the dimethylformamide was removed. The dichloromethane layer was dried over anhydrous MgSO₄, the solvent was removed under vacuum and the crude product was purified by flash chromatography to give compound 11 (4.2

g, 73% yield); ^1H NMR (500 MHz, CDCl_3) δ 4.70 (dd, 2H, $J = 10.73, 6.38$ Hz), 3.75-3.65 (m, 2H), 3.45 (m, 1H), 3.40 (s, 3H), 3.20-3.10 (br q, 1H, $J = 3.72$ Hz), 2.40 (dt, 1H, $J = 14.16, 5.77$ Hz), 2.25 (dt, 1H, $J = 13.67, 3.15$ Hz), 1.85 (m, 1H), 1.65 (dt, 1H, $J = 12.38, 3.9$ Hz); ^{13}C NMR (125 MHz, CDCl_3) δ 118, 96, 75, 61, 56, 55, 32,31,30; HRMS (ESI) found 252.12 $[\text{M} + \text{H}]^+$, calcd 251.11; $[\alpha]_{\text{D}}^{24} = -10.2^\circ$ (c 0.570, CHCl_3).

(1S,2R,4S,5S)-methyl 2,4-diazido-5-hydroxycyclohexanecarboxylate (12) To a solution of Compound 11 (2 g, 7.96 mmol) in methanol was added few drops of conc. sulfuric acid and heated the reaction mixture to reflux for 15 hours, the solvent was removed under vacuum and the crude reaction mixture was neutralized with saturated NaHCO_3 and the product was extracted with dichloromethane, the dichloromethane layer was washed with water, dried over anhydrous MgSO_4 , the solvent was removed under vacuum and the crude product was purified by flash chromatography to give compound 12 as yellow oil (780 mg, 45 %). ^1H NMR (500 MHz, CDCl_3) δ 3.78-3.63 (m, 2H), 3.5 (m, 1H), 3.4 (s, 3H), 3.19 (br d, 1H, $J = 3.42$ Hz), 2.45-2.40 (dt, 1H, $J = 13.94$ Hz, 4.16 Hz), 2.38-2.30 (br dt, 1H, $J = 13.94, 2.93$ Hz), 1.95 (q, 1H, $J = 11.25$ Hz), 1.65 (m, 1H), 1.25 (bs, 1H); ^{13}C NMR (125 MHz, CDCl_3) δ 172, 69, 62, 58, 52, 42, 30, 29; HRMS (ESI) found 263.0863 $[\text{M} + \text{Na}]^+$, calcd 240.09; $[\alpha]_{\text{D}}^{24} = +34.02^\circ$ (c 0.088, CHCl_3).

Methyl(1S,2R,4S,5S)-2,4-bis((tert-butoxycarbonyl)amino)-5-hydroxycyclohexane-1-carboxylate (13). To a solution of compound 12 (800 mg, 3.33 mmol) in methanol (20 mL) were added 10% Pd/C, triethylamine (1.3 mL, 9.43 mmol), and di-*t*-butyl dicarbonate (2.47 g, 11.3 mmol). The reaction mixture was stirred for 12 h at room temperature under hydrogen atmosphere. After completion of reaction, the catalyst was removed by filtration using microfiber filter paper. Evaporation of solvent, followed by flash chromatography on silica gel (1:1 hexanes: ethyl acetate) afford compound 13 as a white solid (1.15 g, 89 %). ^1H NMR (500 MHz,

CDCl₃) δ 5.43 (br s, 1H), 4.71 (br s, 1H), 3.83-3.76 (ddd, $J = 3, 8, 13$ Hz, 2H), 3.70 (s, 3H), 3.45 (ddd, $J = 3, 11, 13$ Hz, 1H), 3.35 (ddd, $J = 2, 10, 11$ Hz, 1H), 2.93 (ddd, $J = 4, 5, 8$ Hz, 1H), 2.40-2.37 (ddd, $J = 2, 4, 14$ Hz, 1H), 2.03-2.00 (ddd, $J = 3, 3, 13$ Hz, 1H), 1.78-1.71 (ddd, $J = 13, 13, 13$ Hz, 1H), 1.65-1.59 (ddd, $J = 5, 10, 14$ Hz, 1H), 1.42 (s, 9H), 1.41 (s, 9H); ¹³C NMR (125 MHz, CDCl₃) δ 174.1, 157.4, 155.3, 80.6, 79.8, 71.9, 55.1, 52.1, 48.3, 43.2, 34.4, 33.9, 28.6, 28.5; HRMS (ESI) Found 388.2232 for [M]⁺; calcd. 388.2209.

2,4-diazido-5-hydroxycyclohexane-1-carboxylic acid (9). To a solution of 13 (1 g, 2.57 mmol) in methanol (50 ml) at 0°C was added a solution of sodium methoxide (486 mg, 9 mmol) in methanol (50 ml) and heated the reaction mixture to 40°C for 6 h. The reaction mixture was made acidic using Amberlite resin and then filtered. The filtrate was concentrated and the compound was purified by flash chromatography to give epimer (400 mg, 40%). To a solution of the epimer (400 mg, 1.03 mmol) in methanol (10 mL) was added LiOH (75 mg, 3.1 mmol) solution dissolved in 5 mL water and stirred the reaction mixture at room temperature for 6 hours, the solvent was removed under vacuum and p^H was adjusted to 2 using 1M HCl and the product was extracted with chloroform. Evaporation of solvent affords the product as a white solid. (220 mg, 57 %). To a solution of the crude product (220 mg, 0.587 mmol) in methylene chloride was added TFA (270 μ l, 3.52 mmol) at room temperature and stirred the reaction mixture for 2 h, after completion of the reaction, reaction mixture was concentrated to afford desired product as yellow oil (210 mg, 100%), which was dissolved in methanol (15 mL), and added potassium carbonate (405 mg, 2.93 mmol), triflyl azide solution (prepared from sodium azide (16 equiv.) and triflic anhydride (12 equiv. in methylene chloride and water) at 0 °C and stirred the reaction mixture at room temperature for overnight and concentrated the solvent, diluted the reaction mixture with methylene chloride (100 mL), washed the organic layer with

water (2×50 mL) and dried over anhydrous MgSO₄, evaporation of solvent followed by column purification on silica gel (1:1 hexanes: ethylacetate) afford compound 9 white solid. Yield: 30%.

(1R,2R,4S,5S)-2,4-diazido-N-((1S,2S,4R,5R)-2,4-diamino-5-methoxycyclohexyl)-5-

hydroxycyclohexanecarboxamide (14). To a solution of 8 (300 mg, 0.83 mmol) and 9 (207 mg, 0.92 mmol) in dry DMF (10 mL) were added HOAt (340 mg, 2.5 mmol), HATU (878 g, 2.5 mmol) and DIPEA (875 µl, 5.0 mmol) at room temperature and heated the reaction mixture to 50 °C for 3 h. The reaction mixture was concentrated in vacuo. The resulting crude was purified by column chromatography on silica gel (3:1 hexanes: ethyl acetate) to afford compound 7 as pale yellow liquid (200 mg, 42%). The compound (200 mg, 0.35 mmol) in methylene chloride was added TFA (270 µl, 3.5 mmol) at room temperature and stirred the reaction mixture for 2 h, after completion of the reaction, reaction mixture was concentrated to afford desired product as yellow oil (210 mg, 100%), which was dissolved in methanol (15 mL), and added potassium carbonate (195 mg, 1.41 mmol), triflyl azide solution (prepared from sodium azide (16 equiv.) and triflic anhydride (12 equiv. in methylene chloride and water)) at 0 °C and stirred the reaction mixture at room temperature for overnight and concentrated the solvent, diluted the reaction mixture with methylene chloride (100 mL), washed the organic layer with water (2×50 mL) and dried over anhydrous MgSO₄, evaporation of solvent followed by column purification on silica gel (1:1 hexanes: ethylacetate) afford compound 14 as colorless oily liquid (100 mg, 68%). ¹HNMR (300MHz, CDCl₃) δ 7.47 (d, 1H, *J* = 8.7Hz), 4.5 (brs, 1H), 3.88-3.65 (m, 2H), 3.52-3.36 (m, 4H), 3.3 (s, 3H), 3.26-3.13 (m, 1H), 2.36-1.9 (m, 6H), 1.57 (q, 1H, *J* = 12.3 Hz), 1.42-1.13 (m, 2H); ¹³CNMR (75MHz, CDCl₃) 205.6, 80.8, 72.3, 64, 62, 61, 59, 56, 50, 48.5, 35, 34.6, 34, 33.6. HRMS (ESI) *m/z* [M+H]⁺ caclcd 420.1969, found 420.2054. [α]_D²⁴ = +9.47° (95 mg/6mL DCM).

(2R,3R,5R,6S)-5-azido-2-(azidomethyl)-6-(((1S,2S,4R,5R)-2,4-diazido-5-(((1S,2S,4R,5R)-2,4-diazido-5-methoxycyclohexyl)carbomoyl)cyclohexyl)oxy)tetrahydro-2H-pyran-3,4-diyl diacetate (16). To a solution of compound 14 (95 mg, 0.226 mmol) in 5:2 diethyl ether: methylene chloride was added compound 15 (110 mg, 0.271 mmol), activated 4Å powdered molecular sieves (1g). The reaction mixture was stirred at room temperature for 2 h, followed by the addition of 1 M solution of Me₂S₂-Tf₂O reagent (408 μL, 0.34 mmol), stirred the reaction mixture for 20 min, quenched the by the addition excess triethylamine, diluted with CH₂Cl₂ (100 mL), filtered, and washed with water. The organic layer was dried over anhydrous MgSO₄, and concentrated, the residue was purified by column chromatography on silica gel (1:1 hexanes: ethylacetate) to afford compound 9 as colorless oily liquid (40 mg.). ¹HNMR (300 MHz, CDCl₃) δ 5.96 (d, 1H, *J* = 8.4Hz), 5.5 (t, 1H, *J* = 9.6Hz), 5.1 (m, 1H), 5.0 (t, 1H, *J* = 9.9Hz), 4.28 (q, 1H, *J* = 10Hz), 3.98-3.73 (m, 2H), 3.63-3.5 (m, 2H), 3.45 (s, 3H), 3.43-3.16 (m, 5H), 2.58-2.15 (m, 5H), 2.08 (s, 3H), 2.06 (s, 3H), 1.53 (t, 2H, *J* = 11Hz), 1.366 (t, 3H, *J* = 12Hz); ¹³CNMR (75MHz, CDCl₃) δ 170.7, 169.88, 169.82, 94.5, 80.5, 76, 70, 69.6, 69.3, 61.3, 61.2, 60.6, 60.5, 58.9, 57.6, 51, 50.3, 48.4, 35, 33.3, 32.7, 30, 20.6. HRMS (ESI) *m/z* [M+H]⁺ caclcd 716.2838, found 716.2908. [α]_D²⁴ = +20° (45 mg/6 mL DCM).

(1R,2R,4S,5S)-2,4-diamino-5-(((2S,3R,4R,5S,6R)-3-amn-6-(aminomethyl)-4,5-dihydroxytetrahydro-2H-pyran-2-yl)oxy)-N-((1S,2S,4R,5R)-2,4-diamino-5-methoxycyclohexyl)cyclohexanecarboxamide (1). To a solution of compound 16 (90 mg, 0.126 mmol) in methanol (10 mL) was added potassium carbonate (70 mg, 0.504 mmol), stirred the reaction mixture at room temperature for 15 min. concentrated the solvent in in vacuo. Diluted the reaction mixture with methylene chloride (25 mL) washed with water (2×15 mL), dried the organic layer over anhydrous MgSO₄, the solvent was concentrated to give the desired

product as colorless liquid (70 mg, 87%), which was dissolved in methanol (5 mL) and water (5 mL), added tributylphosphine (450 μ L, 2.2 mmol) and stirred the reaction mixture for overnight at room temperature. After completion of the reaction, reaction mixture was concentrated in in vacuo. Diluted the reaction mixture with water (25 mL), washed the water layer with methylene chloride (4 \times 20 mL), removed the water by lyophilization to afford desired compound (1) as white solid (14 mg, 27%). ^1H NMR (500MHz, CDCl_3) δ 3.6 (s, 3H), 3.55-3.32 (m, 2H), 3.30-3.04 (m, 4H), 3.0-2.80 (m, 1H), 2.79-2.65 (m, 1H), 2.64-2.46 (m, 2H), 2.30-1.97 (m, 1H), 1.52-1.21 (m, 3H), 1.20- 0.9 (m, 3H), 0.84-0.68 (m, 1H). HRMS (ESI) m/z $[\text{M}+\text{H}]^+$ calcd 476.3197, found 476.3163.

(1R,2R,4S,5S)-2,4-diazido-N-((1S,2S,4R,5R)-2,4-diazido-5-hydroxycyclohexyl)-5-hydroxycyclohexane-1-carboxamide (14). To a solution of 8 (300 mg, 0.83 mmol) and 9 (207 mg, 0.92 mmol) in dry DMF (10 mL) were added HOAt (340 mg, 2.5 mmol), HATU (878 g, 2.5 mmol) and DIPEA (875 μ L, 5.0 mmol) at room temperature and heated the reaction mixture to 50 $^\circ\text{C}$ for 3 h. The reaction mixture was concentrated in vacuo. The resulting crude was purified by column chromatography on silica gel (3:1 hexanes: ethyl acetate) to afford compound 7 as pale yellow liquid (200 mg, 42%). The compound (200 mg, 0.35 mmol) in methylene chloride was added TFA (270 μ L, 3.5 mmol) at room temperature and stirred the reaction mixture for 2 h, after completion of the reaction, reaction mixture was concentrated to afford desired product as yellow oil (210 mg, 100%), which was dissolved in methanol (15 mL), and added potassium carbonate (195 mg, 1.41 mmol), triflyl azide solution (prepared from sodium azide (16 equiv.) and triflic anhydride (12 equiv. in methylene chloride and water) at 0 $^\circ\text{C}$ and stirred the reaction mixture at room temperature for overnight and concentrated the solvent, diluted the reaction mixture with methylene chloride (100 mL), washed the organic layer with water (2 \times 50 mL) and

dried over anhydrous MgSO₄, evaporation of solvent followed by column purification on silica gel (1:1 hexanes: ethylacetate) afford compound 14 as colorless oily liquid (100 mg, 68%).

(1R,2R,4S,5S)-2,4-diamino-N-((1S,2S,4R,5R)-2,4-diamino-5-hydroxycyclohexyl)-5-hydroxycyclohexane-1-carboxamide (2). To a solution of compound 14 (25 mg, 0.55 mmol) in methanol was added Pd/C (20 mol %) and stirred the reaction mixture under hydrogen atmosphere and the catalyst was removed by filtration using microfiber filter paper. Evaporation of the solvent afford compound 2 (15 mg, 81 %) as white solid. ¹H NMR (500MHz, CDCl₃) δ 3.39 (td, *J* = 4, 8 Hz, 1 H), 3.14 (qd, *J* = 4, 8.5 Hz, 2 H), 2.78 (td, *J* = 4, 7.5 Hz, 1H), 2.5 (td, *J* = 4, 7.5 Hz, 1H), 2.42 (qd, *J* = 4, 8Hz, 2H), 1.99 (td, *J* = 3, 9.5 Hz, 1 H), 1.92-1.78 (m, 4H), 1.32 (q, *J* = 11.5 Hz), 1.18, (q, *J* = 12 Hz, 1H), 0.975 (q, *J* = 12 Hz, 2 H); ¹³CNMR (75MHz, CDCl₃) δ 176.1, 74.1, 73.3, 53.6, 53.4, 51.6, 51.4, 49.4, 39.4, 38.0, 36.6, 35.1, 23.3.

1-((1S,2S,4R,5R)-2,4-diamino-5-hydroxycyclohexyl)-3-((1R,2R,4S,5S)-2,4-diamino-5-methoxycyclohexyl)urea (3). To a solution of compound 17 (50 mg, 0.128 mmol) in CH₂Cl₂ was added trimethylamine (54 μL, 0.384 mmol) followed by dropwise addition of Phenyl chloroformate (20 μL, 0.154 mmol) at 0 °C, stirred the reaction mixture for 1hour at room temperature, removed the solvent under vacuum and to the crude reaction mixture in DMSO (2 mL) was added triethyl amine (54 μL, 0.384 mmol) followed by drop wise addition of compound 8 (55.3 mg, 0.154 mmol) by dissolving in small amount of DMSO, stirred the reaction mixture for 2 hours, diluted the reaction mixture with CH₂Cl₂ (20 mL), washed with water (2×15 mL) dried the organic layer, removed the solvent under vacuum and purified the product by flash chromatography on silica gel, the boc groups were deprotected with trifluoroacetic acid (6 equiv) to afford compound 3 as brown solid. ¹HNMR (300 MHz, CDCl₃) δ 3.6-3.38 (m, 3H), 3.3 (s, 3H), 3.25-3.13 (m, 1H), 2.98-2.75 (m, 3H), 2.3- 2.22 (m, 1H), 2.21-2.05 (m, 3H), 1.45-1.29 (m,

4H), 1.22-1.10 (m, 2H); 159.8, 82.9, 73.4, 66.4, 56.3, 55.2, 53.8, 53.6, 53.4, 52.0, 51.8, 51.6,
38.1, 37.9, 22.9, 23.1.

Chapter-3

RNA Binding Studies and Antibacterial Activity of 2-deoxystreptamine Antibiotic Mimics

3.1 RNA Binding Studies and Anti-bacterial Activity

In chapter 2 we discussed the design and synthesis of a new class of molecules based on a 2-deoxystreptamine core with the potential to display high selectivity in RNA binding. These new classes of 2-deoxystreptamine mimics have the potential to act as antibiotics by selectively targeting and binding with bacterial RNA. In this chapter we will briefly discuss several assays used for evaluating selectivity of RNA binding for compounds **1–3** (Figure 3.1), their RNA affinity for binding specific regions in RNA, their antibacterial activity. We will also discuss the correlation between RNA binding affinity and antibacterial activity.

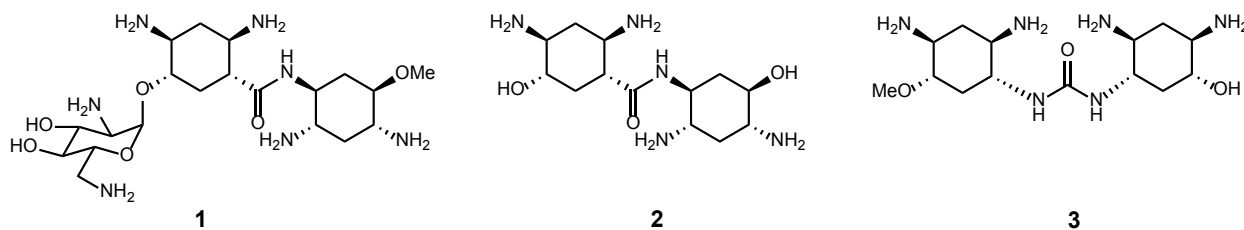


Figure 3.1 Structures of Compounds **1**, **2** and **3**

3.2 Evaluating RNA Binding

The *in vitro* binding affinity of RNA binding ligands cannot be determined through use of a direct enzymatic assay because the target RNAs used for *in vitro* studies usually does not have catalytic activity. However, several quantitative methods are available for the assessment of small molecule-RNA interactions¹. One of the commonly used methods for evaluating RNA binding affinity is NMR-based analysis.² In this method, the direct binding of a ligand to a RNA target is monitored by determining changes in the chemical shifts of protons in the nucleotide

bases. Differences in the chemical shifts of the nucleotide bases between the free ligand and the bound state provide information on both the strength and the region of binding. The drawback of this method is that large quantities of RNA are required for analysis of the chemical shifts. The second approach is to use an electrospray ionization (ESI) mass spectrometry-based method.³ In this method, the molecular weight shift is determined for free RNA, the RNA-binding ligand, and the bound RNA-ligand complexes in the gas phase. A third method involves fluorescent ligand displacement-based assays⁴. In this method, a fluorescent molecule is attached to the ligand and is titrated with RNA and a change in the fluorescence spectrum is recorded. Finally, fluorescently labelled RNA can be used to titrate binding with specific ligands.⁵ In this method, RNA oligonucleotides are made fluorescent by attaching a fluorophore to one end or by incorporating fluorescent nucleotides within or adjacent to the small molecule binding site. The most commonly used fluorescent nucleotide for this assay is 2-aminopurine. This method allows for site-specific binding analysis. In an RNA molecule containing multiple secondary structures, the selective incorporation of 2-aminopurine into one of the secondary structures can allow for detection of binding to only that site of interest. Our investigation into the binding affinity and specificity of our novel RNA binding 2-DOS mimics, we chose to use the latter method involving incorporation of a fluorescent nucleotide into our desired RNA binding partner. Thus, these assays would provide information about the affinity of our 2-DOS mimics (**1–3**) for RNA binding, and about the specificity of our ligands for specific regions of RNA.

3.2.1 RNA Binding Studies of Compound 1

The highly conserved binding interaction of rings I and II of neamine with RNA (Figure 3.2a) and its consistent recognition of the same 5'-GU-3' nucleotides in a variety of aminoglycosides makes neamine a valuable structural scaffold from which sequence specific

RNA binding molecules can be built. Our design of novel neamine mimics for selective RNA binding hinges on the use of the 2-deoxystreptamine core of neamine and incorporating new ring structures capable of introducing additional binding interactions to improve selectivity and binding affinity. Specifically, we introduced an additional 2-deoxystreptamine ring to ring I and II or neamine via an amide bond and a urea bond (compounds 1–3). Our design of sequence specific RNA binding molecules was based on the hypothesis that by extending one or more of the monomeric building blocks (2-deoxystreptamine) onto ring I of neamine, greater specificity for could be obtained for longer sequences of RNA. In particular, we believed that an additional neomiane ring could recognize dsRNAs that contain 5'-GUGU-3' sequence steps next to traditional binding location (A-site). Our neamine derivatives were tested to see if these extensions would be capable of recognizing extended 5'GU-3'/3'-UG-5' base pairs (see Figure 3.2b) and other random sequences. In our studies, we obtained both the binding affinity and the specificity of our compounds toward a variety of RNA structures.

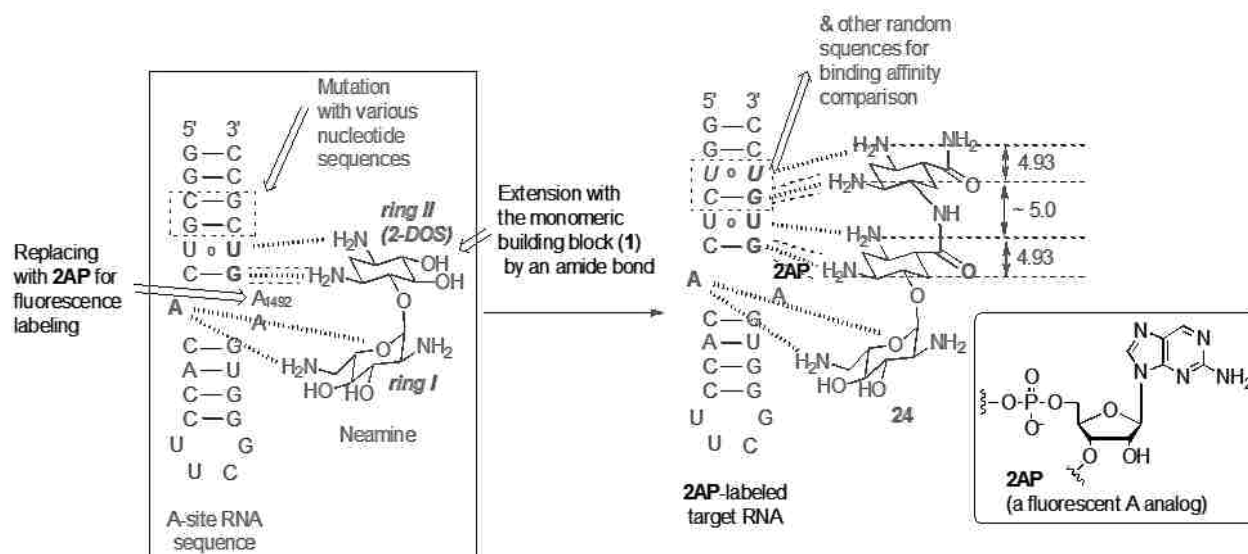


Figure 3.2 Design of sequence specific RNA binding molecules.

Compound **1** was tested for its sequence specific binding against the native A-site RNA sequence (**RNA-1**) and its mutants (**RNA 2-8**) (Figure 3.3). Each of these RNA sequences contains a 2-aminopurine (2-AP) fluorescence probe at the A-site (replacing A1492) to monitor binding. All of the RNA mutants (**RNA 2-8**) were purchased commercially and contain random sequences that replace the 5'-CG-3/5-GC-'3 pair of native A-site RNA. Neamine binds to several nucleotides of A-site RNA through four hydrogen bonds and two electrostatic interactions (Figure 3.4).⁶ All six interactions are conserved when other bulkier aminoglycosides (gentamycin B, kanamycin A, ribostamycin, lividomycin A, and neomycin B) bind to the same A-site RNA. In addition, all of these aminoglycosides contain neamine as a part of their structure. The neamine sub unit recognizes the same RNA sequence in the context of all these aminoglycosides (Figure 3.4).⁶ Based on this observation, our studies focused on structures where neamine was used as a base to which additional neamine and glycosides were appended. Thus, neamine was employed as an anchor to bring its attached 2-deoxystreptamine (2-DOS) mimic into close proximity with the mutated sequences. Therefore, the library of A-site RNA mutants will serve as a good tool to study preferred sequence binding by the 2-DOS mimics attached to neamine in the context of fully base-paired dsRNA.

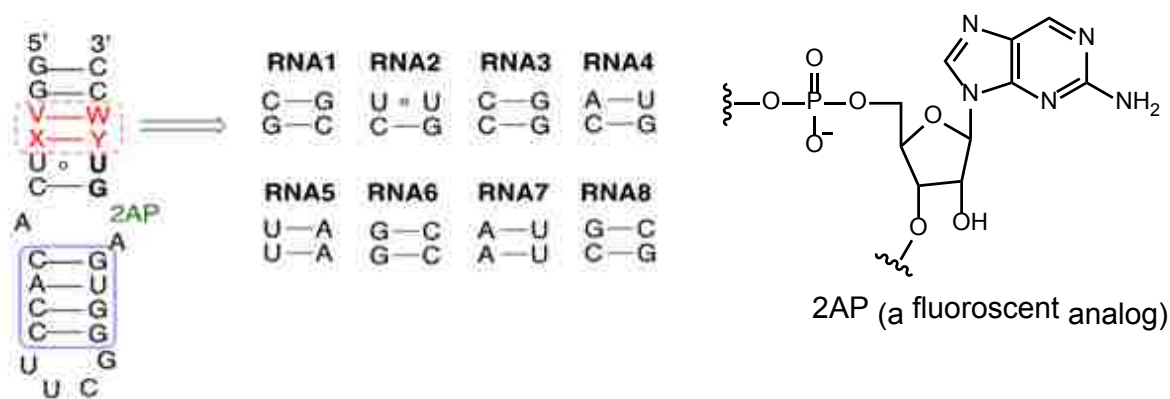


Figure 3.3 Sequences of RNA targets.

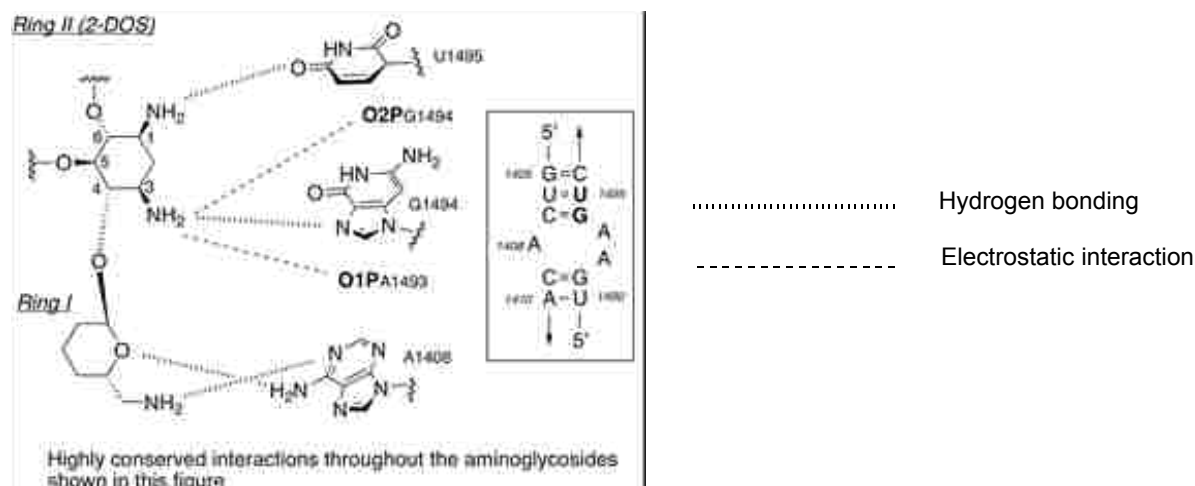


Figure 3.4 Conserved *H*-bonding and electrostatic interactions between aminoglycosides and RNA.

To see if 2-aminopurine-modified A-site RNA could be used for our binding assays, we titrated neomycin against RNA 1. Neomycin is known to form a 1:1 complex with A-site RNA. The titration gave a typical sigmoidal curve with a K_d value of 1.5 μM by scatchard analysis (Figure 3.5a). This result is in good agreement with the literature reported K_d of 0.5 μM for the complex of neomycin and A-site RNA.⁷ RNA 3, 5 and 7 were also treated with neomycin to see if mutations outside of the A-site would affect the binding affinity. All the titrations of RNAs with neomycin showed sigmoidal curves with K_d values between 1.1 to 2.4 μM . This result suggests that mutations to our target RNA outside of the A-site recognized by neomycin minimally affected the binding affinity of the RNAs. Compound 1 was next titrated against each RNA target to determine the binding affinity and sequence selectivity towards different RNA sequences. All the RNAs demonstrated sigmoidal curves as shown in a sample binding curve between RNA 2 and compound 1 (Figure 3.5b). The K_d values were between 0.5 and 2.9 μM (Table 3.1). It was found that RNA 5 is the preferred target for compound 1 and demonstrated six times stronger binding affinity compared to RNA 7. This result demonstrates that compound

1 does show some slight preference for specific DNA pairs adjacent to the A-binding site of RNA1.

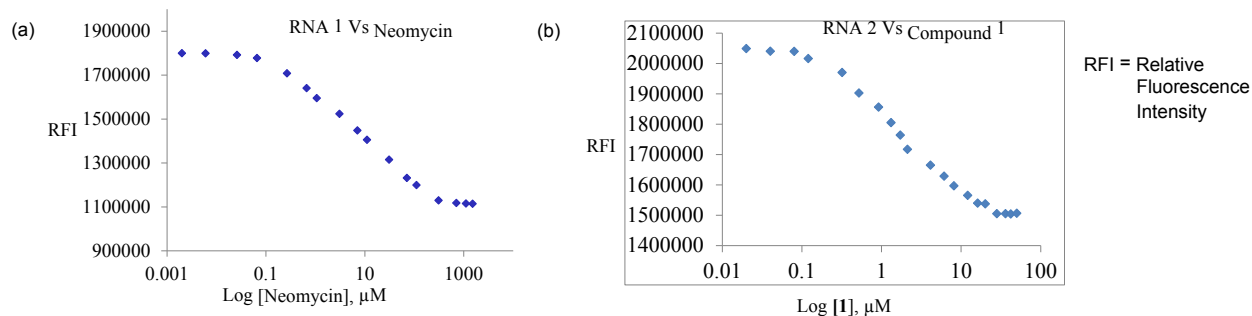


Figure 3.5 (a) titration curve between RNA 1 and Neomycin. (b) Sample titration curve between RNA 2 and Compound 1

Table 3.1. K_d values (μM) for compound **1** against mutant RNA.

entry	RNA1	RNA 2	RNA 3	RNA 4	RNA 5	RNA 6	RNA 7	RNA 8
Compound 1	2.2	1.5	2.2	1.7	0.5	1.4	2.9	1.4

3.2.2 RNA Binding Studies of Compound 2

Compound **2** was titrated similar to compound **1** against **RNA 1** (native A-site RNA) and its mutants **RNA 2-8** (Figure 3.6). As observed with compound **1**, all the RNAs showed sigmoidal regression curves, as shown in a sample binding curve between **RNA 6** and compound **2** (Figure 3.4b). The K_d values ranged between 0.4 and 3.8 μM (Table 3.2), which were comparable to that observed with neomycin. **RNA 1** is the preferred target for compound **2** and demonstrated 10 times stronger affinity compared to **RNA 7**. Both compound **1** and **2** showed lowest binding affinity towards RNA7. These results provide additional evidence that specific sequence binding can be influenced by the addition of additional rings to the neamine core structure.

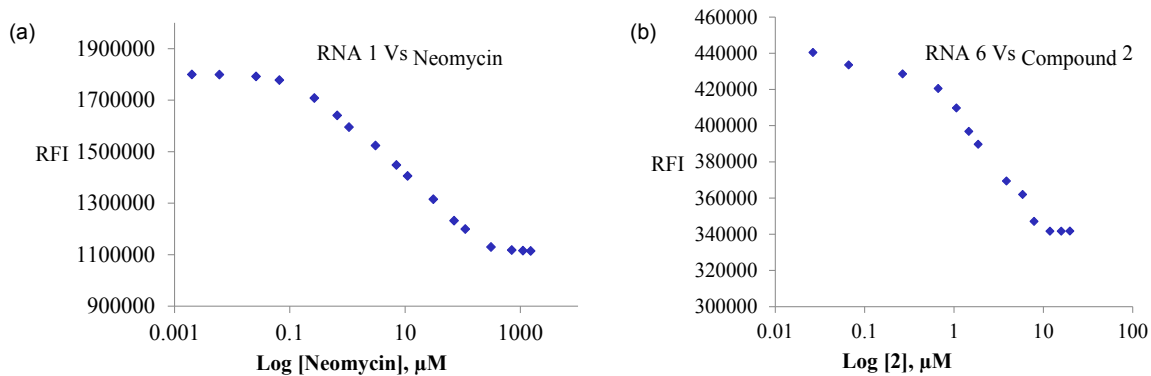


Figure 3.6 (a) Titration curve between RNA 1 and Neomycin. (b) Sample titration curve between RNA 6 and Compound 2

Table 3.2 K_d values (μM) for Compound 2 against RNA mutants

entry	RNA1	RNA 2	RNA 3	RNA 4	RNA 5	RNA 6	RNA 7	RNA 8
Compound 2	0.4	3.2	3.6	1.2	0.68	3.4	3.8	2.2

3.2.3 RNA Binding Studies of Compound 3

Compound 3, which contains a urea bond linking the dimeric 2-DOS mimics, was next tested for binding affinity and sequence selectivity against different RNA sequences. All the RNAs demonstrated sigmoidal binding curves as shown in the sample binding curve between RNA 6 and compound 3 (Figure 3.7b). The K_d values for compound 3 range from 0.36 to 7.7 μM (Table 3.3). Compound 3 showed strong binding affinity towards RNA 3, 4 and 5. RNA 5 is the preferred target for compound 3 and demonstrated 21 times stronger binding affinity compared to RNA 8.

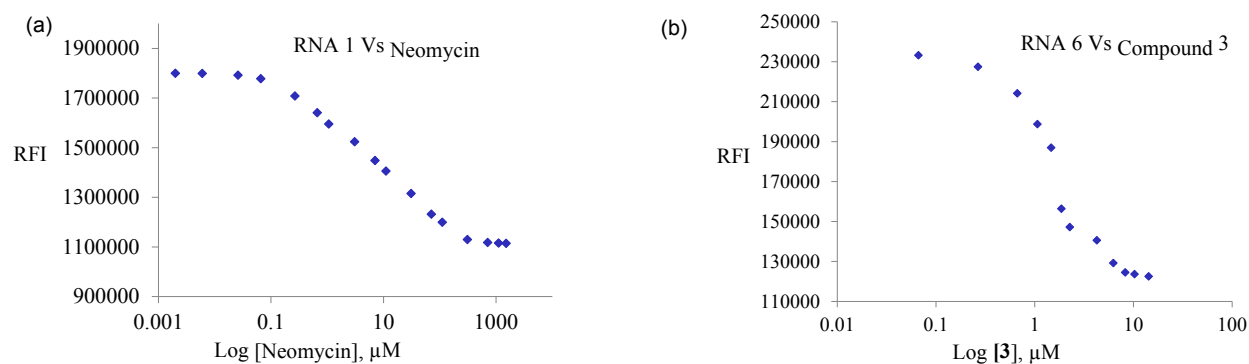


Figure 3.7 (a) titration curve between RNA 1 and Neomycin. (b) Sample titration curve between RNA 6 and Compound 3

Table 3.3 K_d values (μM) for Compound 3.

entry	RNA1	RNA 2	RNA 3	RNA 4	RNA 5	RNA 6	RNA 7	RNA 8
Compound 3	2.5	3.6	0.67	0.65	0.36	4.95	1.18	7.7

The results of these RNA binding studies demonstrate that our 2-deoxystreptamine mimics **1–3** do demonstrate selectivity towards binding different sequences of RNA. Each of our mimics shows specificity for different sequences of RNA adjacent to the standard binding location (A-site), confirming our hypothesis that extension of the aminoglycoside to include additional rings can be used as a strategy for designing new RNA binding molecules that bind to specific sequences. In addition, these results confirm that the structure of the 2-DOS mimic can impact the specificity of binding for different sequences.

3.3 Antibacterial Activity

3.3.1 Antibacterial Activity of Novel 2-DOS Mimics 1–3

Compounds **1**, **2**, and **3** were next tested for antimicrobial activity against *E. Coli TOP10*, *Klebsiella pneumoniae* and *Acinetobacter baumannii*. These strains of bacteria are known to be resistant to aminoglycoside antibiotic. We first tested compound **1** against *E. coli* TOP10, *K.*

pneumoniae JHCK1, and *Acinetobacter baumannii*. Concentrations of compound **1** were 0.05 and 0.25 mg/ml. We did not see any activity against any of these strains with compound **1**. We did not test a full range of concentrations for compound **1** due to the lack of antibacterial activity shown in initial experiments and because of a lack of material with compound **1**. Compound **2** was next tested, and was shown to have no activity against *Acinetobacter baumannii*. It does, however, show some activity against *E. Coli TOP10*, and *Klebsiella pneumoniae*. Concentrations of compound **2** were 1, 2, 4, and 8 mg/ml. We then tested compound **3** against *E. coli TOP10*, *K. pneumoniae* JHCK1, and *Acinetobacter baumannii*. Concentrations of compound **3** were 0.5, 1, 2, 4, and 8 mg/ml. Compound **3** is active against all the three strains. *Klebsiella pneumoniae* JHCK1 and *Acinetobacter baumannii* A155 are resistant to several amino glycosides including amikacin, kanamycin, tobramycin.

In conclusion, we have prepared dimeric 2-DOS mimics (**1–3**) by conjugating two monomeric units by an amide and urea bonds. Their binding affinity was comparable to that of neomycin in RNA binding studies with a variety of mutant RNAs. They demonstrated weak antibacterial activities but show some promising results against *K. Pneumoniae* JHK1, which is known to be resistant to many aminoglycosides. Thus, our novel 2-DOS mimics may be used as templates to build more potent antibiotics.

3.3.2 Comparison of RNA binding Affinity and Antibacterial Activity

In this section we will discuss the correlation between the antibacterial studies and RNA binding affinity studies of aminoglycoside antibiotics. In our recent paper¹³ we published results comparing the binding affinity of eight members of the pyranmycin class of antibiotics (TC001, TC002, TC003, TC005, TC007, TC0012, RR501 and pyrankacin) and two members of

neomycin class (NEOF004 and neokacin) with their antibacterial activity (Figure 3.8). We titrated all the ten aminoglycosides against **RNA1** and **RNA 3** (see Figure 3.3) under the same conditions used for titrations with our 2-DOS mimics presented in the previous section ¹⁴. The minimum inhibitory concentrations (MIC's) against *Escherichia coli* (ATCC 25922) and *Staphylococcus aureus* (ATCC 25923), have been determined previously for all the compounds tested.⁸⁻¹¹

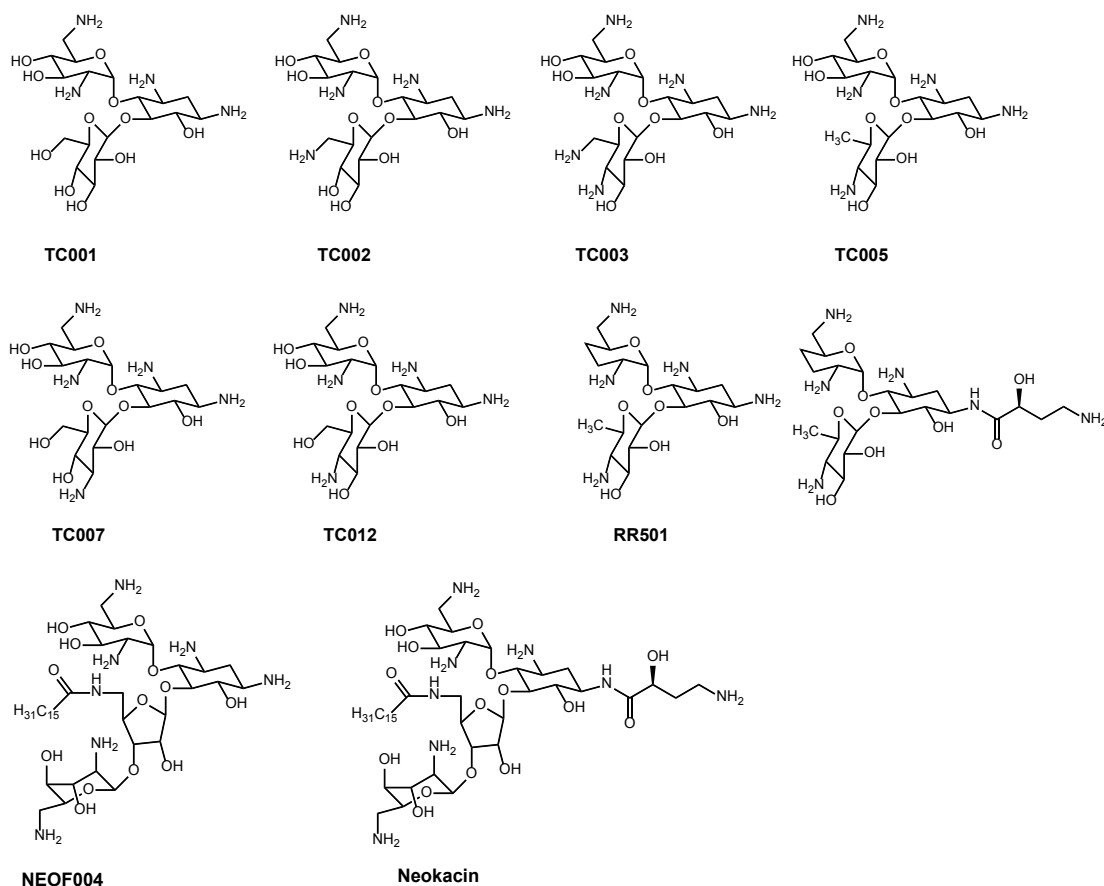


Figure 3.8 Members of pyranmycin and neomycin family used to compare antibacterial activity and binding affinity.

Generally aminoglycosides with more hydrophilic groups (NH_2 or OH) will have higher binding affinity (lower K_d value) towards the target RNAs. For example TC003 with six amino

groups showed the highest binding affinity compared to other pyranmycin members, but TC003 showed less antibacterial activity compared to other members (Table 3.4). RR501 on the other hand has two less hydroxyl groups at 3' and 4' positions and thus shows lower binding affinity. Yet it shows superior antibacterial activity. Similar difference between K_d 's and MIC's has also been previously reported.¹² Compounds TC005, TC007 and neokacin did not show sigmoidal binding curve with RNA 1, instead they show an increase in the fluorescence reading as the concentration of each aminoglycoside is increased. The other members of pyranmycin and neomycin family of antibiotics demonstrated sigmoidal binding curves. This means that these three pyranmycin members may interact differently in the region of RNA1 potentially by non-specific interactions due to the presence of non-natural 2-aminopurine. However, using structurally similar **RNA3** (see Figure 3.3), normal binding mode was observed for all the tested aminoglycosides, including TC005, TC007 and neokacin. Since neomycin showed very similar binding affinities toward both **RNA1** and **RNA3**, we believe that the abnormal binding of TC005, TC007 and neokacin toward RNA1 is due to the presence of the 2-aminopurine. However pyrankacin showed the highest binding affinity and highest antibacterial activity. NEOF0004, which has a much larger hexadecanoyl (C16) group at the 5' position showed stronger binding affinity than several other pyranmycin members and even neomycin, which is interesting since the high lipophilicity of the hexadecanoyl group is not expected to interact closely with the highly charged RNA's. As additional evidence for the disconnect between RNA binding affinity and antibacterial activity, our 2-DOS mimics **1**, **2** and **3** showed stronger binding affinities compared to neomycin. However, all the three 2-DOS mimics showed little antibacterial activity compared to neomycin.

Table 3.4 Binding affinity ($K_d = \mu M$) and minimum inhibitory concentrations (MIC's)

Compound	Binding	Binding	E. coli	S. aureus
	Affinity	Affinity	(ATCC 25922)	(ATCC 25923)
	RNA1	RNA3	MIC	MIC
Neomycin	1.148	1.270	4.4	1.1
TC001	9.667	0.608	92.4	44.4
TC002	26.05	0.845	35.1	14.8
TC003	3.720	0.261	41.8	29.6
TC005	No Binding	0.556	19.8	11.0
TC007	No Binding	1.152	57.2	59.2
TC012	5.675	2.827	44.0	29.6
RR501	1.331	1.203	26.0	6.50
Pyrankacin	0.650	1.357	5.59	2.80
NEOF004	1.269	0.737	4.69	2.35
Neokacin	No Binding	1.642	8.59	2.15

3.4 Conclusion

Our results presented in this chapter suggest that our novel approach to aminoglycoside-based RNA binding molecules could indeed lead to the design of specific and selective RNA binding molecules. These results also imply that the RNA constructs can accommodate diverse structural entities attached onto the naturally occurring aminoglycosides, which can be used as a strategy for developing more specific binders to any RNA sequence. However, our antibacterial studies demonstrate a strong disconnect between the RNA binding capabilities of an aminoglycoside mimic and the actual antibacterial properties. Thus, the use of simple RNA constructs and

binding affinities alone may not be sufficient to predict the actual behavior of synthetic aminoglycosides inside bacteria.

3.5. References

- (1) Thomas, J.R.; Hergenrother, P.J. *Chem. Rev.*, **2008**, *108*, 1172.
- (2) Johnson, E. C.; Feher, V. A.; Peng, J. W.; Moore, J. M.; Williamson, J. R. *J. Am. Chem. Soc.* **2003**, *125*, 15724.
- (3) *for review see*: Hofstadler, S. A.; Griffey, R. H. *Chem. ReV.* 2001, 101, 377 (b) Sannes-Lowery, K. A.; Griffey, R. H.; Hofstadler, S. A. *Anal. Biochem.* **2000**, *280*, 264.
- (4) Tok, J. B.; Cho, J.; Rando, R. R. *Biochemistry*, **1999**, *38*, 199. (b) Matsumoto, C.; Hamasaki, K.; Mihara, H.; Ueno, A. *Bioorg. Med. Chem. Lett.* **2000**, *10*, 1857.
- (5) Yan, Z.; Baranger, A. M. *Bioorg. Med. Chem. Lett.* 2004, *14*, 5889. (b) Lacourciere, K. A.; Stivers, J. T.; Marino, J. P. *Biochemistry*, **2000**, *39*, 5630.
- (6) Francois, B.; Russell, R. J. M.; Murray, J. B.; Aboul-ela, F.; Masquida, B.; Vicens, Q.; Westhof, E. *Nucleic Acids Res.* **2005**, *33*, 5677.
- (7) Fourmy, D.; Recht, M. I.; Puglisi, J. D. *J. Mol. Biol.* **1998**, *277*, 347.
- (8) Wang, J.; Li, J.; Chen, H.-N.; Chang, H.; Tanifum, C. T.; Liu, H.-H.; Czyryca, P. G.; Chang, C.-W. T. *J. Med. Chem.* **2005**, *48*, 6271.
- (9) Elchert, B.; Li, J.; Wang, J.; Hui, Y.; Rai, R.; Ptak, R.; Ward, P.; Takemoto, J. Y.; Bensaci, M.; Chang, C.-W. T. *J. Org. Chem.* **2004**, *69*, 1513.

(10) Zhang, J.; Chiang, F.-I.; Wu, L.; Czyryca, G. P.; Li, D.; Chang, C.-W. T. *J. Med. Chem.* **2008**, *51*, 7563.

(11) Chang, C.-W. T.; Hui, Y.; Elchert, B.; Wang, J.; Li, J.; Rai, R. *Org. Lett.* **2002**, *4*, 4603.

(12) Greenberg, W. A.; Priestley, E. S.; Sears, P. S.; Alper, P. B.; Rosenbohm, C.; Hendrix, M.; Hung, S.-C.; Wong, C.-H. *J. Am. Chem. Soc.* **1999**, *121*, 6527.

(13) Udumula, V.; Ham, Y. W.; Fosso, M. Y.; Chan, K. Y.; Rai, R.; Zhang, Z.; Li, J.; Chang, C.-W. T. *Bioorg. Med. Chem. Lett.* **2013**, *23*, 1671.

(14) Udumula, V.; Chittapragada, M.; Marble, J. B.; Dayton, D. L.; Ham, Y. W. *Bioorg. Med. Chem. Lett.* **2011**, *21*, 4713.

3.6 Experimental Procedures

3.6.1 Fluorescence Binding Assay Condition, Procedures, and Titration Curves

Purification of the compound 1 and neomycin: The compound 1 and neomycin were purified and isolated as the free base form using anion exchange resin (DOWEX MONOSPHERE 550A (OH)). Each (50-100 mg) was loaded on the resin column that had been pre-equilibrated with water. Then, each was eluted using ddI-H₂O water and fractions containing the free base were identified by ninhydrin staining on TLC plate and were combined & lyophilized.

Determination of RNA concentration: Each RNA was purchased from Dharmacon PAGE- purified, 2'-deprotected, & desalted. They were used directly without further purification. RNA constructs were quantified in 50 mM phosphate buffer (pH 7.5) with the following extinction coefficient (260 nm) values (in units of L/mol.cm): RNA1 ($\epsilon = 244,200$),

RNA2 ($\epsilon = 247,300$), RNA3 ($\epsilon = 242,200$), RNA4 ($\epsilon = 249,600$), RNA5 ($\epsilon = 258,900$), RNA6 ($\epsilon = 245,400$), RNA7 ($\epsilon = 255,200$), RNA8 ($\epsilon = 239,100$).

3.6.2 Fluorescence Binding Assay

Fluorescence binding assay was performed in a pH7.0 buffer (150 mM sodium cacodylate, 5 mM MgCl_2). Each 2-AP labeled RNA was excited at 300 nm and emission spectrum was monitored at 330 to 420 nm (emission max at 370 nm). Following is the detailed procedure for the assay: the fluorescence spectrum of a 222.8 μL buffer solution was recorded as the blank. This background fluorescence was observed minimal and subtracted from all subsequent emission spectrum of each binding titration. To the blank buffer was added each RNA labeled with 2-aminopurine (2.25 μL of 50 μM) to give the final 0.5 μM RNA concentration and the fluorescence was recorded. Subsequent aliquots of 0.9 μL of aqueous solution of neomycin or the compound 1 (0.05 μM – 5 mM) was added and the fluorescence spectrum were recorded after each aliquot. The decrease in fluorescence was observed with the addition of each aliquot. Over the entire range of titration, the emission maximum at 370 nm did not significantly vary (<1.0 nm). No “background emission” was observed near 370 nm. As small, concentrated volumes of the ligands were titrated in, the total volume of the sample never changed more than 5%. Titration experiment performed at lower ionic strength used a pH 7.0 buffer containing 20 mM sodium cacodylate, 25 mM KCl, 2 mM MgCl_2 .

Chapter-4

Polymer-Supported Nanoparticle Catalysts for Organic Synthesis

4.1 Introduction

The design and synthesis of nanostructured materials has emerged as a major research direction in several areas such as optics and electronics, sensing, medicine, and catalysis. For each of these applications, the properties of the nanomaterials can be altered by changing their size (surface area), molecular structure and shape, and matrix or support. These types of modifications to nanostructured materials (nanoparticles) are particularly important in the area of catalysis where chemical reactions that occur at the surface of the nanoparticles are highly influenced by the surface composition and physical properties¹. Catalysis has a broad impact on many areas important to modern society, including the development of new medicines (pharmaceuticals), energy (photovoltaics, petroleum utilization), materials (polymers), and agriculture (pesticides, fungicides). Thus, the development of highly reactive and selective nanoparticle catalysts can accelerate the advancement of our modern society in important ways.

Transition metal catalysis is divided into two general classes: heterogeneous catalysts where the catalyst and reactants are in different phases (generally solid/liquid or solid/gas) and homogeneous catalysis where both catalysts are in the same phase (generally dissolved in solvent). Several practical considerations make heterogeneous catalysts more attractive, including their ease of separation, recovery, and reuse, and their high temperature stability. However, heterogeneous catalysis suffers from a general lack of mechanistic understanding that could aid in the development of more selective and efficient catalysts.² Homogeneous catalysis, on the other hand, is very efficient and selective and the electronic and steric properties of the metal catalyst can be tuned by changing the structure of the supporting ligands. In addition,

many reaction mechanisms are known for homogeneous transition metal catalysts that enable rational design of more efficient catalysts. The limitations with homogeneous catalysis include low turnover numbers, low thermal stability, and the difficulty of catalyst separation and recovery¹. Based on the advantages and disadvantages of these two classes of catalysis, it would be highly advantageous to develop catalysts at the interface between homogeneous and heterogeneous catalysis that offer both catalyst stability and recyclability while maintaining selectivity and catalyst tunability.

Nanoparticle catalysis represents a bridge between heterogeneous and homogeneous catalysis for several significant reasons.³ First, the small size and high surface of nanoparticles makes them more reactive than traditional heterogeneous catalysts. Second, product selectivity, catalytic efficiency, and catalyst stability can often be controlled by adding stabilizers (organic ligands or polymers), or by adsorbing the nanoparticles on a solid support such as TiO₂, Al₂O₃, SiO₂, CeO₂, ZrO₂,⁴ porous zeolites or carbon nanotubes.⁵ Nanoparticles can also be encapsulated in dendrimers⁵ or polymers.⁵ Third, the desired nanoparticle catalysts often remain heterogeneous in the reaction mixture, especially when adsorbed onto a solid support, and thus can be easily separated from the reaction mixture and reused without loss of activity. Finally, nanoparticle catalysis is environmentally friendly because the catalysts can be often reused.

This chapter will discuss the design and synthesis of nanoparticle catalysts for applications in organic synthesis. A wealth of knowledge is available on the development of transition metal nanoparticles on solid supports and the application of these nanocatalysts to industrial processes such as Fischer Tropsch hydrocarbon synthesis.⁶ These applications of nanoparticle catalysis have been previously reviewed.⁶⁰ The focus of this chapter is recent advances in the development of tunable nanoparticle catalysis and their application to organic

reactions used in fine chemical synthesis. In general, the mechanisms of these processes are well understood, and corresponding homogeneous catalysts have been developed. Specifically, the formation of unsupported homogeneous nanoparticle catalysts will be discussed, followed by the synthesis and application of supported nanoparticles, including polymer-supported nanoparticle catalysts.

4.2 Preparation Strategies for Nanoparticle Catalysts

While various methods exist for preparing nanostructured materials, the typical procedure for preparation of nanoparticle catalysts is reduction of a homogenous solution of a high valent metal salt in the presence of stabilizers. The reducing agent reduces the corresponding metal ion to zero valent metal, which then aggregates to form nano-sized clusters. Synthesis of nanocatalysts in this way requires no special equipment or instrumentation, making this class of catalyst accessible to any synthetic chemistry laboratory. Chemical reductions are the simplest and most common method of preparing nanoparticles, including the use of metal hydride reductants such as sodium borohydride⁷ or hydrogen gas.⁸ In the latter method, hydrogen gas is either bubbled into a solution containing the metal salt or the reduction is carried out under elevated pressures of hydrogen to reduce the metal salts to zero valent metal atoms. Reduction of metal salts in alcohol⁹ solvents is another common reduction method, where reduction of the metal salt occurs under refluxing conditions. In this reaction, the alcohol acts as the reductant and is subsequently oxidized to the corresponding carbonyl compound. The other common reductants for nanoparticle formation include hydrazine,¹⁰ and sodium citrate solutions.¹¹

During the reduction of metal salts for nanoparticle formation, the addition of stabilizers is often necessary to control particle size and shape, and to prevent formation of bulk heterogeneous metal. Nano-sized metal particles have much higher surface area than bulk

metals, have highly curved surfaces, and often have edges and ridges, all of which can be important to catalytic activity. The addition of stabilizers or heterogeneous supports, which can bind to the surface of nanoparticles or sequester small particles to prevent further aggregation, is often used as a strategy to improve catalytic efficiency. The nature of the support and or additives can influence not only the size, but also the shape of the particles and the electronic properties of the metal surface. The next section will discuss specific examples of how size, shape, and the nature of the support can influence the catalytic performance of the nanoparticle catalysts.

4.3 The Impact of Nanoparticle Structure on Catalytic Activity

4.3.1 Nanoparticle Size and Catalytic Activity

The size of the nanoparticle has a tremendous impact on the catalytic activity and selectivity of a reaction and can often be optimized to improve catalyst performance.¹² In general, nanoparticles with small size are more catalytically active compared to larger ones because of their higher surface area per unit volume. However sometimes optimization of the ideal particle size is necessary for better catalytic activity. For example, Goodman et al.¹³ prepared Au nanoparticles on TiO₂ for CO oxidation with diameters ranging from 2–6 nm. They found that the highest catalytic activity was achieved not with the smallest nanoparticles synthesized, but when a particle size of 3.5 nm was obtained. Several groups have similarly found that gold nanoparticles exhibit maximum catalytic activity when the size of the nanoparticles is between ~2–3 nm. Gangula et al. also showed that the catalytic activity of gold nanoparticles in 4-nitrophenol reduction decreases as the size of the particle increases.¹⁵

Nanoparticle size not only affects catalytic activity, but can also affect the selectivity of a catalyst for different products. Somorjai et al.¹⁴ showed that reduction of pyrrole using platinum nanoparticles on SBA-15 mesoporous silica exclusively forms *n*-butyl amine when the size of the nanoparticle is more than 2 nm (Figure 4.1). When the size of the platinum nanoparticle was decreased to about <2 nm, reduction of pyrrole generated pyrrolidone selectively.

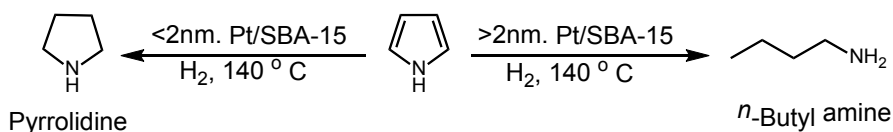


Figure 4.1 Hydrogenation of pyrrole over platinum NPs of different sizes.

4.3.2 Nanoparticle Shape and Catalytic Activity

Nanoparticles exhibit different catalytic activity and selectivity on different exposed facets at the surface of the particle.¹⁶ As the number and types of facets change on a particle surface, the shape also changes as a direct result. Synthetic methods have been developed that generate metal nanoparticles of different shapes, including spheres, cubes, tetrahedrons, octahedrons, rods, wires, and prisms.¹⁷ McGlacken et al.¹⁸ prepared palladium nanoparticles with cubic, cuboctahedral, and octahedral morphologies (Figure 4.2) and compared the catalytic performance for Suzuki-Miyaura coupling reactions. These palladium nanocubes were synthesized from Na_2PdCl_4 using poly(vinylpyrrolidone) (PVP) as a stabilizing agent and ascorbic acid as reducing agent at 80 °C. Octahedral and cuboctahedral nanocrystals were prepared from cubic palladium seeds using PVP as a stabilizing agent and ascorbic acid as reducing agent at 80 °C, followed by the addition of varying amounts of Na_2PdCl_4 dissolved in deionized water. The prepared nanocrystals were separated by centrifugation, immobilized on a heterogeneous carbon support, and then dried in vacuum at 120 °C. In the catalytic studies, they

showed that palladium nanocrystals with {100} surface facets showed superior catalytic activity compared to {111} facets.

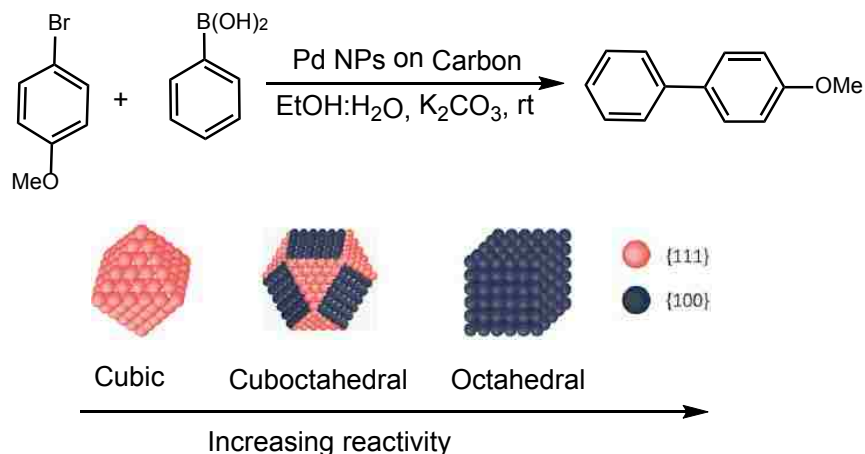


Figure 4.2 Shape sensitivity in palladium nanoparticle-catalyzed Suzuki-Miyaura cross coupling reaction.

Similar to the McGlacken work described thus far, El-Sayed et al.¹⁹ prepared tetrahedral and spherical platinum nanocrystals for Suzuki-Miyaura coupling reaction (Figure 4.3). In their manuscript, they demonstrated that the tetrahedral nanocrystals showed catalytic activity, while spherical nanocrystals did not show any catalytic activity.^{19b} A significant drawback to designing nanoparticle catalysts with structure-based reactivity is that the shape of the nanoparticle may not be preserved during the reaction.¹⁹ Thus, catalytic performance can either increase or decrease as the result in changes to the metal surface during catalysis.

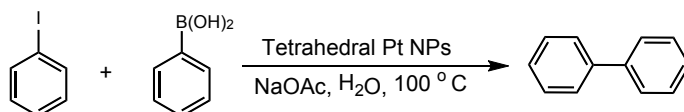


Figure 4.3 Tetrahedral Pt NPs catalyzed Suzuki- Miyaura coupling reaction.

4.3.3 Supporting Ligands and Catalytic Activity

Colloidal (Homogeneous) Nanoparticle catalysis: The use of colloidal or homogeneously dispersed metal nanoparticle catalysts is an attractive approach in nanoparticle catalysis because the nanoparticles are generally freely accessible to reagents in the reaction solution. Thus, excellent catalytic efficiency and selectivity is observed, as compared to supported metal nanoparticle catalysts. However, catalyst recycling is difficult compared to supported, heterogeneous nanoparticle catalysts. Colloidal metal nanoparticles can be prepared via the reduction methods described above from homogeneous metal salt solutions. In colloidal metal nanoparticle synthesis, stabilizers are necessary to prevent nanoparticle agglomeration, which can cause the catalyst to precipitate from solution. Common classes of stabilizers include polymers such as polystyrene,²⁰ polyvinylpyrrolidone (PVP),²¹ ionic polymers,²² polyvinyl alcohol (PVA),²³ and poly (acrylamide) (PAA),²⁴ and surfactants²⁵ like cetyltrimethylammonium bromide (CTAB) and N-alkyl-N-(2-hydroxyethyl)ammonium salts (Figure 4.4). Phosphine ligands,²⁶ dendrimers²⁷ have also been employed. Specific examples of the synthesis of this class of nanoparticle and the impact of ligand structure on catalytic properties will be discussed in the following section.

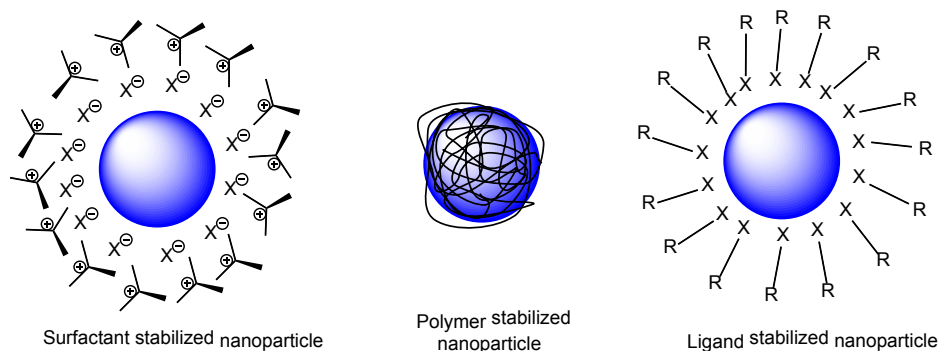


Figure 4.4⁶³ Schematic representation of stabilization of nanoparticles using different protecting groups.

Supported nanoparticle catalysis: In heterogeneous catalysis, metal nanoparticles are adsorbed on inorganic oxides such as TiO₂, Al₂O₃, CeO₂, SiO₂, or carbon, or can be encapsulated by polymers followed by cross linking.²⁸ The adsorption process involves preparing a colloidal suspension of the transition metal nanoparticles and adsorbing these colloidal nanoparticles onto the support. Alternatively, performing the nanoparticle reduction/formation in the presence of the inorganic oxide can lead to formation of the nanoparticle on the support. A significant advantage of supported nanoparticles over colloidal nanoparticles is that catalyst recovery and recycling is very straightforward and can often be accomplished with simple filtrations. In addition, leaching of the metal nanoparticle into solution can be minimized by controlling the concentration of the nanoparticle on the support, or by making modifications to the support. One disadvantage is that the reactivity of supported nanoparticle catalysts can be diminished because the nanoparticle is sequestered in the support (polymers) and or in a separate phase from the reagents. Metal nanoparticles composed of platinum, gold, palladium, ruthenium, nickel and cobalt, among others,²⁹ have been supported on inorganic oxides. These supported catalysts are widely used in synthesis for hydrogenations,³⁰ oxidations of CO³¹ and alcohols,³² NO reductions,³³ nitroarene reduction,³⁴ coupling reactions,³⁵ and Fischer-Tropsch synthesis.³⁶

The main advantage of using organic polymer supports over inorganic supports is that organic polymers can be easily functionalized by incorporating ligands on the polymer.³⁷ This approach allows for tuning of the metal nanoparticles steric and electronic properties, which in turn can control the reactivity and selectivity of the desired transformation. In this fashion, polymer-supported nanoparticle catalysts most closely resemble their homogeneous metal complex counterparts because the reactivity of the nanoparticles can be optimized and tuned by

variation of the polymer ligand structure. Specific examples of the synthesis and catalytic applications of polymer-supported nanoparticle catalysts will be presented below.

4.4 Preparation and Catalytic Performance of Nanoparticle Catalysts for Organic Synthesis

4.4.1 Preparation and Catalytic Activity of Unsupported Metal Nanoparticles

This section provides specific examples of methods to synthesize unsupported ligand-stabilized colloidal metal nanoparticles in liquid phase and in the absence of a solid support. The main emphasis is on the synthesis of nanoparticles for catalytic applications and their reactivity towards different organic reactions. Key to the synthesis and use of homogeneous colloidal nanoparticles is selection of the appropriate stabilizer that not only prevents nanoparticle aggregation and precipitation, but also maintains or enhances the desired catalytic activity. The reports on the synthesis of colloidal metal nanoparticles are extensive, and thus here we only discuss the synthesis of gold, palladium, and silver nanoparticles because they have found the most wide spread application in organic synthesis.

Preparation and Catalytic Activity of Unsupported Gold Nanoparticles: Bulk gold metal is catalytically inactive and historically was not considered as a viable metal for heterogeneous catalysis. Haruta and coworkers were the first to report that gold nanoparticles (NPs) with particle size <10 nm are chemically active in oxidation of CO.⁶¹ Since this initial report, significant attention has been given to the synthesis of catalytically active gold nanoparticles. Gold nanoparticles are generally non-toxic, as compared to other transition metals, and thus much interest has been demonstrated in their potential as catalysts for pharmaceutical synthesis, and as supports for drug delivery applications⁵⁹. Herein we will describe several examples of the synthesis and catalytic applications of gold nanoparticles.

Tsukuda et al.³⁸ prepared monodisperse Au NPs having a mean diameter of 1.3 nm and studied their catalytic activity for the aerobic oxidation of benzylic alcohols (Figure 4.5). Gold nanoparticles were prepared by rapid addition of aqueous NaBH₄ into an aqueous solution of HAuCl₄ containing polyvinylpyrrolidone (PVP) as a stabilizer at room temperature. They also prepared Au NPs having a mean diameter of 9.5 nm by reducing HAuCl₄ with sodium sulfite in the presence of 1.3 nm gold NPs prepared previously and compared the catalytic activity of both the nanoparticles of different sizes. Nanoparticles having mean diameter of 1.3 nm showed superior activity compared to the one nanoparticles of 9.5 nm diameter. The authors attributed the improved catalytic activity to the difference in surface area.

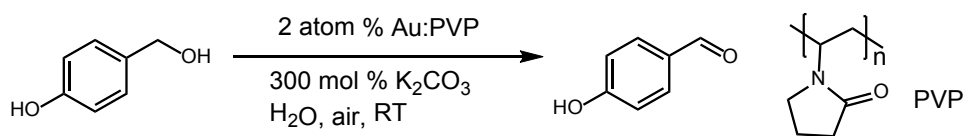


Figure 4.5 PVP stabilized gold NPs catalyzed oxidation of benzyl alcohol

Dyson et al.³⁹ prepared Au NPs by NaBH₄ reduction of HAuCl₄ in water with water soluble ionic polymer poly-(3-((2,4-divinylcyclopentyl)methyl)-1,2-dimethyl-1*H*-imidazolium methanesulfonate) as a stabilizer. They then studied the catalytic activity of the nanoparticles for the reduction of *p*-nitrophenol (Figure 4.6) and hydrogenation of cinnamaldehyde. In the preparation of the nanoparticle catalysts, they demonstrated that the size of the nanoparticle could be controlled by adjusting the ratio of polymer to gold nanoparticle. When a polymer/Au ratio of 50:1 was employed, the particle size distribution was in the range of 1.8 to 2.8 nm. If the ratio of polymer to Au was decreased to 3:1, the resulting particle size distribution changed to the range of 2 to 12 nm. The Au NPs catalyst having polymer/Au ratio of 50:1 showed the best activity toward reduction of *p*-nitrophenol.

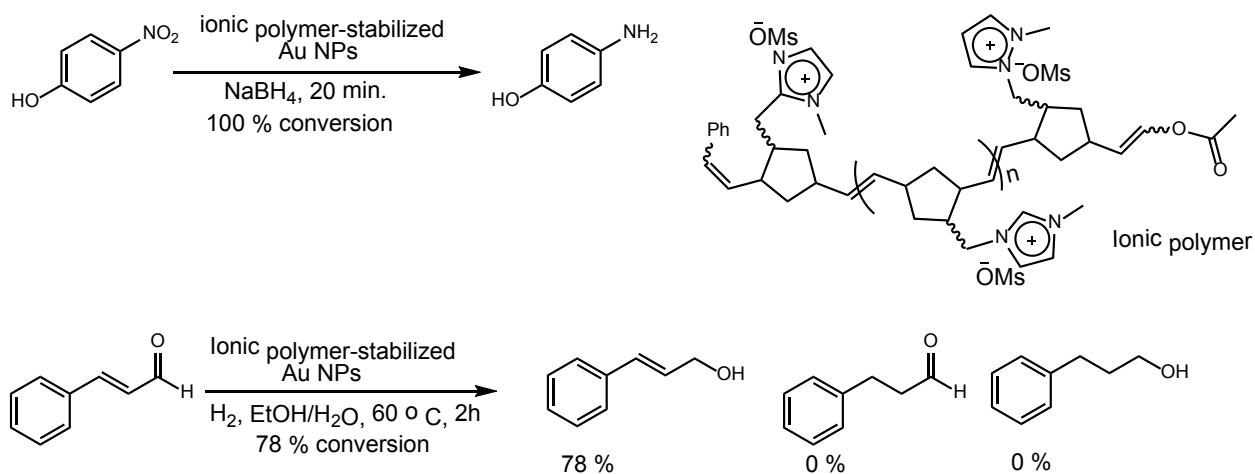


Figure 4.6 Ionic polymer stabilized Au NPs for 4-nitrophenol reduction.

Prati et al.⁴⁰ studied the catalytic activity and stability of Au NPs in the presence of various stabilizing agents, including polyvinyl alcohol (PVA), tetrakis(hydroxypropyl)phosphonium chloride (THPC) and citrate (Figure 4.7). The PVA stabilized Au NPs were prepared by the reduction of aqueous solution of HAuCl_4 by NaBH_4 . THPC and citrate stabilized Au NPs were prepared by reducing the aqueous solution of HAuCl_4 with THPC or citrate as the reductant. The size and catalytic activity of the Au NPs in different stabilizers were then compared. It was found that the size of the Au NPs (2.0 to 2.45) were smaller when sterically bulky stabilizing groups were used (PVA and THPC), and the size of the Au NPs when citrate was used was 9.76 nm. In the catalytic oxidation of glycerol, they found that higher catalytic activity was observed with the smaller particle sizes (Figure 4.7). There was significant difference in the catalytic between PVA and THPC stabilized Au NPs. This result shows that bulky stabilizer (PVP, THPC) was more effective at controlling particle size and thus provide more reactive catalysts for aerobic oxidations.

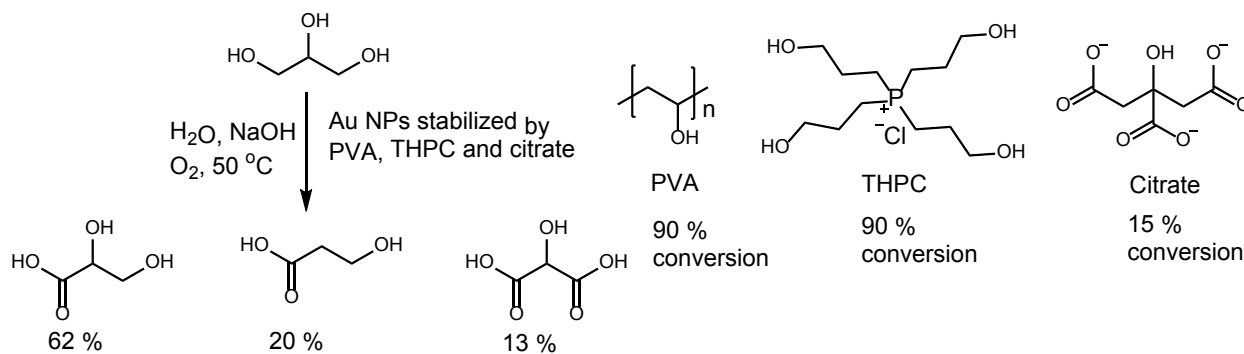


Figure 4.7 PVA, THPC, Citrate stabilized Au NPs for aerobic oxidation of glycerol.

Preparation and Catalytic activity of Unsupported Palladium Nanoparticles: Palladium is one of the most widely used metals in homogeneous transition metal catalysis. In fact, the importance of palladium catalysis to modern chemistry was recently demonstrated when the 2010 Nobel Prize in chemistry was awarded for palladium-catalyzed cross couplings in organic synthesis. Thus, the development of highly active and selective palladium nanoparticle catalysts has the potential to impact a wide range of reactions in organic synthesis, including cross coupling reactions, hydrogenations, and oxidations.

El-Sayed et al.⁴¹ prepared the Palladium NPs for applications to Suzuki cross coupling reactions (Figure 4.8). They prepared their nanoparticle catalysts by heating an aqueous solution of H_2PdCl_4 in the presence polyvinyl pyrrolidone (PVP) as a stabilizer and ethanol as a reducing agent. The mean diameter of the synthesized Pd NPs was 3.6 nm. In catalytic studies, they found that the nanoparticles were capable of performing the Suzuki cross coupling reaction in high yields. However, the catalytic activity of Pd NPs slowly decreased during the course of the reaction because the nanoparticles were shown to agglomerate and precipitate from solution. The authors hypothesized that the high temperatures ($100\text{ }^\circ\text{C}$) necessary for the reaction caused the nanoparticles to escape from the polymer matrix and agglomerate, leading to precipitation.

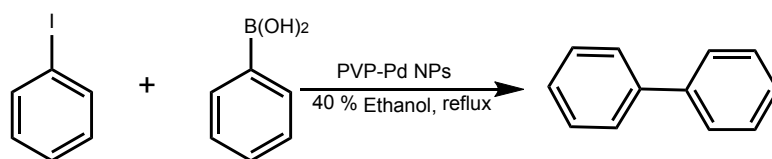


Figure 4.8 PVP-Pd NPs catalyzed Suzuki cross coupling

Fujihara et al.⁴² prepared chiral palladium NPs for enantioselective biaryl formation via asymmetric Suzuki-Miyaura couplings at room temperature (Figure 4.9). The nanoparticles were synthesized from K_2PdCl_4 using chiral, enantioenriched mono and bisphosphines as stabilizers and sodium borohydride as a reducing agent. The mean diameter of the chiral Pd NPs were 1.2 -1.7 nm. The yields and enantiomeric excess of the reaction were moderate to good, the yields and enantioselectivities in the reaction were influenced remarkably by the protective ligand on the chiral Pd NPs (Figure 4.9).

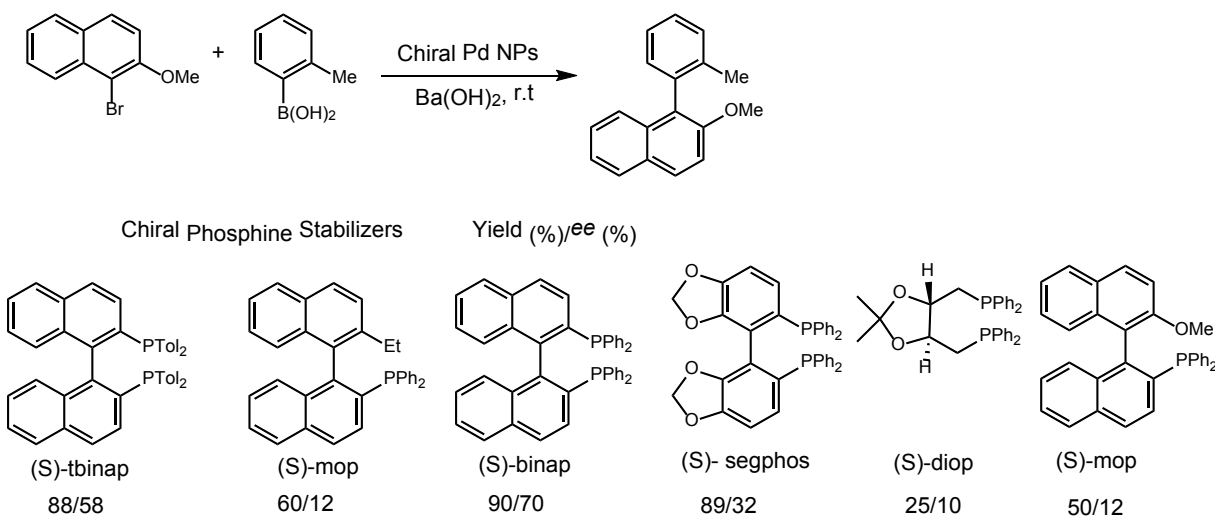


Figure 4.9 Chiral Phosphine stabilized Pd NPs for enantioselective Suzuki-Miyaura coupling reactions.

Reetz et al.⁴³ prepared palladium NPs for application to the Heck cross coupling reaction. The nanoparticles were synthesized from PdCl_2 , $\text{Pd}(\text{OAc})_2$, or $\text{Pd}(\text{NO}_3)_2$ using excess of tetraalkylammonium carboxylates as reducing and stabilizing agent (Figure 4.10a). The tetra-

alkyl ammonium carboxylates stabilize colloidal nanoparticles by forming a monolayer around the metal core (Figure 4.10a) thus preventing them from forming agglomerates. The palladium nanoparticles were shown to have a diameter of 2 nm. The prepared Pd NPs were used for Heck reaction and were found to have high reactivity (Figure 4.10b).

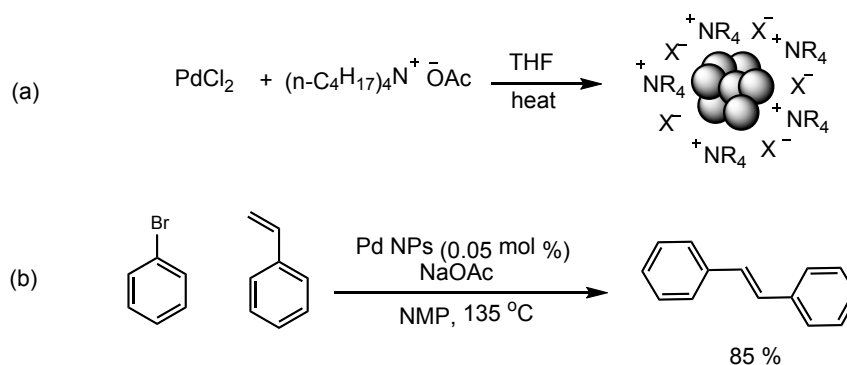


Figure 4.10 (a) Tetraalkylammonium carboxylate-stabilized Pd NPs for Heck reactions. (b) Heck reaction

Preparation and Catalytic activity of Unsupported Ruthenium Nanoparticles: Rousseau et al.⁴⁴ prepared ruthenium NPs and explored their activity in the regio and stereoselective deuteration of pyridines (Figure 4.11). The nanoparticles were prepared from Ru(COD)(COT) in the presence of PVP as stabilizer and hydrogen gas as a reducing agent. Nanoparticles thus prepared were shown to have high catalytic activity for a variety of substrates, including pyridines, quinoliines, indoles and alkyl amines when deuterium gas was employed at room temperature (Figure 4.11).

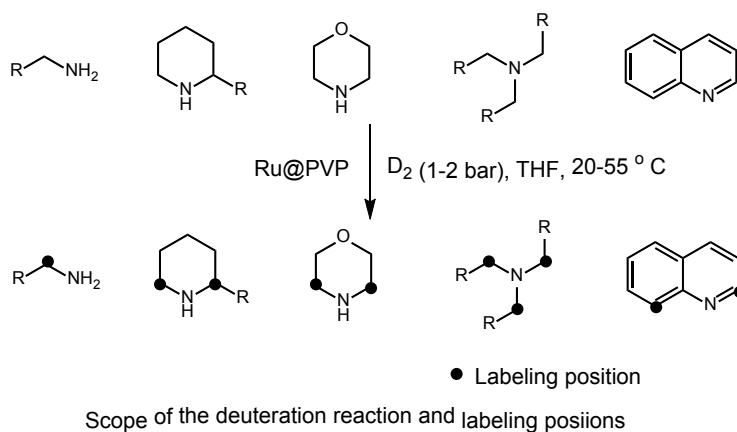


Figure 4.11 PVP stabilized Ru NPs for deuteration of amines.

Leeuwen et al.⁴⁵ prepared ruthenium (Ru) NPs and explored their reactivity in the hydrogenation of *o*-methylanisole (Figure 4.12). The nanocatalysts were again prepared from Ru(COD)(COT) in the presence of different phosphine ligands as stabilizers and hydrogen gas as a reducing agent. The authors prepared various “roof-shaped” diphosphines and monophosphine ligands containing aryl and alkyl groups and studied the effect of phosphine ligands on the size, stability and catalytic activity of the corresponding Ru NPs. The size distribution of alkyl phosphorous stabilized NPs were between 1.35-1.5 nm, whereas the size distribution of aryl phosphorous stabilized NPs were between 1.5-2 nm.

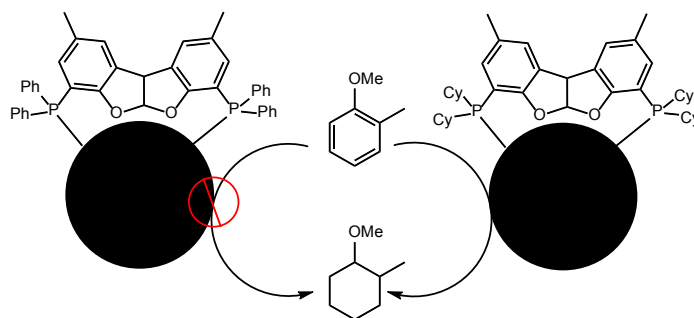


Figure 4.12 Aryl and alkyl groups containing phosphine stabilized Ru NPs for Hydrogenation

The authors found that phosphines containing alkyl groups showed superior catalytic activity compared to phosphine ligands containing aryl groups. The stability is mainly due to strong bond with alkyl phosphorous and weak π - π interaction between the aromatic backbone of the ligand and the ruthenium atoms.

4.4.2 Preparation and Catalytic Applications of Supported Nanoparticles

In supported nanoparticle catalysis, metal nanoparticles are stabilized by absorption onto insoluble solid supports. The insoluble supports are of two types: 1) inorganic supports such as metal oxides and mesoporous silica 2) organic supports such as polymers. One of main advantages of supported nanoparticle catalysts is that separation of the catalyst from the reaction mixture is easy. In addition, the recovered catalysts can often be recycled and perform subsequent reactions with the same reactivity and selectivity. This latter advantage minimizes the use of expensive metals and also decreases the metal-containing waste produced. A final advantage of supported nanoparticle catalysts is that in many instances, no supporting ligands in addition to the support are necessary. In this section we will briefly discuss several preparation methods and catalytic applications of nanoparticles supported on inorganic and polymer-based supports.

Nanoparticles Supported on inorganic supports – Fischer-Tropsch synthesis: Supported metal nanoparticles have found widespread application in catalysis related to the petrochemical industry, including for Fischer-Tropsch synthesis and hydrogenations. Fischer-Tropsch synthesis is a process for conversion of CO/H₂ into liquid hydrocarbon fuels and chemicals. A significant body of research has been generated on the development of catalysts, including nanoparticle

catalysts, for Fischer-Tropsch synthesis.⁶⁰ Thus, only a recent example will be presented here that demonstrates the impact of the solid support identity on catalytic performance.

Wang et al.⁴⁶ reported preparation of cobalt (Co) nanoparticles supported on SiO₂, Al₂O₃, Zeolite H-Y, Zeolite Na-Y, Zeolite H-meso-Y and Zeolite Na-meso-Y for Fischer-Tropsch synthesis. The authors prepared Co NPs by mixing Co(NO₃)₂·6H₂O and solid support using melt infiltration technique at 60 °C followed by thermal treatment in a gas flow of 5 % NO/He at 400 °C. The catalytic activity and product selectivity for C₁₀₋₂₀ hydrocarbons of these nanocatalysts was then compared. Zeolite Na-meso-Y supported Co NPs showed better selectivity for C₁₀₋₂₀ hydrocarbon compared to other supports. The higher selectivity is due small size of Co NPs and small mesopore size of the support.

Nanoparticles Supported on Inorganic Supports for Organic Synthesis:

Somorjai and Toste et al.⁴⁷ prepared platinum nanoparticles of different sizes (1.5, 2.9 and 5.0 nm) for applications in alkene – alkyne cycloisomerization reactions (Figure 4.13). The nanocatalysts were prepared from H₂PtCl₆ with either NaBH₄ or ethylene glycol/NaOH as the reducing agents. The nanoparticles were generated with polyvinylpyrrolidone (PVP) and hydroxyl-terminated polyamidoamine (PAMAM) dendrimers as capping agents. After nanoparticle formation, the resulting stabilized catalysts were deposited on SBA-15 and MCF-17 mesoporous silica at 100 °C for 24 hours. The supported nanoparticles then were tested for the catalytic activity in various cyclization reactions (Figure 4.13). The authors showed equivalent or superior selectivity could be obtained with the heterogeneous catalysts as with previously developed homogeneous catalysts. They also demonstrated that the size of the nanoparticles had a large impact on the catalytic activity, where nanoparticles of small size showed superior

reactivity. The authors also commented that the pores on the mesoporous silica prevent catalyst aggregation and contribute to the high stability of the catalysts.

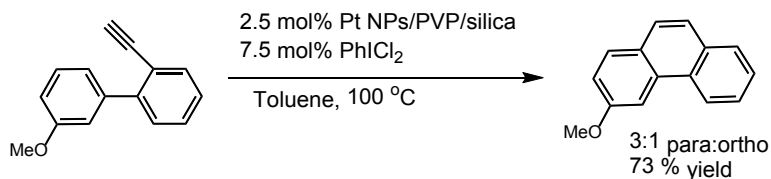


Figure 4.13 Silica supported Platinum NPs for Hydroarylation.

Porco et al.⁴⁸ prepared silica supported silver (Ag) NPs having a mean diameter of 4.5 nm and studied their catalytic activity for the Diels-Alder cycloadditions of 2'-hydroxychalcones (Figure 4.14). The Ag NPs were prepared by addition of tetrabutylammonium borohydride into a solution of silver tetra fluoroborate (AgBF₄) in CH₂Cl₂ in the presence of silica gel. The solid was filtered and dried at 160 °C for 12 hours to give silica supported Ag NPs. The nanoparticles had both high reactivity and high selectivity in the Diels-Alder reaction of highly advanced synthetic intermediates. The authors did the same Diels-Alder reaction under homogeneous conditions using AgBF₄, the yields and selectivity for endo:exo were slightly better than silica supported Ag NPs, with AgBF₄ (Yield: >99%, endo/exo: 78:22), with silica supported Ag NPs (Yield: 98%, endo/exo: 65:35), however the silica supported Ag NPs are reusable.

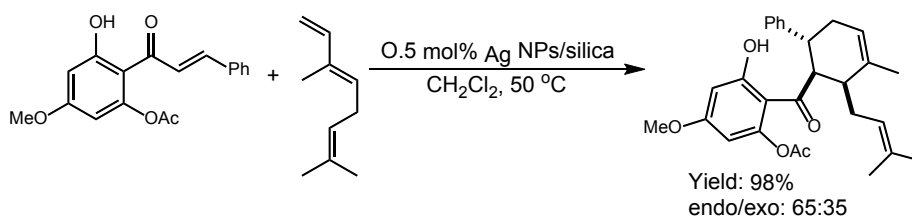


Figure 4.14 Silica supported silver NPs for Diels-Alder reactions.

Shiraishi et al.⁴⁹ prepared TiO₂ and CeO₂ supported gold (Au) NPs for application to catalytic aerobic oxidation reactions in the presence of UV-Visible light (Figure 4.15). The Au NPs were prepared by adding TiO₂ (P25) to a solution of water containing HAuCl₄.H₂O. The solution PH was adjusted to 7 with 1M NaOH and the mixture stirred at 80 °C for 3 hours. The Au NPs were recovered by centrifugation and solid was dried under air at 80 °C for 12 hours and powders were calcined in air at 200 °C to 600 °C. The resulting nanoparticles had a mean diameter of 3.7 to 45.3 nm. The size of the nanoparticles was controlled by changing the ratio of the supports. Au/CeO₂ nanoparticle catalysts were prepared in a similar manner. The nanoparticles with <5 nm showed better catalytic activity in aerobic oxidations compared to nanoparticles of larger size (Figure 4.15).

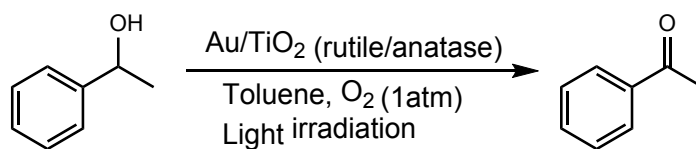


Figure 4.15 TiO₂ supported gold NPs catalyzed aerobic oxidation of alcohols.

Synthesis and Catalytic Activity of Polymer Supported Nanoparticles: Organic polymers offer some advantages over inorganic supports. Organic polymers can be easily functionalized by incorporating supporting ligands onto the polymer. Thus, polymer-modification can be used to tune the electronic and steric properties of the metal nanoparticles. Polymer-supported nanoparticles can act as both homogeneous and heterogeneous catalysts where the homogeneous polymers (such as those supported in polyvinyl pyrrolidone) can be easily separated from the reaction by adjusting the polarity of the solvent, leading to catalyst precipitation. The use of homogeneous polymer supported nanoparticle catalysts was previously discussed in section 4.4.1. The most common polymer used in polymer supported nanoparticle synthesis is

polystyrene because it is easy to synthesize and can be easily functionalized to introduce supporting ligands. Polystyrene-based polymers can also be cross-linked by adding small amounts of divinylbenzene as a cross linker.⁵⁰ Cross-linking in this manner generates insoluble polymer supports, which can be easy to separate from the reaction mixture. Alternatively, polystyrene-based polymers can be cross linked by introduction of reactive groups⁵² that can react with one another and cross-link the polymer upon heating. This section discusses the synthesis and catalytic activity of insoluble polymer supported nanoparticles.

Somorjai et al.⁵¹ and others have reported that organic molecules such as benzene can weakly interact with gold surfaces through formation of weak interactions between the π -electrons of the benzene ring and the metal surface. Kobayashi et al.⁵² prepared gold nanoclusters in polystyrene based polymers to see if the benzene rings of the polymers can stabilize the gold nanoclusters through interaction with the π -electrons. They first prepared gold nanoclusters from PPh_3AuCl in THF using sodium borohydride as reducing agent without any stabilizing agent. After addition sodium borohydride, the solution immediately turned from colorless to wine red, which suggest the formation of gold (0) particles. However, after stirring the solution for several minutes, aggregation of nanoclusters occurred to afford a black precipitate. They next reduced PPh_3AuCl under the same conditions and in the presence of polystyrene to see if nanoparticle stabilization would result. In this case, the solution remained a deep red color, indicating nanoparticle formation, but no black precipitate was observed, even after stirring the solution for 12 hours. This suggests that gold nanoclusters can be stabilized by the π -electrons of the benzene rings in polystyrene.

Using polystyrene supported nanoparticles, Kobayashi and coworkers developed heterogeneous polymer-supported gold nanoparticle catalysts for aerobic oxidation reactions

(Figure 4.16). In their report, they co-polymerized epoxide- and alcohol-containing styrene monomers to generate a cross-linkable polymer support. After the introduction of gold nanoparticles into the polymer by sodium borohydride reduction, the catalyst was heated to initiate cross-linking via epoxide opening reactions. The authors were able to show that the resulting cross-linked polymers remained heterogeneous in the reaction, had high catalytic activity in aerobic oxidation reactions, and that cross-linking prevented the leaching of the gold nanocluster from the polymer into solution (Figure 4.17).

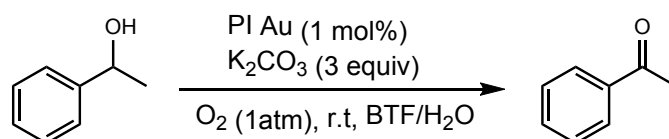


Figure 4.16 Aerobic oxidation of 1-phenylethanol using polymer incarcerated gold NPs

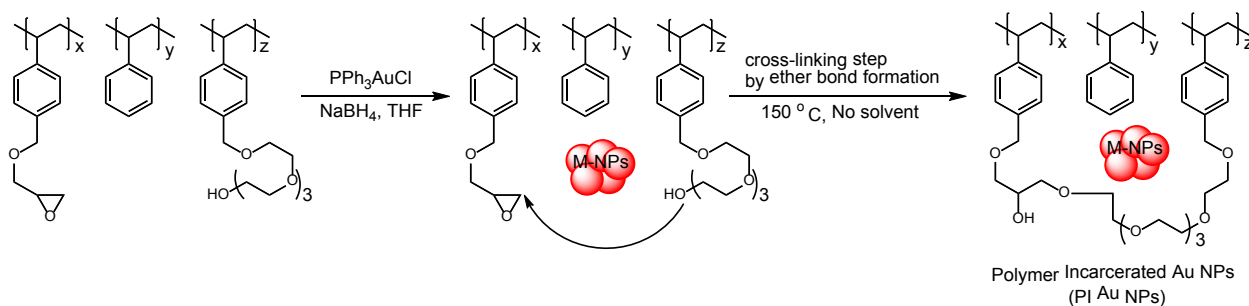


Figure 4.17 PI Gold NPs prepared by cross linking the epoxide and alcohol functional groups of the polymer

Kobayashi and coworkers⁵³ also reported the synthesis of phosphinated cross-linkable polymers capable of stabilizing palladium nanoparticle catalysts (Figure 4.18). These palladium nanoparticle catalysts were later applied to Suzuki-Miyaura coupling reactions where addition exogenous phosphine was unnecessary for high catalytic activity. The authors reported the synthesis several polystyrene-based polymers containing diphenylphosphine groups attached to the polystyrene. The cross-linkable polymers (epoxide-containing) were synthesized with

different ratios of the copolymers to vary the amount of phosphine and cross-linking agent in the polymer. The catalyst was prepared by adding $\text{Pd}(\text{PPh}_3)_4$ to a solution of copolymer in THF at room temperature, followed by stirring at room temperature for 24 hours. The polymer encapsulated palladium nanoparticles were precipitated from the solution by addition of hexanes and the polymer was cross linked by heating at $120\text{ }^\circ\text{C}$ for 2 hours. The catalytic activity of polymer-incarcerated nanoparticles was excellent when the ratio of diphenylphosphino groups to palladium in the polymer was 2:1. The authors also synthesized a polymer without phosphine groups and did the reaction by the addition of external triphenylphosphine. Importantly, the addition of exogenous phosphine did not lead to high catalytic activity compared to the diphenylphosphine-containing polymer.

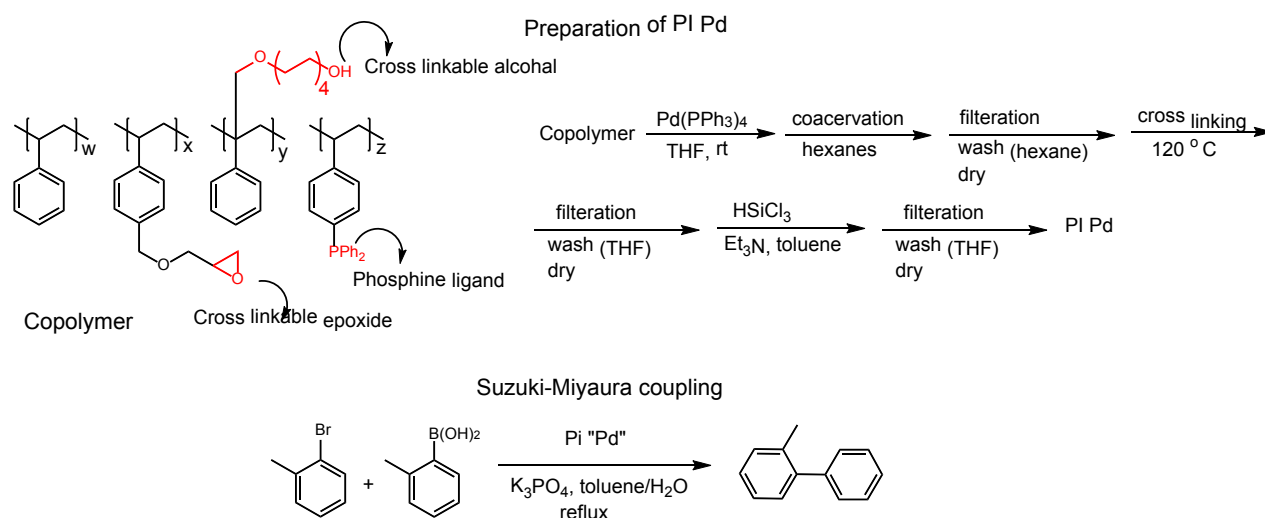


Figure 4.18 schematic representation of copolymer used to prepare Pd NPs for Suzuki-Miyaura coupling

The Kobayashi group also reported the synthesis nickel nanoparticles stabilized by polystyrene containing *N*-heterocyclic carbene ligands for use in the Corriu-Kumada-Tamao

reaction (Figure 4.19).⁵⁴ The polymer-incarcerated nickel nanoparticles was prepared by adding $\text{NiBr}_2(\text{PPh}_3)_2$ to a solution of THF containing an imidazole-containing copolymer and ketjen black. The catalyst was then reduced using lithium triethylborohydride. The solid formed was then filtered, washed, and dried. Cross-linking of the polymer was then accomplished by reaction of the imidazole with an alkyl bromide upon heating to 150 °C for 12 hours under argon. The resulting imidazolium-containing polymer contained the requisite N-heterocyclic carbene (NHC) precursor that was hypothesized to activate nickel for cross coupling during the reaction. The resulting nickel nanoparticles have a mean diameter of 1-4 nm. The authors then compared the reactivity of the nickel nanoparticles stabilized in the imidazolium-containing polymer (Figure 4.20a) to nickel nanoparticles stabilized by their original cross-linked polystyrene polymer (Figure 4.20b). They reported that the polymer that has no N-heterocyclic carbene on the polymer is inactive whereas the polymer that has N-heterocyclic carbene highly is active in cross coupling reactions (Figure 4.19).

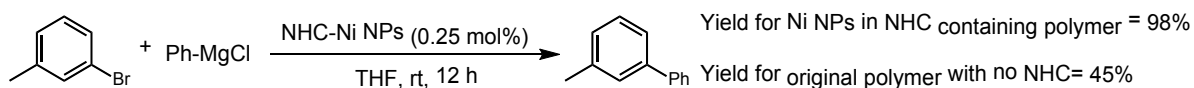


Figure 4.19 *Corriu-Kumada-Tamao reaction*

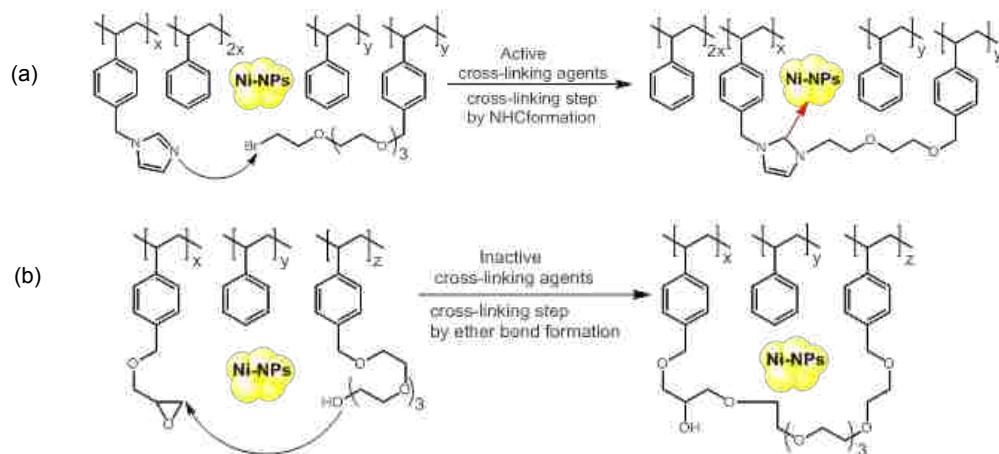


Figure 4.20 (a) Ni NPs in original cross-linked polymer with no *N*-heterocyclic carbene. (b) Nickel NPs stabilized in the cross-linked imidazolium-containing polymer with *N*-heterocyclic carbene (NHC) formation.

Guo et al.⁵⁵ prepared highly stable gold (Au) NPs of different sizes (1.0, 2.0 and 5.0 nm) supported on poly (2-aminothiophenol) (PATP) for Suzuki-Miyaura cross coupling reactions (Figure 4.21). The PATP-stabilized gold NPs were prepared by stirring 2-aminothiophenol in an aqueous HCl solution, followed by the addition of an aqueous solution of HAuCl₄. After stirring the reaction mixture for 24 hours at room temperature, the PATP supported Au NPs were precipitated, filtered, washed with deionized water, and dried under vacuum at 60 °C. Nanoparticles with sizes 1nm, 2nm and 5nm was prepared by altering the molar ratio of HAuCl₄ to 2-aminothiophenol. The conjugated π -electrons of benzene rings and thiol groups of the PATP significantly control the size and stability of the gold NPs. The authors reported that both the size of the nanoparticles and the percent loading of the nanoparticles in polymer played an important role in catalytic activity of gold NPs in Suzuki-Miyaura cross-coupling reaction. They found that the catalytic was highest when the small particles were used, and that the higher weight percent of nanoparticle in the polymer also led to higher catalyst activity.

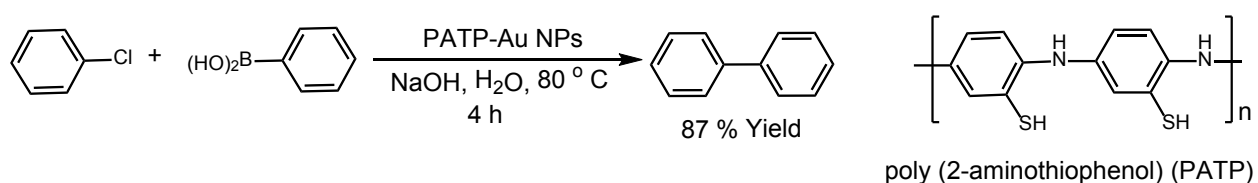


Figure 4.21 PATP-Stabilized Gold Nanoparticle Catalysts for Suzuki-Miyaura Coupling of Chlorobenzene and Phenylboronic Acid

Diaconescu et al.⁵⁶ prepared palladium NPs supported on polyaniline nanofibers for Suzuki coupling reactions (Figure 4.22). Palladium NPs supported on polyaniline were prepared by adding palladium (II) nitrate to a suspension of polyaniline in water, followed by incubation for one day. The resulting solution was purified by dialysis to remove any remaining palladium

(II) nitrate. These polyaniline-supported Pd NPs prepared via this protocol showed good yields and selectivity's in the cross coupling reaction. (Yield: 88 to 99%, time: 2-6 h)

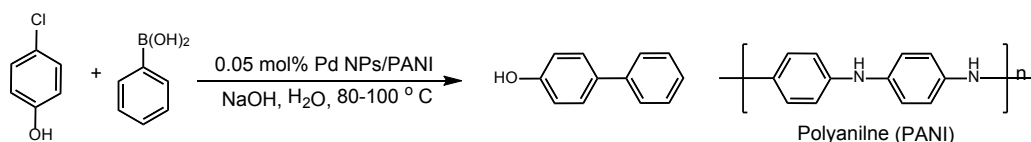


Figure 4.22 Polyaniline supported Pd NPs for Suzuki coupling

Synthesis of Polymer Supported Bimetallic Nanoparticle catalyst: An alternative strategy for improving the reactivity of polymer-supported nanoparticle catalysts is incorporating a second metal into the polymer to form a bimetallic nanoparticle. Three different classes of bimetallic nanoparticle catalysts can be formed, depending on the procedure and type of metals employed. First, bimetallic alloys may form; second, bimetallic core shell nanoparticles may form; and third, mixtures of monometallic nanoparticles may form. The alloy form has different properties compared to monometallic nanoparticles, bimetallic core shell nanoparticles, and mixtures of individual monometallic nanoparticles. In addition, different catalytic activity and selectivity can be observed for each type of catalyst. This section discusses the synthesis and catalytic applications of some important polymer supported bimetallic nanoparticles.

Kobayashi et al.⁵⁷ reported the synthesis of amides from alcohols and amines under aerobic conditions using polymer incarcerated carbon black (PICB) supported bimetallic gold/iron, gold/nickel and gold/cobalt nanoparticles (Figure 4.23). The bimetallic nanoparticles were prepared by reducing the corresponding the solution of precatalysts (PPh₃AuCl, NiF₂, FeCl₂, and CoCl₂) in diglyme using sodium borohydride followed by filtering the precipitate by adding diethyl ether and cross linking the polymer at 150 °C for 4 hours. When monometallic gold nanoparticles were used to make the amide from benzyl alcohol and benzyl

amine, only 45 % of the amide was formed. Incorporating inexpensive metals like Iron, nickel, cobalt nanoparticles led to improved yield and selectivity for amide product formation when compared to monometallic gold nanoparticles. In addition, the ratio of M_1 and M_2 had a huge impact on the selectivity and yield. Gold/cobalt bimetallic nanoparticles (2.36 nm) showed better selectivity and yield compared to gold/iron or gold/nickel nanoparticles.

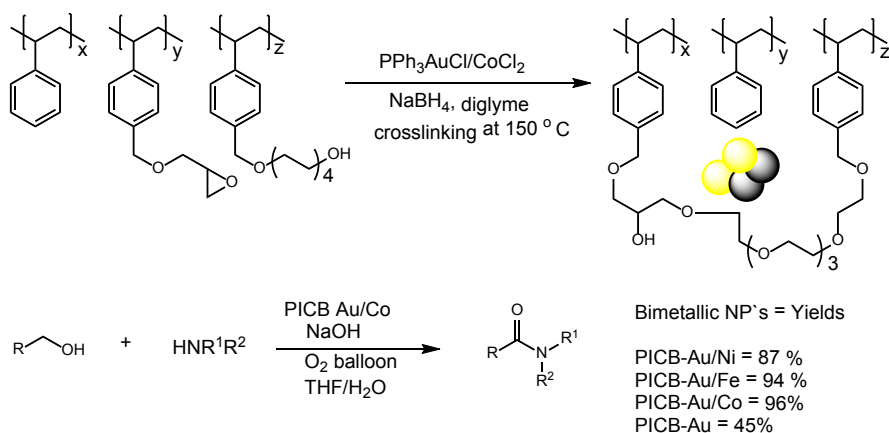


Figure 4.23 Polymer incarcerated (PI) Au/Co NPs for amide synthesis from alcohols and amines.

Kobayashi et al.⁵⁸ also reported the aerobic oxidations of alcohols to form aldehydes, ketones and esters using polymer incarcerated carbon-supported (PICB) bimetallic gold/platinum and gold/palladium nanoparticles (Figure 4.24). The polymer incarcerated bimetallic nanoparticles were prepared by the reducing the corresponding metals salts (PPh_3AuCl , $\text{Na}_2\text{PtCl}_6 \cdot 6\text{H}_2\text{O}$, $\text{Pd}(\text{OAc})_2$ in diglyme using sodium borohydride followed by filtering the precipitate by adding diethyl ether and cross linking the polymer at 150 °C for 4 hours. Under neutral reaction conditions, monometallic polymer incarcerated gold, palladium and platinum nanoparticles did not show any catalytic activity in the aerobic oxidation of alcohols. However, bimetallic gold/platinum nanoparticles showed excellent activity and selectivity for aerobic oxidation of alcohols to aldehydes and ketones in benzotrifluoride/water solvent. Under basic

conditions, alcohols were converted selectively to acids with the same nanoparticle catalysts. With methanol as solvent, alcohols were converted to methyl esters in good yields. Bimetallic gold/palladium nanoparticles did not show any catalytic activity for aerobic oxidation of alcohols under neutral or basic conditions.

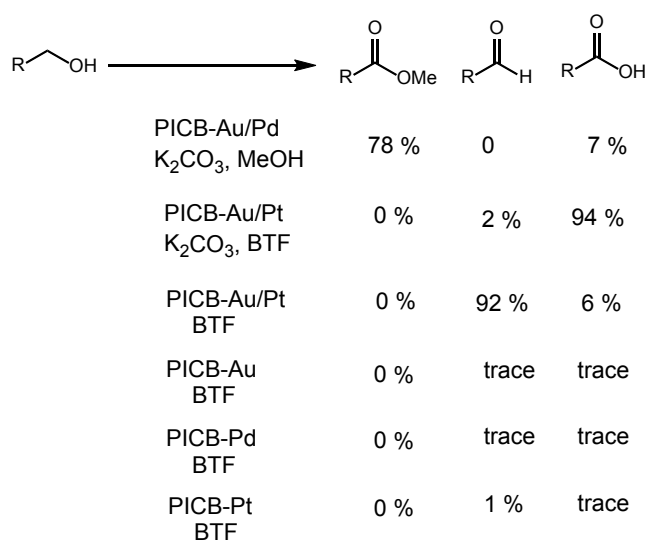


Figure 4.24 Selectivity to different products using bimetallic nanoparticles

4.5 Conclusion and Outlook

Nanoparticle catalysis is now well advanced, with the development of several preparation methods and modern characterization techniques. Nanoparticle catalysts are tunable, recoverable and recyclable catalysts, thereby acting as bridge between homogeneous and heterogeneous catalysis. Several different preparation methods, supports, and stabilizers are available to make metal nanoparticles. Bimetallic nanoparticles are often more efficient than single metal nanoparticles, and the shape of the nanoparticle has huge impact on catalytic activity. Polymer supported nanoparticles have the added advantage over traditional inorganic supports in that the electronic properties of the particle can be tuned by attaching ligand to the polymer, like in homogeneous catalysis.

My work in the Michaelis laboratory has focused on the use of polymer-supported nanoparticle catalysts for the development of highly reactive and selective catalysts for organic synthesis. We are interested in the potential of the polystyrene to act as a tunable ligand capable of tuning catalytic activity and selectivity in catalysts. Several of the examples presented above demonstrated that incorporation of supporting ligands into the polymer structure can be used to vary catalytic activity. In addition, the use of mixed-metal nanoparticles is also a viable strategy for generating highly effective catalysts. In our research, we have focused on the potential to change the steric and electronic structure of the polystyrene itself in order to vary the strength of the metal-polymer interaction. Our hypothesis is that subtle changes to the strength of the interaction between the π -electrons of the polymer and the metal surface can influence catalyst activity and lead to more reactive and selective catalysts.

In our recent first publication on the topic⁶², we showed that both modification of the polystyrene support structure and varying the $M_1:M_2$ ratios in a bimetallic nanoparticle led to enhanced reactivity in nitroarene reductions with ruthenium-cobalt nanoparticle catalysts. This dual optimization approach produced highly active and chemoselective catalysts for nitroarene reductions (Figure 4.25). We also demonstrated for the first time that polymer electronic structure could significantly impact catalyst activity.

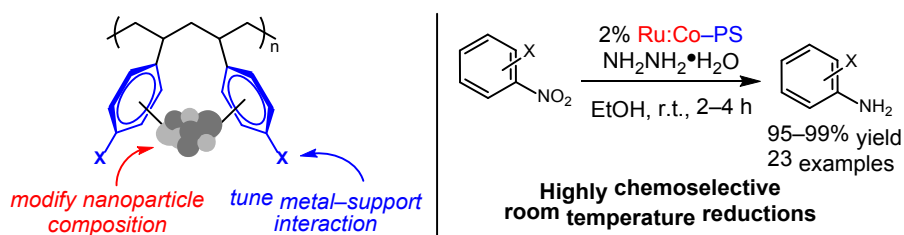


Figure 4.25 *Modifying the nanoparticle composition and tuning the metal-support interaction for nitro reduction*

Further work in our laboratory has demonstrated that highly chemoselective azide reductions can be facilitated by polystyrene-supported ruthenium, even in the presence of highly reactive nitro functional groups. We have also demonstrated that modification of the nanoparticle catalyst activity can lead to selective partial reduction of nitroarenes to provide diarylhydrazine products in high yield (Figure 4.26). These works are currently being prepared for publication.

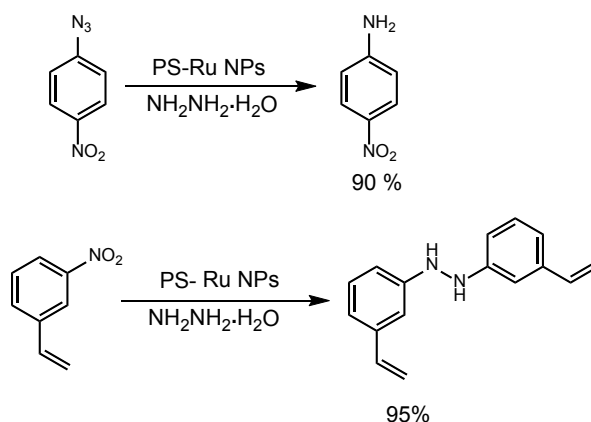


Figure 4.26 *Selective reduction of azides in the presence of nitro group and partial reduction of nitro group to form diarylhydrazine product.*

Although nanoparticle catalysis has emerged as an effective approach to catalyst development, the application of these catalysts to organic synthesis is still in its infancy. The application of nanoparticle catalysts to the synthesis of complex molecules and pharmaceuticals reduce the cost, waste associated with chemical synthesis, while at the same time providing processes with higher efficiency that maintain high levels of selectivity. Thus, the application of nanoparticle catalysis to organic synthesis will continue to be an important research pursuit in the decades to come.

4.6 References

(1) For reviews, see: Na, K.; Zhang, Q.; somorjai, G.A. *J. Cluster. Sci.* **2014**, *25*, 83. (b) Zaera, F. *Chem. Soc. Rev.* **2013**, *42*, 2746. (c) Mondloch, J. E.; Bayram, E.; Finke, R.G. *J. Mol. Catal. A: Chem.* **2012**, *355*, 1. (d) Gates, B.C.; *Chem. Rev.* **1995**, *95*, 511. (e) Copéret, C.; Chabanas, M.; Saint-Arroman, R.P.; Basset, J-M. *Angew. Chem. Int. Ed.* **2003**, *42*, 156. (F) Wieckowski, A.; Savinova, E. R.; Vayenas, C. G. *Catal. Electrocatal. Nano. Surf.* **2003**, 847.

(2) (a) *Transition-metal Nanoparticles in Catalysis: From Historical Background to the State-of-the Art*, (Prof. Dr. Didier Astruc), Wiley, 2008. (b) *Homogeneous Transition Metal Catalyzed Reaction*, (Moser, W.R.; Slocum, D.W.) American Chemical Society, 1992.

(3) For recent reviews on transition - metal NP - catalyzed reactions, see: Astruc, D.; Lu, F.; Aranzaes, R.J.; *Angew. Chem. Int. Ed.* **2005**, *44*, 7399. (b) De-Vries, G. J. *Dalton Trans.* **2006**, 421. (c) Astruc, D. *Inorg. Chem.* **2007**, *46*, 1884. (d) Schmid, G. *Chem. Rev.* **1992**, *92*, 1709; (e) Lewis, L.N. *Chem. Rev.* **1993**, *93*, 2693.

(4) Konova, P.; Naydenov, A.; Venkov, Cv.; Mehandjiev, D.; Andreeva, D.; Tabakova, T. *J. Mol. Catal. A: Chem.*, **2004**, *213*, 235. (b) Ishiguro, A.; Nakajima, T.; Iwata, T.; Fujita, M.; Minato, T.; Kiyotaki, F.; Izumi, Y.; Aika, K.; Uchida, M.; Kimoto, K.; Matsui, Y.; Wakatsuki, Y. *Chem. Eur. J.* **2002**, *8*, 3260. (c) Ingelsten, H. H.; Beziat, J.; Bergkvist, K.; Palmqvist, A.; Skoglundh, M.; Hu, Q.; Falk, L. K. L.; Holmberg, K. *Langmuir*, **2002**, *18*, 1811. (d) Liu, Z.; Lee, J. Y.; Chen, W.; Han, M.; Gan, L. M. *Langmuir*, **2004**, *20*, 181.

(5) Xiang, Y.; Kong, L.; Xie, P.; Xu, T.; Wang, J.; Li, X. *Ind. Eng. Chem. Res.*, **2014**, *53*, 2197. (b) Crooks, R.M.; Zhao, M.; Sun, L.; Chechik, V.; Yeung, L.K. *Acc. Chem. Res.*, **2001**, *34*, 181.

- (c) Kralik, M.; Biffis, A. *J. Mol. Catal. A: Chem.* **2001**, *177*, 113. (d) Chen, C.-W.; Chen, M.-Q.; Serizawa, T.; Akashi, M. *Chem. Commun.* **1998**, 831.
- (6) Koh, T.; Koo, H.M.; Yu, T.; Lim, B.; Bae, J.W. *ACS Catal.* **2014**, *4*, 1054. (b) Wan, H.; Wu, B.; Xiang, H.; Li, Y. *ACS Catal.*, **2012**, *2*, 1877. (c) Munnik, p.; Krans, N.A.; Jongh, P.E.; Jong, K.P. *ACS Catal.*, **2014**, *4*, 3219.
- (7) Zhao, M.; Sun, L.; Crooks, R. M. *J. Am. Chem. Soc.* **1998**, *120*, 4877. (b) Zhao, M.; Crooks, R. M. *Angew. Chem., Int. Ed.* **1999**, *38*, 364. (c) Schulz, J.; Roucoux, A.; Patin, H., *Chem. Eur. J.* **2000**, *6*, 618.
- (8) Ahmadi, T. S.; Wang, Z. L.; Green, T. C.; Henglein, A.; El-Sayed, M. A. *Science*, **1996**, *272*, 1924. (b) Aiken, J. D., III; Finke, R. G. *J. Am. Chem. Soc.* **1999**, *121*, 8803. (c) Ohde, H.; Wai, C. M.; Kim, H.; Kim, J., Ohde, M. *J. Am. Chem. Soc.* **2002**, *124*, 4540. (d) Henglein, A. *J. Phys. Chem. B*, **2000**, *104*, 2201.
- (9) Li, Y.; Hong, X. M.; Collard, D. M.; El-Sayed, M. A. *Org. Lett.* **2000**, *2*, 2385. (b) Narayanan, R.; El-Sayed, M. A. *J. Am. Chem. Soc.* **2003**, *125*, 8340. (c) Chen, C. W.; Akashi, M., *Langmuir*, **1997**, *13*, 6465. (d) Narayanan, R.; El-Sayed, M. A. *J. Phys. Chem. B*, **2003**, *107*, 12416.
- (10) Demir, M. M.; Gulgun, M. A.; Menciloglu, Y. Z.; Erman, B.; Abramchuk, S. S.; Makhaeva, E. E.; Khokhlov, A. R.; Matveeva, V. G.; Sulman, M. G. *Macromol.* **2004**, *37*, 1787. (b) Wu, S. H.; Chen, D.H., *Chem. Lett.* **2004**, *33*, 406. (c) Wu, S. H.; Chen, D.H., *J. Coll. Interf. Sci.* **2003**, *259*, 282.

- (11) Harriman, A.; Thomas, J. M.; Millward, G. R. *New J. Chem.* **1987**, *11*, 757. (b) Bastús, N.G.; Comenge, J.; Puentes, V. *Langmuir*, **2011**, *27*, 11098.
- (12) Zhou, X.; Xu, W.; Liu, G.; Panda, D.; Chen, P. *J. Am. Chem. Soc.*, **2010**, *132*, 138. (b) Isaifan, R.J.; Ntais, S.J.; Baranova, E.A. *Applied Catalysis A: General*, 2013, 464-465, 87. (c) Laoufi, Saint-Lager, M-C.; Lazzari, R.; Jupille, J.; Robach, O.; Garaudée, S.; Cabailh, G.; Dolle, P.; Cruguel, H.; Bailly, A. *J. Phys. Chem. C*, **2011**, *115*, 4673. (d) Rhee, C.K.; Kim, B-J.; Ham, C.; Kim, Y-J.; Song, K.; Kwon, K. *Langmuir*, **2009**, *25*, 7140.
- (13) Valden, M.; Pak, S.; Lai, X.; Goodman, .W. *Catalysis letters*, **1998**, *56*, 7.
- (14) Tsung, C-K.; Kuhn, J.N.; Huang, W.; Aliaga, C.; Hung, L-I.; Somorjai, G.A.; Yang, P. *J. Am. Chem. Soc.* **2009**, *131*, 5816.
- (15) Gangula, A.; Podila, R.; Ramakrishna, M.; Karanam, L.; Janardhana, C.; Rao, A.M. *Langmuir*, **2011**, *27*, 15268.
- (16) Mustafa, S.; Behafarid, F.; Croy, J.R.; Ono, L.K.; Li, L.; Yang, J.C.; Frenkel, A.I.; Roldan-Cuenya, B. *J. Am. Chem. Soc.* **2010**, *132*, 15714.
- (17) Xiong, Y.; Wiley, B.J.; Xia, Y. *Angew. Chem., Int. Ed.* **2007**, *46*, 7157. (b) Li, Y.; Liu, Q.; Shen, W. *Dalton Trans.* **2011**, *40*, 5811.
- (18) Collins, G.; Schmidt, M.; Dwyer, C. O.; Holmes, J.D.; McGlacken, G.P. *Angew. Chem. Int. Ed.* **2014**, *53*, 4142.
- (19) Narayanan, R.; El-Sayed, M.A. *J. Phys. Chem. B*, **2005**, *109*, 12663. (b) Thathagar, M.B.; Beckers, J.; Rothenberg, G. *J. Am. Chem. Soc.* **2002**, *124*, 11858.

(20) Miyamura, H.; Yasukawa, T.; Kobayashi, S. *Green Chem.* **2010**, *12*, 776. (b) Lucchesi, C.; Inasaki, T.; Miyamura, H.; Matsubara, R.; Kobayashi, S. *Adv. Synth. Catal.* **2008**, *350*, 1996. (c) Miyamura, H.; Matsubara, R.; Miyazaki, Y.; Kobayashi, S. *Angew. Chem., Int. Ed.* **2007**, *46*, 4151.

(21) Tsunoyama, H.; Sakurai, H.; Negishi, Y.; Tsukuda, T. *J. Am. Chem. Soc.* **2005**, *127*, 9374. (b) Tsunoyama, H.; Ichikuni, N.; Sakurai, N.; Tsukuda, T. *J. Am. Chem. Soc.* **2009**, *131*, 7086. (c) Tsunoyama, H.; Sakurai, H.; Ichikuni, N.; Negishi, Y.; Tsukuda, T. *Langmuir*, **2004**, *20*, 11293. (d) Mertens, P.G.N.; Vandezande, P.; Ye, X.; Poelman, H.; Vankelecom, I.F.J.; De Vos, D.E. *Appl. Catal. A*, **2009**, *355*, 176.

(22) Biondi, I.; Laurency, G.; Dyson, P.J. *Inorg. Chem.* **2011**, *50*, 8038. (b) Shan, C.; Li, F.; Yuan, F.; Yang, G.; Niu, L.; Zhang, Q. *Nanotechnology*, **2008**, *19*, 285601.

(23) Ananth, A.N.; Daniel, S. C.; Sironmani, T.A.; Umapathi, S. *Colloids Surf B Biointerfaces*. **2011**, *85*, 138.

(24) Chen, M.; Wang, L-Y.; Han, J-T.; Zhang, J-H.; Li, Z-Y.; Qian, D-J. *J. Phys. Chem. B*, **2006**, *110*, 11224. (b) Pal, A.; Shah, S.; Chakraborty, D.; Devi, S. *Aust. J. Chem*, **2008**, *61*, 833.

25) Wang, T.; Aili, D.; Selegård, R.; Tay, Y.; Baltzer, L.; Zhang, H.; Liedberg, B. *J. Mater. Chem.* **2012**, *22*, 20368. (b) Fenger, R.; Fertitta, E.; Kirmse, H.; Thünemann, A.F.; Rademann, K. *Phys. Chem. Chem. Phys.* **2012**, *14*, 9343. Lin, Y.; Finke, R. G. *J. Am. Chem. Soc.* **1994**, *116*, 8335.

(26) Sun, S.U.; Jang, Y.; Yoon, K.Y.; Kang, E.; Hyeon, T. *Nano Lett.* **2004**, *4*, 1147. (b) Tamura, M.; Fujihara, H. *J. Am. Chem. Soc.* **2003**, *125*, 15742. (c) Tatumi, R.; Akita, T.; Fujihara, H. *Chem. Comm.* **2006**, *31*, 3349.

27) Esumi, K.; Isono, R.; Yoshimura, T. *Langmuir*, **2004**, *20*, 237. (b) Scott, Robert W. J.; Datye, Abhaya K.; Crooks, Richard M., *J. Am. Chem. Soc.* **2003**, *125*, 3708. (c) Rahim, E. H.; Kamounah, F. S.; Frederiksen, J.; Christensen, J. B., *Nano Lett.* **2001**, *1*, 499.

(28) For reviews, see: Akiyama, R.; Kobayashi, S. *Chem. Rev.* **2009**, *109*, 594. (b) Kaizuka, K.; Miyamura, H.; Kobayashi, S. *J. Am. Chem. Soc.* **2010**, *132*, 15096.

(29) Liu, Z.; Lee, J. Y.; Chen, W.; Han, M.; Gan, L. M. *Langmuir*, **2004**, *20*, 181. (b) Liu, Z.; Ling, X. Y.; Lee, J. Y.; Su, X.; Gan, L. M., *J. Mat. Chem.* **2003**, *13*, 3049. (c) Nakagawa, K.; Yamagishi, M.; Nishimoto, H.; Ikenaga, N.; Suzuki, T.; Kobayashi, T.; Nishitani-Gamo, M.; Ando, T. *Chem. Mat.*, **2003**, *15*, 4571. (d) . Khodakov, A. Y.; Bechara, R.; Griboval-Constant, A., *Appl. Catal. A: Gen.* **2003**, *254*, 273 (e) Yang, C.; Kalwei, M.; Schuth, F.; Chao, K., *Appl. Catal. A: Gen.* **2003**, *254*, 289.

(30) Boudjahem, A. G.; Monteverdi, S.; Mercy, M.; Bettahar, M. M. *J. Catal.* **2004**, *221*, 325. (b) Horvath, A.; Beck, A.; Koppány, Z.; Sarkány, A.; Gucci, L., *J. Mol. Catal. A: Chem.* **2002**, *182-183*, 295.

(31) Lang, H.; May, R. A.; Iversen, B. L.; Chandler, B. D., *J. Am. Chem. Soc.* **2003**, *125*, 14832. (b) Yang, C.; Kalwei, M.; Schuth, F.; Chao, K., *Appl. Catal. A: Gen.* **2003**, *254*, 289.

(32) Tsukamoto, D.; Shiraishi, Y.; Sugano, Y.; Ichikawa, S.; Tanaka, S.; Hirai, T. *J. Am. Chem. Soc.* **2012**, *134* 6309.

- (33) Balint, I.; Miyazaki, A.; Aika, K., *Phys. Chem. Chem. Phys.* **2004**, *6*, 2000.
- (34) Zhu, H.; Ke, X.; Yang, X.; Sarina, S.; Liu, H. *Angew. Chem. Int. Ed.* **2010**, *49*, 9657. (b) Vasilikogiannaki, E.; Gryparis, C.; Kotzabasaki, V.; Lykakis, L. N.; Stratakisa, M. *Adv. Synth. Catal.* **2013**, *355*, 907.
- (35) Pittelkow, M.; Moth-Poulsen, K.; Boas, U.; Christensen, J. B., *Langmuir*, **2003**, *19*, 7682.
- (b) Li, Y.; El-Sayed, M.A., *J. Phys. Chem. B.* **2001**, *105*, 8938. (c) Gopidas, K. R.; Whitesell, J. K.; Fox, M. A., *Nano Lett.* **2003**, *3*, 1757.
- (36) Khodakov, A. Y.; Bechara, R.; Griboval-Constant, A., *Appl. Catal. A: Gen.* **2003**, *254*, 273.
- (37) Obrey, S. J.; Barron, A. R. *Macromolecules*, **2002**, *35*, 1499. (b) Mishra, D. K.; Dabbawala, A. A.; Hwang, J-S. *Catalysis Communications*, **2013**, *41*, 52. (c) Sulman, E.; Bodrova, Yu.; Matveeva, V.; Semagina, N.; Cervený, L.; Kurte, V.; Bronstein, L.; Platonova, O.; and Valetsky, P.; *Appl. Catal. A: General*, **1999**, *75*, 176. (d) Ornelas, C.; Diallo, A. K.; Ruiz, J.; Astruca, D. *Adv. Synth. Catal.* **2009**, *351*, 2147.
- (38) Tsunoyama, H.; Sakurai, H.; Negishi, Y.; Tsukuda, T. *J. Am. Chem. Soc.* **2005**, *127*, 9374.
- (39) Biondi, I.; Laurency, G.; Dyson, P.J. *Inorg. Chem.* **2011**, *50*, 8038.
- (40) Villa, A.; Wang, D.; Su, D.S.; Prati, L. *ChemCatChem.* **2009**, *1*, 510. (b) Prati, L.; Spontoni, P.; Gaiassi, A. *Top. Catal.* **2009**, *52*, 288.
- (41) Li, Y.; Hong, X.M.; Collard, D.M.; El-Sayed, M. A. *Org. Lett.* **2000**, *2*, 2385.
- (42) Sawai, K.; Tatumi, R.; Nakahodo, T.; Fujihara, H. *Angew. Chem. Int. Ed.* **2008**, *47*, 6917.
- (43) Reetza, M.T.; de Vries, G.J. *Chem. Comm.* **2004**, 1559.

- (44) Pieters, G.; Taglang, C.; Bonnefille, E.; Gutmann, T.; Puente, C.; Berthet, J-C.; Dugave, C.; Chaudret, B.; Rousseau B. *Angew. Chem. Int. Ed.* **2014**, *53*, 230.
- (45) Gonzalez-Galvez, D.; Nolis, P.; Philippot, K.; Chaudret, B.; van Leeuwen, P. W. N. M. *ACS Catal.* **2012**, *2*, 317.
- (46) Peng, X.; Cheng, K.; Kang, J.; Gu, B.; Yu, X.; Zhang, Q.; Wang, Y. *Angew. Chem. Int. Ed.* **2015**, *54*, 4553. (b) Kang, J.; Cheng, K.; Zhang, L.; Zhang, Q.; Ding, J.; Hua, W.; Lou, Y.; Zhai, Q.; Wang, Y. *Angew. Chem. Int. Ed.* **2011**, *50*, 5200.
- (47) Witham, C.A.; Huang, W.; Tsung, C-K.; Kuhn, J.N.; Somorjai G. A.; Toste, D.F. *Nature Chemistry*, **2010**, *2*, 36.
- (48) Cong, H.; Becker, C. F.; Elliott, S.J.; Grinstaff, M. W.; Porco, Jr, J. A. *J. Am. Chem. Soc.* **2010**, *132*, 7514.
- (49) Tsukamoto, D.; Shiraishi, Y.; Sugano, Y.; Ichikawa, S.; Tanaka, S.; Hirai, T. *J. Am. Chem. Soc.* **2012**, *134* 6309.
- (50) Groppo, E.; Agostini, G.; Borfecchia, E.; Wei, L.; Giannici, F.; Portale, G.; Longo, A.; Lamberti, C. J. *Phys. Chem. C* **2014**, *118*, 8406.
- (51) Nakazawa, M.; Somorjai, G. A. *Appl. Surf. Sci.* **1993**, *68*, 517. (b) Kumar, A.; Mandal, S.; Mathew, S. P.; Selvakannan, P.R.; Mandale, A. B.; Chaudhari, R. V.; Sastry, M. *Langmuir* **2002**, *18*, 6478. (c) Ramanath, G.; DKArcy-Gall, J.; Maddaninath, T.; Ellis, A. V.; Ganesan, P. G.; Goswami, R.; Kumar, A.; Vijayamohanan, K.; *Langmuir* **2004**, *20*, 5583.
- (52) Miyamura, H.; Matsubara, R.; Miyazaki, Y.; Kobayashi, S. *Angew. Chem. Int. Ed.* **2007**, *46*, 4151.

- (53) Okamoto, K.; Akiyama, R.; Kobayashi, S. *Org. Lett.* **2004**, *6*, 1987. (b) Nishio, R.; Sugiura, M.; Kobayashi, S. *Org. Lett.* **2005**, *7*, 4831.
- (54) Soule, J-F.; Miyamura, H.; Kobayashi, S. *J. Am. Chem. Soc.* **2013**, *135*, 10602.
- (55) Han, J.; Liu, Y.; Guo, R. *J. Am. Chem. Soc.* **2009**, *131*, 2060.
- (56) Gallon, B. J.; Kojima, R. W.; Kaner, R. B.; Diaconescu, P.L. *Angew. Chem. Int. Ed.* **2007**, *46*, 7251.
- (57) Soule, J-F.; Miyamura, H.; Kobayashi, S. *J. Am. Chem. Soc.* **2011**, *133*, 18550.
- (58) Kaizuka, K.; Miyamura, H.; Kobayashi, S. *J. Am. Chem. Soc.* **2010**, *132*, 15096.
- (59) Murawala, P.; Tirmale, A.; Shiras, A.; Prasad, B. L. V. *Mater. Sci. Eng. C* **2014**, *34*, 158. (b) Sun, X.; Zhang, G.; Keynton, R. S.; O'Toole, M. G.; Patel, D.; Gobin, A. M. *Nanomed: Nanotech. Biol Med.* **2013**, *9*, 1214.
- (60) Shi, D.; Faria, A. J.; Rownaghi, A. A.; Huhnke, R. L.; Resasco, D. E. *Energy Fuels*, **2013**, *27*, 6118. (b) Zhu, Y.; Ye, Y.; Zhang, S.; Leong, M. E.; Tao, F. *Langmuir*, **2012**, *28*, 8275. (c) Yu, G.; Sun, B.; Pei, Y.; Xie, S.; Yan, S.; Qiao, M.; Fan, K.; Zhang, X.; Zong, B. *J. Am. Chem. Soc.* **2010**, *132*, 935. (d) Calderone, V. R.; Shiju, N. R.; Chambrey, S.; Curulla-Ferre, D.; Chambrey, S.; Khodakov, A.; Rose, A.; Thiessen, J.; Jess, A.; Rothenberg, G. *Angew. Chem. Int. Ed.* **2013**, *52*, 4397.
- (61) Haruta, M. *Catal. Today*, **1997**, *36*, 153.
- (62) Udumula, V.; Tyler, J.H.; Davis, D.A.; Wang, H.; Linford, M. R.; Minson, P. S.; Michaelis, D.J. *ACS Catal.* **2015**, *5*, 3457.

(63) Cookson, J.; *Platinum Metals Rev.* 2012, 56, 83–98

Chapter-5

A Dual Nanoparticle Approach to Bimetallic Nanoparticle Catalysis: Impact of $M_1:M_2$ Ratio and Supporting Polymer on Reactivity in Nitroarene Reductions

5.1 Introduction

The development of highly reactive, tunable, recoverable, and recyclable heterogeneous nanoparticle catalysts has the potential to make a significant impact in organic synthesis.¹ The challenge associated with traditional heterogeneous catalysts is the difficulty of designing catalysts that are highly reactive and at the same time selective. Nanoparticle catalysts could potentially address this challenge because of the ability to modify nanoparticle reactivity and selectivity by varying the properties of the nanoparticle support. Inorganic supports such as metal oxides (TiO_2 , Al_2O_3 , CeO_2 , ZrO_2) and porous zeolites are commonly used for supporting metal nanoparticles, which help control the nanoparticle size and agglomeration state.² While modifications to these inorganic supports can impact catalytic activity, it is often difficult to predict how these modifications will impact catalysis.

Recent developments in the synthesis of polymer-supported nanoparticle catalysts has demonstrated that organic polymers can be used to control nanoparticle size and reactivity. Our group is interested in the potential of polymer supports to tune the reactivity of supported nanoparticles via formation of metal-polymer interactions. Our main objective is to develop nanoparticle catalysts where reactivity and selectivity can be controlled by modifying the electronic and steric properties of the polymer support. In this chapter, we will discuss the development of polystyrene-supported bimetallic ruthenium-cobalt nanoparticles for nitroarene

reductions where the electronic properties of the polymer support are shown to influence catalyst activity in a predictable way.

Several literature reports demonstrate that variations to a nanoparticle support material can affect the size, shape, and electronic state of the metal nanoparticles, thereby effecting the catalytic activity.³ Somorjai et al.⁴ reported the preparation of platinum nanoparticles of uniform size on mesoporous SiO₂, CeO₂, MnO₂, Fe₂O₃, NiO and Co₃O₄ supports for methanol oxidation. They found that the Pt/MnO₂ catalyst was 135 times less active and the Pt/CeO₂ catalyst was 12 times more active than Pt/SiO₂. Song et al.⁵ reported the preparation of platinum nanoparticles supported on CeO₂, Nb₂O₅, TiO₂ and SiO₂ having uniform size. These nanoparticle supported on different metal oxides were tested for activity in the carbon monoxide oxidation reaction. The catalytic activity showed the general trend of CeO₂ > Nb₂O₅ > TiO₂ > SiO₂. Ebatani et al.⁶ reported the preparation of hydrotalcite-supported platinum nanoparticles for aerobic oxidations using starch, Polyvinylpyrrolidone and polyvinyl alcohol as stabilizers to generate nanoparticles with uniform particle size (Figure 5.1). These nanoparticles were then tested in the oxidation of 1, 2-propanediol to lactic acid. Nanoparticles stabilized using starch showed better catalytic activity than polyvinyl alcohol, and polyvinyl alcohol showed better catalytic activity compared to polyvinyl pyrrolidone. The authors reasoned that the starch-stabilized nanoparticles showed better catalytic activity because of an increased number of free hydroxyl groups that can donate electrons to the platinum nanoparticles. This enhanced donation makes oxygen activation more efficient and enhances the catalytic activity (Figure 5.1). These results show that interactions between the metal nanoparticle and the inorganic support or the polymer stabilizer can be used to enhance the catalytic activity of metal nanoparticles.

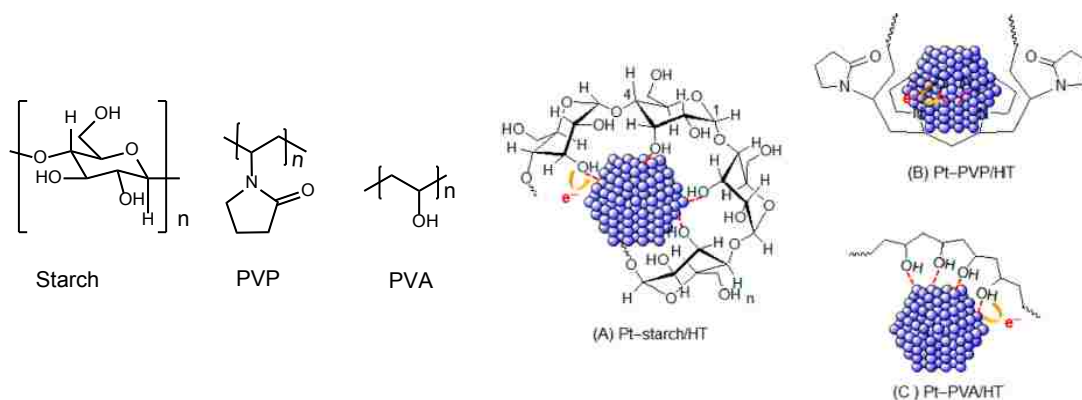


Figure 5.1 Possible electron donations from polymers to platinum nanoparticles

The Kobayashi laboratory recently reported a strategy for developing polymer-stabilized metal nanoparticle catalysts. In these catalysts, the catalytic activity and selectivity of the polymer supported nanoparticle can be optimized by incorporating supporting ligands into the polymer structure,⁷ or by formation of bimetallic nanoparticle catalysts.⁸ Formation of mixed-metal nanoparticle catalysts is a widely used approach in nanoparticle catalysis, where the second metal can either enhance the catalytic activity or change the selectivity of a reaction by changing the electronic properties or the crystal structure of the first metal.⁹ In traditional polymer-supported nanoparticle catalysis, polymers are used as supports to control the size and prevent aggregation and precipitation of the metal nanoparticles. The polymer is also used to facilitate recovery and recycling of the catalyst. In our laboratory, we are interested in developing tunable polymer-supported nanoparticle catalysts where modification to the structure and electronic properties of the polymers can be used to enhance catalytic activity and selectivity. The ability to tune nanoparticle catalysts in predictable ways would mimic ligand optimization in homogeneous transition metal catalysis where electronic properties of the metal can be tuned by ligand modification¹³. The ability to predictably tune nanoparticle catalysts would greatly enhance the

utility of nanoparticle catalysts and accelerate the development of highly reactive and selective heterogeneous catalysts for organic synthesis.

In this section we will discuss the development of polystyrene-supported Ru-Co bimetallic nanoparticles as catalysts for nitroarene reductions. We will present a dual optimization approach where modification of the bimetallic nanoparticle composition ($M_1:M_2$ ratio) and the electronic properties of the supporting polymer generate exceptional catalysts for room temperature nitroarene reductions with hydrazine hydrate. (Figure 5.2). We will demonstrate that variation of the electronic character of the aryl rings on the polymer support via incorporation of electron-donating and electron-withdrawing substituents can lead to predictable changes in catalytic activity.¹⁴ We will also show that the polymer structure can affect not only the rate of nitroarene reductions, but can also influence the mechanism of the reaction. To the best of our knowledge, this is the first example of using the electronic properties of a polystyrene polymer to influence the activity of the nanoparticle catalysts in a predictable way.

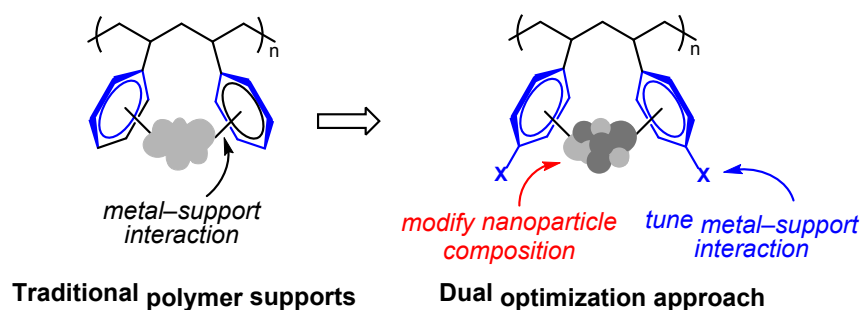


Figure 5.2 *Polymer supported nanoparticle catalysts*

The chemoselective reduction of nitro compounds to amines is an important reaction for the preparation of pharmaceuticals, pesticides and dyes.¹⁰ Nanoparticle-catalyzed reductions represent a particularly attractive approach to aniline formation because the catalysts exhibit

exceptional reactivity, are easily recovered after the reaction, and can often be recycled.¹⁴ While a variety of nanoparticle catalysts have been developed for nitroarene reductions, these methods suffer from several drawbacks, including low yields, high reaction temperatures, and a lack of functional group tolerance. The nitro reduction reaction was selected as a model reaction for our polymer optimization studies due to importance of this reaction in the synthesis of pharmaceutically important compounds. An important aspect of these studies is the modification of polymer structure to generate highly selective catalyst for nitroarene reductions to anilines that proceed in the presence of easily reducible functional groups¹⁵. The main objective of this work is to prepare inexpensive, easily synthesized and recyclable catalyst for nitroreductions at room temperature¹⁶.

5.2 Results and Discussion

5.2.1 Catalyst Optimization Studies

We first prepared monometallic ruthenium (Ru) nanoparticles supported on polystyrene for nitroarene reductions. The nanoparticles were prepared according to a reported procedure using sodium borohydride as the reducing agent and in the presence of a homogeneous solution of polystyrene (MW 35,000) (Figure 5.3)¹⁷. The polymer-supported nanoparticles were then precipitated from solution, washed with deionized water to remove salts and unsupported nanoparticles, and dried under vacuum. The black powder obtained through this process can be easily recovered from the reaction mixture by simple filtration. Bimetallic nanoparticle catalysts were also synthesized via this method by addition of the reducing agent to a homogeneous solution containing both metal salts.

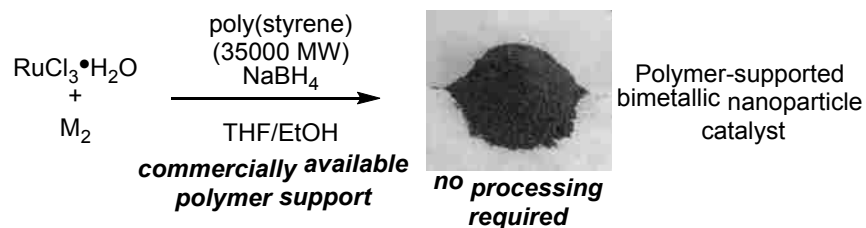
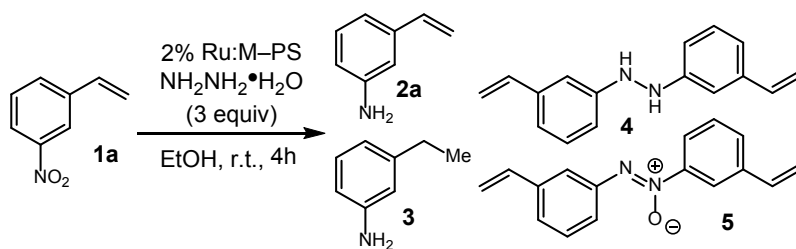


Figure 5.3 *Synthesis of bimetallic nanoparticle catalysts*

The ruthenium nanoparticle catalyst was first tested for catalytic activity in the chemoselective reduction of 3-nitrostyrene with hydrazine hydrate as the stoichiometric reductant (Table 5.1). The monometallic ruthenium nanoparticles showed good chemoselectivity for reduction of the nitro functional group in the presence of the easily reduced olefin. However, the yield of the transformation was low because of the formation of partially reduced byproducts (entry 1). We next explored the potential of bimetallic Ru-M nanoparticles to increase the catalytic activity and chemoselectivity through metal-metal cooperativity (entries 2–5)⁸. While incorporation of copper and nickel did not improve the catalytic activity of the nanoparticles, both iron and cobalt provided nanoparticles with enhanced reactivity (entries 4 and 5). At this stage, we decided to focus our optimization studies on Ru-Co bimetallic nanoparticles because Ru-Fe bimetallic nanoparticles provided lower selectivity with a variety of substrates (see experimental section). We next investigated the impact of the Ru to Co ratio in the nanoparticle on catalytic activity. These studies showed that a higher percentage of ruthenium to cobalt was beneficial for obtaining a highly active catalyst when the loading of ruthenium was held constant in the reaction at 2 mol% (Table 1, entries 5–9). The Ru-Co bimetallic catalysts (5.1 %_(81Ru19Co)/PS) is among the most active nanoparticle catalysts for nitroarene reductions, leading to complete and selective reduction of the nitro functionality in just 2 hours at room temperature.

Table 5.1 Catalyst Optimization Studies

entry ^a	catalyst	catalyst composition ^{b,c}	% conv. ^d	selectivity (2:3:4:5) ^c
1	Ru	6.7%(₁₀₀ Ru)/PS	100	60:0:18:22
2	Ru : Cu	5.4%(₅₁ Ru ₄₉ Cu)/PS	100	63:4:32:1
3	Ru : Ni	6.7%(₄₄ Ru ₅₆ Ni)/PS	100	41:2:32:25
4	Ru : Fe	7.0%(₂₄ Ru ₇₆ Fe)/PS	100	95:4:0:1
5	Ru : Co	5.6%(₄₆ Ru ₅₄ Co)/PS	100	83:14:0:3
6	Ru : Co	3.6%(₆₁ Ru ₃₉ Co)/PS	100	28:10:14:48
7	Ru : Co	5.7%(₃₅ Ru ₆₅ Co)/PS	100	45:8:0:47
8	Ru : Co	7.8%(₂₃ Ru ₇₇ Co)/PS	100	17:8:25:50
9	Ru : Co	5.1%(₈₁ Ru ₁₉ Co)/PS	100	97:3:0:0

^a Reactions conditions: **1a** (0.4 mmol), catalyst (2 mol% wrt Ru), and $\text{NH}_2\text{NH}_2 \cdot \text{H}_2\text{O}$ (3 equiv) in EtOH at room temp. ^b Catalyst composition represented as $n\%(xM1yM2)/\text{support}$, where n is total wt% metals in support, and x and y are the relative wt% of M1 and M2. ^c Metal ratios determined by ICP analysis (see supporting information). ^d Determined by ^1H NMR analysis of the crude reaction mixture. PS = polystyrene, MW 35,000.

After optimizing the Ru:Co bimetallic catalyst, we next studied the substrate scope and chemoselectivity with various substrates containing easily reduced functional groups (Figure 5.4). We showed that efficient and selective reductions can be performed in the presence of alkenes, stilbenes, allyl ethers, alkynes, propargyl ethers, halides, nitriles, phenols, carboxylic acids and ketones. Nitro groups on heteroaromatic compounds can also be easily reduced with Ru-Co bimetallic compounds. Each of these reactions was performed on 0.4 mmol scale with 2 mol% Ru

loading (2.5:1 Ru:Co in polystyrene), and $\text{NH}_2\text{NH}_2 \cdot \text{H}_2\text{O}$ (3 equiv) in ethanol (2 mL) at room temperature. The typical reaction time for this reduction was about 2 hours. In all the cases tested, the products were isolated in near quantitative yield by simply removing the catalyst by filtration and then evaporating the solvent. No chromatography was needed due to the high purity of the crude aniline products.

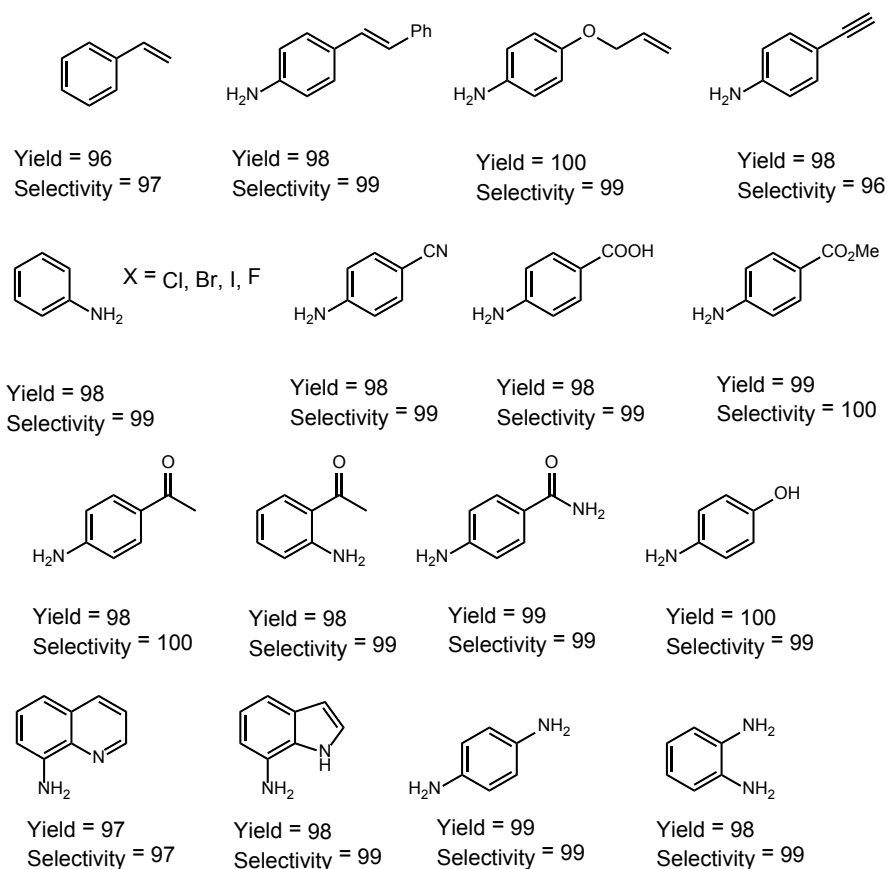
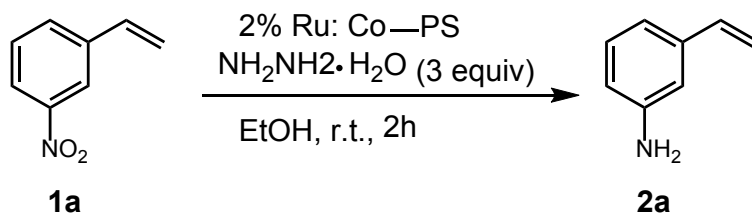


Figure 5.4 *Substrate Scope of Nitroarene Reduction*

5.2.2 Recyclability studies

We next studied whether the heterogeneous polystyrene supported Ru:Co nanoparticles could be recycled without loss of activity. We found that our nanoparticle catalysts could be recycled various times by simply filtering off the reaction mixture, washing the heterogeneous

catalyst with ethanol, and then re-adding reagents for the subsequent reaction. No catalyst reactivation step was required. We also found that our catalysts could be reused up to five times without significant loss in product yield or reaction chemoselectivity (Scheme 5.1).



	Run 1	Run 2	Run 3	Run 4
yield/selectivity	99/97	99/96	98/97	96/96

Reactions conditions: 1a (0.4 mmol), catalyst (2 mol% wrt Ru, 2.5:1 Ru:Co), and NH₂NH₂•H₂O (3 equiv) in ethanol at room temp.

Scheme 5.1 Catalyst Recyclability Studies

5.2.3 Leaching Studies

We next investigated the leaching of Ru-Co bimetallic nanoparticles into solution to see if the reaction was catalyzed by homogeneous nanoparticles that leached from the polymer matrix. The reaction mixture was filtered off after completion of the reduction and the metal content of the filtered solution was determined by ICP-MS analysis. We found that 1.2 % of the ruthenium and 1.3 % of the cobalt nanoparticles (with respect to original catalyst added) was leached out into the reaction mixture from the polymer matrix. We also removed the catalyst from the reaction after partial conversion by filtering through a sintered glass funnel. After removal of the catalyst, no further conversion of the starting material (monitored by NMR) was observed (Figure 5.5). When the catalyst was added back to the reaction mixture after several hours the reduction reaction resumed (similar to Cat-in-a-Cup test)¹⁸. These results suggest that heterogeneous

polymer supported nanoparticles are responsible for the observed catalysis and not homogeneous metal nanoparticles that have leached from the polymer matrix.

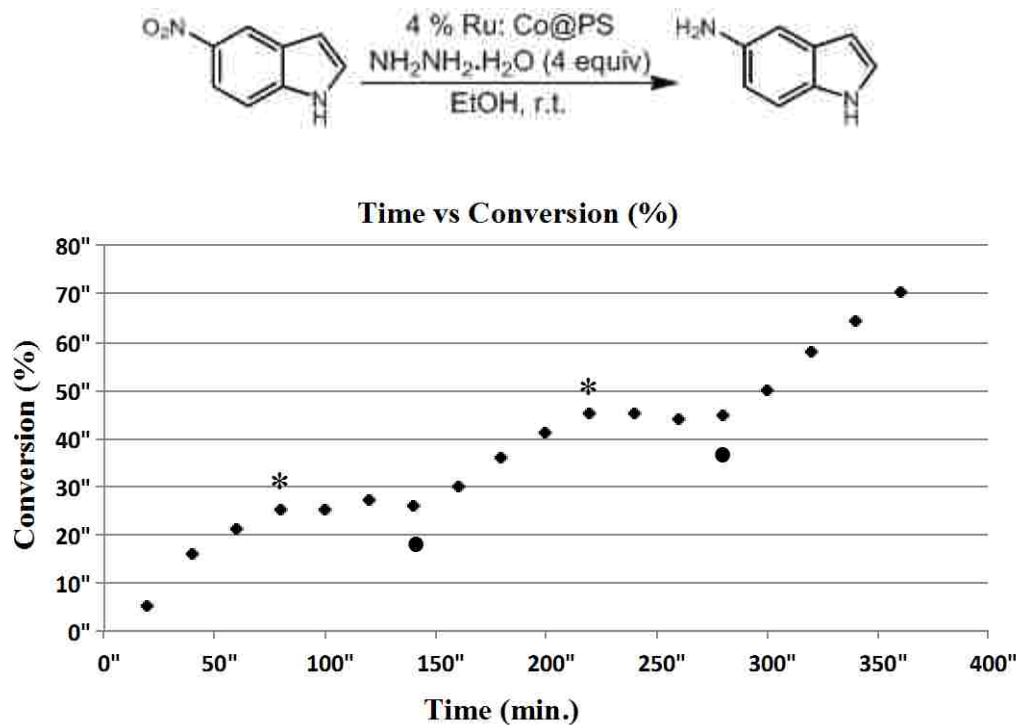


Figure 5.5 Test for homogeneous nanoparticles. Catalyst was removed by filtration at time points indicated with *. Catalyst was added back to the reaction mixture at time points indicated by ●.

5.2.4 Effect of Polymer Structure on Catalyst Activity

We next studied the effect of the polymer structure on the rate and selectivity of the Ru-Co bimetallic nanoparticle catalysts. Previous reports suggest that metal nanoparticles supported by polystyrene polymers are stabilized by weak interactions with the π -electrons of the benzene rings of the polymer¹⁹. We hypothesized that these weak interactions could be tuned by changing the electronic properties of the aromatic rings. To test our hypothesis, we synthesized several polymers containing electron-donating and electron-withdrawing substituents as supports for Ru-Co bimetallic nanoparticles. We found that these variations had a dramatic effect on the catalytic activity of Ru-Co bimetallic nanoparticles (Figure 5.6). Electron deficient poly(4-

trifluoromethylstyrene) supported bimetallic nanoparticles catalyzed the nitroarene reductions in just 20 minutes at room temperature, while electron rich poly(4-methylstyrene) and poly(4-methoxystyrene) supported bimetallic nanoparticles took 10 h and 5.5 h, respectively, to go to completion. We believe that this effect on reactivity is caused by two potential factors. First, the weak interaction between the π -electrons of benzene ring of the polymer and nanoparticle surface could lead to arene ligand dissociation from the nanoparticle surface, opening up more catalytic metal sites to facilitate reductions. Second, the electronic property of the polymer could change the electron density at the metal surface, thus making the catalyst more reactive.

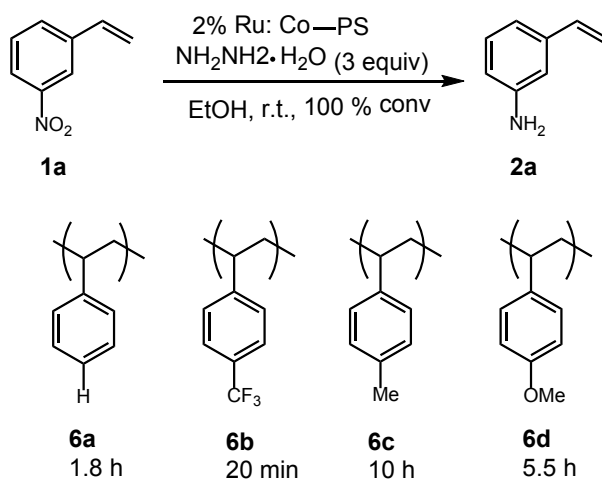


Figure 5.6 *Electronic effects of polymer supports*

We next synthesized polymers containing donating heterocycles with subtle differences between their Lewis basic characters. This included polymers containing amide, urea, and amine functional groups (Figure 5.7). These functionalized polymers were designed to mimic the properties of poly(*N*-vinyl-2-pyrrolidone) (PVP), which is widely used as polymer support in the nanoparticle synthesis. PVP stabilizes and influences the nanoparticle catalytic activity through coordination of Lewis basic amide oxygen with the nanoparticle surface. These heterocyclic

polymer supported bimetallic nanoparticles (**6e-6g**) also showed similar trends to what we observed for polystyrene polymers (**6a-6d**). The pyrrolidinone-containing polymer (**6e**) led to complete conversion in 8 h, while imidazolidinone polymer (**6f**) took 10h. The most Lewis basic amine-containing polymer (**6g**) required 10 h to reach 60% conversion. Thus, the most electron donating polymers led to the slowest catalysis, as observed for the most donating polystyrene polymers discussed above. These results suggest that the electronic properties of the polymer can be used to tune the reactivity of the nanoparticle catalysts in predictable ways.

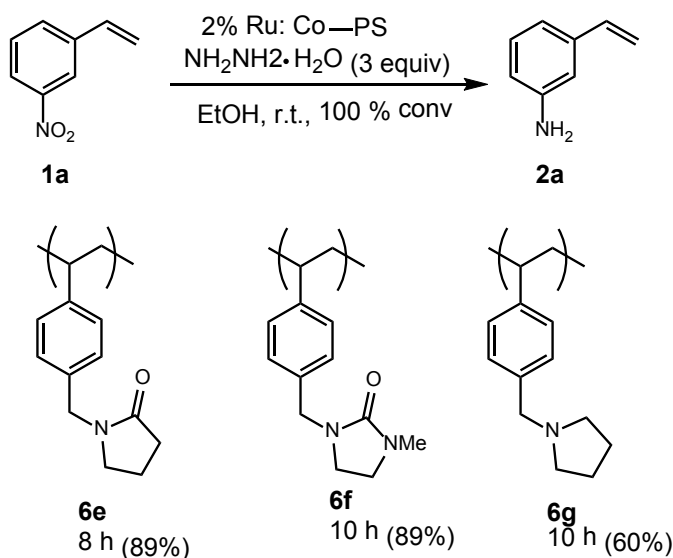
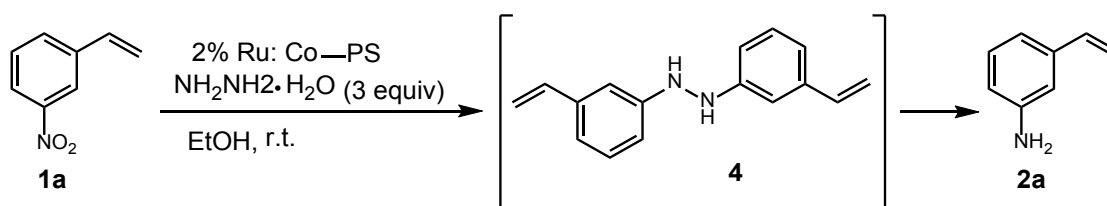


Figure 5.7 *Electronic effects of Lewis basic functional groups on catalysis*

5.2.5 Mechanism of Nitroarene Reduction

We next studied the reaction mechanism for reduction of 3-nitrostyrene using electron deficient and electron rich polymer supported bimetallic nanoparticles (**6a-6d**). When the reduction of 3-nitrostyrene **1a** was conducted with Ru:Co bimetallic catalysts supported on **6a**, **6c**, **6d** and **6e**, the starting material **1a** is converted to intermediate hydrazine **4** before a significant amount of product **2a** is formed (Scheme 5.2). However, when the electron-withdrawing

polymer supported Ru-Co bimetallic nanoparticles (**6b**) was used, no hydrazine intermediate **4** was observed during the course of the reaction. With this catalyst, starting material directly converts to product **2a**. The observed difference in the reaction might be because of the fast reduction of hydrazine **4** to **2a** by catalyst **6b** or due to inability of the catalyst **6b** to catalyze formation of **4**. These results also support the hypothesis that the electronic properties of the nanoparticles can be influenced by the electronic structure of the polymer.



Scheme 5.2 *Intermediate formation in nitroarene reduction*

5.2.6 Analysis of Nanoparticles

To characterize our catalysts, we first measured the size of the Ru-Co nanoparticles using scanning transmission electron microscopy (STEM). One goal was to see if the difference in the reactivity of our different polymer-supported nanoparticles was because of the difference in the size of the nanoparticles. STEM images showed that the size of the nanoparticles in polymers (**6a-6d**) were between ~1-2 nm in diameter. In addition, the nanoparticles are in the form of agglomerates in the polymer matrix that range from single particles to 30-40 nm bundles (Figure 5.8a). Statistical analysis of the nanoparticle size distribution for polymers **6a-6d** shows nearly equal size distribution ($CF_3 = 2.0$ nm, H = 1.9 nm, OMe = 1.75 nm and Me = 1.50 nm) for all the four polymers. The subtle difference in the nanoparticle size may be responsible for the catalytic activity but, that does not explain the observed change in reaction mechanism. Therefore, we believe that the observed difference in the catalytic activity of our polymer supported bimetallic

nanoparticles is due to a combination of subtle differences in size and variations in the strength of metal-polymer interactions. These results suggest that the catalytic activity of polymer supported metal nanoparticles can be enhanced by changing the supporting polymer structure, similar to homogeneous catalysis where the electronic properties of a metal can be tuned by modifying the ligands.

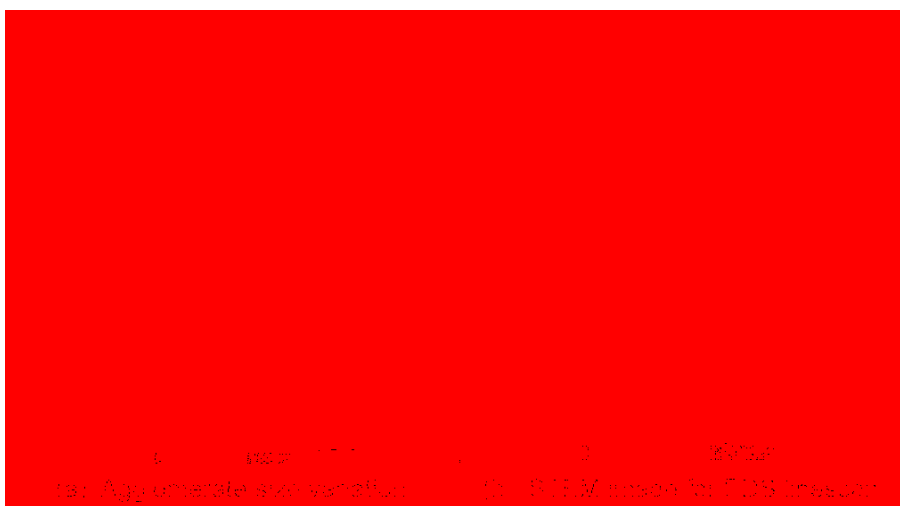
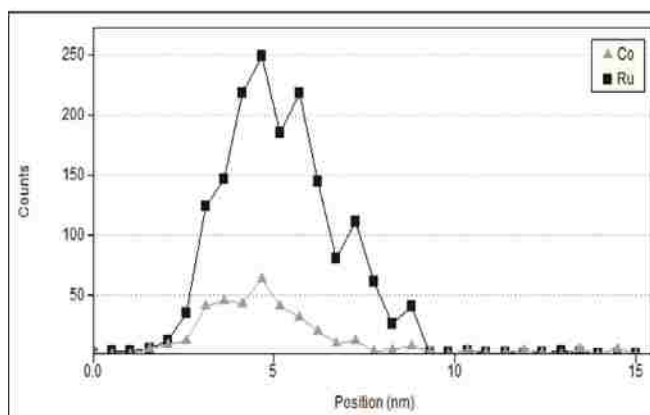


Figure 5.8 Nanoparticle Characterization. (a) STEM image showing agglomerate size variation (b) STEM image showing EDS line scan location



(c) EDS linescan results showing Co tracking Ru

Figure 5.8 (c) Energy-dispersive X-ray spectroscopy (EDS) Line scan of Ru-Co nanoparticles in polystyrene.

We also used STEM, energy-dispersive X-ray spectroscopy (EDS) to study to see if the Ru-Co bimetallic nanoparticles are individual particles or in alloy form. EDS line scan shows that ruthenium and cobalt are localized within the particle, but not individual monometallic nanoparticles (Figure 5.8b, 5.8c). The localization of both ruthenium and cobalt in a single nanoparticle might be responsible for the increased catalytic activity of the bimetallic nanoparticles. We also estimated the Ru:Co ratio at various locations of the bimetallic nanoparticle sample and found that the ratios of Ru to Co is consistent throughout the sample. X-ray photoelectron spectroscopy (XPS) analysis of bimetallic nanoparticle catalysts shows that ruthenium is in metallic (0) form while cobalt is in oxide form. This suggests that ruthenium is completely reduced and cobalt is not completely reduced during nanoparticle formation. We also used time of flight secondary ion mass spectrometry (ToF-Sims) to confirm the presence of ruthenium and cobalt in our sample. ToF-Sims confirmed the presence of both ruthenium and cobalt in the polystyrene polymer matrix.

5.3. Conclusion

Our dual optimization approach to nanoparticle catalysis is an attractive strategy for catalyst optimization due to the ability to predictably control reaction rates and selectivities. We have demonstrated that the electronic properties of the polymer and the nanoparticle composition can be tuned to enhance the catalytic activity of the nanoparticles for nitroarene reductions. Rational design of the polymer structures that lead to predictable changes in the catalytic activity is an attractive strategy for improving the catalytic activity and selectivity of a reaction. The preparation of our bimetallic nanoparticles is very straightforward and required only commercially available materials. Thus, the catalysts are easily accessible to chemists for nitroarene reductions. In addition, the catalysts can be easily recovered and reused after

completion of the reaction by simple filtration without significant loss in the catalytic activity. Thus, our Ru-Co bimetallic nanoparticles showed exceptional catalytic activity, high chemoselectivity and high yields towards nitroarene reductions.

5.4 References

(1) For reviews, see: (a) *Nanocatalysis: Synthesis and Applications*, (eds. Polshettiwar, V.; Asefa, T.), Wiley, New Jersey, 2013. (b) Cong, H.; Porco, Jr., J. A. *ACS Catal.* **2012**, *2*, 65. (c) Yasukawa, T.; Miyamura, H.; Kobayashi, S. *Chem. Soc. Rev.* **2014**, *43*, 1450. (d) Pachón, L. D.; Rothenberg, G. *Appl. Organometal. Chem.* **2008**, *22*, 288. (e) Astruc, D. in *Nanoparticles and Catalysis*. (Ed: D. Astruc), Wiley-VCH, Weinheim, 2008, pp. 1. (f) Astruc, D.; Lu, F.; Ruiz Aranzaes, J. *Angew. Chem. Int. Ed.* **2005**, *44*, 7852.

(2) For reviews, see: Na, K.; Zhang, Q.; Somorjai, G. A. *J. Cluster. Sci.* **2014**, *25*, 83. (b) Zaera, F. *Chem. Soc. Rev.* **2013**, *42*, 2746. (c) Mondloch, J. E.; Bayram, E.; Finke, R. G. *J. Mol. Catal. A: Chem.* **2012**, *355*, 1. (d) Gates, B. C. *Chem. Rev.* **1995**, *95*, 511.

(3) Xia, Y.; Xiong, Y.; Lim, B.; Skrabalak, S.E. *Angew. Chem. Int. Ed.* **2009**, *48*, 60. (b) Tongsakul, D.; Nishimura, S.; Ebitani, K. *J. Phys. Chem. C* **2014**, *118*, 11723.

(4) Wang, H.; An, K.; Sapi, A.; Liu, F.; Somorjai, G.A. *Chem. Lett.* **2014**, *11*, 144. (b) Vayssilov, G.N.; Lykhach, Y.; Migani, A.; Staudt, T.; Petrova, G.P.; Tsud, N.; Skála, T.; Bruix, A.; Illas, F.; Prince, K.C.; Matolin, V.; Neyman, K.N.; Libuda, J. *Nature Materials*, **2011**, *10*, 310.

(5) Park, D.; Kim, S.M.; Kim, S.K.; Yun, J.Y.; Park, J. Y. *Applied Catalysis A: General*, **2014**, *480*, 25.

(6) Tongsakul, D.; Nishimura, S.; Ebitani, K. *J. Phys. Chem. C* **2014**, *118*, 11723.

(7) (a) Akiyama, R.; Kobayashi, S. *Angew. Chem. Int. Ed.* **2001**, *40*, 3469. (b) Akiyama, R.; Kobayashi, S. *J. Am. Chem. Soc.* **2003**, *125*, 3412. For reviews, see: (c) Miyamura, H.; Kobayashi, S. *Acc. Chem. Res.* **2014**, *47*, 1054. (d) Kobayashi, S.; Miyamura, H. *Aldrichimica Acta* **2013**, *46*, 3–19. (e) Kobayashi, S.; Miyamura, H. *Chem. Rec.* **2010**, *10*, 271. (f) Akiyama, R.; Kobayashi, S. *Chem Rev.* **2009**, *109*, 594. (g) Shenhar, R.; Norsten, T. B.; Rotello, V. M. *Adv. Mater.* **2005**, *17*, 657.

(8) (a) Yuan, H.; Yoo, W.-J.; Miyamura, H.; Kobayashi, S. *J. Am. Chem. Soc.* **2012**, *134*, 13970. (b) Yasukawa, T.; Miyamura, H.; Kobayashi, S. *J. Am. Chem. Soc.* **2012**, *134*, 16963. (c) Yuan, H.; Yoo, W.-J.; Miyamura, H.; Kobayashi, S. *Adv. Synth. Catal.* **2012**, *354*, 2899. (d) Yoo, W.-J.; Miyamura, H.; Kobayashi, S. *J. Am. Chem. Soc.* **2011**, *133*, 3095. (e) Miyamura, H.; Matsubara, R.; Kobayashi, S. *Chem. Commun.* **2008**, 2031. (f) Kaizuka, K.; Miyamura, H.; Kobayashi, S. *J. Am. Chem. Soc.* **2010**, *132*, 15096.

(9) (a) An, K.; Somorjai, G. A. *Catal. Lett.* **2015**, *145*, 233. (b) Notar Francesco, I.; Fontaine-Vive, F.; Antoniotti, S. *ChemCatChem* **2014**, *6*, 2784. (c) Calderone, V. R.; Shiju, N. R.; Curulla-Ferré, D.; Chambrey, S.; Khodakov, A.; Rose, A.; Thiessen, J.; Jess, A.; Rothenberg, G. *Angew. Chem. Int. Ed.* **2013**, *52*, 4397. (d) Calderone, V. R.; Shiju, N. R.; Curulla-Ferré, D.; Rothenberg, G. *Green Chem.* **2011**, *13*, 1950.

(10) Blaser, H.-U.; Steiner, H.; Studer, M. *ChemCatChem* **2009**, *1*, 210. (b) Blaser, H.-U.; Siegrist, U.; Steiner, H. In *Fine Chemicals Through Heterogeneous Catalysis: Aromatic Nitro Compounds*; R. A. Sheldon, H. van Bekkum Eds.; Wiley: New York, 2001; pp. 389.

(11) (a) Vu, K. B.; Bukhryakov, K. V.; Anjum, D. H.; Rodionov, V. O. *ACS Catal.* **2015**, *5*, 2529. (b) Yan, N.; Yuan, Y.; Dyson, P. J. *Dalton Trans.* **2013**, *42*, 13294.

(12) For recent examples of nanoparticle-polymer support interactions, see: (a) Zhanga, J.; Yuanc, Y.; Kilpinc, K. J.; Koua, Y.; Dyson, P. J.; Yan, N. *J. Mol. Catal. A: Chem.* **2013**, *371*, 29. (b) Borodko, Y.; Humphrey, S. M.; Tilley, T. D.; Frei, H.; Somorjai, G. A. *Phys. Chem. C* **2007**, *111*, 6288. (c) Galow, T. H.; Drechsler, U.; Hanson, J. A.; Rotello, V. M. *Chem. Commun.* **2002**, 1076.

(13) Blaser, H.-U.; Steiner, H.; Studer, M. *ChemCatChem* **2009**, *1*, 210. (b) Blaser, H.-U.; Siegrist, U.; Steiner, H. In *Fine Chemicals Through Heterogeneous Catalysis: Aromatic Nitro Compounds*; R. A. Sheldon, H. van Bekkum Eds.; Wiley: New York, 2001; pp. 389.

(14) (a) Petkar, D. R.; Kadu, D. S.; Chikate, R. C. *RCS Adv.* **2014**, *4*, 8004. (b) Ganji, S.; Enumula, S. S.; Marella, R. K.; Rao, K. S. R.; Burri, D. R. *Catal. Sci. Technol.* **2014**, *4*, 1813. (c) He, L.; Wang, L.-C.; Sun, H.; Ni, J.; Cao, Y.; He, H.-Y.; Fan, K.-N. *Angew. Chem. Int. Ed.* **2009**, *48*, 9538.

(15) Soule, J.F.; Miyamura, H.; Kobayashi, S.; *J. Am. Chem. Soc.*, **2011**, *133*, 18550.

(16) Gaikwad, A. V.; Boffa, V.; ten Elshof, J. E.; Rothenberg, G. *Angew. Chem. Int. Ed.* **2008**, *47*, 5407.

(17) (a) Kumar, A.; Mandal, S.; Mathew, S. P.; Selvakannan, P. R.; Mandale, A. B.; Chaudhari, R. V.; Sastry, M. *Langmuir* **2002**, *18*, 6478; (b) Ramanath, G.; D ~~Arby~~ J.; Maddaninath, T.; Ellis, A. V.; Ganesan, P. G.; Goswami, R.; Kumar, A.; Vijayamohanan, K. *Langmuir* **2004**, *20*, 5583; (c) Maddanimath, T.; Kumar, A.; D-Arcy-Gall, J.; Ganesan, P. G.; Vijayamohanan, K.; Ramanath, G. *Chem. Commun.* **2005**, 1435; (d) Nakazawa, M.; Somorjai, A. *Appl. Surf. Sci.* **1993**, *68*, 517.

(18) Rahaim, R. J.; Maleczka, R. E.; *Org. Lett.* **2005**, *7*, 5087.

(19) Alper, H.; Amaratunga, S. *Tetrahedron Lett.* **1980**, *21*, 2603.

5.5 Experimental Section

General Information

All reactions were carried out in oven-dried glassware with magnetic stirring, unless otherwise indicated. All the reagents were used as obtained unless otherwise noted. Analytical thin-layer chromatography was performed with 0.25 mm coated commercial silica gel plates (E. Merck, DC-Plastikfolien, kieselgel 60 F254). Flash Chromatography was performed with EM Science silica gel (0.040-0.063 μ m grade) Proton nuclear magnetic resonance ($^1\text{H-NMR}$) data were acquired on a Inova 300 (300 MHz) or on a Inova-500 (500 MHz) spectrometer. Chemical shifts are reported in delta (δ) units, in parts per million (ppm) downfield from tetramethylsilane. Carbon-13 nuclear magnetic resonance ($^{13}\text{C-NMR}$) data were acquired on a Inova 500 at 125 MHz. Signals are reported as follows: s (singlet), d (doublet), t (triplet), q (quartet), dd (doublet of doublets), qd (quartet of doublets), brs (broad singlet), m (multiplet). Coupling constants are reported in hertz (Hz). Chemical shifts are reported in ppm relative to the center line of a triplet at 77.23 ppm for chloroform-d. Mass spectral data were obtained using ESI techniques (Agilent, 6210 TOF). The content of all metals in the final material was determined by ICP analysis using a Shimadzu ICPS-7510 instrument. STEM images and EDS analyses were obtained using a JEOL JEM-2100F instrument operated at 5.0 kV. All STEM specimens were prepared by placing a drop of a homogeneous chloroform solution of the respective polymer-nanoparticle composite on a carbon coated copper grid and allowed to dry in air without staining. Polystyrene (MW 35,000) and cobalt (II) chloride hexahydrate were purchased from Aldrich. Ruthenium (III) chloride hydrate was purchased from Oakwood Chemicals.

Synthesis of 4-Methyl polystyrene (6b)

To a stirred solution of 4-Methyl styrene (5 g, 42.3 mmol) in 15 mL of chloroform was added AIBN (347 mg, 2.11 mmol) and the mixture was heated to reflux for 12 h. The resulting polymer solution was poured into methanol. The precipitated polymer was filtered and washed with methanol several times and dried under vacuum to afford desired polymer as white solid (4.8 g, 96 % yield). ¹H NMR (500 MHz, CDCl₃): 7.15-6.15 (br m, 4H), 2.4-2.16 (br m, 3H), 2.0-1.2 (br m, 3H).

Synthesis of 4-Methoxy polystyrene (6c)

To a stirred solution of 4-methoxystyrene (5 g, 37.26 mmol) in 15 mL of chloroform was added AIBN (306 mg, 1.86 mmol) and the reaction was heated to reflux for 12 h. The resulting polymer solution was poured into methanol. The precipitated polymer was filtered and washed with methanol several times and dried under vacuum to afford the desired polymer as white solid (4.5 g, 90 % yield). ¹H NMR (500 MHz, CDCl₃): 7.0-6.2 (br m, 4H), 3.82-3.63 (br m, 3H), 1.85-1.2 (br m, 3H).

Synthesis of 4-Trifluoromethyl polystyrene (6c)

To a stirred solution of 4-(trifluoromethyl) styrene (2 g, 11.61 mmol) in 15 mL of chloroform was added AIBN (95.4 mg, 0.55 mmol) and the reaction was heated to reflux for 36 h. The resulting polymer solution was poured into diethyl ether. The precipitated polymer was filtered and washed with methanol several times and dried under vacuum to afford desired polymer as white solid (1.8 g, 90 % yield). ¹H NMR (500 MHz, CDCl₃): 7.6-6.4 (m, 4H), 2.0-1.4 (m, 3H).

Synthesis of Ruthenium-Polystyrene nanoparticles

Polystyrene (1g) was added to 25 mL of THF and 8 mL of ethanol and the mixture was stirred using a Teflon-coated magnetic stir bar until polystyrene was completely dissolved. Ruthenium (III) chloride hydrate (100 mg, 0.482 mmol) anhydrous basis was added and the mixture was stirred until the solution became homogenous. Sodium borohydride (182.5 mg, 4.82 mmol) was then added portion wise. The reaction was stirred under argon atmosphere for 10 h giving a black homogeneous solution, indicating the formation of nanoparticles. The solvent was then evaporated and millipore water was added to the resulting solid and the mixture was stirred for 15 minutes then filtered. The solid was then washed with millipore water (20 mL× 5) and dried under vacuum to give a black solid, which was finely ground with a mortar and pestle before use.

Synthesis of Ru-Co NP's@Polystyrene.

General Procedure for Bimetallic nanoparticle Synthesis: Polystyrene (1g) was added to 25 mL of THF and 8 mL of ethanol and the mixture was stirred using a Teflon-coated magnetic stir bar until polystyrene was completely dissolved. Ruthenium (III) chloride hydrate (100 mg, 0.482 mmol) anhydrous basis and Cobalt (II) chloride hexahydrate (50 mg, 0.21 mmol) were added and the mixture was stirred until the solution became homogenous. Sodium borohydride (223 mg, 5.89 mmol) was then added portionwise. The reaction stirred under and argon atmosphere for 10 h giving a black homogeneous solution, indicating the formation of nanoparticles. Solvent was evaporated, millipore water was added to the resulting solid and the mixture was stirred for 15 minutes then filtered. The solid was then washed with millipore water (20 mL× 5) and dried under vacuum to give a black solid, which was finely ground with a mortar and pestle before use.

The same procedure was followed to prepare Ru-Co nanoparticles in poly(4-methylstyrene), poly(4-methoxystyrene), poly(4-trifluoromethylstyrene) with similar metal loadings and Ru:Co ratios. See Table S1 for Ru:Co loadings and ratios.

The general procedure was followed to prepare Ru-M₂ (M₂ = Ni, Cu, Fe and Au) nanoparticles in polystyrene. The respective amounts of metal salts used in the synthesis of nanoparticle-polymer conjugates with 1 g of polystyrene are listed below. The yields for each bimetallic nanoparticle composite are also provided. Metal loadings for each polymer and M₁:M₂ ratios, as determined by ICP analysis, are listed in Table S1.

RuCl₃.XH₂O (100 mg): NiCl₂.6H₂O (210 mg)

RuCl₃.XH₂O (100 mg): Cu(OAc)₂ (100 mg)

RuCl₃.XH₂O (100 mg): FeCl₂ (210 mg)

Synthesis of 1-(4-polyvinylbenzyl) pyrrolidine (6g)

To a stirred solution of pyrrolidine (512 mg, 7.2 mmol) in DMF (20 mL) was added 60% sodium hydride (363 mg, 10.8 mmol), and the reaction was stirred for 10 minutes at room temperature. A solution of poly (vinylbenzyl chloride) (1 g, 6.55 mmol) in DMF (15 mL) was added drop wise and the reaction mixture was stirred at room temperature for 8 h. The reaction was then diluted with H₂O (25 mL), the precipitated solid was filtered and concentrated under vacuum to afford 1-(4-polyvinylbenzyl) pyrrolidine as off-white solid (1.1 g, 90 %). ¹H NMR (500 MHz, CDCl₃): 7.2-6.2 (br m, 4H), 3.65-3.2 (br m, 2 H), 2.6-2.2 (br, m, 4H), 1.85-1.6 (br m, 4H), 2.0-1.2 (br m, 3H).

Synthesis of 1-(4-polyvinylbenzyl) pyrrolidin-2-one (6e)

To a stirred solution of 2-pyrrolidone (613 mg, 7.2 mmol) in DMF (20 mL) was added 60% sodium hydride (363 mg, 10.8 mmol), and the reaction stirred for 10 minutes at room temperature. A solution of poly (vinylbenzyl chloride) (1 g, 6.55 mmol) in DMF (15 mL) was added drop wise and the reaction mixture was stirred at room temperature for 8 h. The reaction was then diluted with H₂O (25 mL) and the aqueous phase was extracted with CH₂Cl₂ (3 × 30 mL). The combined organic layers were concentrated under vacuum to afford 1-(4-polyvinylbenzyl) pyrrolidin-2-one as white solid (1.0 g, 77 %). ¹H NMR (500 MHz, CDCl₃): 7.2-6.2 (br m, 4H), 4.5-4.2 (br m, 2 H), 3.4-3.0 (br, m, 2H), 2.5-2.3 (br m, 2H), 2.1-1.9 (br m, 2H), 1.8-1.0 (br m, 3 H)

Synthesis of 1-methyl-3-(4-polyvinylbenzyl) imidazolidin-2-one. (6f)

To a stirred solution of 1-methyl imidazolidin-2-one (722 mg, 7.2 mmol) in DMF (20 mL) was added 60% sodium hydride (363 mg, 10.8 mmol) and the mixture was stirred for 10 minutes at room temperature. A solution of poly (vinylbenzyl chloride) (1 g, 6.55 mmol) in DMF (15 mL) was then added drop wise and the reaction mixture was stirred at room temperature for 8 h. The reaction was diluted with H₂O (25 mL) and the aqueous phase was extracted with CH₂Cl₂ (3 × 30 mL). The combined organic layers were concentrated under vacuum to afford 1-methyl-3-(4-polyvinylbenzyl) imidazolidin-2-one as white solid (1.12 g, 79 %). ¹H NMR (500 MHz, CDCl₃): 7.2-6.2 (br m, 4H), 4.4-4.1 (br m, 2 H), 3.4-3.0 (br, m, 4H), 2.9-2.7-1.6 (br s, 3H), 2.0-1.0 (br m, 3H).

The ratio of M₁:M₂ are shown in ICP table

Preparation of the sample for ICP-analysis

To 10 mg of polymer-nanoparticle catalyst was added 1 ml conc. H₂SO₄ and the mixture heated at 140 °C. HNO₃ was then slowly added and the solution was heated for 10 min. 1 ml of aqua regia was then added and the mixture cooled to room temperature and diluted to 500 mL in a volumetric flask. Metal concentrations were then determined by ICP analysis by comparison to standard solutions.

Table S5.1 Loading of catalysts determined by ICP

Catalyst	Ruthenium conc. (M ₁)	M ₂ conc.	Ratio M ₁ :M ₂	Catalyst Classification
Ru: Ni	0.295 mmol/g	0.637 mmol/g	1:2.1	6.7%(₄₄ Ru ₅₆ Ni)/polystyrene
Ru: Cu	0.272 mmol/g	0.416 mmol/g	1:1.5	5.4%(₅₁ Ru ₄₉ Cu)/polystyrene
Ru:Fe	0.170 mmol/g	0.949 mmol/g	1:5.5	7.0%(₂₄ Ru ₇₆ Fe)/polystyrene
Ru: Co	0.256 mmol/g	0.506 mmol/g	1:2	5.6%(₄₆ Ru ₅₄ Co)/polystyrene
Ru: Co	0.219 mmol/g	0.242 mmol/g	1:1.1	3.6%(₆₁ Ru ₃₉ Co)/polystyrene
Ru: Co	0.198 mmol/g	0.625 mmol/g	1:3.1	5.7%(₃₅ Ru ₆₅ Co)/polystyrene
Ru:Co	0.176 mmol/g	1.03 mmol/g	1:5.8	7.8%(₂₃ Ru ₇₇ Co)/polystyrene
Ru:Co (6a)	0.408 mmol/g	0.159 mmol/g	2.5:1	5.1%(₈₁ Ru ₁₉ Co)/polystyrene
Ru:Co (4-CF ₃ -polystyrene) (6b)	0.285 mmol/g	0.123 mmol/g	2.3:1	3.6%(₈₀ Ru ₂₀ Co)/6b
Ru:Co (4-Methyl-polystyrene)	0.370 mmol/g	0.152 mmol/g	2.4:1	4.6%(₈₁ Ru ₁₉ Co)/6c

(6c)				
Ru:Co (4-OMe-polystyrene) (6d)	0.341 mmol/g	0.135 mmol/g	2.5::1	5.6%_(81Ru₁₉Co)/6d
Ru:Co (1-(4-polyvinylbenzyl) pyrrolidin-2-one (6e)	0.288 mmol/g	0.169 mmol/g	1.7: 1	3.9%_(75Ru₂₅Co)/6e
Ru:Co (1-methyl-3-(4- polyvinylbenzyl) imidazolidin-2-one (6f)	0.374 mmol/g	0.201 mmol/g	1.86:1	5.0%_(76Ru₂₄Co)/6f
Ru:Co (1-(4-polyvinylbenzyl) pyrrolidine (6g)	0.284 mmol/g	0.157 mmol/g	1.8:1	3.8%_(76Ru₂₄Co)/6g

Optimization studies with Ru:Fe catalysts.

We initially performed optimization studies with Ru:Fe bimetallic nanoparticle catalysts. These studies showed that a bimetallic catalyst of composition 11.4%_(16Ru₈₄Fe)/polystyrene performed nitroarene reduction of **1a** in 30 minutes with a nitroarene concentration of 1.3M in Ethanol and 1 mol% ruthenium loading (99% yield, 99% selectivity). However, substituted nitroarenes containing ketones (**2m**) or fluorine (**2f**) led to decomposition of the products and low yields in the presence of the Ru-Fe catalysts. Thus, optimization studies were focused on Ru-Co nanoparticles, which display much higher chemoselectivity and avoid these decomposition products.

Reuse experiments of Ru-Co-Polystyrene nanoparticles.

The reduction of 3-nitropolystyrene was performed under the typical reaction conditions in a flask containing a frit of medium porosity and a bottom stopcock. After completion of the reaction, the solution was removed via filtration through the frit. The flask was then rinsed with EtOH (3 ml)

and the filtrate evaporated and the isolated yield and selectivity were determined. To the remaining nanoparticle catalyst was added a new set of reagents and solvents and the reaction was allowed to proceed for the same time. This procedure was repeated 5 times, and the results are presented in Scheme 1.

Leaching studies

After completion of the reaction, polymeric catalyst was filtered off through a plug of cotton and the flask and nanoparticles were rinsed with 1 ml EtOH to collect all reaction materials. The solvent was then removed from the filtrate. 0.5 ml of conc. H₂SO₄ was then added to the resulting residue and the mixture heated to 140 ° C for 30 min. 0.5 ml of conc. HNO₃ was then slowly added and the solution was heated for 10 min at the same temperature. 1 ml of aqua regia was then added and the mixture cooled to room temperature and diluted to 10 ml in a volumetric flask. Metal concentrations were then determined by ICP analysis by comparison to standard solutions. The concentrations were then compared to the original amount of Ru–Co polymer added to the reaction, and the percent leaching was calculated.

Amount of Ruthenium leached: 1.2 %

Amount of Cobalt leached: 1.28%

In order to test for the presence of active homogeneous nanoparticle catalysts that could potentially leach from the polymer support, catalyst was removed part way through the reaction via filtration and reaction progress monitored. This procedure mimics the Cat-in-a-Cup protocol described previously. As noted in Figure S1 below, after removal of the nanoparticle catalyst by filtration through a sintered glass funnel of medium porosity, all reaction progress is halted. Readdition of the catalyst after several hours leads to further consumption of starting material.

This study confirms that the polymer-supported nanoparticles are the active catalyst and that homogeneous nanoparticles that have leached from the polymer matrix are not responsible for catalysis.

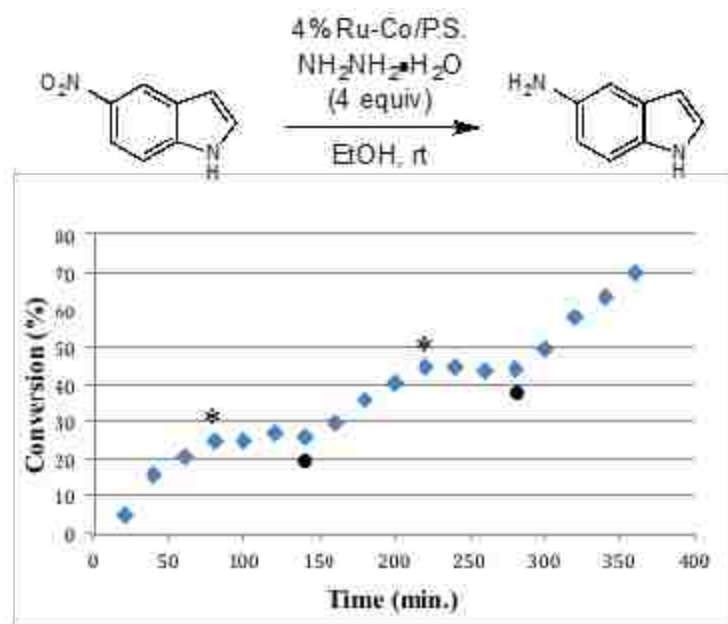


Figure S5.1 Nanoparticle Leaching study. Conversion determined by ^1H NMR of the crude reaction mixture at each time point.

To 5-nitroindole (150 mg, 0.925 mmol) in a round bottom flask was added 6 mL of ethanol, polystyrene supported Ruthenium nanoparticles (82 mg, 4mol %) and hydrazine hydrate (180 μL , 3.7 mmol, 4 equiv). The reaction vessel was then closed with a septum and allowed to react at room temperature. Small aliquots (~ 0.1 ml) of the reaction were removed at the time points indicated in figure 5.9 and the aliquots were filtered through a small plug of silica gel and eluted with 2 ml EtOH to remove any metal catalyst. The solvent was then removed and the reaction conversion was determined by ^1H NMR analysis. After removal of an aliquot at 80 minutes, the entire reaction was filtered through a sintered glass funnel of medium porosity into a

new round bottom flask to remove any heterogeneous catalyst and 135 μ L Three additional equivalents of hydrazine hydrate (135 μ L, 2.8 mmol, 3 equiv) was added to the reaction at this stage and the flask was again capped with a septum. After a total of 140 min, 82 mg of catalyst was added to the reaction just after removal of the aliquot used to determine reaction conversion. The filtration (*) /catalyst readdition (•) sequence was performed a second time at 220 min and 280 minutes respectively. The results of this study are presented in Figure S5.1

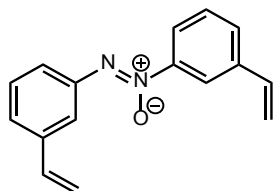
Reduction of 3-nitrostyrene (1a).²

General Procedure: A typical procedure for the reduction of nitro compounds by Ru-Co (2.5:1)-PS is as follows: 5.1%(₈₁Ru₁₉Co)/polystyrene catalyst (23 mg , 2 mol% wrt ruthenium) was placed in a 25 mL test tube containing a Teflon-coated magnetic stir bar, followed by the addition of ethanol (2.5 mL), 3-nitrostyrene (50 mg, 0.335 mmol), and dropwise addition of hydrazine monohydrate (1 mmol, 48.8 μ L, 3 equiv) at room temperature. The reaction vessel was then sealed with a glass stopper and stirred for 3.5 h. After the reaction, the heterogeneous catalyst was removed by filtration through a small plug of silica gel in a pipet, and the solids washed several times with ethanol. The filtrate was collected, and the solvent removed under reduced pressure on a rotary evaporator to provide the product (39.6 mg, 0.332 mmol, 99% yield, 97% selectivity) in excellent purity, which did not require further purification. The selectivity of the reaction was determined by ¹H NMR analysis of the pure product obtained as described. Yield: 38.5 mg, 96 % (96.7)

¹H NMR (300 MHz, CDCl₃): 7.13 (t, J = 7.5 Hz, 1H), 6.83 (d, J = 7.5 Hz, 1H), 6.75 (br s, 1H), 6.64 (dd, J₁ = 18.0 Hz, J₂ = 10.0 Hz, 1H), 6.60 (d, J = 7.5 Hz, 1H), 5.71 (dd, J₁ = 18.0 Hz, J₂ =

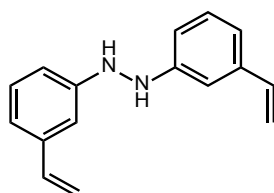
1.0 Hz, 1H), 5.22 (dd, $J_1 = 10.0$ Hz, $J_2 = 1.0$ Hz, 1H); ^{13}C NMR (75 MHz, CDCl_3): 146.5, 138.6, 137.0, 129.4, 116.9, 114.8, 113.6, 112.7.

1, 2-bis (3-vinylphenyl) diazene oxide (5) ²



^1H NMR (300 MHz, CDCl_3): δ 5.32 (d, $J = 10.9$ Hz, 1 H), 5.39 (d, $J = 10.9$ Hz, 1 H), 5.86 (t, $J = 17.4$ Hz, 2 H), 6.78 (ddd, $J = 5.7, 10.9, 17.0$ Hz, 2 H), 7.45 (m, 3 H), 7.58 (m, 1 H), 8.08 (dd, $J = 3.2$ Hz, 5.8 Hz, 1 H), 8.18 (m, 2 H), 8.33 (d, $J = 1.6$ Hz, 1 H) ppm. ^{13}C NMR (75 MHz, CDCl_3): δ 114.8, 115.9, 119.9, 121.4, 123.4, 124.6, 127.3, 128.8, 128.9, 129.2, 135.5, 136.2, 138.1, 138.6, 144.2

1, 2-bis (3-vinylphenyl) hydrazine (4) ³



^1H NMR (300 MHz, CDCl_3): 7.29-7.16 (m, 4H), 6.67-6.59 (m, 2H), 6.82-6.77 (m, 2H), 6.68-6.60 (dd, $J_1 = 18.0$ Hz, $J_2 = 10.0$ Hz, 2H), 5.76 (dd, $J_1 = 18.0$ Hz, $J_2 = 1.0$ Hz, 2H), 5.26 (dd, $J_1 = 10.0$ Hz, $J_2 = 1.0$ Hz, 2H) ppm. ^{13}C NMR (75 MHz, CDCl_3): δ 149.27, 138.9, 137.11, 129.7, 118.3, 114.1, 112.1, 110.1.

4-vinylaniline: Yield: 38.8 mg, 97% (97). Spectral data for the product matched literature values.⁹

2-vinyylaniline: ¹⁰ Spectral data for the product matched literature values.

¹H NMR (500 MHz, CDCl₃) δ 7.33 (d, J = 7.6 Hz, 1H), 7.12 (m, 1H, ArH), 6.80 (m, 2H), 6.70 (d, J = 7.9 Hz, 1H), 5.66 (dd, J = 1.2, 17.4 Hz), 5.35 (dd, J = 1.3, 11.1 Hz, 1H), 3.8 (s, br, NH₂). ¹³C NMR (125 MHz, CDCl₃) δ 143.6, 132.6, 128.7, 127.2, 124.0, 118.8, 116.0, 115.6. Yield: 38.7 mg 97 %, (97)

4-chloroaniline: ¹ Spectral data for the product matched literature values.

¹H NMR (300 MHz, CDCl₃): 7.10 (d, J = 8.5 Hz, 2H), 6.61 (d, J = 8.5 Hz, 2H), 3.34 (br s, 2H); ¹³C NMR (75 MHz, CDCl₃): 144.8, 129.0, 123.2, 116.2. Yield: 40 mg 98 %, (99)

2-chloroaniline: ¹ Spectral data for the product matched literature values.

¹H NMR (300 MHz, CDCl₃) 7.27 (d, J = 7.9 Hz, 1H), 7.09 (t, J = 7.09 Hz, 1H), 6.78 (d, J = 8.0 Hz, 1H), 6.72 (t, J = 7.9 Hz, 1H), 4.03 (s, 2H); ¹³C NMR (75 MHz, CDCl₃) δ 142.9, 129.4, 127.6, 119.2, 119.0, 115.8. Yield: 40 mg, 98 %, (99).

4-fluoroaniline: ¹ Spectral data for the product matched literature values.

¹H NMR (300 MHz, CDCl₃): 6.83 (m, 2H), 6.60 (m, 2H), 3.51 (bs, 2H); ¹³C NMR (75 MHz, CDCl₃): 157.9, 154.7, 142.3, 116.0, 115.9, 115.7, 115.4. Yield: 38 mg, 96 %, (99)

4-bromoaniline: ¹ Spectral data for the product matched literature values.

¹H NMR (300 MHz, CDCl₃): 7.23 (d, J = 8.5 Hz, 2H), 6.55 (d, J = 8.5 Hz, 2H), 3.55 (br s, 2H); ¹³C NMR (75 MHz, CDCl₃): 145.4, 132.0, 116.7, 110.2. Yield: 41.5 mg, 97 %, (99)

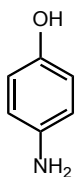
4-iodoaniline: ¹ Spectral data for the product matched literature values.

¹H NMR (300 MHz, CDCl₃) δ 7.42 (d, J = 8.7 Hz, 2H), 6.48 (d, J = 8.7 Hz, 2H), 3.59 (s, J = 53.3 Hz, 2H). ¹³C NMR (75 MHz, CDCl₃) δ 146.0, 137.9, 117.3, 79.3. Yield: 49 mg, 98 %, (99)

4-aminobenzonitrile: ⁶ Spectral data for the product matched literature values.

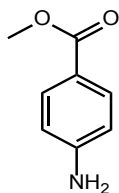
¹H NMR (300 MHz, CDCl₃): 7.83 (s, 1H), 7.37 (d, J = 8.79 Hz, 2H), 7.29 (bs, 1H), 6.87 (d, J = 8.24 Hz, 2H); ¹³C NMR (75 MHz, CDCl₃): 154.5, 133.5, 132.9, 119.7, 114.1, 112.8, 102.1. Yield: 39 mg, 98 %, (99)

4-aminophenol: ¹ Spectral data for the product matched literature values.



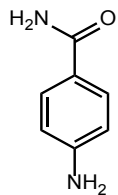
¹H NMR (300 MHz, CD₃OD): 6.65 (d, J = 9.0 Hz, 2H), 6.60 (d, J = 9.0 Hz, 2H); ¹³C NMR (75 MHz, CD₃OD): 149.9, 138.6, 117.2, 115.4. Yield: 30.5 mg, 98 % yield, (99)

Methyl 4-aminobenzoate: ⁹ Spectral data for the product matched literature values.



¹H NMR (300 MHz, CDCl₃): 7.83 (d, J = 8.5 Hz, 2H), 6.62 (d, J = 7.5 Hz, 2H), 4.10 (br s, 2H), 3.84 (s, 3H); ¹³C NMR (75 MHz, CDCl₃): 167.2, 150.9, 131.5, 119.6, 113.7, 51.5. Yield: 41.5 mg, 99% (99)

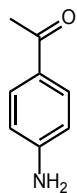
4-Aminobenzamide: ⁶ Spectral data for the product matched literature values.



¹H NMR (300 MHz, DMSO-*d*₆) δ 5.57 (bs, 2H), 6.50 (d, *J* = 8.2 Hz, 2H), 6.79 (bs, 1H), 7.47 (bs, 1H), 7.56 (d, *J* = 8.2 Hz, 2H); ¹³C NMR (75 MHz, DMSO-*d*₆) δ 112.5, 121.0, 129.1, 151.7, 168.1.

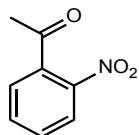
Yield: 40.8 mg, 99% (99)

4-Aminoacetophenone: ⁶ Spectral data for the product matched literature values.



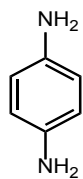
¹H-NMR (300 MHz, CDCl₃) δ 7.84-7.78 (m, 2H), 6.68-6.62 (m, 2H), 4.11 (bs, 3H); ¹³C-NMR (125 MHz, CDCl₃) δ 196.6, 151.0, 131.0, 127.9, 113.7, 26.1. Yield: 40 mg, 98% (99)

2-Aminoacetophenone: ⁸ Spectral data for the product matched literature values.



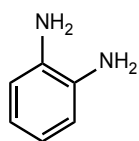
¹H NMR (300 MHz, CDCl₃) δ 7.71 (1H, d, *J* = 8.0 Hz), 7.30 –7.10 (3H, m), 6.76 (1H, d, *J* = 8.0 Hz), 6.53 (1H, t, *J* = 8.0 Hz), 2.50 (3H, s); ¹³C NMR (125 MHz, CDCl₃) δ 200.15, 151.04, 134.17, 132.22, 116.85, 114.38, 27.84 (+ one aromatic signal overlapping). Yield 40 mg, 98% (99).

Benzene-1, 4-diamine: ¹ Spectral data for the product matched literature values.



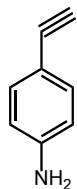
^1H NMR (300 MHz, CDCl_3): 6.57 (s, 4H), 3.30 (br s, 4H); ^{13}C NMR (75 MHz, CDCl_3): 138.5, 116.7.

Benzene-1, 2-diamine: ¹ Spectral data for the product matched literature values.



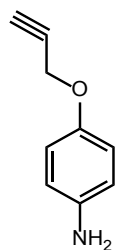
^1H NMR (300 MHz, CDCl_3): 6.6-6.56 (m, 2H), 6.48-6.45 (m, 2H), 4.40 (br s, 4H); ^{13}C NMR (75 MHz, CDCl_3): 134.3, 117, 114.2 Yield: 40.5 mg, 99%, (99).

4-Ethynylaniline: ⁴ Spectral data for the product matched literature values.



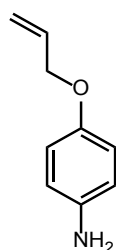
^1H NMR (300 MHz, CDCl_3): δ 7.29 (d, 2H, $J = 8.64$ Hz), 6.59 (d, 2H, $J = 8.67$ Hz), 3.81 (s, 2H), 2.96 (s, 1H). ^{13}C NMR (75 MHz, CDCl_3): δ 146.98, 133.41, 114.53, 111.21, 84.36, 74.89. Yield: 38.6 mg, 97% (97).

4-(Ethynyloxy) aniline: ⁹ Spectral data for the product matched literature values.



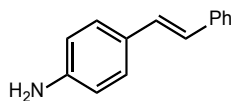
Yield: 40.4 mg, 97% (97)

4-(Vinyloxy) aniline:⁹ Spectral data for the product matched literature values.



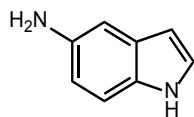
¹H-NMR (300 MHz, CDCl₃) δ 6.78-6.75 (m, 2H), 6.65-6.62 (m, 2H), 6.07-6.02 (m, 1H), 5.41-5.37 (m, 1H), 5.27-5.25 (m, 1H) ppm; ¹³C NMR (125 MHz, CDCl₃) δ 151.8, 140.2, 133.9, 117.3, 116.4, 116.0, 69.6. Yield: 40.8 mg, 98 (99).

(E)-4-Styrylaniline:⁵ Spectral data for the product matched literature values.



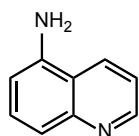
¹H-NMR (300 MHz, CDCl₃) δ 7.50-7.44 (m, 2H), 7.37-7.29 (m, 4H), 7.24-7.17 (m, 1H), 7.03 (d, J = 16.3 Hz, 1H), 6.91 (d, J = 16.3 Hz, 1H), 6.71-6.65 (m, 2H), 3.74 (bs, 2H) ppm; ¹³C NMR (125 MHz, CDCl₃) δ 146.2, 137.9, 128.7, 128.6, 128.0, 127.8, 126.9, 126.1, 125.1, 115.2. Yield: 43 mg, 98 % (99).

5-Aminoindole:¹ Spectral data for the product matched literature values.



^1H NMR (300 MHz, $\text{DMSO-}d_6$) δ 10.57 (s, 1H), 7.12 (t, $J = 2.7$ Hz, 1H), 7.09 (d, $J = 8.5$ Hz, 1H), 6.69 (d, $J = 2.0$ Hz, 1H), 6.49 (dd, $J = 8.5, 2.1$ Hz, 1H), 6.23 – 6.00 (m, 1H), 4.44 (s, 2H). ^{13}C NMR (75 MHz, $\text{DMSO-}d_6$) δ 141.4, 130.1, 128.9, 125.1, 112.2, 111.8, 103.6, 100.0. Yield: 40 mg, 98% (99).

8-Aminoquinoline: 1 Spectral data for the product matched literature values.



^1H NMR (300MHz, CDCl_3) δ : 8.65 (d, $J = 3.6$, 1H), 7.89 (t, $J = 8.2$, 2H), 7.26 (m, 1H), 7.15 (d, $J = 8.0$, 1H), 6.88 (d, $J = 2.8$, 1H), 3.88 (s, 2H). 40 mg, 97% (90).

5.6 Nanoparticle Characterization

Characterization of Ru-Co/polystyrene nanoparticles: Statistical analysis of the size distribution of the nanoparticles was performed to demonstrate that the average particle size in each of the 4 polymer supports (6a–6d) was similar, and that variations in nanoparticle size was not principally responsible for variations in the catalytic activity of the nanoparticle catalysts. For metal loadings in each polymer, see figure S5.2-5.5.

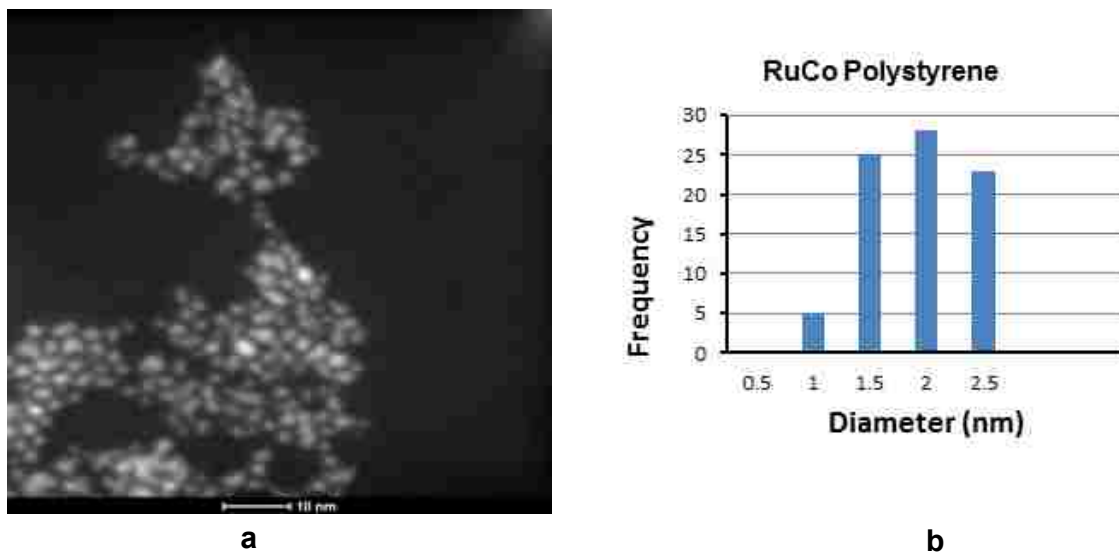


Figure S5.2 STEM image Ru-Co polystyrene catalyst (6a). (a) STEM Image of polymer-encapsulated nanoparticles. (b) Statistical analysis of nanoparticle size (average size: 1.9 nm).

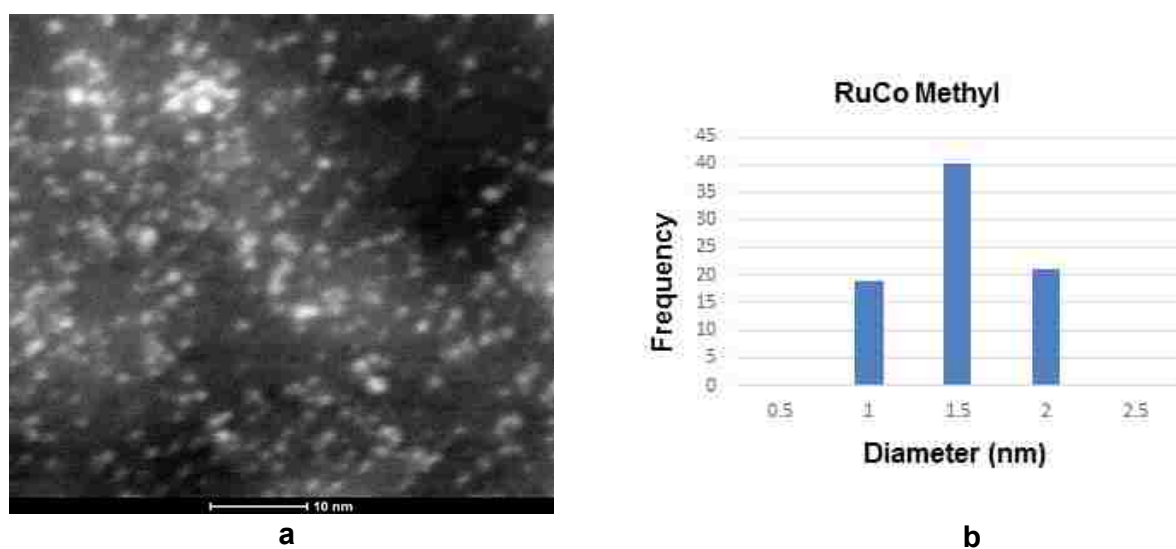


Figure S5.3 STEM image of Ru-Co poly (4-Methylstyrene) catalyst (6c). (a) STEM Image of polymer-encapsulated nanoparticles. (b) Statistical analysis of nanoparticle size (average size: 1.5 nm)

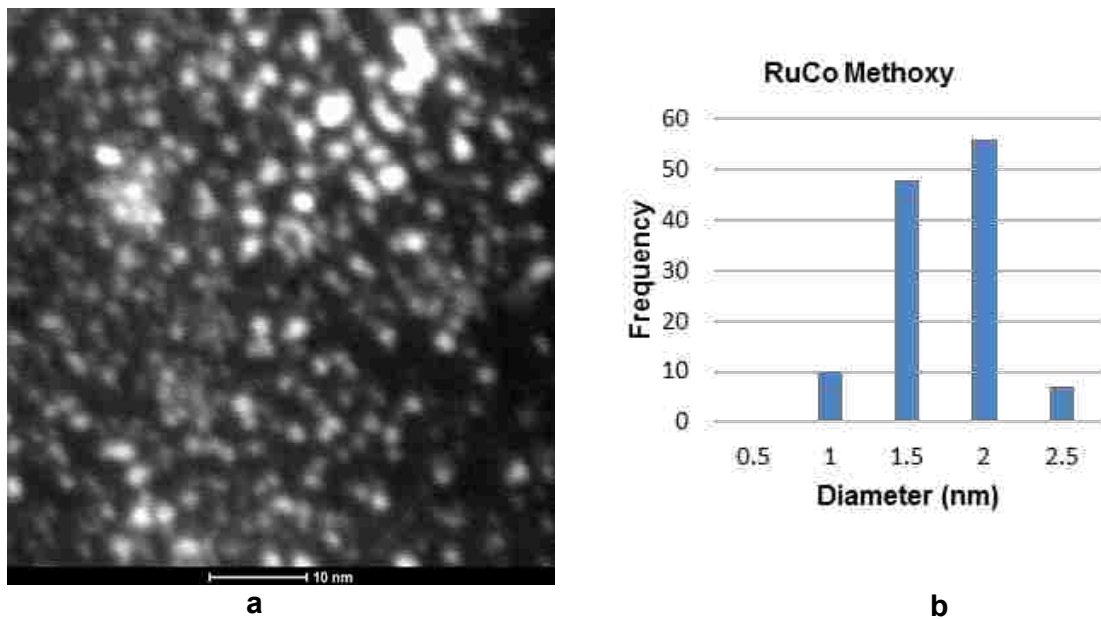


Figure S5.4 *STEM image Ru-Co (poly-4-methoxystyrene) catalyst (6d). (a) STEM Image of polymer-encapsulated nanoparticles. (b) Statistical analysis of nanoparticle size (average size: 1.75 nm).*

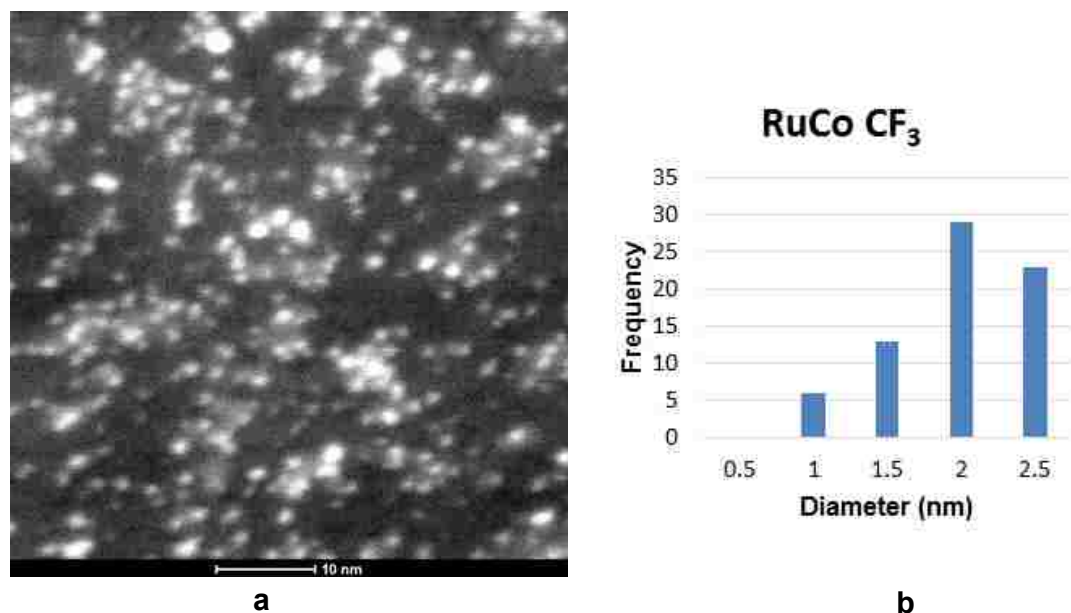


Figure S5.5 *Ru-Co poly(4-CF₃styrene) catalyst (6b). (a) STEM Image of polymer-encapsulated nanoparticles. (b) Statistical analysis of nanoparticle size (average size: 2.0 nm).*

5.7 References

1. Cantillo, D.; Baghbanzadeh, M.; Kappe, C. O. *Angew. Chem. Int. Ed.* **2012**, *51*, 10190.
2. Kim, J. H.; Park, J. H.; Chung, Y. K.; Park, K. H. *Adv. Synth. Catal.* **2012**, *354*, 2412.
3. Yu, C.; Liu, B.; Hu, L. *J. Org. Chem.* **2001**, *66*, 919.
4. Serwinski, P. R.; Lahti, P. M. *Org. Lett.* **2003**, *5*, 2099.
5. Schabel, T.; Belger, C.; Plietker, B. *Org. Lett.*, **2013**, *15*, 2858.
6. Wang, D.; Ding, Q. C. K. *Adv. Synth. Catal.* **2009**, *351*, 1722.
7. Ahammed, S.; Saha, A.; Ranu, B. C. *J. Org. Chem.*, **2011**, *76*, 7235.
8. Thakur, K. G.; Ganapathy, D.; Sekar, G. *Chem. Commun.* **2011**, *47*, 5076.
9. Dey, R.; Mukherjee, N.; Ahammed, S.; Ranu, B. C. *Chem. Commun.* **2012**, *48*, 7982.
10. Vo, G. D.; Hartwig, J. F. *J. Am. Chem. Soc.* **2009**, *131*, 11049.

5.8 XPS and ToF-SIMS Studies:

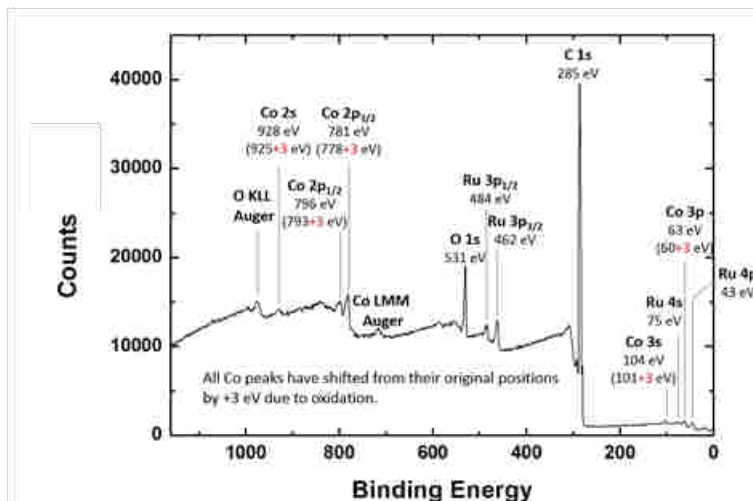


Figure S5.6. XPS survey spectrum of Co-Ru nanoparticles in a polystyrene matrix. The peak energies are labeled with their maxima from the corresponding narrow scans, with the exception of the C 1s spectrum (see Figure 6.5).

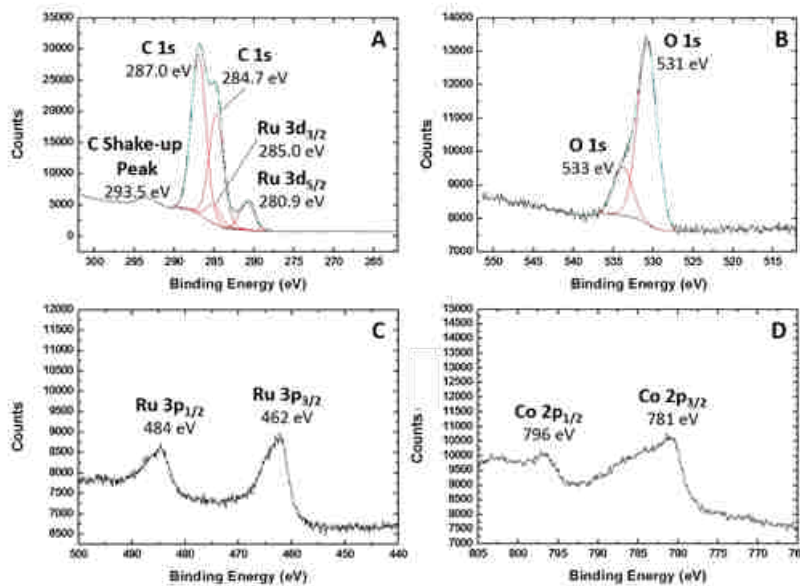


Figure S5.7. XPS narrow scans of Co-Ru nanoparticles in a polystyrene matrix. (A) Carbon (C 1s), (B) Oxygen (O 1s), (C) Ruthenium (Ru 3p), and (D) Cobalt (Co 2p)

Figure S5.6 is an X-ray photoelectron spectroscopy (XPS) survey scan of Co-Ru nanoparticles dispersed in a polystyrene (PS) matrix, and Figure 6.5 shows the corresponding C *1s*, O *1s*, Ru *3p*, and Co *2p* XPS narrow scans. We now describe the analysis of this data below, element by element, as follows:

- *Oxygen* A modest O *1s* signal is present in the survey spectrum along with its corresponding *KLL* Auger signal at ca. 978 eV. The O *1s* narrow scan was peak fitted. The portion of the peak at 531 eV (see Figure S7B) is consistent with the presence of metal oxide, and the shifted O *1s* peak at 533 eV suggests oxygen bonded to carbon.¹⁻³
- *Carbon* The carbon *1s* signal was complex. The small peak at ca. 280 eV in the C *1s* narrow scan is attributed to the Ru *3d_{5/2}* signal. The overlap of the Ru and C signals at ca. 285 eV is well known. Accordingly, there should be a Ru *3d_{3/2}* peak +4.17 eV from the Ru *3d_{5/2}* signal,⁴ and theoretically these peaks should have a 3:2 area ratio. Excluding the signal at ca. 294 eV, which was attributed to the carbon shake-up peak from aromatic carbon in polystyrene, we attempted to fit the remainder of the C *1s* envelope to a single C *1s* signal and to two appropriately constrained Ru *3d* signals. After a series of unsuccessful attempts, we added an additional carbon signal. A good fit to the data was obtained with these four peaks. It is not entirely clear what the source of the two C *1s* signals is. For example, there is the possibility that the catalyst is in some way interacting with or altering the polystyrene matrix around it, leaving some of the carbon in a reduced state and some of it in a more oxidized state. More work in this area will be needed to fully understand these results. The positions of the peaks in the fit were: Ru *3d* signals: 280.9 eV and 285.0 eV, and C *1s* signals: 284.7 eV and 287.0 eV. It is very common to reference XPS spectra to the C *1s* peak position, which is often taken at 284.6 eV or 285.0

eV. Unfortunately, due to the ambiguity inherent in peak fitting, the overlap of these signals left us without a good reference point that we could apply to the remainder of the data.

- *Cobalt* A series of peaks for Co ($3p$ at 63 eV, $3s$ at 104 eV, $2p_{3/2}$ at 781 eV, $2p_{1/2}$ at 796 eV, and $2s$ at 928 eV) is present in the survey spectrum, which leaves little doubt as to the presence of this element. The peak shapes for the Co $2p$ signals in Figure S7 suggest that Co is in a +2 or +3 oxidation state.^{3, 5-6} The presence of oxidized Co would be consistent with at least some of the O $1s$ signal at ca. 531 eV.
- *Ruthenium* A series of peaks for Ru ($4p$ at 43 eV, $4s$ at 75 eV, $3p_{3/2}$ at 462 eV, and $3p_{1/2}$ at 484 eV) are present in the survey spectrum, which again provides strong proof for the presence of this element in the sample.

Given the overlap of the Ru $3d$ and C $1s$ signals/lack of a clear reference point, we undertook the following analysis to determine the oxidation states of Co and Ru in the sample. Table S1 gives the peak positions for the Ru $3p$ and Co $2p$ signals from the reduced (metallic) metals, which were obtained from the literature, and also from the Ru and Co narrow scans in Figure S7. For metallic Co and Ru, the spacings between the Co $2p_{3/2}$ and Ru $3p_{3/2}$ peaks and between the Co $2p_{1/2}$ and Ru $3p_{1/2}$ peaks are 316 eV and 309 eV, respectively. The spacings between these peaks in the narrow scans in Figure S7 are 318.7 eV and 312.1 eV, respectively. Given the fact that (i) the Ru peaks in the spectra are within an eV of where they would be for metallic Ru, and (ii) the Co peaks in the spectra are shifted about +3 eV from where they would be in metallic Co, we believe that the shift between these peaks (+3 eV greater than the shift between the peaks in the metallic elements) indicates that Co is in an oxidized state and that Ru is in a reduced state.

Unfortunately, the literature is not entirely clear as to whether Co is in a +2 or a +3 oxidized state.⁷

Overall, the sample composition of this material by XPS is 88.9 at.% C, 7.8 at.% O, 1.6 at.% Co, and 1.7 at.% Ru.

Figure S8 is a positive ion time-of-flight secondary ion mass spectrometry (ToF-SIMS) spectrum of the sample. The large peak at $m/z = 59$ is from cobalt (Co^+), and the series of peaks from 96 to 104 are from isotopes of Ru, which are present in good agreement with their natural abundances (see Table S4). Thus, ToF-SIMS provides a strong confirmation of the presence of Co and Ru in this sample. The Na^+ peak at $m/z = 23$ is attributed to sample treatment with NaBH_4 . The signals at $m/z = 91$ (the tropylium cation), 103, and 105 are known fragments from the PS matrix (shown in Figure S8).

Table S5.2. Positions of the Co $2p_{3/2}$, Co $2p_{1/2}$, Ru $3p_{3/2}$, and Ru $3p_{1/2}$ peaks in metallic Co and Ru (from the literature), and from Co/Ru nanoparticles in a polystyrene matrix.

Peak	Co $2p_{3/2}$	Ru $3p_{3/2}$	Co $2p_{1/2}$	Ru $3p_{1/2}$	B. E. Difference
B. E. (experimental)/eV	781	462			319
B. E. (reference)/eV	778	462			316
B. E. (experimental)/eV			797	485	312
B. E. (reference)/eV			793	484	309

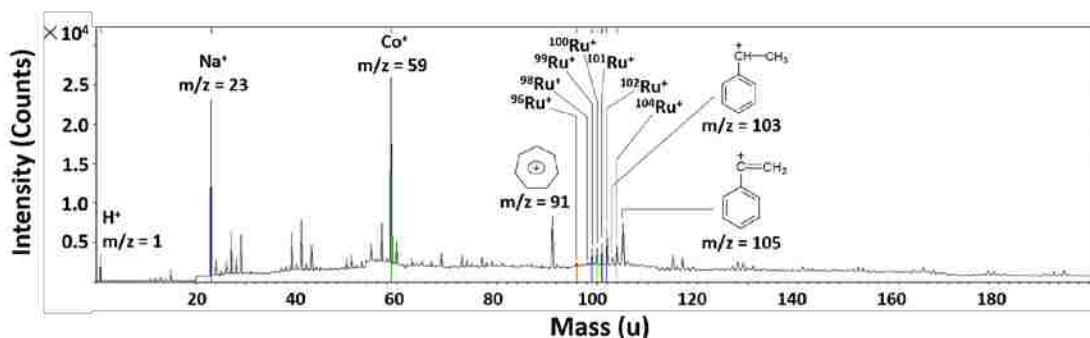


Figure S5.8 Positive ion time-of-flight (TOF)-secondary ion mass spectrometry of Co-Ru nanoparticles in a polystyrene matrix.

Table S5.3 Natural abundances of Ru isotopes and experimental peak areas of Ru⁺ signals from Co/Ru nanoparticles in a polystyrene matrix.

Isotope	Natural Abundance	ToF-SIMS Peak Area
⁹⁶ Ru	5.54 %	5.22 %
⁹⁸ Ru	1.87 %	1.98 %
⁹⁹ Ru	12.76 %	14.60 %
¹⁰⁰ Ru	12.60 %	15.58 %
¹⁰¹ Ru	17.06 %	19.10 %
¹⁰² Ru	31.55 %	27.26 %
¹⁰⁴ Ru	18.62 %	16.25 %

5.9 Instrumentation

X-ray photoelectron spectroscopy (XPS) XPS was performed with an SSX-100 instrument (Surface Science, serviced by Service Physics, Bend, OR). Monochromatic Al K_a X-rays were the excitation source, the take off angle was 35°, and a hemispherical analyzer was used. Sample charging was controlled with an electron flood gun. The following parameters were used for high resolution data acquisition: window width: 40 eV for C, O, and Ru, and 60 eV for Co, eV/step: 0.065 eV, resolution: 3 (pass energy: 100 eV), number of scans: 40, and spot size: 500 μm. The C 1s spectrum, including the Ru 3d signals were fitted as follows. A Shirley background was employed. All of the peaks were constrained to have the same widths, which floated in the fit to a

value of 2.1 eV. The peaks were 90:10 Gaussian: Lorentzians without asymmetry. The heights of the Ru 3d signals were constrained to have their theoretical 3:2 ratio.

Static time-of-flight secondary ion mass spectrometry (ToF-SIMS) was performed on a TOF-SIMS IV instrument (ION-TOF GmbH, Münster, Germany) with a 25 keV Ga⁺ source over a 250 x 250 μm² sample area. The sample was not observed to charge so no charge compensation (electron flood gun) was employed. For each sample, three spots were analyzed in positive ion mode and three in the negative mode. Care was taken not to analyze the same area of the sample twice. The total ion flux (7.2 x 10¹¹ ions/cm²) was controlled to keep the experiment within the static limit.

5.10 References for XPS and ToF-SIMS studies

1. Beamson, G.; Briggs, D., Appendices 3.1 & 3.2. In *High Resolution XPS of Organic Polymers - The Scienta ESCA300 Database*, Wiley Interscience: 1992.
2. Nohira, H.; Tsai, W.; Besling, W.; Young, E.; Petry, J.; Conard, T.; Vandervorst, W.; De Gendt, S.; Heyns, M.; Maes, J.; Tuominen, M. *J. Non-Cryst. Solids* **2002**, *303*, 83.
3. Biesinger, M. C.; Payne, B. P.; Grosvenor, A. P.; Lau, L. W. M.; Gerson, A. R.; Smart, R. *S. C. Appl. Surf. Sci.* **2011**, *257*, 2717.
4. <http://www.xpsfitting.com/search/label/Ruthenium>.
5. <http://www.xpsfitting.com/2012/01/cobalt.html>.
6. Yang, J.; Liu, H.; Martens, W. N.; Frost, R. L. *J. Phys. Chem C* **2010**, *114* (1), 111.

7. Moulder, J. F.; Stickle, W. F.; Sobol, P. E.; Bomben, K. D. *Handbook of X-ray Photoelectron Spectroscopy*, 1st ed.; Chastain, J.; R C King, J., Ed.; Physical Electronics, Inc.: Eden Prairie, Minnesota, 1995.

Chapter-6

Chemo and Regioselective Alkyl and Aryl Azide Reductions with Recoverable Heterogeneous Nanoparticle Catalysts

6.1 Introduction

Amines are an important functional group in pharmaceuticals, dyes and polymers. One of the most common routes to make amines is by reduction of the corresponding azide. Azides are excellent nucleophiles and, due to their low Lewis basicity, act like protected amines that can be easily deprotected via reduction.¹⁻³ Selective reduction of azides in the presence of other easily reducible functional groups is a significant challenge in organic synthesis because azides are generally reduced near the end of a synthesis when other sensitive functional groups are present. The two state-of-the-art approaches to azide reductions include hydrogenations in the presence of transition metal catalysts like palladium and platinum (Figure 6.1a), and Staudinger reductions with electron-rich phosphines⁴⁻⁵ (Figure 6.1b). Hydrogenation using transition metal catalysts is an effective method to reduce azides to amines,¹¹ but often proceeds with limited chemoselectivity. Staudinger reductions are known to proceed with excellent chemoselectivity compared to transition metal catalyzed hydrogenations, but Staudinger reductions generates stoichiometric amounts of phosphines oxide waste, which is hazardous to the environment and can require tedious separations to remove.

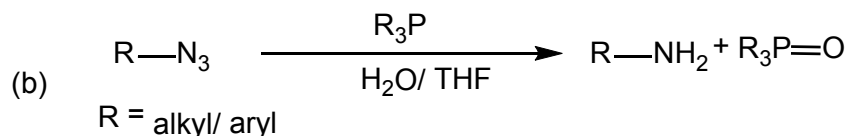
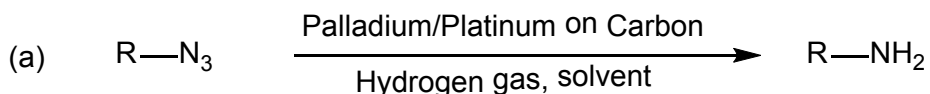


Figure 6.1 *Common methods used for azide reductions to amines*

Recent developments in the design and synthesis of catalytically active transition metal nanoparticle catalysts have demonstrated that polymer-supported nanoparticles can serve as highly efficient catalysts for organic synthesis. Transition metal nanoparticles are highly efficient catalysts due to their high surface to volume ratio, which increases the number of active sites at the metal surface. Our group is particularly interested in the potential to tune not only the reactivity of nanoparticle catalysts, but also influence the selectivity of reactions mediated by these catalysts. In nanoparticle catalysis, selectivity and catalytic activity can potentially be enhanced by modifying the nanoparticle composition, by control of size, shape and morphology, and by careful selection of a suitable nanoparticle support/stabilizer. In the previous chapter, we described our efforts to use polymer structure to control the catalytic activity of Ru-Co nanoparticle catalysts for chemoselective nitroarene reductions. This chapter will discuss our efforts to develop highly chemoselective and regioselective catalysts for azide reductions using monometallic ruthenium nanoparticles supported on commercially available polystyrene. Regioselective reductions of one azide in the presence of multiple azides is also demonstrated. This report represents the first example of transition metal nanoparticle catalyzed regioselective reduction of azides in the presence of multiple azides.

While several recent publications report that nanoparticle catalysts can perform azide reduction reactions, these reductions require high temperature and/or stoichiometric amounts of reducing metals. Kappe et al.⁶ reported the reduction of aromatic azides and nitro compounds to amines using iron oxide nanoparticles in the presence of hydrazine hydrate as a reducing agent. These reactions were shown to proceed rapidly at 150-170 °C under microwave irradiation conditions (Figure 6.2). Chemoselectivity in this transformation was not demonstrated, and is

presumed to be low due to the forcing reaction conditions. In addition, concerns arise regarding the safety of heating the azide-containing compounds to such high temperatures on large scale.

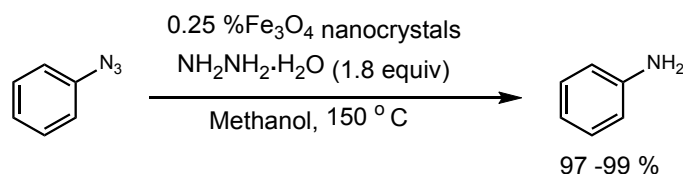


Figure 6.2 Reduction of azides to amines using iron oxide nanoparticles

Ranu et al.⁷ reported the reduction of aromatic azides to amines using copper nanoparticles in the presence of ammonium formate as reducing agent at 100 °C (Figure 6.3). While this reaction proceeded in high yield, the optimized conditions require significant metal loadings (50 mol%), and no reductions alkyl azides or chemoselectivity studies were presented.

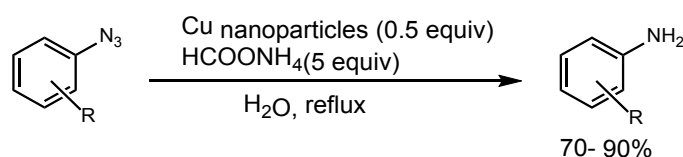


Figure 6.3 Reduction of azides to amines using copper nanoparticles

Garcia-Garibay et al.⁸ reported photocatalytic reductions of aromatic azides to amines using cadmium sulfide (CdS) and cadmium selenide (CdSe) nanoparticles in the presence of sodium formate (Figure 6.4). In this reduction, the yields of meta substituted compounds are comparatively lower than ortho- and para-substituted compounds. In addition, this reduction was only shown to proceed with aromatic azides, and no information on the potential synthetic utility or chemoselectivity was provided.

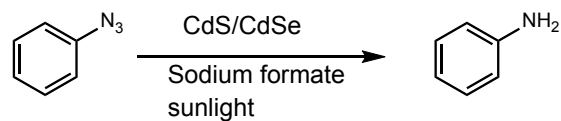


Figure 6.4 Reduction of aromatic azides to amines using CdS/CdSe nanoparticles

In the examples presented above, the application of the nanoparticle catalysts is limited because of low chemoselectivity for azide reduction, the need for high temperatures, and a lack of information on the substrate scope of the transformations. Due to the limitations associated with current methods for chemoselective azide reduction reactions, our goal was to demonstrate that polymer-supported nanoparticle catalysts could act as highly efficient and chemoselective catalysts for azide reductions that proceed under mild reaction conditions. In addition, we desired to develop catalysts capable of performing both aliphatic and aromatic azide reductions. We also desired to investigate whether our nanoparticle catalysts could achieve high regioselectivity in the mono-reduction of bis and multi-azide containing molecules. This latter effect could provide an attractive route to the synthesis of differentially-functionalized diamine products.

Our group recently demonstrated the utility of polymer-supported Ru-Co bimetallic nanoparticles in nitro arene reductions⁹. In our report, we showed that catalytic activity could be optimized by modification of the supporting polymer structure. During the course of these studies, we found that the reduction of aryl azides could occur with high chemoselectivity in the presence of an easily reduced nitro functional group (Figure 6.5). This exceptional chemoselectivity for azide reduction has not been demonstrated in nanoparticle catalysis. In this chapter, we report that polystyrene-supported ruthenium nanoparticles are highly chemoselective catalysts for azide reductions and that selective mono reductions of multi-azide substrates can be attained with high levels of regioselectivity.

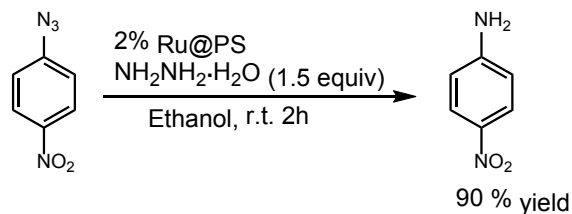


Figure 6.5 Reduction of 1-azido-4-nitrobenzene using Ru NPs supported on polystyrene

6.2. Results and Discussions

6.2.1 Catalyst Preparation

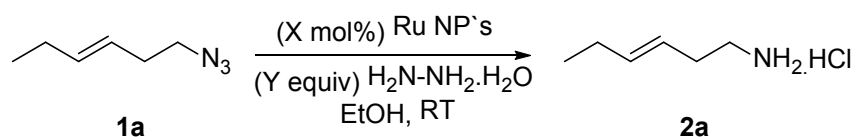
We prepared polystyrene supported ruthenium nanoparticles according to a modified literature procedure via NaBH_4 reduction of a homogeneous solution of ruthenium trichloride hydrate and polystyrene (MW 35,000). The polymer supported nanoparticles were then precipitated from solution, washed with deionized water and dried under vacuum. The black powder thus obtained can be easily recovered and reused from the reaction mixtures by simple filtration⁹. The preparation of ruthenium nanoparticles stabilized by polymers of differing electronic properties was also prepared according to this method.

6.2.2 Catalyst Optimization Studies

The polystyrene-supported ruthenium nanoparticles prepared above were first tested for catalytic activity and chemoselectivity in the reduction of 1-azidohex-3-ene (Table 6.1). With 3 mol% of our ruthenium catalyst and 3 equivalents of hydrazine hydrate, the azide reduction reaction goes to completion in just 1 hour with nearly quantitative yield (entry 1). The ruthenium nanoparticles showed good reactivity and chemoselectivity for reduction of the azide functional group in the presence of an olefin. In our optimization studies, we found that efficient reduction

could occur with as little as 1.5 equivalents of hydrazine hydrate (entries 1–3), and with as little as 1 mol% ruthenium catalyst (entries 4–8). For our optimized conditions, we found that reductions in the presence of 2 mol% ruthenium and with 3 equivalents hydrazine hydrate provided the most reproducible results over a wide range of substrates

Table 6.1 Optimization of the catalyst



entry	Ru@PS (X mol%)	NH ₂ NH ₂ ·H ₂ O (Y equiv)	Time (h)	Yield (%)
1	3	3	1	99
2	3	2	1.4	97
3	3	1.5	2.1	98
4	2	3	2	98
5	2	2	2.5	98
6	2	1.5	3.0	72
7	1	3	3.0	94
8	1	2	3.0	86

Reactions run using 0.37 mmol **1**, X mol% ruthenium nanoparticles (0.401 mmol/g in polystyrene) in 2 mL EtOH unless otherwise noted.

We next investigated the impact of the metal loading in the polymer and the composition of the nanoparticle catalyst had on catalytic activity (Table 6.2). This study showed that the metal loading in the polymer was inconsequential for catalytic activity (entries 1–4). Thus, the highest polymer loading (0.4 mmol Ruthenium per gram of polystyrene) was chosen to minimize the amount of polymer-supported nanoparticle that was required for efficient conversions. We also investigated whether the Ru-Co nanoparticles used previously for nitroarene reductions were better catalysts for azide reductions than monometallic ruthenium nanoparticles (entry 5). We

found that incorporation of cobalt into the nanoparticle had negligible effects on catalytic activity, and so pure ruthenium nanoparticle catalysts were used for the remainder of our studies.

Table 6.2 Effect of metal loading and nanoparticle composition on catalytic activity.

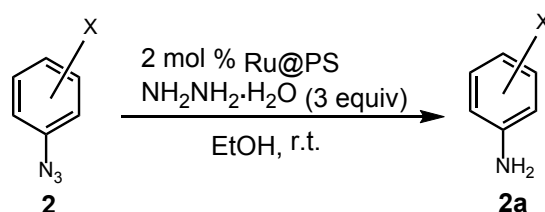
entry ^a	Ru NPs (mmol/g)	Ru NPs (Xmol %)	NH ₂ NH ₂ ·H ₂ O (equiv)	Time (h)	Yield (%)
1	0.4	2	3	2	97
2	0.3	2	3	2	97
3	0.2	2	3	2	96
4	0.1	2	3	2	94
5 ^b	0.4	2	3	2	97

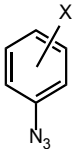
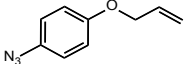
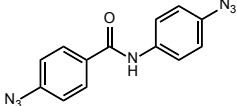
^a Reactions run using 0.37 mmol **1**, X mol% ruthenium nanoparticles (0.401 mmol/g in polystyrene) in 1 ml EtOH unless otherwise noted. ^b Ru-Co (2.5:1) on polystyrene was used.

6.2.3 Substrate Scope of azide reduction

After developing optimal reactions conditions for azide reductions, we next studied the functional group tolerance of the nanoparticle catalyst for the reduction of aromatic azides (Table 6.3). These studies showed that aromatic halides (entries 1–3), amides (entry 4), carboxylic acids (entry 5), esters (entry 6), anilines (entry 7), phenols (entry 8), cyanides (entry 9), ketones (entry 10), and allylic ethers (entry 11) could all be tolerated in the reaction and underwent no observed reduction. Aromatic bis azides (entry 12) also readily reduce to give the di-aniline product in high yield. In all the cases tested, the products were obtained in nearly quantitative yield after removal of the catalyst by filtration and solvent removal.

Table 6.3 Aromatic compounds used in azide reduction. Yields/Selectivity



entry ^a	Substrate 2	X		Time (h)	Yield/ Select. ^b
1		4-Cl	2b	4	98/98
2		4-Br	2c	4	96/98
3		4-I	2d	4	96/97
4		4-CONH ₂	2e	5	98/99
5		4-COOH	2f	5	99/99
6		4-CO ₂ Me	2g	5	99/100
7		4-NO ₂	2h	8	98/90
8		4-NH ₂	2i	5	99/99
9		4-OH	2j	4	98/99
10		4-CN	2k	4	94/99
11		4-Ac	2l	4	99/99
12			2m	10	98/100 ^c
13			2n	6	98/100

^aReaction conditions: **2** (0.38 mmol), catalyst (2 mol % Ru), NH₂NH₂.H₂O (3 equiv.) Ethanol (1mL) at ambient temp. ^bIsolated yields, ^c4 mol% catalyst, NH₂NH₂.H₂O (4 equiv.)

We also studied the chemoselectivity of azide reductions with more synthetically valuable aliphatic substrates (Figure 6.6). These classes of substrates are easily accessed via substitution reactions, and thus are widely used in the synthesis of amine-containing molecules. We found that

benzylic azides containing alkene (**3a** and **3b**) reduce in high yield with high chemoselectivity. Primary (**3o**), secondary (**3e**, **3j**), and tertiary (**3m**) azides are all efficiently reduced under our standard conditions. Azides containing double bonds (**1**, **3b**, **3p**), triple bonds (**3c**, **3d**, **3f**), silyl ethers (**3h**), alcohols (**3j**), and acetals (**3i**), all reacted in excellent yields and almost perfect chemoselectivity. Azides are often common intermediates in the synthesis of complex, amine-containing biomolecules, and thus we desired to investigate whether our method could be used in the synthesis of these valuable intermediates. We found that cholesterol azides (**3k**), azido sugars (**3n**, **3q**), nucleosides (**3l**), and amino acids (**3e**) all reacted in high yield and with good chemoselectivity. In all cases tested, the catalytic activity of our polystyrene supported ruthenium nanoparticles was very good. One limitation to our methodology is that alkyne-containing benzylic substrates reacted in only moderate yield and with slightly diminished chemoselectivity (**3c**, **3d**). However, the yield and selectivity of aliphatic alkynes is excellent (**3f**).

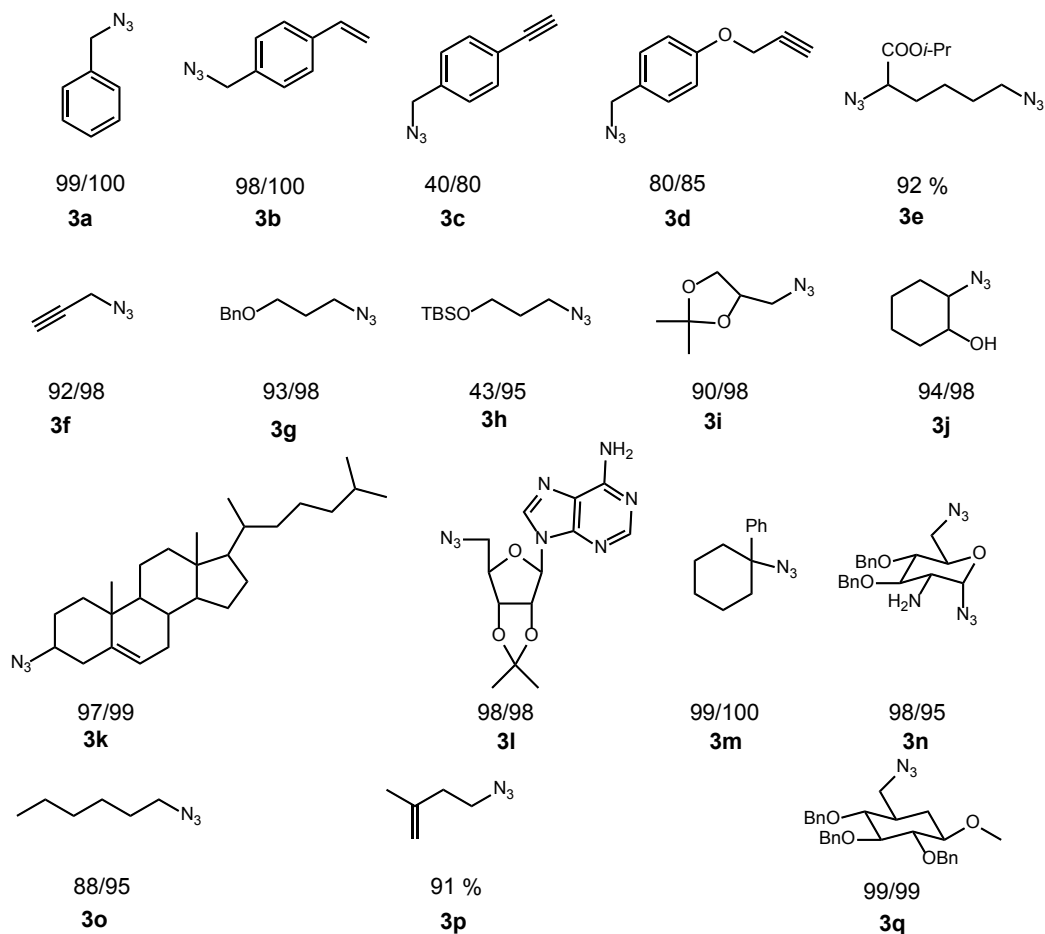
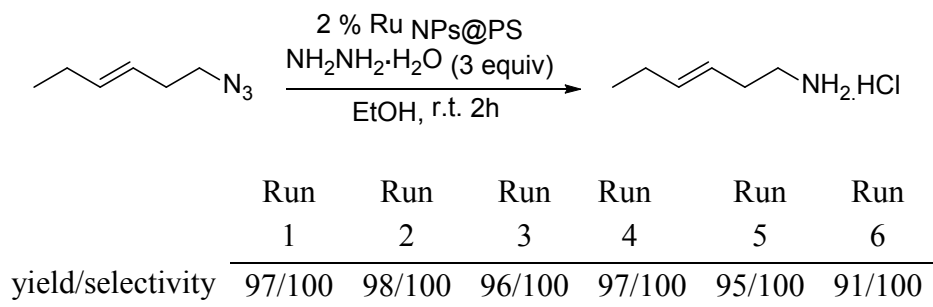


Figure 6.6 Aliphatic substrates used in azide reduction. Yield/Selectivity.

6.2.4 Recyclability studies

We next studied whether the heterogeneous polystyrene supported Ru nanoparticles could be recycled without loss of activity. We found that our nanoparticle catalysts could be recycled various times by simply filtering off the reaction mixture, washing the heterogeneous catalyst with ethanol, and then re-adding reagents for the subsequent reaction. No catalyst reactivation step was required. We also found that our catalysts could be reused up to six times without significant loss in product yield or reaction chemoselectivity.



Scheme 6.1 *Catalyst Recyclability Studies*

6.2.5 Leaching Studies

We next investigated the leaching of Ru nanoparticles into solution to see if the reaction was catalyzed by homogeneous nanoparticles that leached from the polymer matrix. We removed the catalyst from the reaction after partial conversion by filtering through a sintered glass funnel. After removal of the catalyst was added another 4 equivalents of hydrazine hydrate and no further conversion of the starting material (monitored by NMR) was observed. When the catalyst was added back to the reaction mixture after several hours the reduction reaction resumed (similar to Cat-in-a-Cup test)¹⁸. These results suggest that heterogeneous polymer supported nanoparticles are responsible for the observed catalysis and not homogeneous metal nanoparticles that have leached from the polymer matrix (figure 6.7).

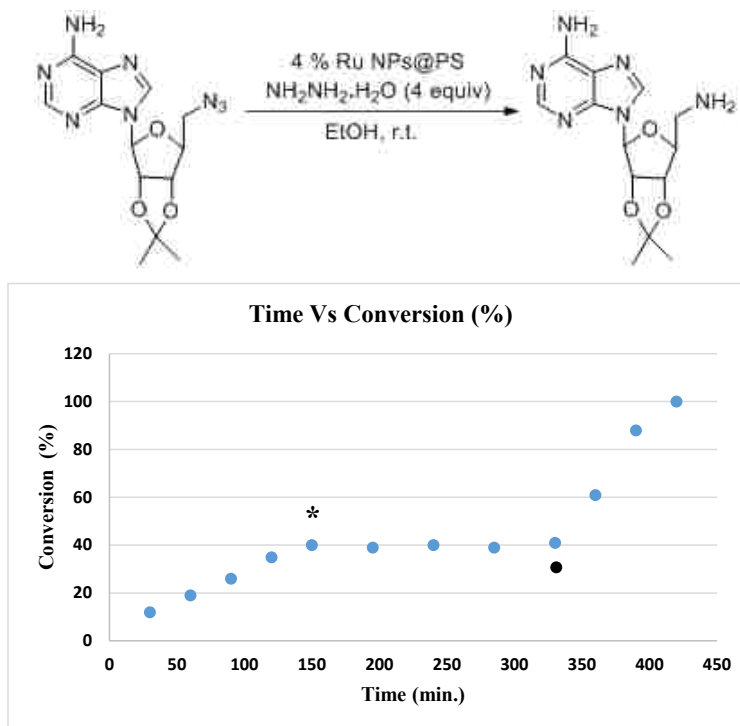


Figure 6.7 Test for homogeneous nanoparticles. Catalyst was removed by filtration at time points indicated with *. Catalyst was added back to the reaction at time points indicated by ●.

6.2.6 Regioselectivity in Azide Reductions

The regioselective mono-reduction of substrates containing multiple azide functional groups represents an attractive strategy for synthesizing differentially functionalized polyamine products. Several groups have reported regioselective reductions of electronically different azide functional groups with electron-rich phosphines. For example, Wong et al.¹⁰ reported the regioselective azide reduction of bis azide **3** using trimethyl phosphine at -78 °C to room temperature (Figure 6.7). In this method, electronic factors play an important role in obtaining high regioselectivity in the reduction of bis azides. The azide closer to the more electron withdrawing acetate functional groups was shown to reduce more quickly. In this section we discuss our efforts to optimize both the reaction conditions and the catalyst structure to obtain high regioselectivity in the mono-reduction of bis(azide) containing substrates. We show that

high regioselectivity for reduction of the sterically most accessible azide is accomplished with our nanoparticle catalysts.

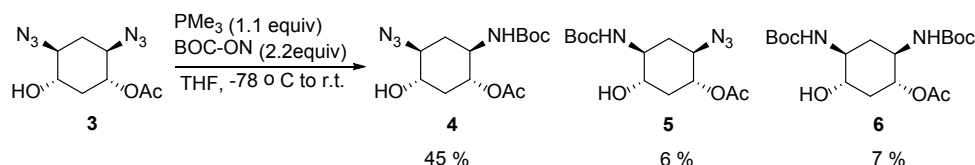
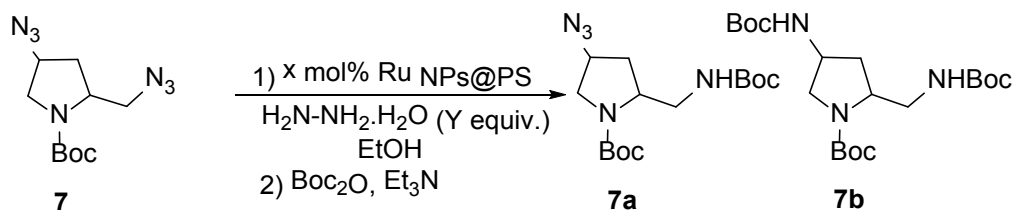


Figure 6.8 Regioselective reduction of bis-azides using trimethyl phosphine.

We initiated our investigations into regioselective azide reductions using proline-derived azide bis(azide) **7**, which contains both a primary and secondary azido group (Table 6.3). Under previously-developed conditions for selective azide reductions with electron-rich phosphines, a 1:1 mixture of mono and bis reduced product was formed (entry 1). While our nanoparticle catalysts did not react at low temperatures (entries 2–3), moderate conversions were observed at 0 °C (entries 4–5). When the reactions was initiated at 0 °C and then warmed to room temperature, good yield and chemoselectivity was obtained for the mono-reduction of the most sterically accessible primary azide (entry 6). These preliminary results confirm that regioselectivity can be obtained for monoreduction of bis(azide) containing substrates.

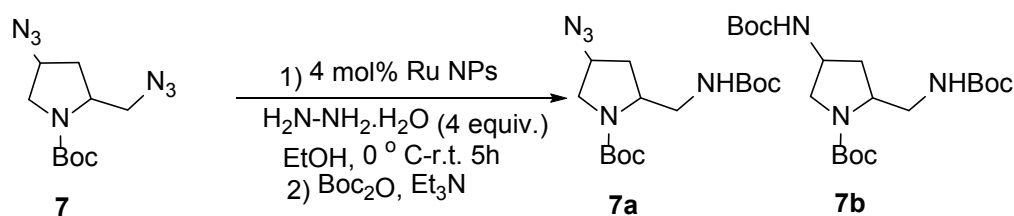
Table 6.3 Optimization of regioselectivity by changing the temperature



entry	Ru NPs (X mol %)	NH ₂ NH ₂ .H ₂ O (Y equiv)	Temp. (° C)	Time (h)	SM recovered (%Yield)	7a (% Yield)	7b (%Yield)
1	0	1.05eq PMe ₃	-78	12	5	54	29

2	4	4	-78	1	100	0	0
3	4	4	-78	4	97	3	0
4	4	4	0	1	76	20	3
5	4	4	0	4	20	60	20
6	4	4	0-rt	5 at rt	5	68	23

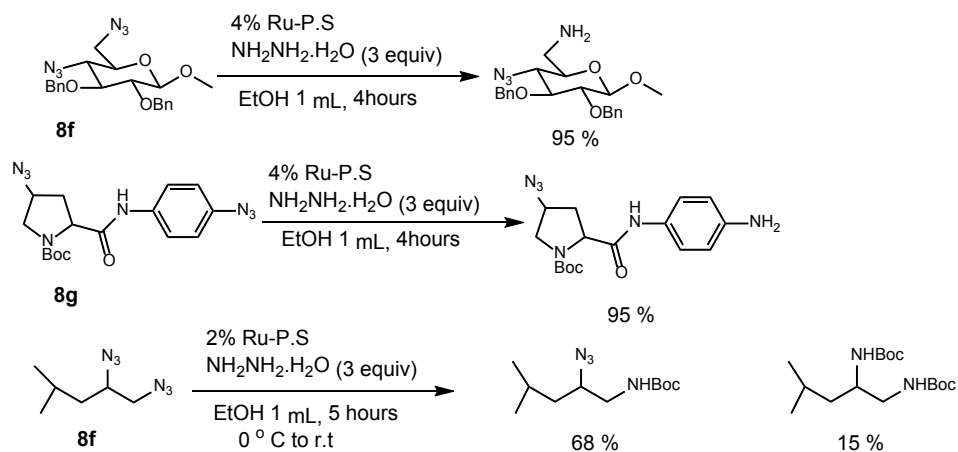
We next investigated the impact of polymer structure on the regioselectivity of our nanoparticle catalysts. Our hypothesis was that by controlling the activity of the nanoparticle by varying the electronic properties of the nanoparticle, higher selectivity for reduction of the sterically less hindered azide could be achieved. In our study, we found that the polymer structure did in fact have a significant influence on the selectivity of the catalyst for mono azide reduction (Figure 6.8). Unfortunately, the impact of electronic structure on the ratio of products formed did not follow any clear trend. In addition, none of the functionalized polymers tested provided higher selectivity than the corresponding polystyrene polymer. Thus, our additional studies focused on the use of our polystyrene-supported ruthenium nanoparticles for regioselective azide reductions.



	R = H	70 %	22 %
	R = Me	23 %	73%
	R = OMe	22 %	38 %
	R = t-Bu	5 %	90%
	R = Cl	53 %	44 %
	R = COO <i>i</i> -Pr	54 %	19 %
	R = CF ₃	28 %	68 %

Figure 6.9 Effect of polymer support on regioselectivity

Having established that our nanoparticle catalysts are capable of regioselective azide reductions, we explored the regioselectivity for reduction of primary over secondary azides in a variety of substrates (Figure 6.9). Primary azides are readily reduced in the presence of electronically activated benzylic azides (**8a–8e**). Aromatic azides also reduce with high regioselectivity over alkyl azides (**8g**). This regioselective reduction is also amenable to mono-reductions of azido sugars (**8f**) and alkyl bis-azides. In all cases, good yields and moderate to excellent selectivities could be obtained for the mono-reduction product (Figure 6.10)



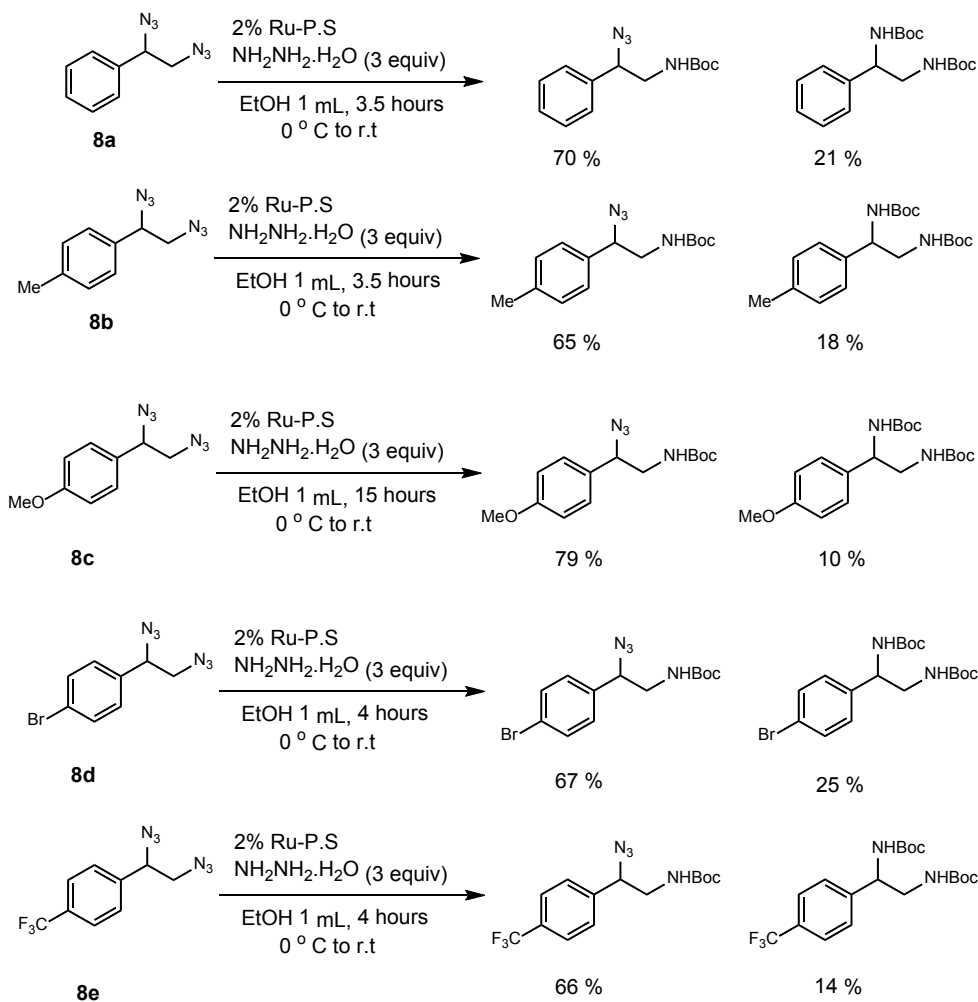


Figure 7.0 Regioselective reduction of bis-azides.

6.3 Conclusion

The chemoselective reduction of azides to amines in the presence of easily reducible functional groups is an important reaction in organic synthesis. We have developed mild and highly chemoselective reduction of azides that has broad substrate scope including sugars, nucleosides, and steroids using polystyrene supported ruthenium nanoparticles. Our ruthenium nanoparticles also show good regioselectivity for the reduction of primary azides over secondary, primary azides over benzylic azides, aromatic azides over alkyl azides, and primary over

secondary azides in sugars. In addition, our polystyrene supported ruthenium nanoparticles are easily recoverable and recyclable after completion of the reaction by simple filtration.

6.4 References

1. Roestamadji, J.; Grapsas, I.; Mobashery, S. *J. Am. Chem. Soc.* **1995**, *117*, 11060.
2. Alper, P. B.; Hung, S.-C.; Wong, C.-H. *Tetrahedron Lett.* **1996**, *37*, 6029.
3. Alper, P. B.; Hendrix, M.; Sears, P.; Wong, C.-H. *J. Am. Chem. Soc.* **1998**, *120*, 1965.
4. Gololobov, Y. G.; Zhmurova, I. N.; Kasukhin, L. F. *Tetrahedron*, **1981**, *37*, 437.
5. Gololobov, Y. G.; Kasukhin, L. F. *Tetrahedron*, **1992**, *48*, 1353.
6. Cantillo, D.; Mirhosseini, M.; Kappe, C. O. *J. Org. Chem.* **2013**, *78*, 4530.
7. Ahammed, S.; Saha, A.; Ranu, B. C. *J. Org. Chem.* **2011**, *76*, 7235.
8. Warriar, M.; Lo, M. K. F.; Monbouquette, L. H.; Garcia-Garibay, M. A. *Photochem. Photobiol. Sci.*, **2004**, *3*, 859.
9. Udumula, V.; Tyler, J.H.; Davis, D. A.; Wang, H.; Linford, M. R.; Minson, P.S.; Michaelis, D. J. *ACS Catal.* **2015**, *5*, 3457.
10. Nyffeler, P. T.; Liang, C-H.; Koeller, K. M.; Wong, C-H. *J. Am. Chem. Soc.* **2002**, *124*, 10778.
11. Hemantha, H. P.; Sureshbabu, V. V. *Org. Biomol. Chem.* **2011**, *9*, 2597.

6.5 Experimental Section

General Information

All reactions were carried out in oven-dried glassware with magnetic stirring, unless otherwise indicated. All the reagents were used as obtained unless otherwise noted. Analytical thin-layer chromatography was performed with 0.25 mm coated commercial silica gel plates (E. Merck, DC-Plastikfolien, kieselgel 60 F254). Flash Chromatography was performed with EM Science silica gel (0.040-0.063 μ m grade) Proton nuclear magnetic resonance ($^1\text{H-NMR}$) data were acquired on a Inova 300 (300 MHz) or on a Inova-500 (500 MHz) spectrometer. Chemical shifts are reported in delta (δ) units, in parts per million (ppm) downfield from tetramethylsilane. Carbon-13 nuclear magnetic resonance ($^{13}\text{C-NMR}$) data were acquired on a Inova 500 at 125 MHz. Signals are reported as follows: s (singlet), d (doublet), t (triplet), q (quartet), dd (doublet of doublets), qd (quartet of doublets), brs (broad singlet), m (multiplet). Coupling constants are reported in hertz (Hz). Chemical shifts are reported in ppm relative to the center line of a triplet at 77.23 ppm for chloroform-d. Mass spectral data were obtained using ESI techniques (Agilent, 6210 TOF). The content of all metals in the final material was determined by ICP analysis using a Shimadzu ICPS-7510 instrument. STEM images and EDS analyses were obtained using a JEOL JEM-2100F instrument operated at 5.0 kV. All STEM specimens were prepared by placing a drop of a homogeneous chloroform solution of the respective polymer-nanoparticle composite on a carbon coated copper grid and allowed to dry in air without staining. Polystyrene (MW 35,000) were purchased from Aldrich. Ruthenium (III) chloride hydrate was purchased from Strem Chemicals.

Synthesis of Ru NP's@Polystyrene

Polystyrene (1g) was added to 25 mL of THF and the mixture was stirred using a Teflon-coated magnetic stir bar until polystyrene was completely dissolved then 10 mL of ethanol and Ruthenium (III) chloride hydrate (100 mg, 0.482 mmol) anhydrous basis was added and the mixture was stirred until the solution became homogenous. Sodium borohydride (182.5 mg, 4.82 mmol) was then added portion wise. The reaction was stirred under argon atmosphere for 10 h giving a black homogeneous solution, indicating the formation of nanoparticles. The solvent was then evaporated and millipore water was added to the resulting solid and the mixture was stirred for 15 minutes then filtered. The solid was then washed with millipore water (20 mL× 5) and dried under vacuum to give a black solid, which was finely ground with a mortar and pestle before use.

Characterization of Ru/polystyrene nanoparticles:

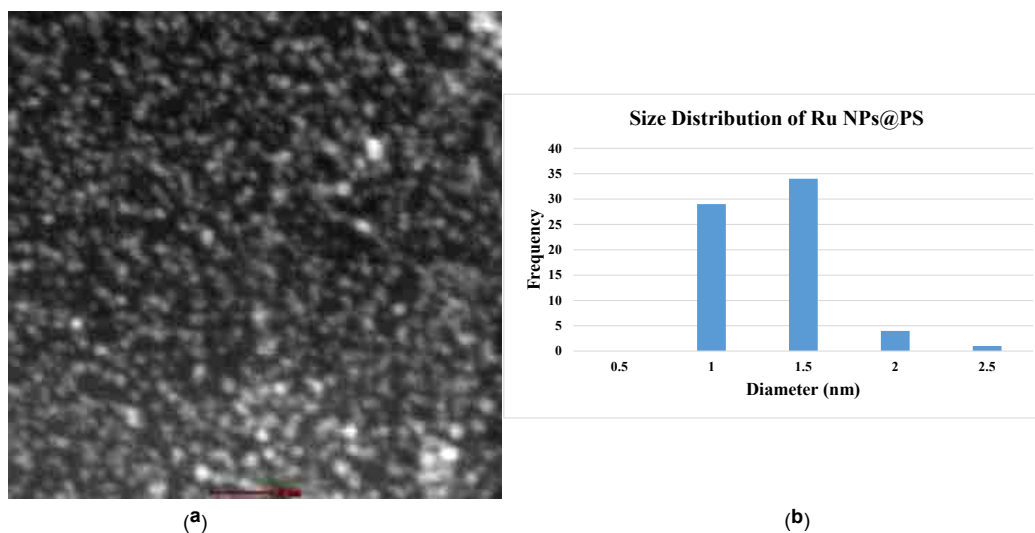


Figure 7.1 STEM image of Ru NPs in polystyrene catalyst. (a) STEM Image of polymer-encapsulated nanoparticles. (b) Statistical analysis of nanoparticle size (average size: 1.33 nm)

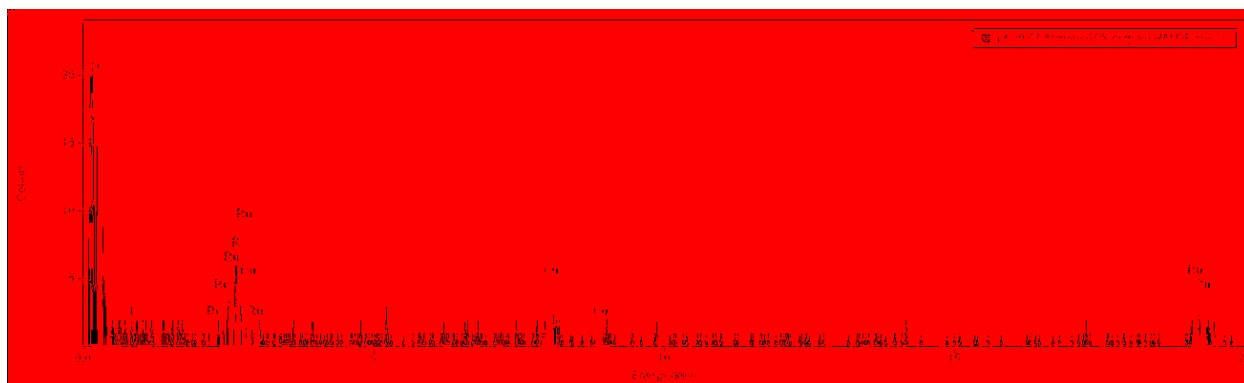


Figure 7.2 EDS spectrum of the Ru nanoparticles showing the presence of the main components Ru. Cu and C peak are background from the TEM support grid.

Preparation of the sample for ICP-analysis

To 10 mg of polymer-nanoparticle catalyst was added 1 ml conc. H₂SO₄ and the mixture heated at 140 °C. HNO₃ was then slowly added and the solution was heated for 10 min. 1 mL of aqua regia was then added and the mixture cooled to room temperature and diluted to 500 mL in a volumetric flask. Metal concentrations were then determined by ICP analysis by comparison to standard solutions.

Reuse experiments of Ru NP's@Polystyrene

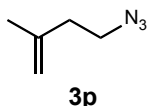
The reduction of (*E*)-1-azidohex-3-ene was performed under the typical reaction conditions in a flask containing a frit of medium porosity and a bottom stopcock. After completion of the reaction, the solution was removed via filtration through the frit. The flask was then rinsed with EtOH (3 ml), 2.0 M HCl in diethylether was added and the filtrate evaporated, to the filtrate chloroform was added and filtered the solid (unreacted hydrazine), evaporated the filtrate and the isolated yield and selectivity were determined. To the remaining nanoparticle catalyst was added a

new set of reagents and solvents and the reaction was allowed to proceed for the same time. This procedure was repeated 6 times (scheme 6.1)

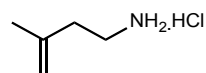
Reduction of (*E*)-1-azidohex-3-ene (**1a**)

General Procedure:

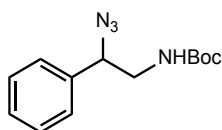
A typical procedure for the reduction of azido compounds by Ru NPs@Polystyrene is as follows: Ru NPs@Polystyrene (17 mg, 2 mol% wrt ruthenium) was placed in a 10 mL test tube containing a Teflon-coated magnetic stir bar, followed by the addition of ethanol (1 mL), (*E*)-1-azidohex-3-ene (50 mg, 0.399 mmol), and dropwise addition of hydrazine monohydrate (1.19 mmol, 58 μ L, 3 equiv) at room temperature. The reaction vessel was then sealed with a glass stopper and stirred for 2 h. After the reaction, Ru NPs@Polystyrene was removed by filtration through a small plug of silicagel in a pipet, and the solids washed several times with ethanol. The filtrate was collected, and the solvent removed under reduced pressure on a rotary evaporator to provide the product (39.6 mg, 0.332 mmol, 98% yield, and 100% selectivity) in excellent purity, which did not require further purification. The selectivity of the reaction was determined by ^1H NMR analysis of the pure product obtained as described. (2a) ^1H NMR (500 MHz, CDCl_3): 8.2 (br m, 4H), 4.4-4.1 (brs, 1 H), 5.7-5.6 (m, 1H), 5.38-5.33 (m, 1H), 3.13-2.91 (m, 2H), 2.58-2.35 (m, 2H), 2.0 (t, 2H, $J = 6.9$ Hz), 0.98 (t, 3H, $J = 7.2\text{Hz}$); ^{13}C NMR (125 MHz, CDCl_3): 137.2, 122.5, 39.7, 30.5, 25.5, 13.4. Yield: 98 % (100)



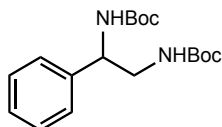
^1H NMR (500 MHz, CDCl_3) δ 4.85–4.79 (d, 2H), 3.38 (t, $J = 7.2$ Hz, 2H), 2.31 (t, $J = 7.2$ Hz, 2H), 1.76 (s, 3H); ^{13}C NMR (125 MHz, CDCl_3): 141.7, 112.6, 49.4, 36.7, 22.25.



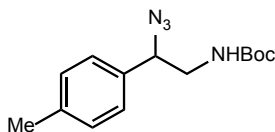
^1H NMR (500 MHz, CDCl_3) δ 4.88 (d, 2H), 3.14 (t, $J = 7.2$ Hz, 2H), 2.49 (t, $J = 7.2$ Hz, 2H), 1.77 (s, 3H); ^{13}C NMR (125 MHz, CDCl_3) δ 140, 113.7, 37.9, 35.2, 22.2. Yield: (92 % (100)).



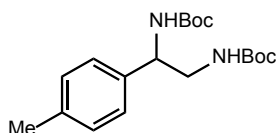
^1H NMR (500 MHz, CDCl_3) δ 7.44–7.30 (m, 5H), 4.86 (brs, 1H), 4.75–4.67 (m, 1H), 3.33–3.19 (m, 1H), 1.46 (s, 9H); ^{13}C NMR (125 MHz, CDCl_3) δ 155.7, 137.1, 128.9, 128.8, 128.6, 128, 126.5, 79.8, 65.6, 55.6, 46.11, 28.35. Yield: 70 %



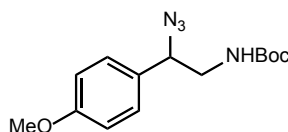
^1H NMR (500 MHz, CDCl_3) δ 7.41–7.25 (m, 5H), 5.55 (brs, 1H), 4.94–4.67 (m, 2H), 3.59–3.32 (m, 2H), 1.47 (s, 9H), 1.44 (s, 9H); ^{13}C NMR (125 MHz, CDCl_3) δ 128.7, 127.6, 126.3, 80.5, 55.9, 45.8, 28.36. Yield: 21 %



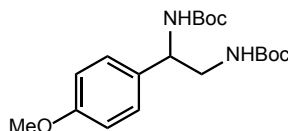
^1H NMR (500 MHz, CDCl_3) δ 7.13 (s, 4H), 4.81–4.71 (m, 1H), 4.63–4.54 (m, 1H), 3.44–3.30 (m, 1H), 3.20–3.10 (m, 1H), 2.28 (s, 3H), 1.37 (s, 9H); ^{13}C NMR (125 MHz, CDCl_3) δ 155.7, 138.5, 134, 129.6, 126.9, 65.4, 46.0, 28.3, 21.1. Yield: 65 %



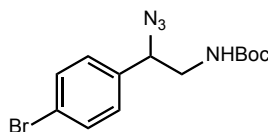
^1H NMR (500 MHz, CDCl_3) δ 7.15 (s, 4H), 5.47 (brs, 1H), 4.89 (brs, 1H), 4.71 (brs, 1H), 3.56–3.20 (m, 2H), 2.33 (s, 3H), 1.44 (s, 9H), 1.42 (s, 9H); ^{13}C NMR (125 MHz, CDCl_3) δ 156.8, 155.7, 137.2, 129.4, 126.2, 79.6, 55.6, 45.9, 28.3, 21.1. Yield: 18 %



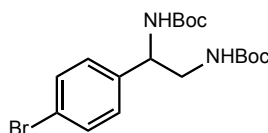
^1H NMR (500 MHz, CDCl_3) δ 7.27 (d, $J = 9$ Hz, 2H), 6.95 (d, $J = 8.8$ Hz, 2H), 4.84 (brs, 1H), 4.71–4.58 (m, 1H), 3.84 (s, 3H), 3.53–3.39 (m, 1H), 3.32–3.18 (m, 1H), 1.47 (s, 9H); ^{13}C NMR (125 MHz, CDCl_3) δ 159.8, 129, 128.2, 127.7, 114.3, 114.2, 65.2, 55.3, 46.0, 28.2. Yield: 79 %



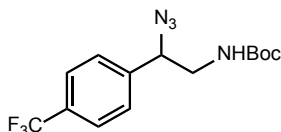
^1H NMR (500 MHz, CDCl_3) δ 7.20 (d, $J = 8$ Hz, 2H), 6.88 (d, $J = 9$ Hz, 2H), 5.39 (brs, 1H), 4.82 (brs, 1H), 4.74–4.64 (m, 1H), 3.8 (s, 3H), 3.55–3.25 (m, 2H), 1.45 (s, 9H); ^{13}C NMR (125 MHz, CDCl_3) δ 159, 127.5, 114.11, 113.8, 55.29, 45.8, 29.7, 28.3, 28.2. Yield: 10 %



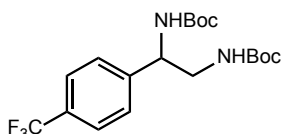
^1H NMR (500 MHz, CDCl_3) δ 7.53 (d, $J = 8.5$ Hz, 2H), 7.21 (d, $J = 8$ Hz, 2H), 4.85 (brs, 1H), 4.72–4.65 (m, 1H), 3.49–3.39 (m, 1H), 3.25–3.14 (m, 1H), 1.45 (s, 9H); ^{13}C NMR (125 MHz, CDCl_3) δ 155.6, 136.2, 132.1, 128.6, 122.6, 80.0, 65.0, 55.4, 46.1, 28.3. Yield: 67 %



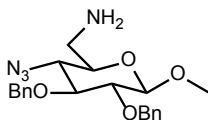
^1H NMR (500 MHz, CDCl_3) δ 7.49 (d, $J = 8.4$ Hz, 2H), 7.20 (d, $J = 8.4$ Hz, 2H), 5.6 (brs, 1H), 4.8 (brs, 1H), 4.76–4.60 (m, 1H), 3.53–3.27 (m, 2H), 1.47 (s, 9H), 1.43 (s, 9H); ^{13}C NMR (125 MHz, CDCl_3) δ 157.0, 155.6, 131.8, 128.1, 121.4, 80.0, 55.8, 45.6, 28.3, 28.1. Yield: 25 %



^1H NMR (500 MHz, CDCl_3) δ 7.7–7.2 (m, 2H), 7.51–7.43 (m, 2H), 4.89 (brs, 1H), 4.81 (brs, 1H), 3.54–3.45 (m, 1H), 3.28–3.19 (m, 1H), 1.44 (s, 9H); ^{13}C NMR (125 MHz, CDCl_3) δ 155.6, 154.9, 141.2, 130.9, 130.6, 130.3, 127.3, 126.9, 125.9–15.77 (m), 80.0, 65.0, 55.4, 46.2, 28.3. Yield: 66 %

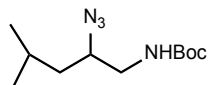


^1H NMR (500 MHz, CDCl_3) δ 7.63 (d, $J = 8.1$ Hz, 2H), 7.43 (d, $J = 8.1$ Hz, 2H), 5.78 (brs, 1H), 4.82 (brs, 2H), 3.42 (brs, 2H), 1.47 (s, 9H), 1.44 (s, 9H). Yield: 14 %

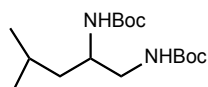


^1H NMR (500 MHz, CDCl_3) δ 7.42–7.2 (m, 10H), 4.87–4.70 (m, 3H), 4.68–4.52 (m, 2H), 4.0–3.96 (m, 1H), 3.92–3.77 (m, 2H), 3.69–3.58 (m, 1H), 3.36 (s, 3H), 3.0–2.87 (m, 1H),

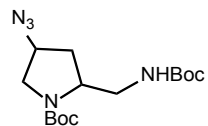
2.78–2.65 (m, 1H); ^{13}C NMR (125 MHz, CDCl_3) δ 128.5, 128.4, 128.1, 128.0, 127.9, 127.8, 127.7, 127.0, 98.6, 78.1, 76.6, 73.8, 73.2, 70.0, 62.0, 55.4, 43.1. Yield: 95 %



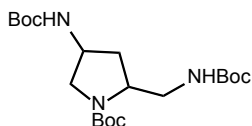
^1H NMR (500 MHz, CDCl_3) δ 4.86 (brs, 1H), 3.58–3.51 (m, 1H), 3.42–3.34 (m, 1H), 3.0–2.93 (m, 1H), 1.84–1.75 (m, 1H), 1.44 (s, 9H), 1.43–1.38 (m, 1H), 1.32–1.24 (m, 1H), 0.97–0.93 (m, 6H); ^{13}C NMR (125 MHz, CDCl_3) δ 155.8, 60.8, 44.7, 40.7, 28.3, 24.9, 22.9, 22.0. Yield: 68 %



^1H NMR (500 MHz, CDCl_3) δ 4.88 (brs, 1H), 4.49 (brs, 1H), 3.72 (brs, 1H), 3.27–3.07 (m, 2H), 1.74–1.64 (m, 1H), 1.35–1.18 (m, 2H), 0.97–0.83 (m, 6H); ^{13}C NMR (125 MHz, CDCl_3) δ 156.5, 156.18, 79.2, 49.3, 45.4, 42.1, 28.4, 28.3, 24.8, 23.0, 22.2. Yield: 15 %

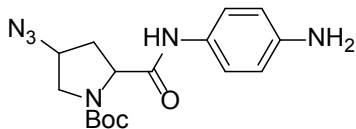


^1H NMR (500 MHz, CDCl_3) δ 5.1 (brs, 1H), 4.2–3.8 (m, 3H), 3.3–3.28 (m, 1H), 3.15–3.05 (m, 1H), 2.43–2.3 (m, 1H), 1.8–1.72 (m, 1H), 1.46 (s, 18 H); ^{13}C NMR (125 MHz, CDCl_3) δ 155.3, 154.4, 80.2, 79.7, 55.7, 53.3, 52.7, 48.5, 34.7, 28.4, 28.3, 28.2. Yield: 70 %



^1H NMR (500 MHz, CDCl_3) δ 5.4 (brs, 1H), 5.2 (brs, 1H), 4.0 (brs, 1H), 3.82–3.68 (m, 2H), 3.4–3.0 (m, 3H), 2.32–2.08 (m, 1H), 1.7–1.57 (m, 1H), 1.38 (s, 27 H); ^{13}C NMR (125 MHz,

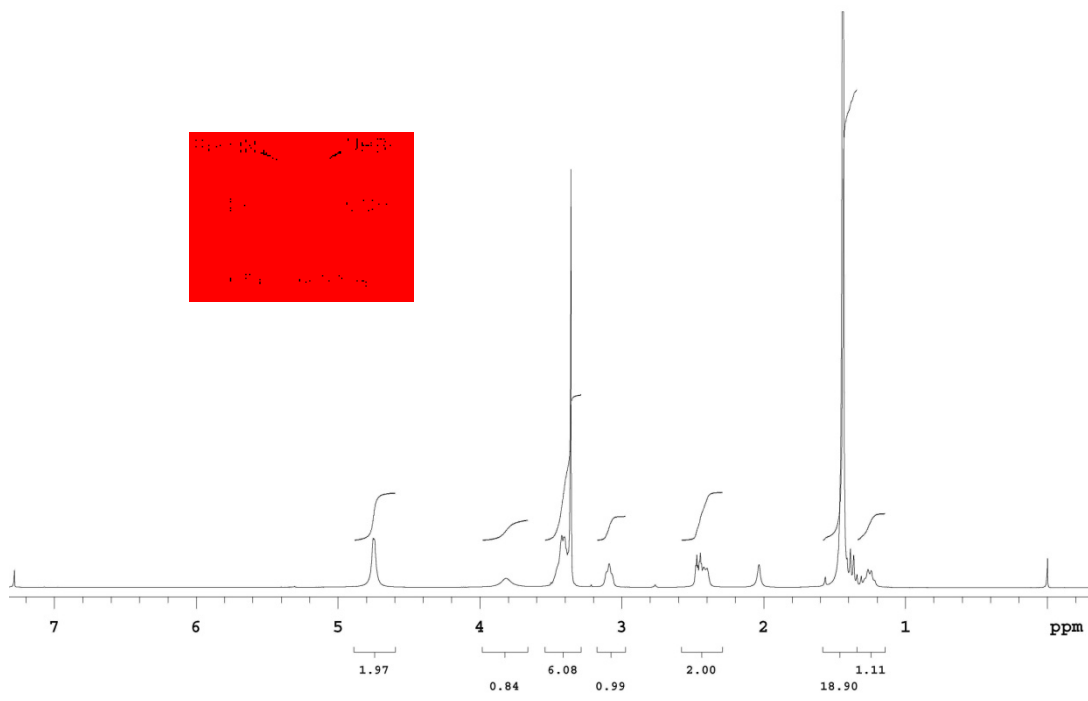
CDCl₃) δ 156.7, 155.6, 154.2, 80.1, 79.5, 56.8, 53.4, 49.4, 43.9, 34.2, 30.9, 28.4, 28.3. Yield: 22 %.

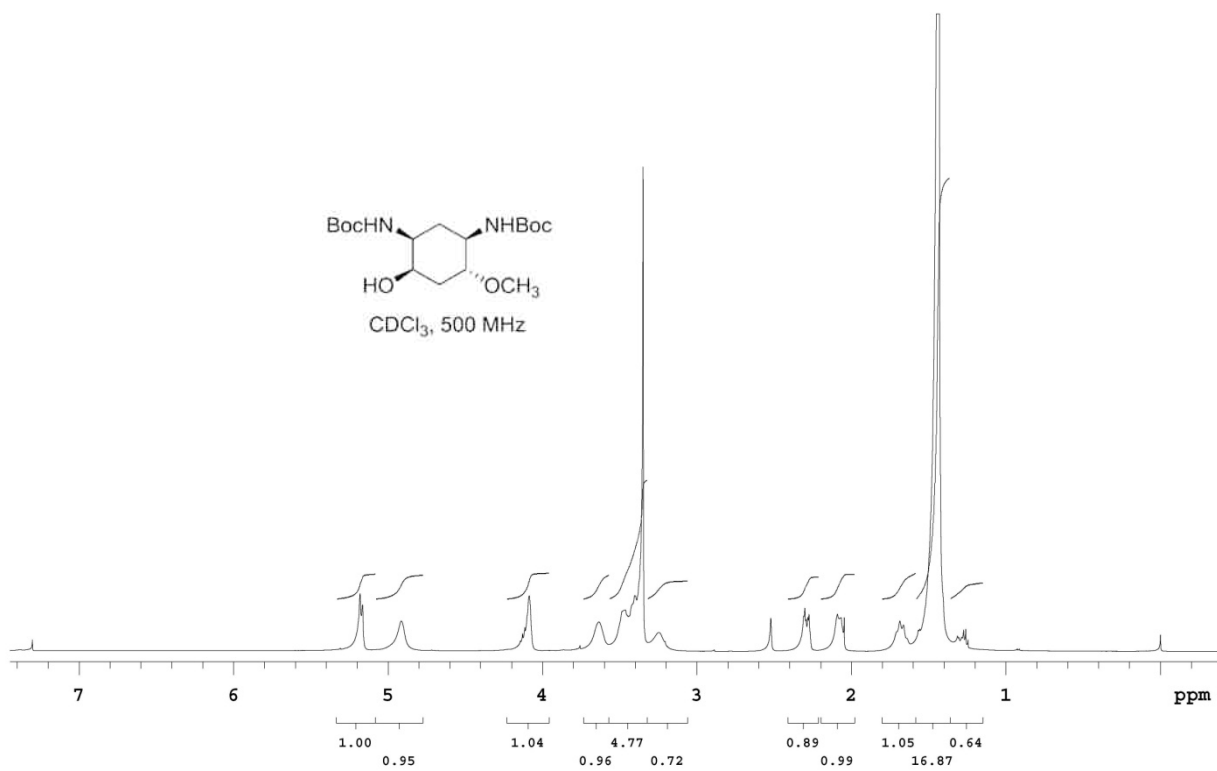
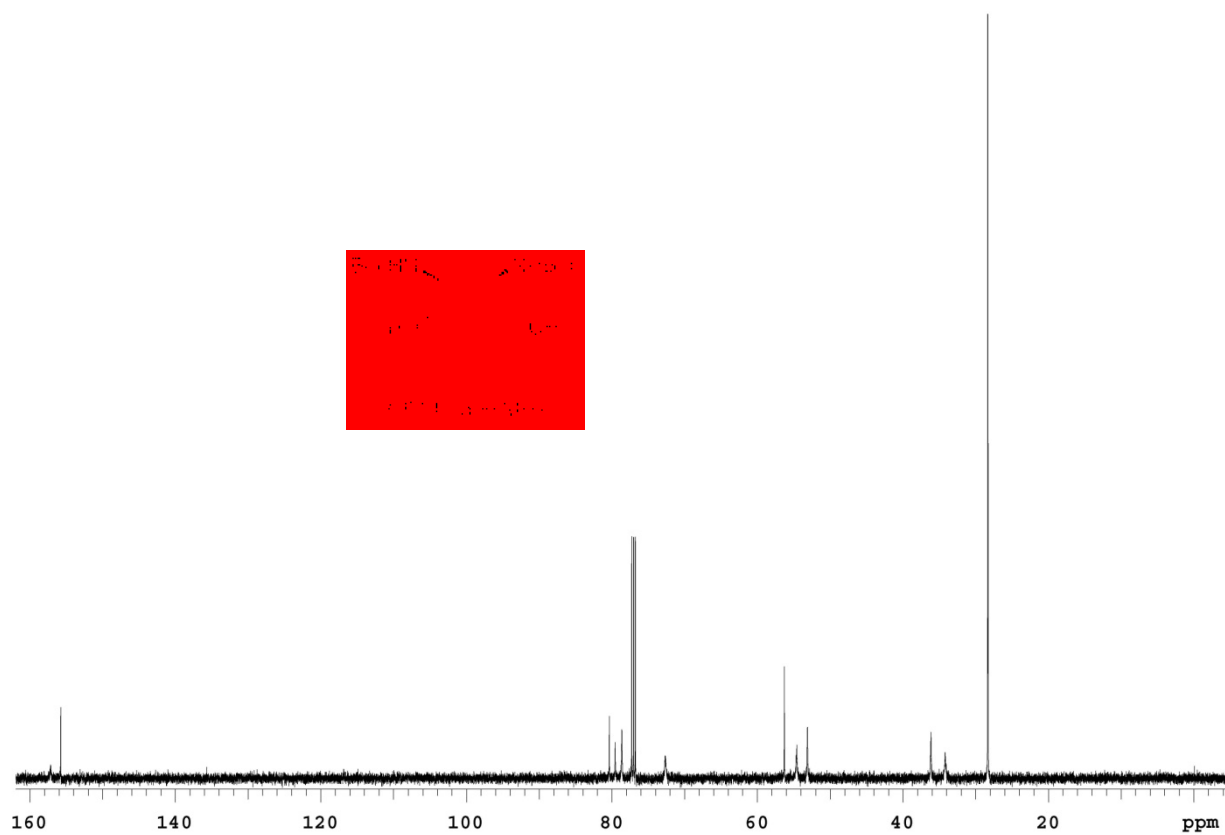


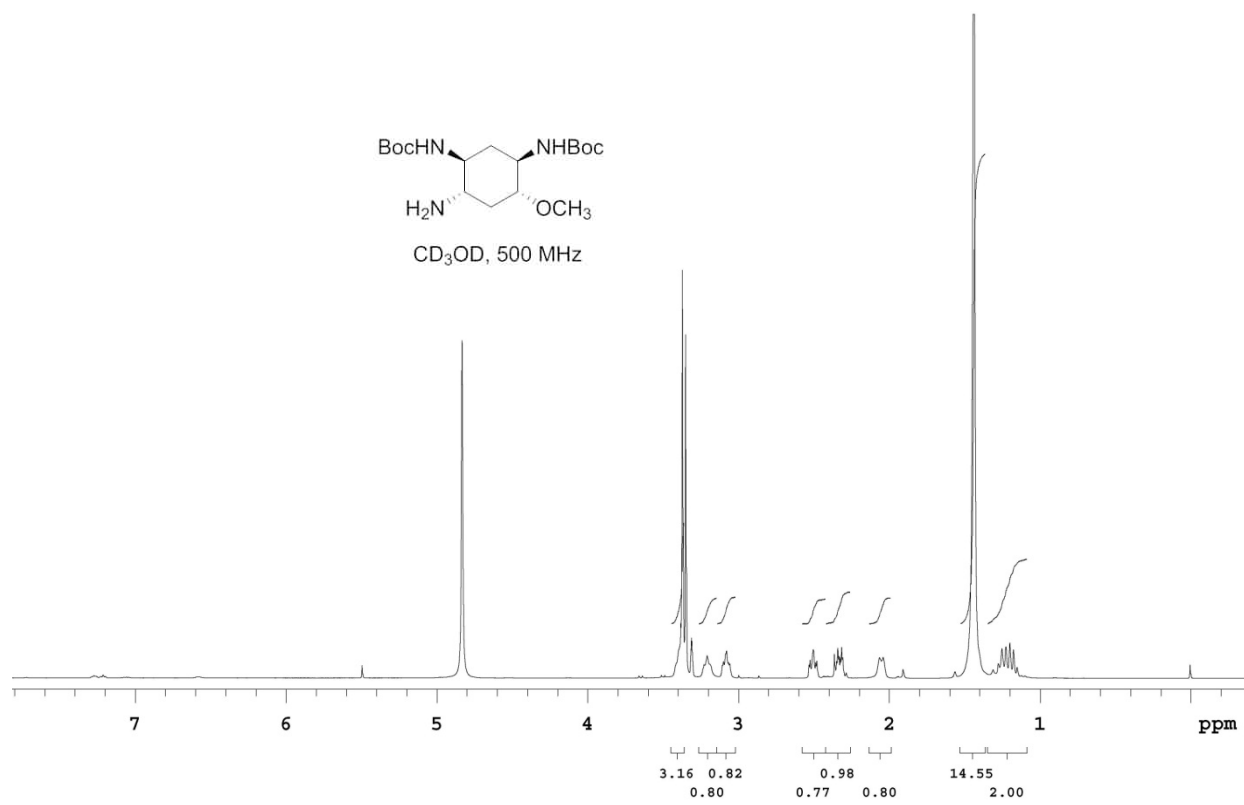
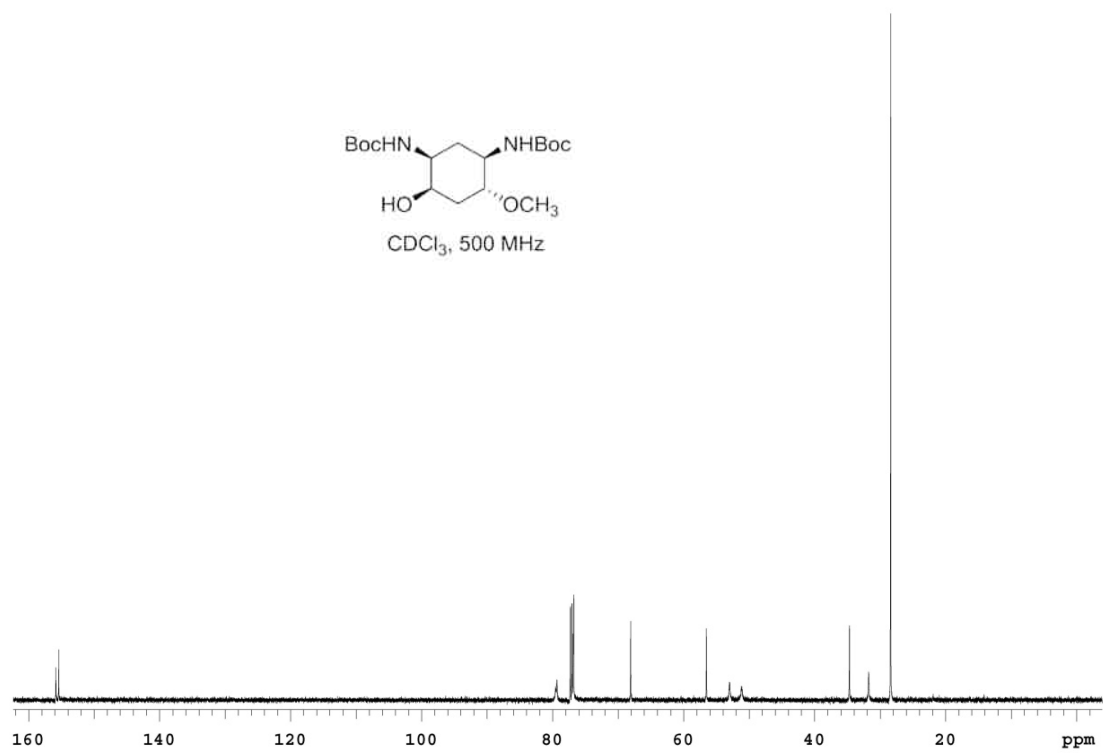
¹H NMR (500 MHz, CDCl₃) δ 7.28, (t, J = 8.5 Hz), 6.64 (t, J = 8 Hz), 4.57-4.16 (m, 1H), 3.8-3.3 (m, 3H), 2.59-2.17 (m, 1H), 2.04, 1.87 (m, 1H), 1.4 (d, 9H). Yield (95%).

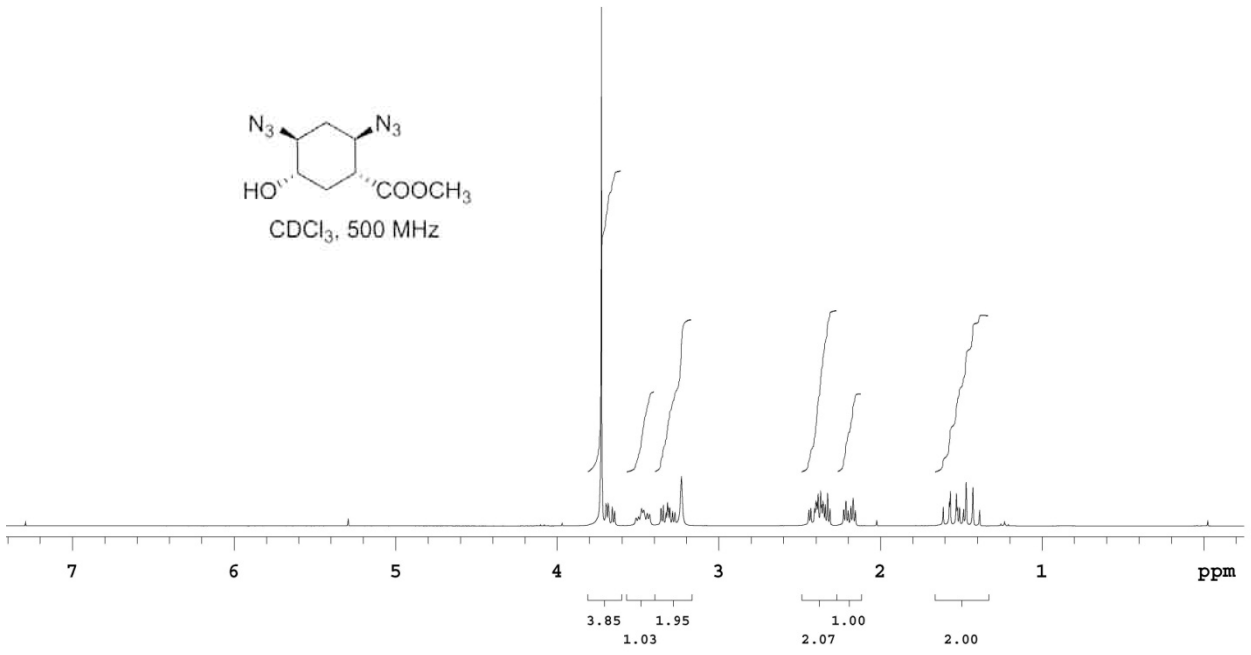
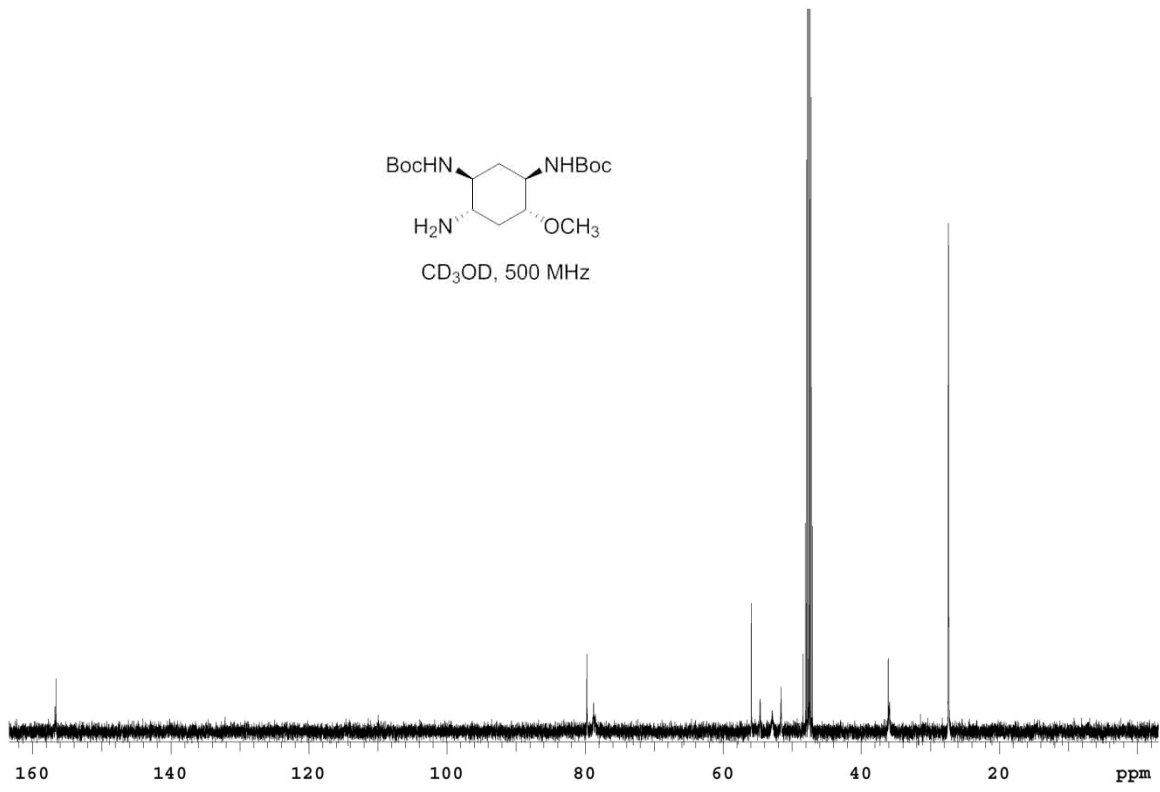
Appendix A

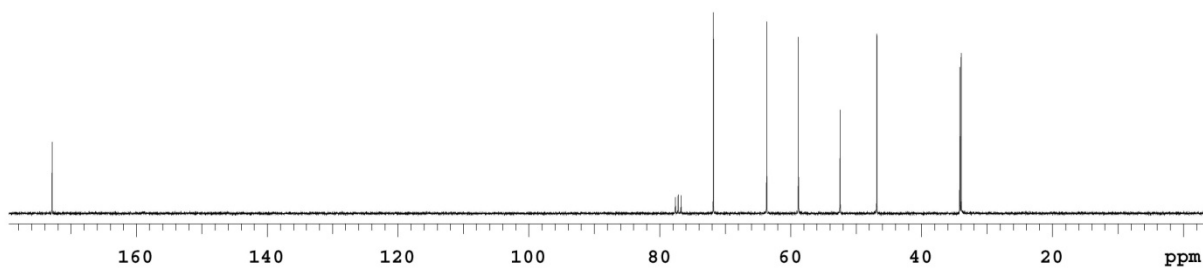
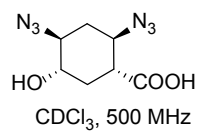
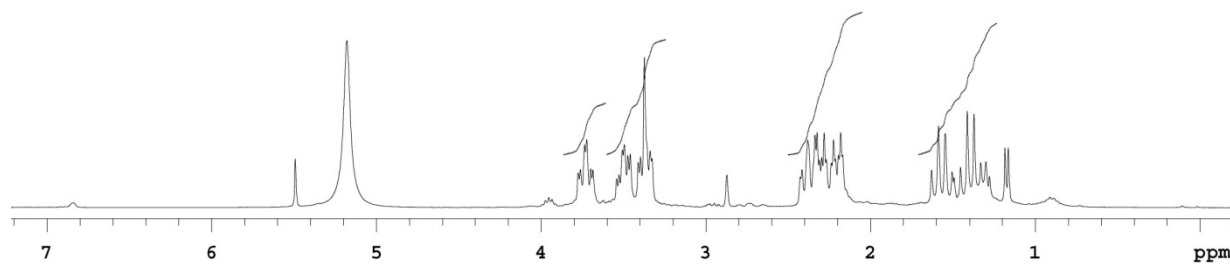
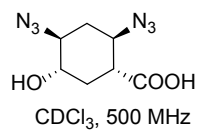
Spectral images for Chapters 2, 5 and 6

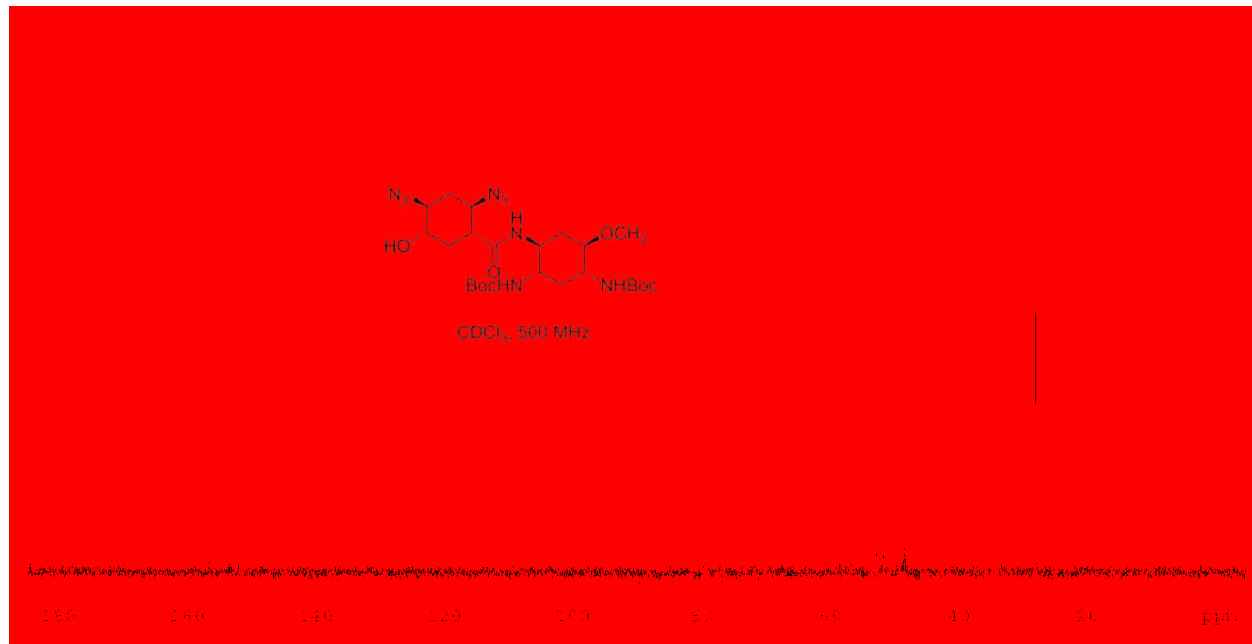
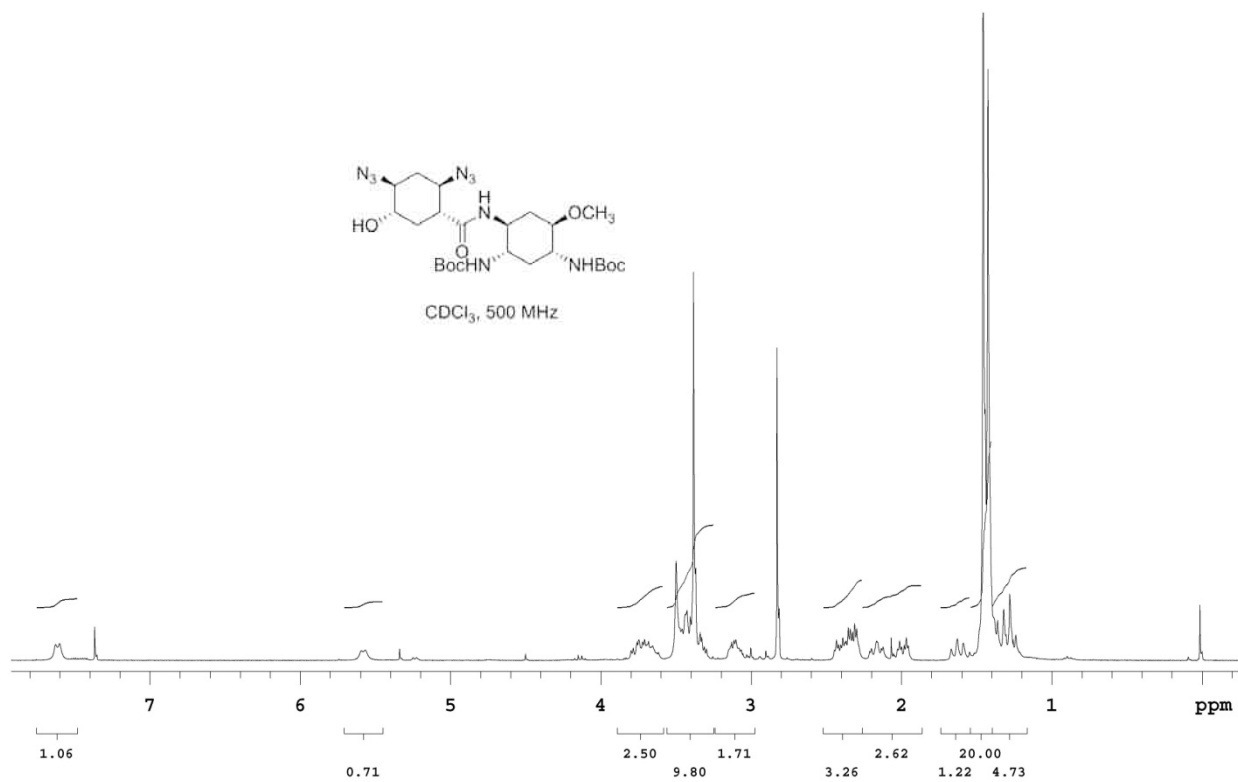


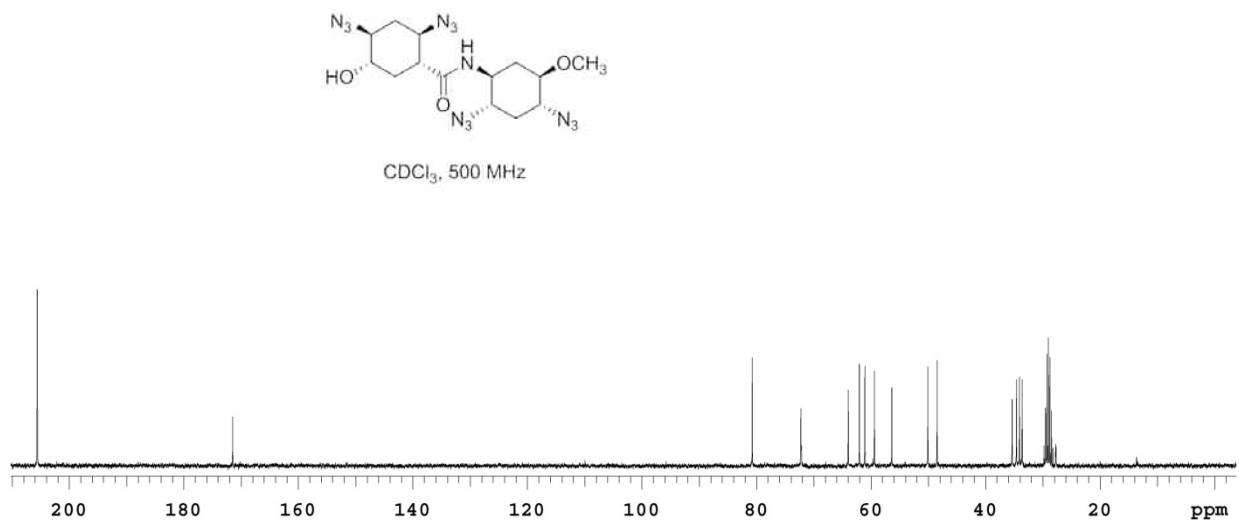
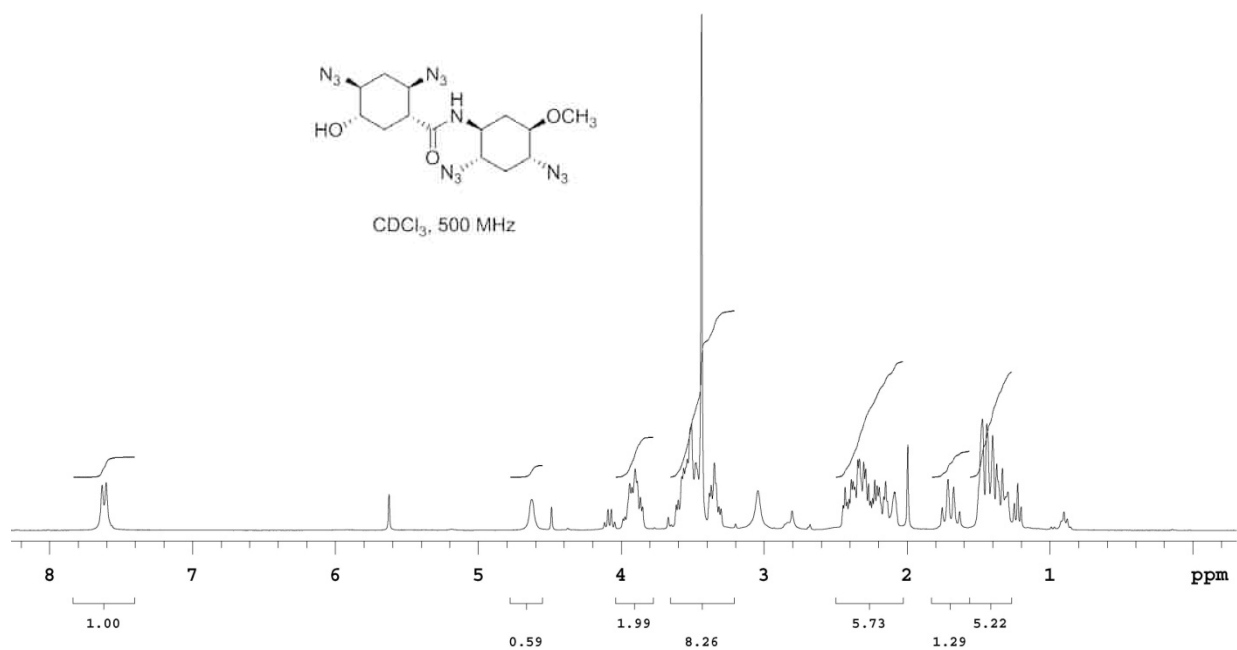


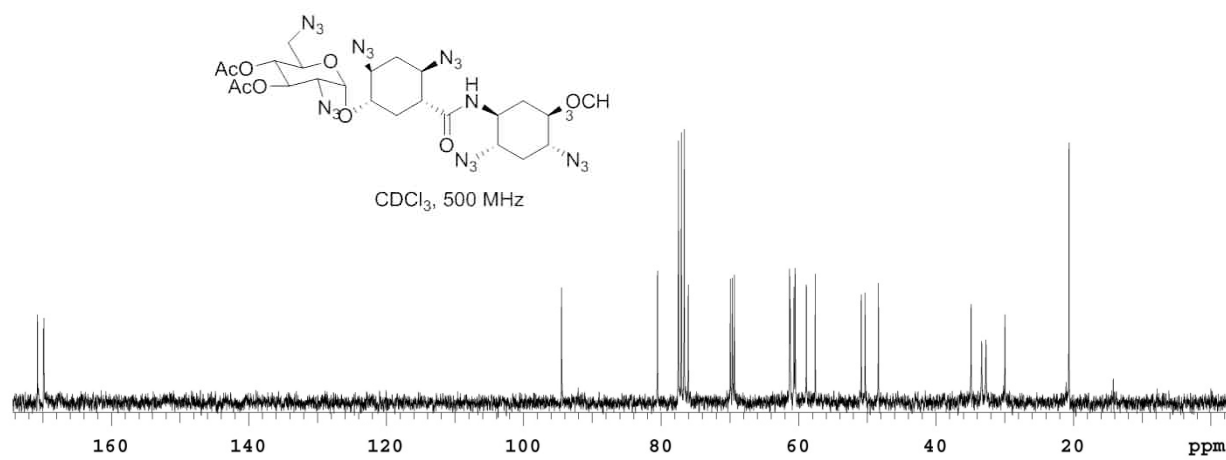
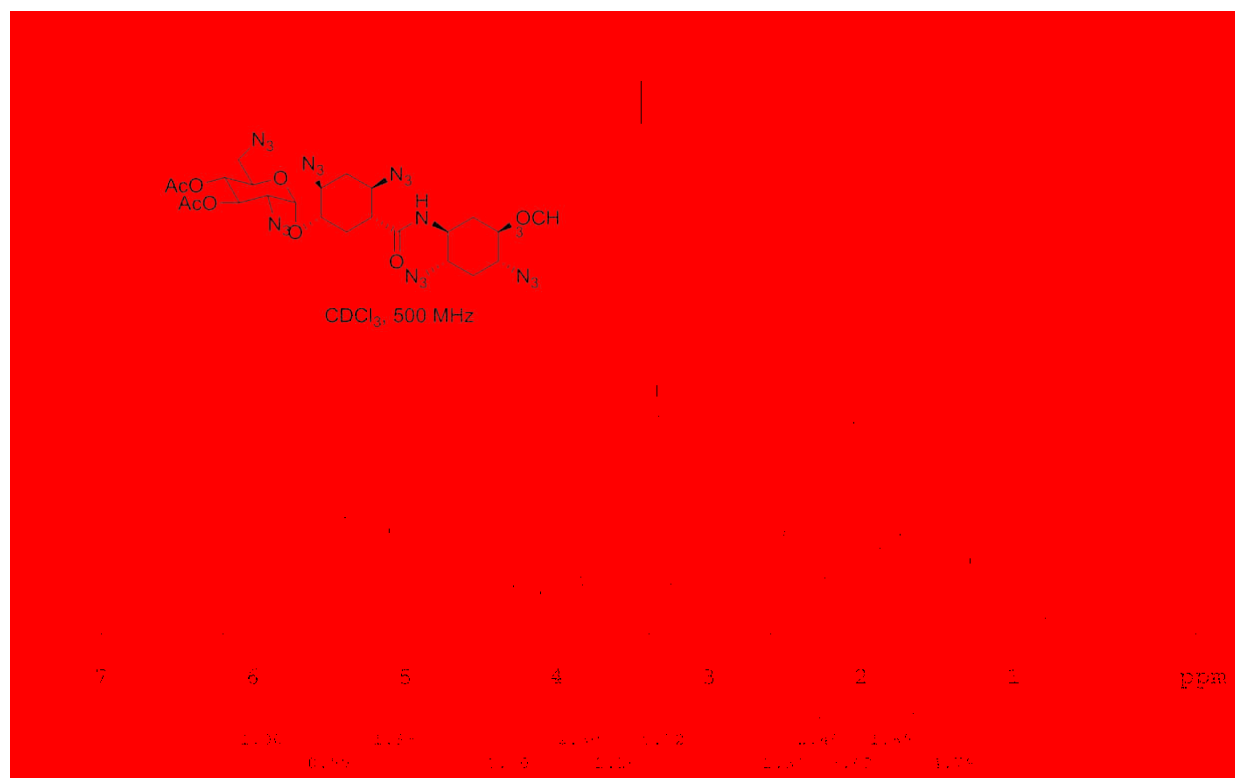


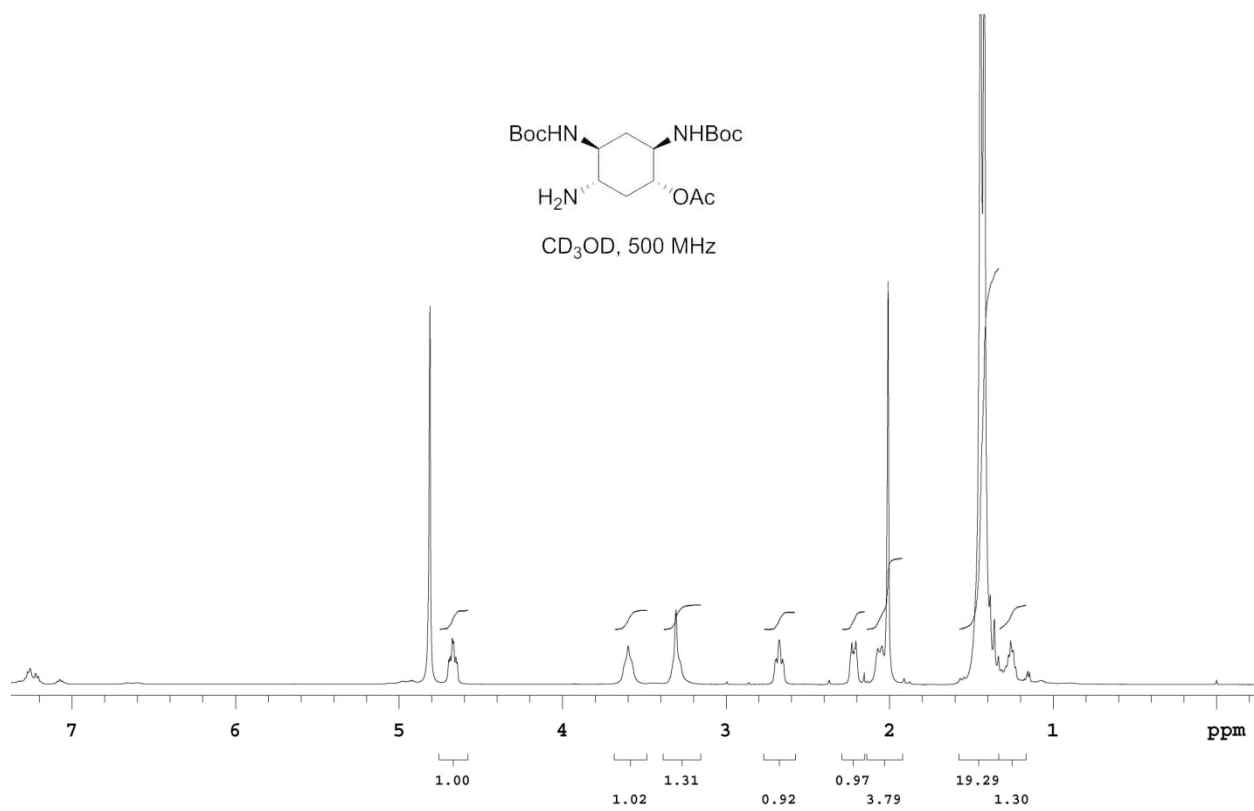
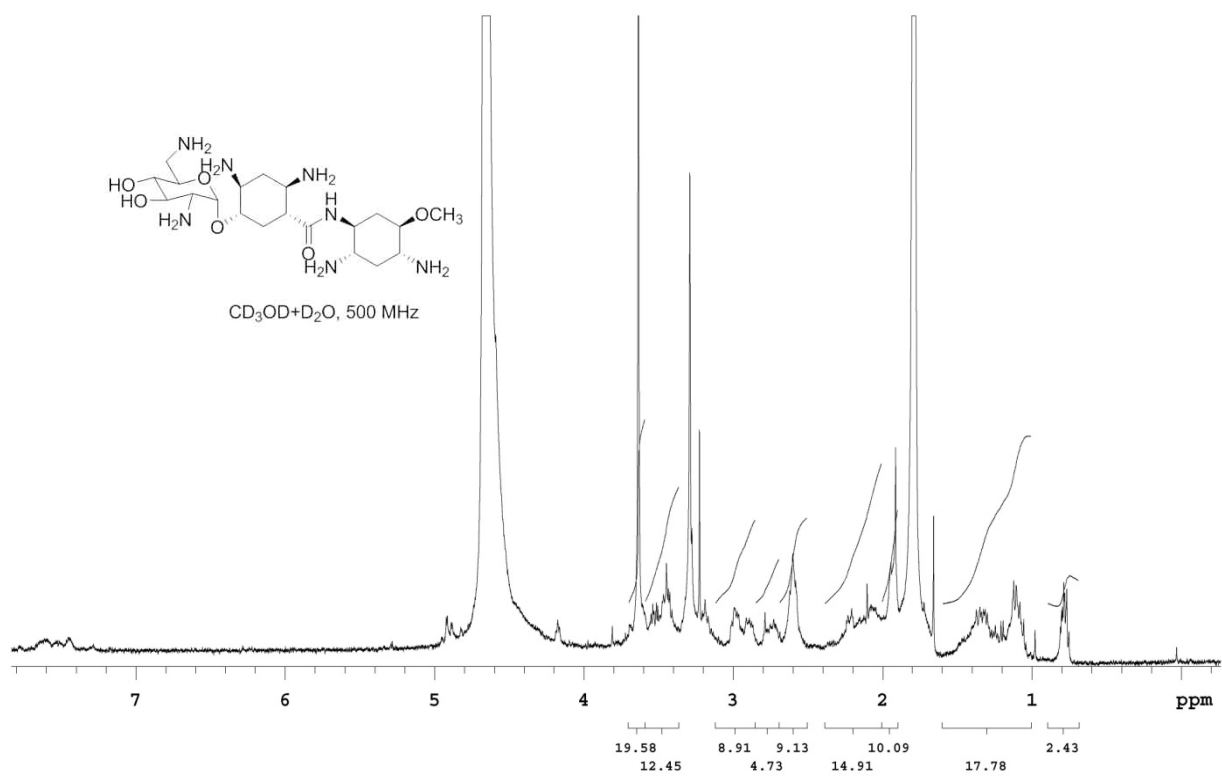


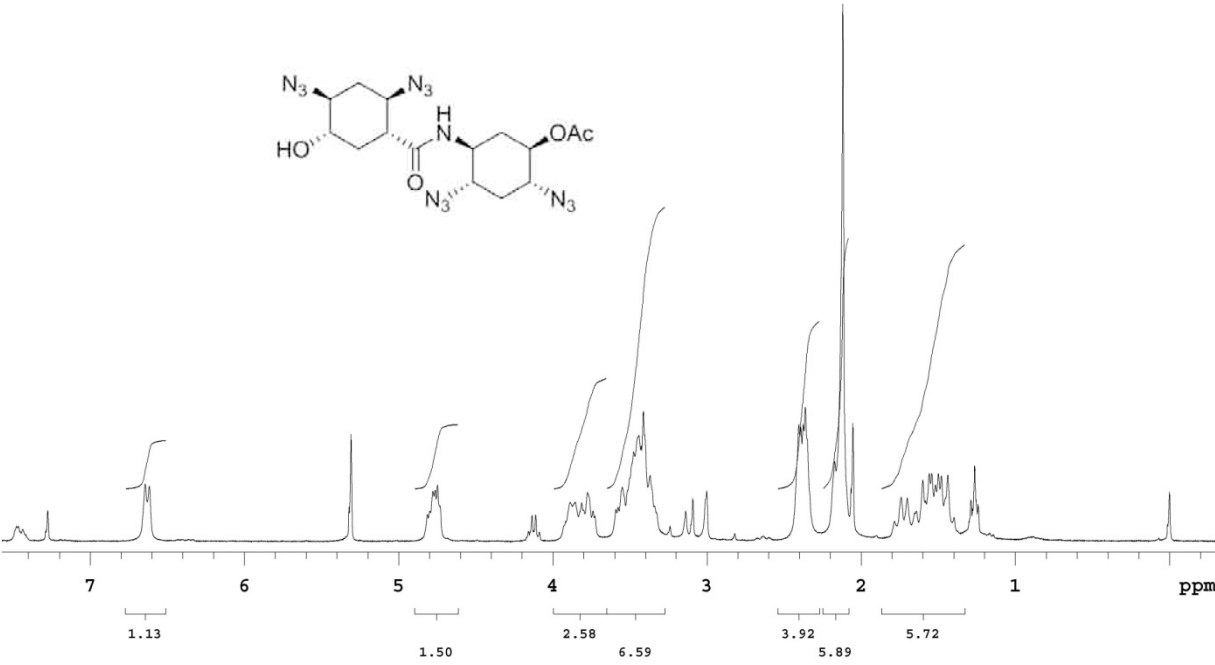
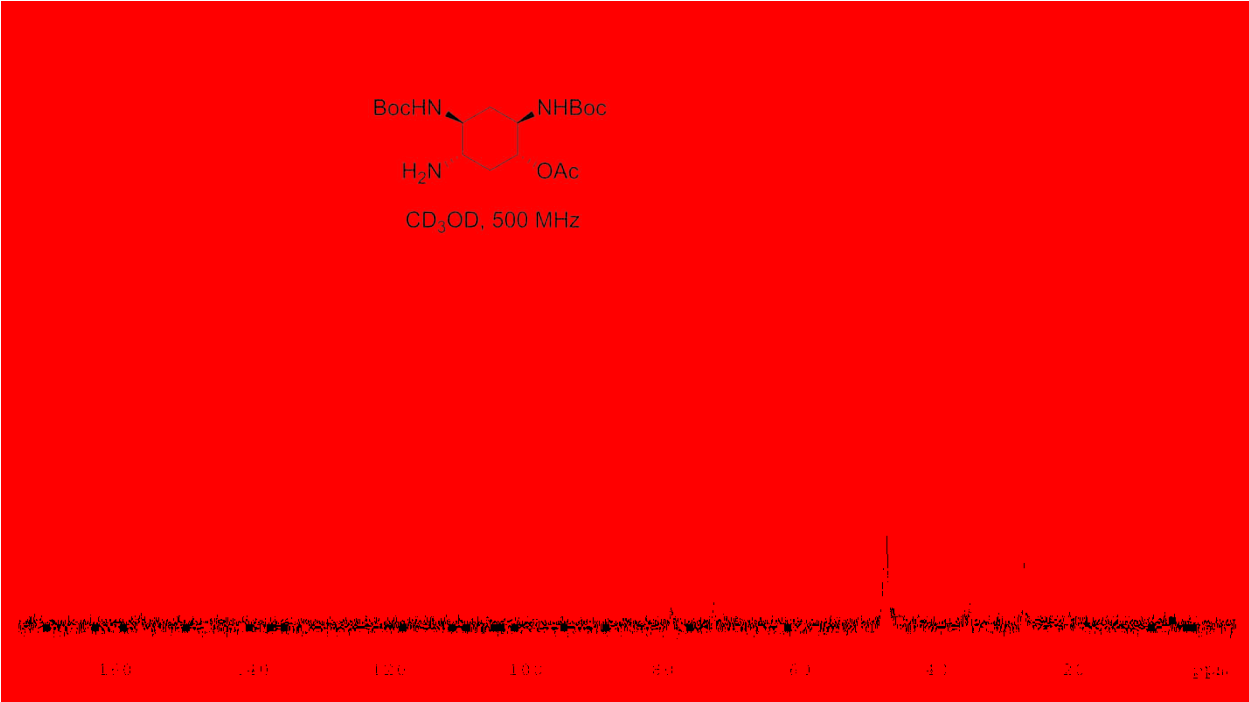


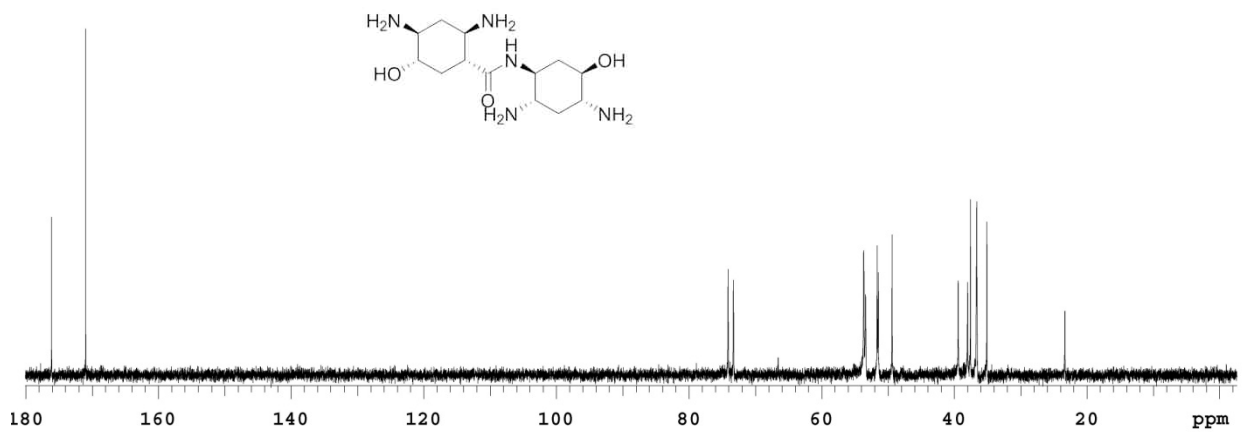
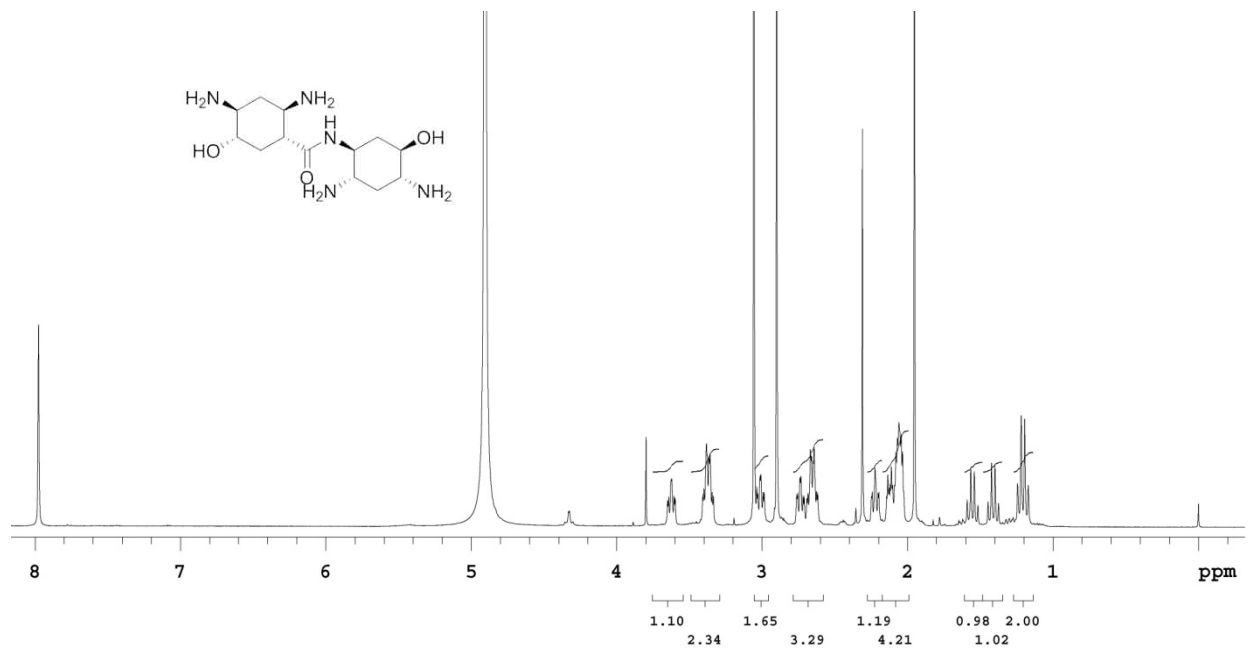


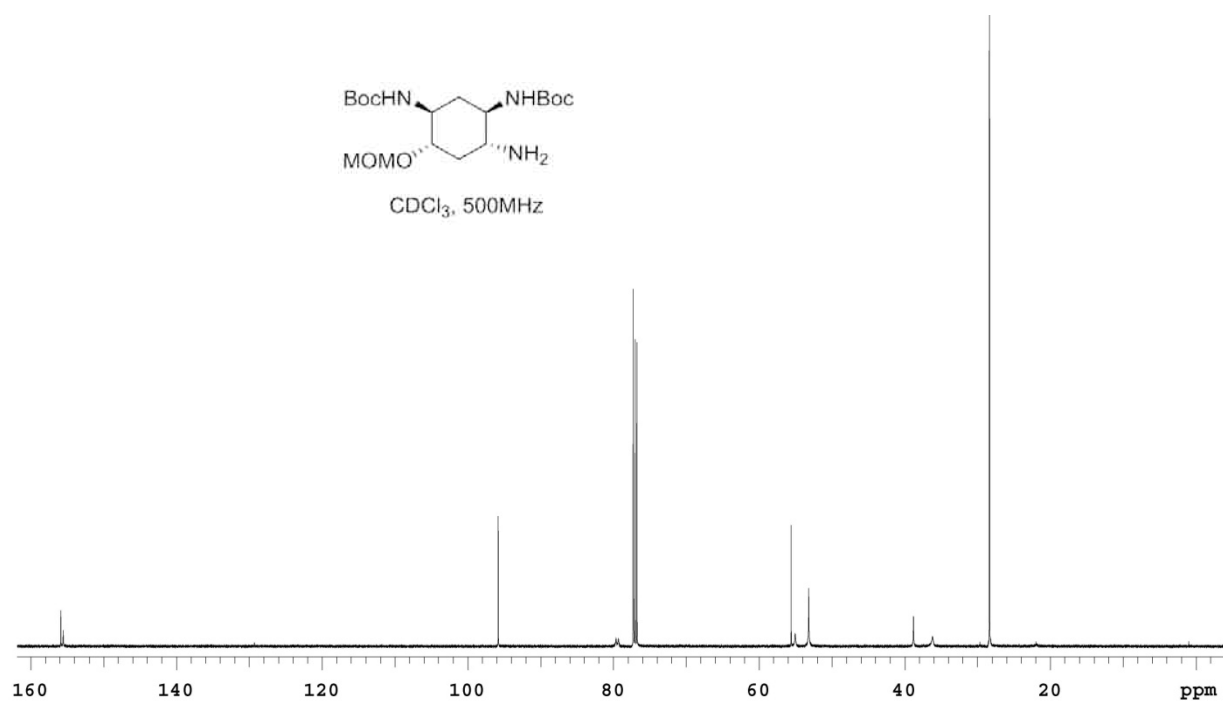
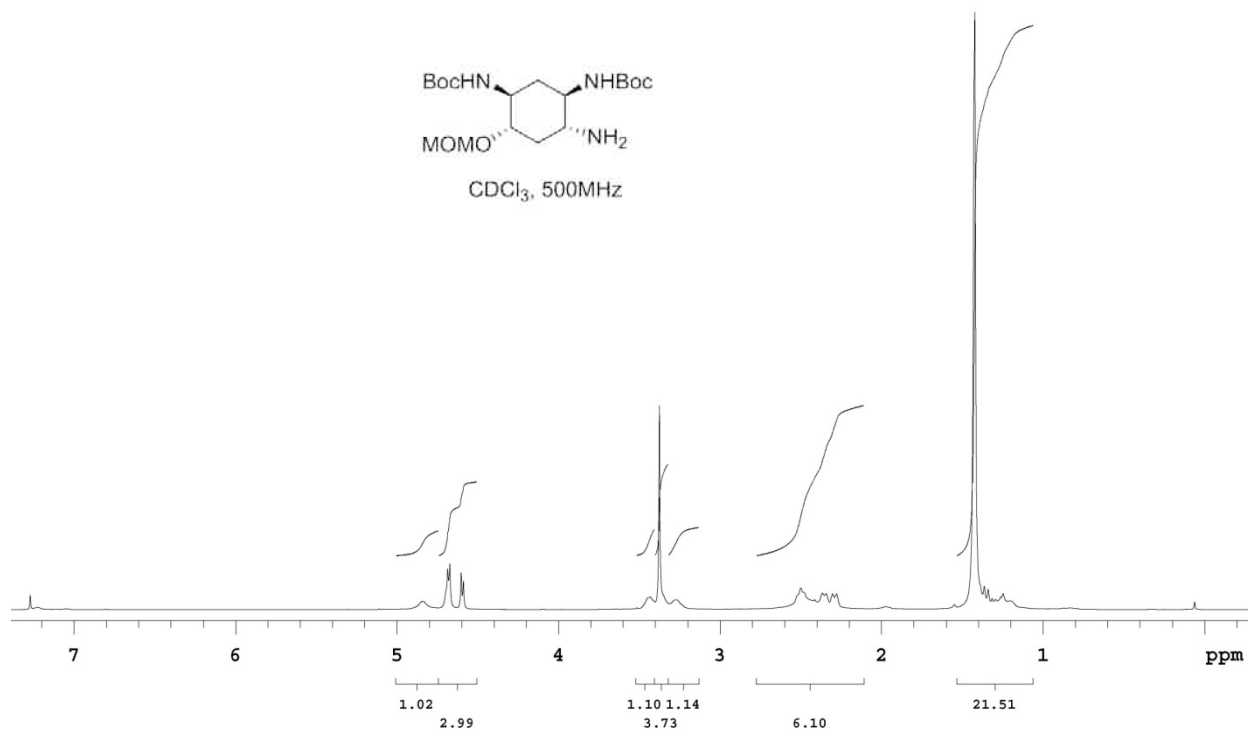


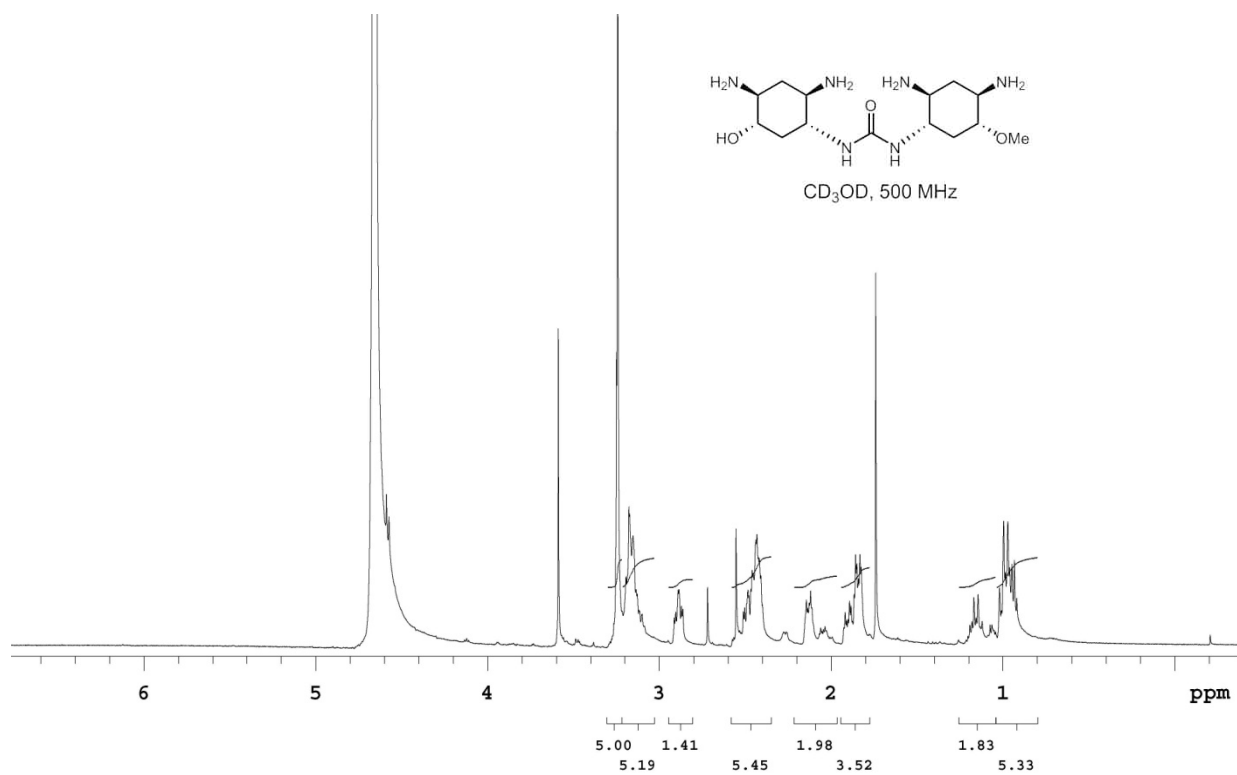
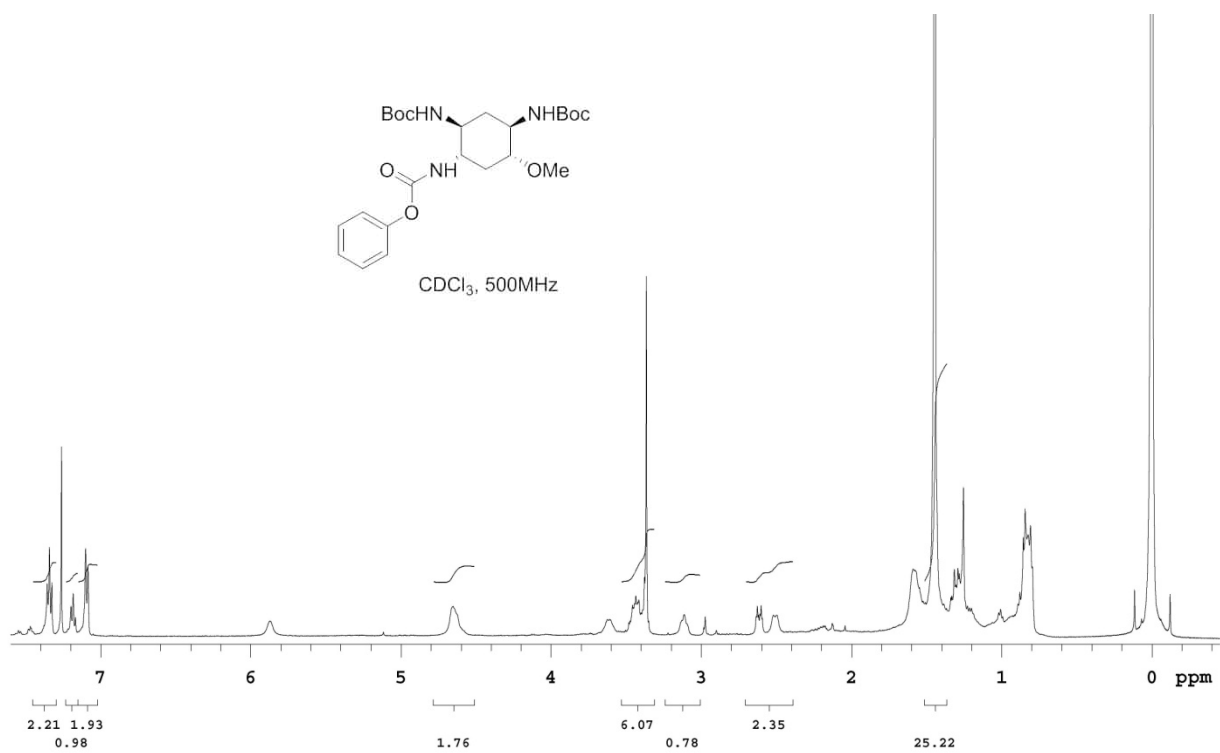


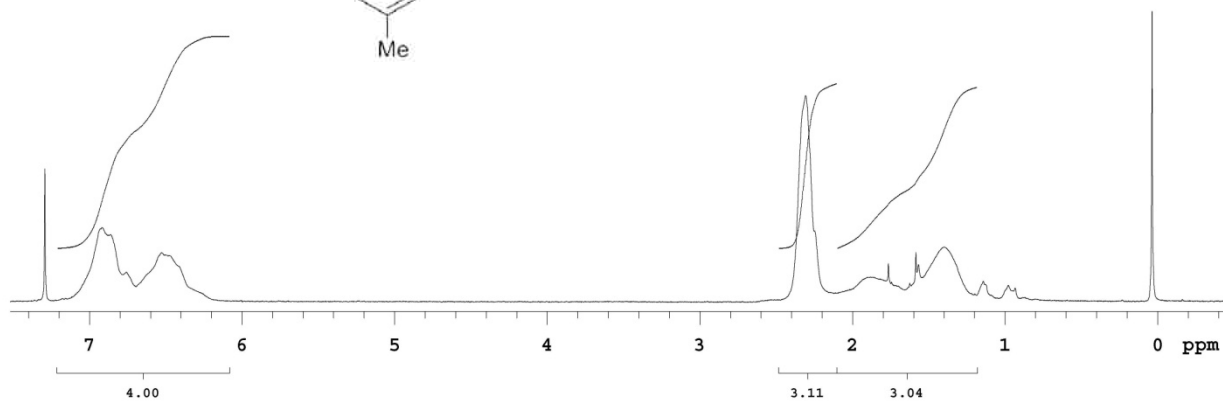
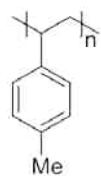
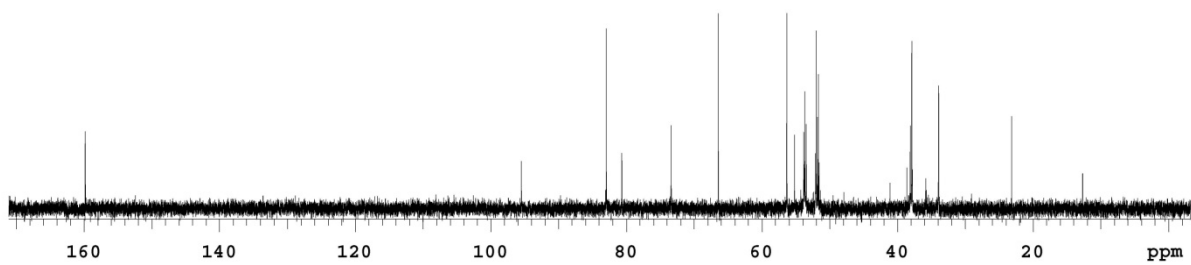
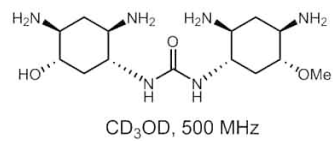


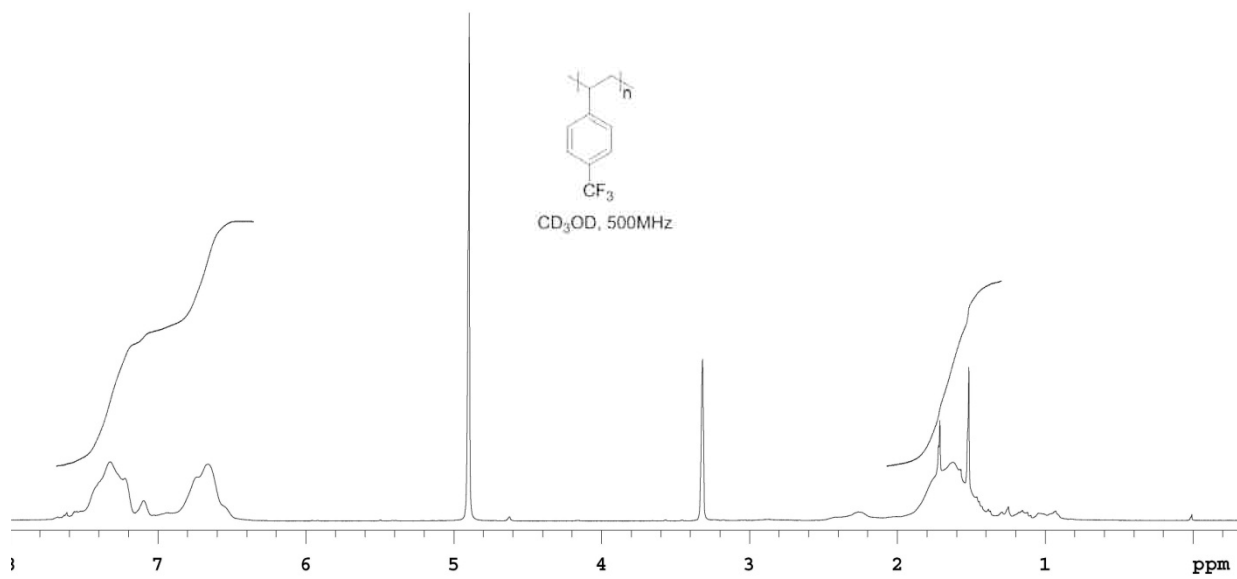
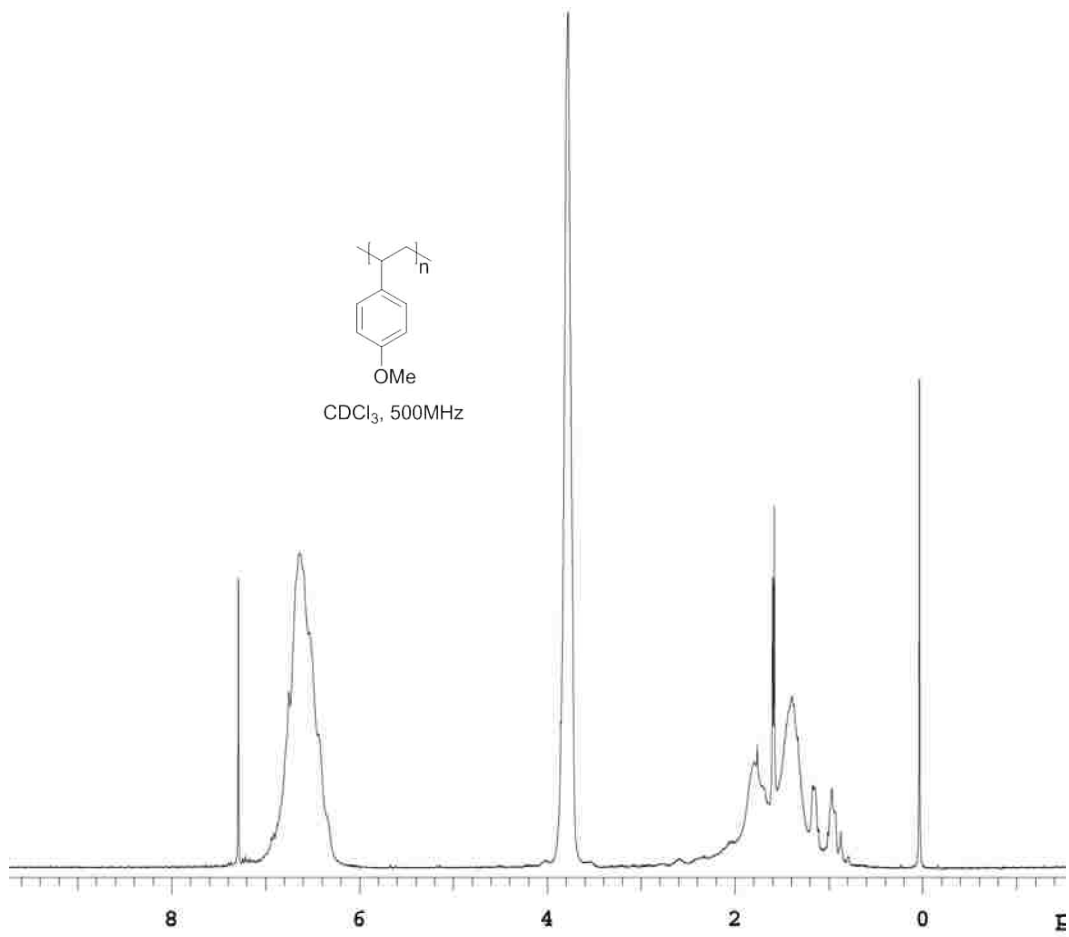


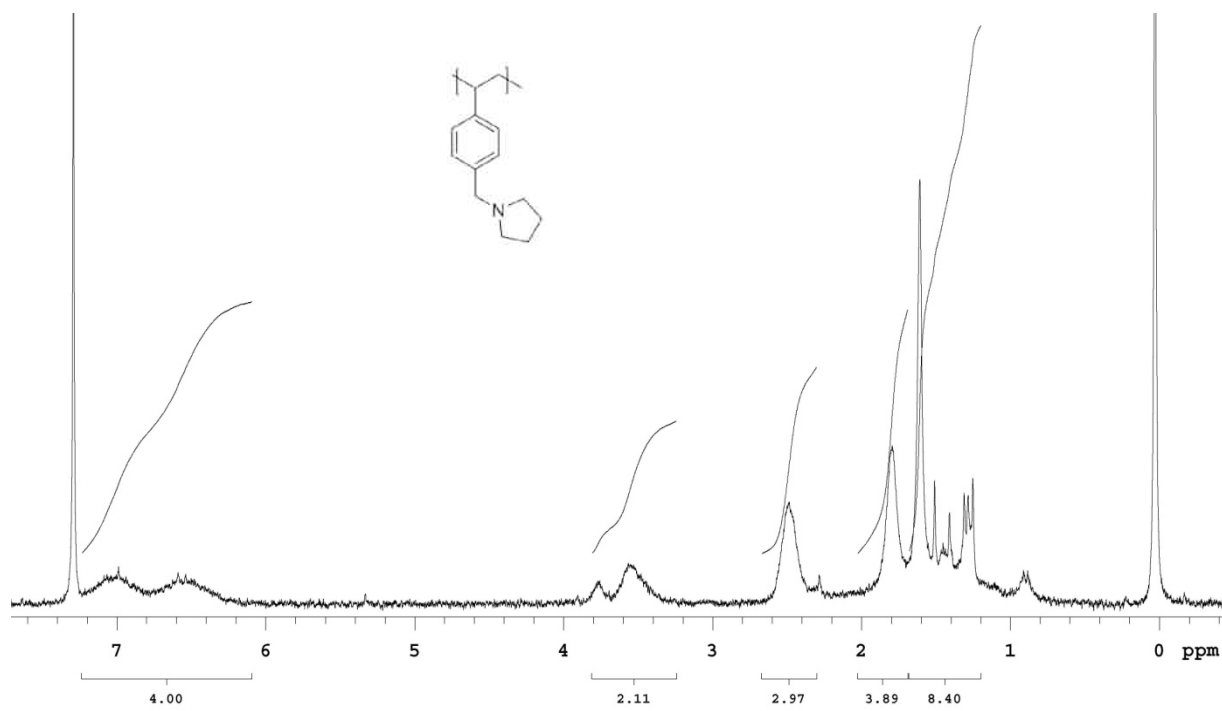
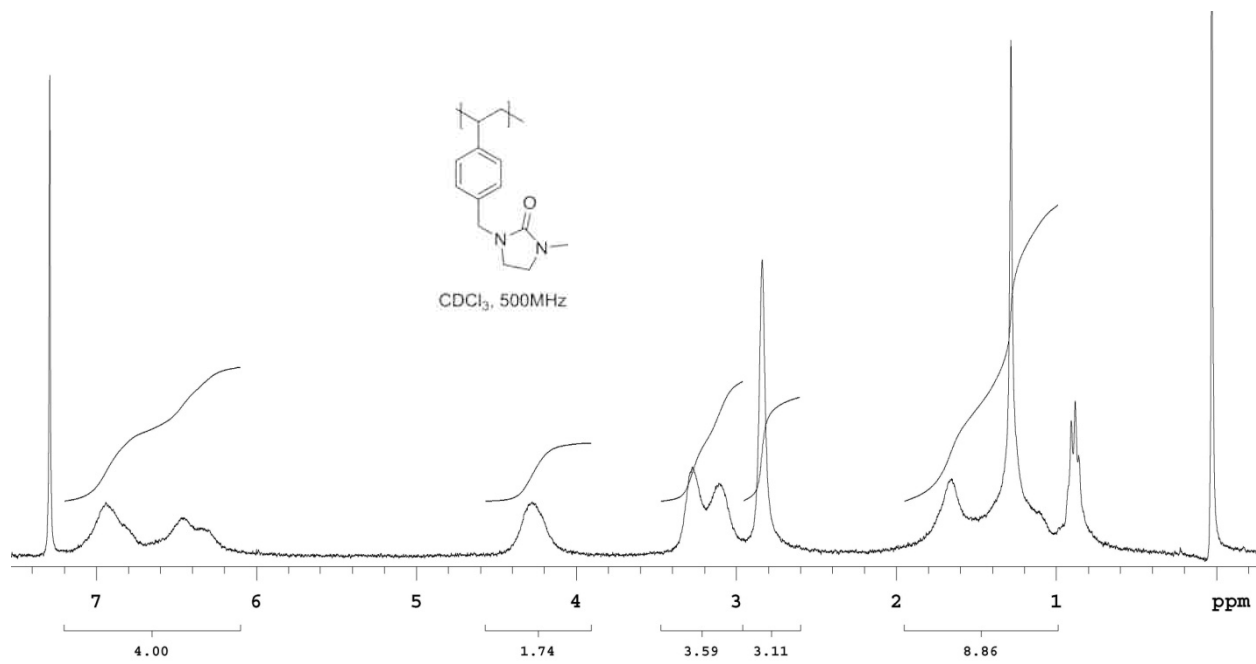


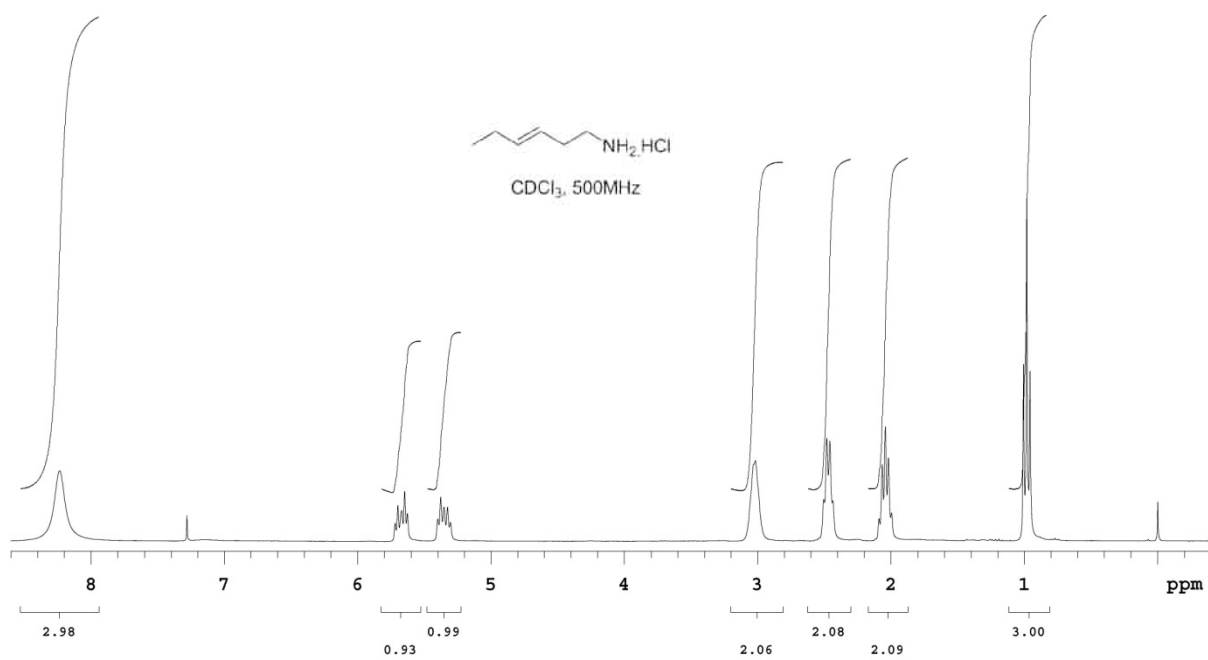
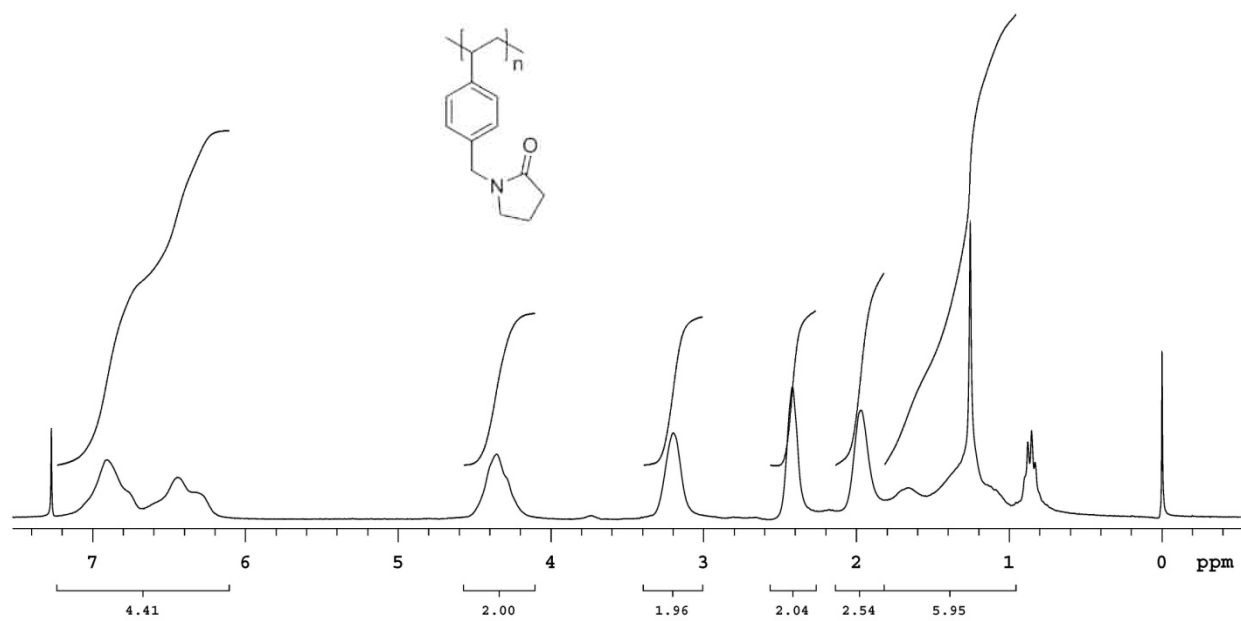


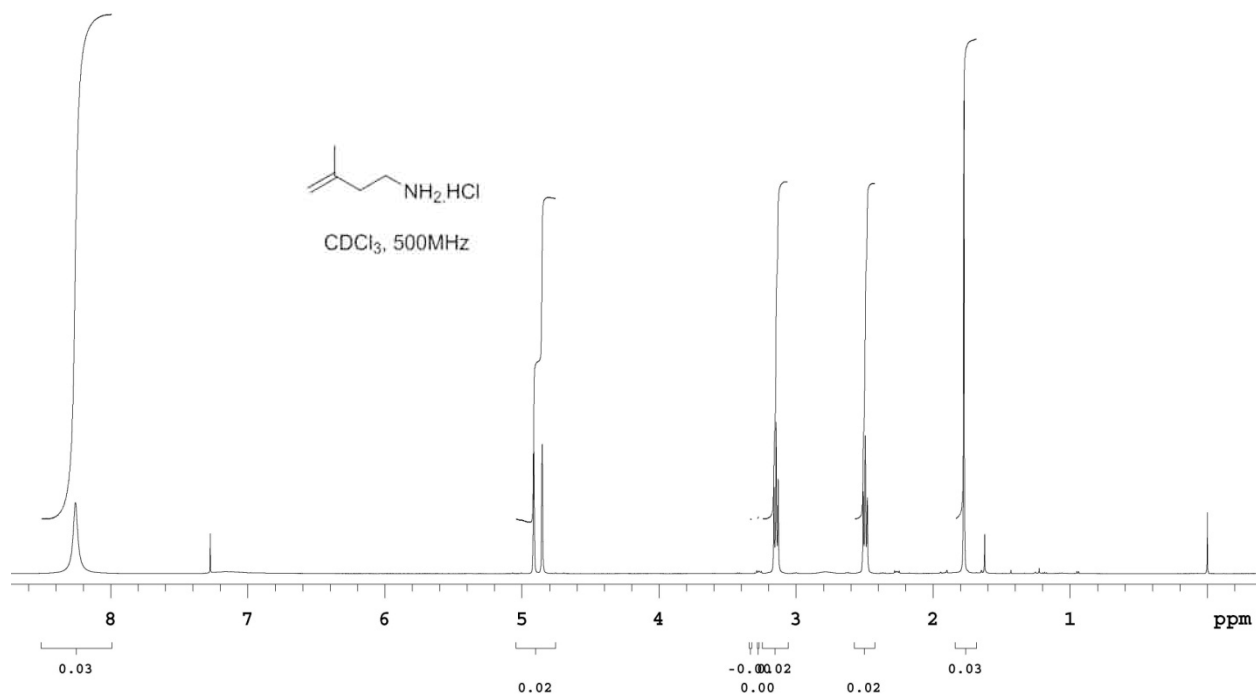
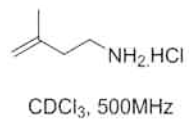
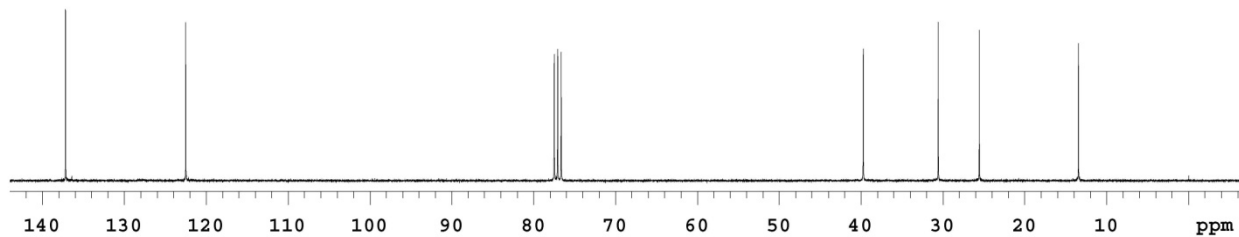
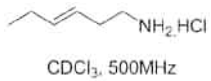


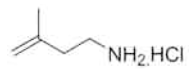




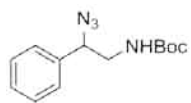
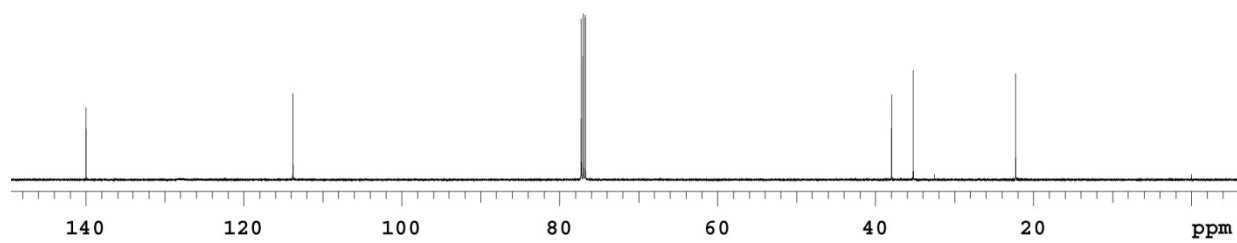








CDCl₃, 500MHz



CDCl₃, 500MHz

